STUDIES ON CARBON-ENHANCED METAL-POOR (CEMP) STARS

A THESIS

SUBMITTED FOR THE DEGREE OF

DOCTOR OF PHILOSOPHY IN PHYSICS

IN

THE FACULTY OF SCIENCE
BANGALORE UNIVERSITY
JNANA BHARATHI, BANGALORE, KARNATAKA 560056

BY

DRISYA K

UNDER THE SUPERVISION OF

PROF. ARUNA GOSWAMI

INDIAN INSTITUTE OF ASTROPHYSICS
BANGALORE, KARNATAKA 560 034

MARCH 2015

To my beloved parents.....

Though my soul may set in darkness, it will rise in perfect light; I have loved the stars too fondly to be fearful of the night..

DECLARATION

I hereby declare that the matter contained in the thesis entitled **"Studies on Carbon-Enhanced Metal-Poor (CEMP) stars"** is the result of investigations carried out by me at the Indian Institute of Astrophysics under the supervision of Prof. Aruna Goswami. This thesis has not been submitted for the award of any other degree, diploma, associateship, fellowship etc. of any University or Institute.

Drisya K
(Candidate)

Indian Institute of Astrophysics
Bangalore-560034, India

CERTIFICATE

This is to certify that the matter contained in the thesis entitled "**Studies on Carbon-Enhanced Metal-Poor (CEMP) stars**" submitted to the Bangalore University by **Mrs. Drisya K** for the award of the degree of Doctor of Philosophy in the Faculty of Science, is based on the results of investigations carried out by her under my supervision and guidance, at the Indian Institute of Astrophysics. This thesis has not been submitted for the award of any other degree, diploma, associateship, fellowship etc. of any University or Institute.

Prof. Aruna Goswami
(Thesis supervisor)

Indian Institute of Astrophysics
Bangalore-560034, India

ACKNOWLEDGEMENTS

This thesis would not have been possible without the help of many individuals, who one or the otherway helped me to complete my work.

First and foremost, I thank God almighty for giving me this wonderful opportunity to pursue a PhD and to complete my work. With the same respect and affection I thank my thesis supervisor **Prof. Aruna Goswami** for her guidance, support, love and motherly care throughout the years. My dream would not have come true without you Ma'am. Thank you so much for your encouragement, enthusiasm and faith in me throughout my time with you.

I thank the Directors, Prof S. S Hasan and Prof P. Sreekumar, Indian Institute of Astrophysics, for providing me all the facilities required for the research work. I also thank the Deans, Prof. H. C Bhat, Prof. T. P Prabhu and Prof. Rangarajan for their support.

I thank all the administrative and library staff members at the Indian Institute of Astrophysics for their constant help and support. I thank Dr. Shanti Kumar for his help during the observations with HCT. I also thank the research trainees at CREST for their support throughout these years. Special thanks to Aman, Ravi, Ritu, Pramod, Venkitesh, Rahul and Gouri for their guidance and support during my nights at CREST.

I take this opportunity to thank all my teachers from primary to MSc who helped me to reach at this level. Special thanks to Prof. Kagali, Prof. Anvekar, Prof. Sharat Anatha Murthy and Prof. Damle of Department of Physics, Bangalore University for helping me regarding all the administrative matters in the university. I also thank Prof. Vijayakumar Doddamani for his help and support.

I am grateful to CSIR (9/890(0003)/12 EMR I) and DST project (SR/S2/HEP-09/2007) for the financial support for the PhD work.

I know this is the only way to express my love and thankfulness to my dear friends who stood there for me always. Special thanks to Jessy jose and Smitha subramanian for all your support and encouragement. Thanks to Bharat Kumar and Sudhakar reddy for their comments and suggestions regarding the high resolution analysis. Special thanks to Honey, Annu, Ambili, Anantha, Hema, Nirmal, Sreejith, Joice, Vineeth, Sajal, Dinesh, Manpreet, Arya, Prashanth, Manjunath for making my life at IIA a memorable one. Thanks to my seniors Rumpa, Ramya. S, Blesson, Koshy, Nagaraj, Uday and Vigeesh for their help and support. I also thank Sreeja and Subramania Athiray for their guidance

and support at the beginning of this journey. Thank you Arun for helping me with your extra ordinary programming skills. Thank you Ramya. P and Susmitha for their support in a special way which made me confident to face all the problems in a cheerful manner. Last but not the least, thank you Sindhuja and Indu for their love, care and faith both in academic as well as personal matters.

I take this opportunity to thank all my family members, who stood there as strong pillars for me always and without them I am nothing. Remembering my beloved grand parents, who wanted me to reach greater heights in life and if I have achieved anything that is only because of their love and blessings. Words can not express how grateful I am to my parents Mr. Devadathan Nair and Mrs. Syamala for all of the sacrifices that they have made on my behalf and showing me the right way in all the ups and downs in my life. Your prayer for me was what sustained me thus far. Thank you Deepu for being a wonderful brother and caring uncle. Definitely I could not achieve this without your sleepless nights and days. Minu, thank you so much for all your love and concern towards me. I also thank my in laws Mr. Unnikrishnan Nambiar and Mrs. Prema for being as my parents and giving me all the freedom to choose whatever I want in life. Thank you Sari and Hema for being there for me always. Finally, to conclude, Nijil and Sivani, I dont know how will I express my love and thanks to them for moulding their routines as per my needs. Nijil, I know how much I disturbed you with my tensions but your ”Everything will be ok” is everything to me. Sivani, my little bundle of joy, whenever I was tensed or hard pressed by time, though you were too small to unedrstand, your smile and laughter made me relaxed. Thank you almighty for making my world with these wonderful people.

TABLE OF CONTENTS

ABSTRACT **4**

LIST OF PUBLICATIONS **7**

LIST OF FIGURES **9**

LIST OF TABLES **13**

1 Introduction **15**

1.1 Carbon-Enhanced Metal-Poor (CEMP) stars 15
1.2 Stellar evolution and Nucleosynthetic processes leading to a carbon star . 16
1.3 Intrinsic properties of carbon stars 20
1.3.1 Spectral classification of carbon stars 20
1.3.2 C−R stars 21
1.3.3 C−N stars 21
1.3.4 C−J stars 21
1.3.5 CH stars 21
1.3.6 CH-like stars 22
1.4 Metal-poor stars and carbon-enhancements 22
1.4.1 Neutron-capture nucleosynthesis and production scenarios 24
1.4.2 CEMP- sub-groups and origin of abundance patterns 26
1.5 Abundance trends with metallicity in CEMP stars 28
1.6 [hs/ls]: An indicator to s-process efficiency 28
1.7 $^{12}C/^{13}C$ ratio as a probe of stellar evolution 29
1.8 Binary nature and mass transfer mechanisms 30
1.8.1 Roche-lobe overflow and Wind mass transfer 31
1.9 Evolutionary link between CH and Ba stars 33
1.10 Outline of the thesis 33

2 Data and Analysis **35**
2.1 Introduction . . . 35
2.2 Astronomical techniques . . . 35
2.2.1 Spectrograph . . . 36
2.2.2 Factors affecting the quality of a spectrum . . . 38
2.3 Observations and Data . . . 39
2.3.1 Low resolution spectroscopy . . . 39
2.3.2 High resolution spectroscopy . . . 40
2.3.3 Data reduction . . . 41
2.4 Data analysis . . . 42
2.4.1 Bolometric magnitudes . . . 42
2.4.2 Luminosity . . . 42
2.4.3 Effective temperature . . . 42
2.4.4 Surface gravity . . . 43
2.4.5 Micro-turbulence . . . 43
2.4.6 Equiwalent width . . . 43
2.4.7 Optical depth and opacity . . . 45
2.4.8 Model atmospheres . . . 45
2.4.9 Estimation of radial velocity . . . 46
2.4.10 Calculation of photometric temperature . . . 46
2.4.11 Stellar Atmospheric parameters . . . 48
2.4.12 Calculation of Chemical abundances . . . 48
2.4.13 Hyperfine splitting and chemical abundances . . . 50
2.5 Parametric model based study . . . 50
2.6 Luminosities and Masses . . . 50
2.7 Error Analysis . . . 51

3 Low resolution spectroscopic study of CEMP (CH) stars **52**
3.1 Introduction . . . 52
3.2 Selection of programme stars . . . 52
3.3 Different types of carbon stars and their spectral characteristics . . . 53
3.3.1 Location of the candidate CH stars on (J−H) vs (H−K) plot . . . 61
3.3.2 Effective temperatures of the programme stars . . . 61
3.3.3 Isotopic ratio $^{12}C/^{13}C$ from molecular band depths . . . 71
3.4 Spectral characteristics of the candidate CH stars . . . 71
3.5 Candidate C−R stars . . . 84

3.6 Candidate C−N stars . . . 85
3.7 Low resolution spectroscopy of stars from the CH star catalogue of Bartkevicius (1996) . . . 87
3.8 Conclusion . . . 88

4 Spectroscopic analysis of CH stars I: Basic observational properties 90
4.1 Introduction . . . 90
4.2 High resolution spectra of the programme stars . . . 92
4.3 Radial velocity . . . 92
4.4 Temperatures from photometric data . . . 93
4.5 Stellar masses . . . 99
4.6 Linelist and Equivalent widths . . . 102
4.7 Conclusions . . . 103

5 Spectroscopic analysis of CH stars II: Atmospheric parameters and chemical abundances 105
5.1 Introduction . . . 105
5.2 Stellar Atmospheric parameters . . . 106
5.3 Abundance analysis . . . 108
5.3.1 Carbon . . . 109
5.3.2 Na and Al . . . 110
5.3.3 Mg, Si, Ca, Sc, Ti, V . . . 111
5.3.4 Cr, Co, Mn, Ni, Zn . . . 112
5.3.5 Sr, Y, Zr . . . 115
5.3.6 Ba, La, Ce, Pr, Nd, Sm, Eu, Dy . . . 115
5.4 Discussion on individual stars . . . 122
5.5 Parametric model based study . . . 133
5.6 Conclusion . . . 138

6 Summary and Conclusion 144
6.1 Future plans . . . 146

A Linelists and equivalent widths 148

REFERENCES **230**

Abstract

Chemical composition of metal-poor stars are crucial to develop an understanding of the nature of the earliest stars formed in the universe, the nucleosynthesis events associated with them, as well as, to redefine the models of galaxy formation. Elements heavier than the iron peak are made via two principal processes: the rapid neutron-capture process (r-process) and the slow neutron-capture process (s-process). Insight into the astrophysical sites and the production mechanisms of neutron-capture elements can be obtained by studying chemical composition of stars that exhibit large enhancement of neutron-capture elements such as the Carbon-Enhanced Metal-Poor (CEMP) stars. Among the CEMP stars, CEMP-s stars exhibit the presence of strongly enhanced s-process elements and CEMP-r stars are with strong enhancement of r-process elements. A number of CEMP stars are also known to exhibit enhancement of both r- and s-process elements, the CEMP-r/s stars (Hill et al. 2000, Goswami et al. 2006, Jonsell et al. 2006 etc.). Till now, the upper limit in the metallicity of stars showing double enhancement is [Fe/H] $\leq$ -2 (HE 1305+0007 with [Fe/H] = -2.0, (Goswami et al. 2006)). In spite of several efforts, a physical explanation for the observed double enhancement is still lacking (Qian & Wasserburg 2003; Wanajo et al. 2006). A few CEMP stars are known that show no enhancement of neutron-capture elements, the CEMP-no stars.

Identification of an explicit stellar site for s-process nucleosynthesis started with the works of Weigert (1966) and Schwarzschild & Härm (1967) on the thermal pulse calculations. Slow neutron-capture elements are now believed to be produced due to partial mixing of protons into the radiative C-rich layers during thermal pulses that initiate the chain of reactions $^{12}C(p,\gamma)\ ^{13}N(\beta)\ ^{13}C(\alpha,n)^{16}O$ in a narrow mass region of the He intershell during the inter-pulse phases of a low-mass AGB stars. Rapid neutron-capture process elements are thought to be produced during SN explosions or accretion induced collapse.

High resolution spectroscopic analyses of CEMP stars have established that the largest group of CEMP stars are s-process rich (CEMP-s) stars and accounts for about 80 per cent of all CEMP stars (Aoki et al. 2007). Chemical composition studies of CEMP stars (Barbuy et al. 2005; Norris et al. 1997a,b, 2002; Aoki et al. 2001, 2002; Goswami et al. 2006, 2010a) also have suggested that a variety of production mechanisms are needed to explain the observed range of elemental abundance patterns in them; however, the binary scenario of CH star formation is currently considered as the most likely formation mechanism also for CEMP-s stars. This idea has gained further support with the demonstration by Lucatello et al. (2005), that the fraction of CEMP-s stars with detected radial velocity

variations is consistent with the hypothesis of all being members of binary systems.

CH stars characterized by iron deficiency, enhanced carbon and s-process elements are known to be post-mass-transfer binaries (McClure & Woodsworth 1990) in which the companion (primary) has evolved to white dwarf passing through an AGB stage of evolution. The chemical composition of CH stars (secondaries) bear the signature of the nucleosynthesis processes occurring in the companion AGB stars due to mass transfer. Roche-Lobe Overflow (RLOF) and wind accretion are among the suggested mass transfer mechanisms. Recent hydrodynamical simulations have shown in the case of the slow and dense winds, typical of AGB stars, that efficient wind mass transfer is possible through a mechanism called Wind Roche-Lobe Overflow (WRLOF) Mohamed & Podsiadlowski 2007; Abate et al. 2013. CH stars (secondaries) thus form ideal targets for studying the operation of s-process occurring in AGB stars. Chemical abundances of key elements such as Ba, Eu etc. and their abundance ratios could provide insight in this regard. In our studies along this line we have considered a sample of eighty nine faint high latitude carbon stars from the Hamburg/ESO survey (Christlieb et al. 2001) and based on medium resolution spectroscopy found about 33% of the objects to be potential CH star candidates (Chapter 3). Inspite of their usefulness, literature survey shows that detailed chemical composition studies of many of the objects belonging to the CH star catalogue of Bartkevicius (1996) are currently not available. A few studies that exist are either limited by resolution or the wavelength range. The CH star catalogue of Bartkevicius (1996) lists about 261 objects, 17 of which belong to ω Cen globular cluster. Many of the objects listed in this catalogue have no information on binary status. It is worthwhile to compare and examine the abundance patterns of elements observed in the confirmed binaries with their counterparts in objects that have no information on binary status. While long-term radial velocity monitoring are expected to throw light on the binary status, detailed chemical composition studies could also reflect on the binary origin. We have therefore undertaken to carry out chemical composition studies for a selected sample of CH stars from this catalogue using high resolution spectra. Towards this end, we have considered twenty two objects from the catalogue of Bartkevicius (1996) for a detailed chemical composition study (Chapter 4 and Chapter 5). Detailed high resolution spectroscopic analyses for this sample of objects are either not available in the literature or limited by resolution or wavelength range. The sample includes five confirmed binaries, six objects that are known to show radial velocity variability, and for the rest eleven objects, none of these two information is available. In the following text, for convenience, we will refer the objects that are confirmed binaries as group I objects, those with limited

radial velocity information as group II objects and the objects for which none of these information are available as group III objects. One of our primary objectives is to estimate the abundances of heavy elements in all the stars of these three groups of objects and critically examine the abundance patterns and abundance ratios if they exhibit characteristic abundance patterns of CH stars.

Polarimetric studies of carbon stars by Goswami & Karinkuzhi (2013) include six objects from this sample. Among these, three objects show percentage V-band polarization at a level $\sim 0.2\%$ (HD 55496 ($p_v\% \sim 0.18$), HD 111721 ($p_v\% \sim 0.22$, and HD 164922 ($p_v\% \sim 0.28$)) indicating presence of circumstellar dust distribution in non-spherically symmetric envelopes. The other three objects, HD 92545, HD 107574 and HD 126681, show V-band percentage polarization at a level $< 0.1\%$.

Among CEMP stars, the group of CEMP-r/s stars show enhancement of both r- and s-process elements ($0 <$ [Ba/Eu] < 0.5, (Beers & Christlieb 2005)). [Ba/Eu] ratio for our programme stars are not falling in this range. The two neutron-capture processes, the s-process and the r-process require entirely different astrophysical environments, different time-scales and neutron flux for their occurrence. While slow neutron-capture elements are believed to be produced in the inter pulse phases of low mass AGB stars, the rapid neutron-capture process requires very high temperatures and neutron flux and are expected to be produced during supernova explosions. To understand the contribution of these two processes to the chemical abundance of the neutron-capture elements we have conducted a parametric model based study. Our study indicates seven objects in our sample to have abundances of heavy elements with major contributions coming from the s-process.

The primary objectives of this study are:

• Determination of chemical compositions of a selected sample of metal-poor objects with special emphasis on the production and distribution of carbon and neutron-capture elements.

• To determine the contribution of s- and r-process to the elemental abundances in the framework of a parametric model and hence the origin of neutron-capture elements.

• To complement our spectroscopic studies with photometric as well as other studies available in literature.

List of Publications

- **Refereed Journals**

  Drisya Karinkuzhi, Aruna Goswami
  Chemical analysis of CH stars II: atmospheric parameters and elemental abundances , 2015, MNRAS, 446, 2348

  Drisya Karinkuzhi, Aruna Goswami
  Chemical analysis of CH stars I: atmospheric parameters and elemental abundances , 2014, MNRAS, 440, 1095

  Aruna Goswami, Drisya Karinkuzhi
  Polarimetric studies of carbon stars at high Galactic latitude , 2013, A&A, 549, 68

  Aruna Goswami, Drisya Karinkuzhi, N. S. Shanti Kumar
  HE 1015-2050: Discovery of a hydrogen-deficient carbon star at high Galactic latitude , 2010, ApJL, 723, L238

  Aruna Goswami, Drisya Karinkuzhi, N. S. Shanti Kumar
  The CH fraction of carbon stars at high Galactic latitudes , 2010, MNRAS, 402, 1111

- **Conference proceedings**

  Drisya Karinkuzhi, Aruna Goswami
  Understanding AGB nucleosynthesis from the chemical analysis studies of CH stars , (Submitted to ASP proceedings)

  Drisya Karinkuzhi, Aruna Goswami
  High resolution spectroscopic study of CH stars , ASIC, 2013, 9Q, 124

  Aruna Goswami, Drisya Karinkuzhi
  Neutron-Capture nucleosynthesis in HdC stars: the case of HE1015-2050 , ASInC, 2013, 9, 112

Aruna Goswami, Drisya Karinkuzhi, P. Subramania Athiray
Elemental abundances in CEMP stars: r- and s- process elements , 2010, rast.conf, page 211 -216

LIST OF FIGURES

1.1 H-R diagram 17
1.2 Schematic evolution in the H-R diagram of a 1 M⊙ stellar model and solar metallicity. All of the major evolutionary phases discussed in the section 1.2 are indicated (Busso et al. 1999). 18
1.3 Same as in Figure 1.2, for a 5 M⊙ stellar model and solar metallicity (Busso et al. 1999). 18
1.4 Schematic structure of an AGB star (Karakas 2010) 19
1.5 [C/Fe] versus [Fe/H] for a literature sample (open squares) including the metal-poor stars (solid circles) from Beers et al. (1992). Figure is from Rossi et al. (1999) 23
1.6 s-process peaks (Karakas 2010) 25
1.7 [Ba/Fe] versus [Eu/Fe] for the different group of CEMP classes mentioned in Table 1.1, where low-s stars are defined as CEMP stars with [Ba/Fe] < 1.0 and [Ba/Eu] > 0.0. Tiny black dots and tiny red triangles indicate Classical Ba stars and black crosses represents CEMP-no stars. Other classes are marked in the figure itself. Figure is taken from Masseron et al. (2010). 27
1.8 A contour plot of the effective potential due to gravity and the centrifugal force of a two-body system in a rotating frame of reference. The arrows indicate the gradients of the potential around the five Lagrange points. (http://pages.uoregon.edu) 31
1.9 Roche-lobe overflow. (http://www.daviddarling.info/encyclopedia/R/Roche-lobe.html) 32

2.1 schematic of an astronomical spectrograph incorporating a transmission grating (http://www.vikdhillon.staff.shef.ac.uk/teaching) 37
2.2 Equivalent width (W) of an absorption line is the total area inside the absorption line, if we create a rectangular box of the same area, extending from the continuum to the 0 flux line, the width of this box is the equivalent width. This measurement is used to describe the strength of the line (the higher the value, the stronger the line)(http://www.bdnyc.org/2012/03/02) 44

3.1 A two colour J−H versus H−K diagram of the candidate CH stars. The thick box on the lower left represents the location of CH stars and the thin box on the upper right represents the location of C−N stars (Totten et al. 2000). Majority of the candidate CH stars listed in Table 3.3 (represented by open circles) fall well within the CH box. The positions of the two outliers are shown with open squares. C−N stars found in our sample are represented by solid triangles. The location of the comparison stars are labeled and marked with solid squares. Location of the three dwarf carbon stars are indicated by open triangles. 72
3.2 The spectra of the comparison stars in the wavelength region 3860 – 6800 Å. Prominent features seen on the spectra are indicated. 73
3.3 An example of each of the HE stars corresponding to the comparison stars presented in Figure 3.2, in the top to bottom sequence, in the wavelength region 3860 – 6800 Å. The locations of the prominent features seen in the spectra are marked on the figure. 74
3.4 A comparison of the spectra of three HE stars in the wavelength region 3870 – 5400 Å with the spectrum of the comparison star HD 26. Prominent features noticed in the spectra are marked on the figure. 75
3.5 A comparison of the spectra of three HE stars in the wavelength region 3870 – 5400 Å with the spectrum of the comparison star HD 209621. Prominent features noticed in the spectra are marked on the figure. 78
3.6 A comparison of the spectra of three HE stars in the wavelength region 3880 – 5400 Å with the spectrum of the comparison star HD 5223. Prominent features noticed in the spectra are marked on the figure. 82
3.7 The spectra of three dwarf carbon stars in the wavelength region 4500 – 6800 Å. Prominent features noticed in the spectra are marked on the figure. 83
3.8 A comparison of the spectra of the candidate C−N stars with the spectrum of V460 Cyg in the wavelength region 4500 – 6800 Å. The bandheads of the prominent molecular bands, Na I D and H_α are marked on the figure. 86
3.9 Spectra for the CH stars from the catalogue of Bartkevicius (1996) 87
3.10 Same as Figure 3.9 88

4.1 Sample spectra of a few programme stars in the wavelength region 5161 to 5190 Å 93
4.2 Spectra showing the wavelength region 6481 to 6510 Å, for the same stars as in Figure 4.1. 94
4.3 The location of HD 125079, HD 216219, HD 4395 and HD 5395 are indicated in the H-R diagram. The masses are derived using the evolutionary tracks of Girardi et al. (2000). The evolutionary tracks for masses 1, 1.1, 1.2, 1.3 1.4, 1.5, 1.6 1.7, 1.8, 1.9 and 1.95 $M_\odot$ from bottom to top are shown in the Figure. 99
4.4 Same as Figure 4.3, but for objects HD 81192, HD 16458, HD 201626 and HD 48565. 100

4.5 The location of HD 188650, and HD 214714 are indicated in the H-R diagram. The evolutionary tracks of Girardi et al. (2000) are shown for masses 2, 2.2, 2.5, 3.0, 3.5, 4.0 and 4.5 $M_\odot$ from bottom to top. 100
4.6 Same as figure 4.3, but for the objects HD 92545, HD 167768, HD 111721 and HD 55496. 101
4.7 The location of HD 148897, HD 204613, HD 107574 and HD 104979 are indicated in the H-R diagram. The masses are derived using the evolutionary tracks of Girardi et al. (2000). The evolutionary tracks are shown for masses 0.6, 0.7, 0.8, 0.9, 1.0, 1.1, 1.2, 1.3 1.4, 1.5, 1.6 1.7, 1.8, 1.9 and 1.95 $M_\odot$ from bottom to top. 101

5.1 The iron abundances of stars are shown for individual Fe I and Fe II lines as a function of excitation potential. The solid circles indicate Fe I lines and solid triangles indicate Fe II lines. 107
5.2 The iron abundances of stars are shown for individual Fe I and Fe II lines as a function of equivalent width. The solid circles indicate Fe I lines and solid triangles indicate Fe II lines. 107
5.3 Spectral-synthesis fits of Sc II line at 6245.637 Å. The dotted lines indicate the synthesized spectra and the solid lines indicate the observed line profiles. Two alternative synthetic spectra for [X/Fe] = +0.3 (long-dashed line) and [X/Fe] = −0.3 (short-dashed line) are shown to demonstrate the sensitivity of the line strength to the abundances. 112
5.4 Spectral-synthesis fits of Ba II line at 5853.67 Å. The dotted lines indicate the synthesized spectra and the solid lines indicate the observed line profiles. Two alternative synthetic spectra for [X/Fe] = +0.3 (long-dashed line) and [X/Fe] = −0.3 (short-dashed line) are shown to demonstrate the sensitivity of the line strength to the abundances. 116
5.5 Spectral-synthesis fits of La II line at 4921.78 Å. The dotted lines indicate the synthesized spectra and the solid lines indicate the observed line profiles. Two alternative synthetic spectra for [X/Fe] = +0.3 (long-dashed line) and [X/Fe] = −0.3 (short-dashed line) are shown to demonstrate the sensitivity of the line strength to the abundances. 117
5.6 Solid curve represent the best fit for the parametric model function $\log\epsilon = A_s N_{si} + A_r N_{ri}$, where N_{si} and N_{ri} represent the abundances due to s- and r-process respectively (Arlandini et al. (1999), Stellar model, scaled to the metallicity of the star). The points with errorbars indicate the observed abundances in HD 16458. 134
5.7 Same as Figure 5.6, but for HD 48565. 135
5.8 Same as Figure 5.6, but for HD 92545. 135
5.9 Same as Figure 5.6, but for HD 104979. 136
5.10 Same as Figure 5.6, but for HD 107574 136
5.11 Same as Figure 5.6, but for HD 125079. 137
5.12 Same as Figure 5.6, but for HD 204613. 137
5.13 Same as Figure 5.6, but for HD 216219. 138

5.14 Abundance ratios of heavy elements observed in the program stars with respect to [Fe/H]. The confirmed binaries are shown with solid circles, the objects with limited radial velocity information are shown with open circles, and the rest of the objects are indicated with solid triangles. The abundance ratios show a large scatter with respect to metallicity. 142
5.15 Same as figure 5.14. But the estimated abundance ratios of Ba, La, Ce and Eu with respect to Fe plotted in this figure are compared with the abundance ratios observed in CEMP stars (solid pentagons) from Masseron et al. (2010) and Ba stars (solid squares) from Allen & Barbuy (2006a). . 143

LIST OF TABLES

1.1 Definition of sub-classes of CEMP stars 26

3.1 HE stars with prominent C_2 molecular bands observed during 2007 − 2009 54
3.2 HE stars without prominent C_2 molecular bands observed during 2007 − 2009 58
3.3 Potential CH star candidates 59
3.4 Estimated effective temperatures from semi empirical relations, T_{eff} from (J−H), (V−K) and (B−V) for metallicity −0.5, −1.0, −1.5, −2.0, −2.5 from top to bottom 61

4.1 Basic data for the programme stars 95
4.2 Radial velocities for the programme stars 96
4.3 Photometric temperatures of the programme stars 97
4.4 Stellar masses 102

5.1 Derived atmospheric parameters and carbon isotopic ratios for the programme stars 108
5.2 Elemental abundance ratios: Light elements 113
5.3 Elemental abundance ratios : Heavy elements 119
5.4 [ls/Fe], [hs/Fe] and [hs/ls] for the programme stars 121
5.5 Atmospheric parameters from literature 126
5.6 Literature values of heavy element abundances 130
5.7 Best fit coefficients and reduced chi-square values 134

A.1 Fe lines used for deriving atmospheric parameters for HD 4395, HD 5395, HD 16458, HD 48565, HD 81192, HD 125079, HD 188650 , HD 201626, HD 214714 and HD 216219 149
A.2 Fe lines used for deriving atmospheric parameters for HD 55496, HD 92545, HD 89668, HD 104979, HD 107574, HD 111721 160
A.3 Fe lines used for deriving atmospheric parameters for HD 122202, HD 126681, HD 148897, HD 164922, HD 167768, HD 204613 171
A.4 Lines used for the calculation of elemental abundances for HD 4395, HD 5395, HD 16458, HD 48565, HD 81192, HD 125079, HD 188650 , HD 201626, HD 214714 and HD 216219 182
A.5 Lines used for the calculation of elemental abundances for HD 55496, HD 89668, HD 92545, HD 104979, HD 107574, HD 111721 196

A.6 Lines used for the calculation of elemental abundances for HD 122202, HD 126681, HD 148897, HD 164922, HD 167768, HD 204613 210
A.7 Elemental abundances: Light elements C, Na, Mg, Ca and Ti 224
A.8 Elemental abundances: Light elements V, Cr, Mn, Co, Ni and Zn 226
A.9 Elemental abundances : Heavy elements 228

CHAPTER 1

INTRODUCTION

1.1 Carbon-Enhanced Metal-Poor (CEMP) stars

Carbon stars are an important class of chemically peculiar stars; a large fraction of them show enhancement of carbon and heavy elements. They are known to populate the halo of the Galaxy (Wallerstein & Knapp 1998; Evans 2010). In the past 20 years, abundance studies using solid state detectors and echelle spectrograph revealed a wealth of new information about these objects leading to an understanding of their role in the much more complicated and multifaceted picture of stellar evolution. This in turn helps us to constrain the formation and evolution of the Galaxy. An interesting phenomenon is that the number of stars showing carbon enhancement increases with decreasing metallicity (Norris et al. 1997a; Rossi et al. 1999). The objects that show enhancement of carbon and metallicity ([Fe/H]) [*] ≤ -1 are called Carbon-Enhanced Metal-Poor (CEMP) stars. They are found in different evolutionary states and include Asymptotic Giant Branch (AGB) stars, giant stars, subgiant stars and also dwarf carbon stars. Since carbon plays an important role in the post main-sequence evolution of the stars it is important to study these objects in detail for understanding the origin of carbon and heavy elements. CEMP stars may also be considered as a fossil record' of the early Universe. However, most of these stars are faint and rare and thus the number of these stars for which detailed chemical abundances have been measured is small. The surface chemical composition of a star can be altered by different mechanisms which include internal nucleosynthesis and the mixing of these materials to the stellar surface, mass transfer in a binary system and compositional differences in the gas from which they form. The detailed chemical

[*] $[Fe/H] = log_{10}(\frac{N_{Fe}}{N_H})_* - log_{10}(\frac{N_{Fe}}{N_H})_\odot$, where N_{Fe} and N_H are number densities of iron and hydrogen atoms respectively.

analysis of stars help to understand the origin of these elemental abundance patterns in them. CEMP stars in the Galactic halo have been known as CH stars (Keenan 1942). They are metal-deficient high velocity carbon stars with enhanced abundances of the neutron-capture elements and are called classical CH stars. These stars are generally divided into two groups; intrinsic and extrinsic. In intrinsic carbon stars, carbon enrichment results from a deep mixing process that pollute the envelop with carbon produced by internal nucleosynthesis. In case of extrinsic carbon stars, carbon enrichment results from transfer of carbon rich material in a binary system. The main goal of this thesis is to conduct detailed chemical composition study of a large sample of CEMP stars including CH stars to understand the nucleosynthetic origin of the observed abundance patterns.

1.2 Stellar evolution and Nucleosynthetic processes leading to a carbon star

Before going to the discussion on carbon stars it is necessary to understand the evolutionary stages and nucleosynthetic processes a star passes through to become a carbon star. Many review articles are available in literature with detailed discussions on the evolution and nucleosynthesis taking place at different evolutionary states of low and high-mass stars to AGB stage (Iben 1991; Busso et al. 1999; Karakas 2010); here we briefly discuss the same that is relevent to our proposed work. Properties of stars are generally discussed on the basis of its position in the Hertzsprung-Russel (H-R) diagram. Most of the stars when plotted in H-R diagram (Figure 1.1) are found to be in a diagonal line called main-sequence, where the hydrogen is burning to form helium, producing the necessary energy to maintain a stable equilibrium. This hydrogen burning takes place, depending on the mass of the stars, either by proton-proton chain ($M \leq 2M_{\odot}$) or by CNO cycle ($M \geq 2M_{\odot}$). Most of the stars spend about 90 per cent of the lifetime in main-sequence. When the star uses up the core hydrogen the post main-sequence evolution starts that depends entirely on the star's mass. For the low-mass stars, after the hydrogen has been exhausted the core must contract to balance the deficit of energy since there is no energy generation in the core. Due to the contraction, core heats itself as well as the layers just above it. Hence the temperature increases making the hydrogen to burn in a shell just outside the hydrogen exhausted core. The energy produced in the core is not enough to burn the helium. The core continues to contract. To balance the increase in surface gravity at the border of the core the pressure has to increase either by increasing the density or by increasing the temperature. Due to this increase star expands and there by increasing the total radius R.

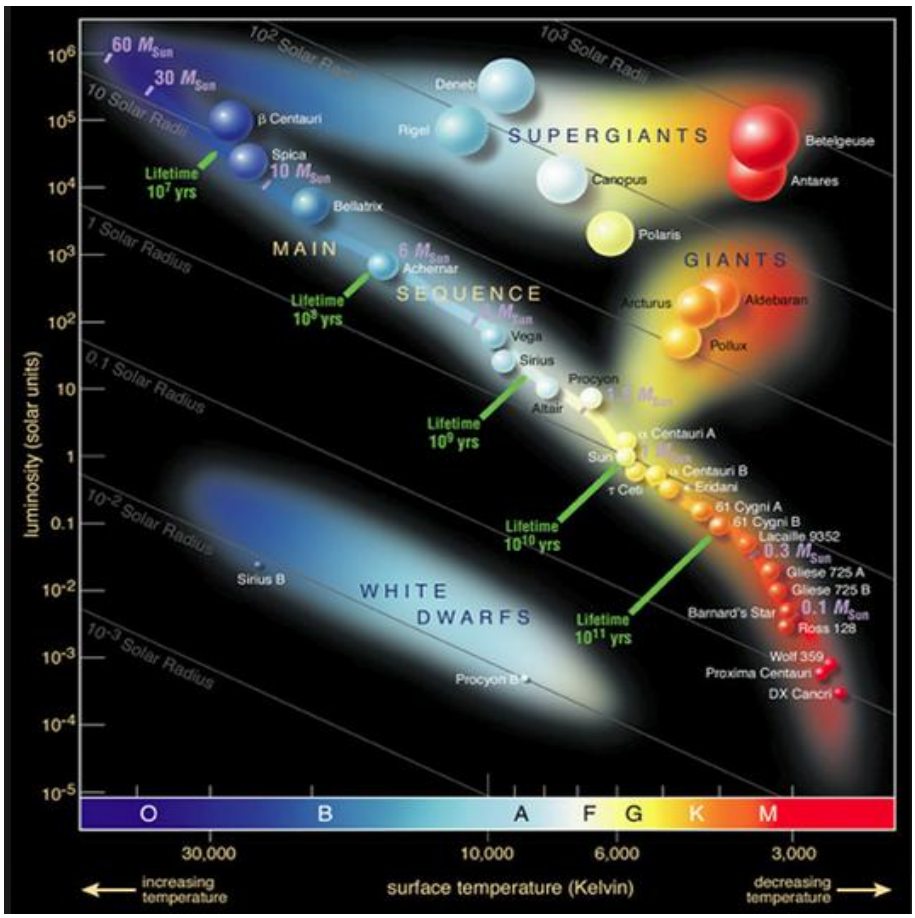

Figure 1.1: H-R diagram

The luminosity has to be constant thus effective temperature decreases according to the relation

$$L = 4\pi R^2 \sigma T^4$$

This immediate post main-sequence evolution of the star therefore moves the stars position more or less horizontally to the right in the H-R diagram turning the star into a subgiant. As the star expands the effective temperature cannot fall below a particular value. This temperature barrier causes the evolutionary track of the low-mass stars to move vertically upwards turning the subgiant into a red giant star. At this stage the entire envelop becomes convective. As the star expands, the convective layer penetrates into the regions which has already experienced partial CN processing during main sequence evolution and this dredges up the material into the surface which in turn changes the surface chemical composition of the star. This is called the First Dredge-Up (FDU) and is marked in Figures 1.2 and 1.3.

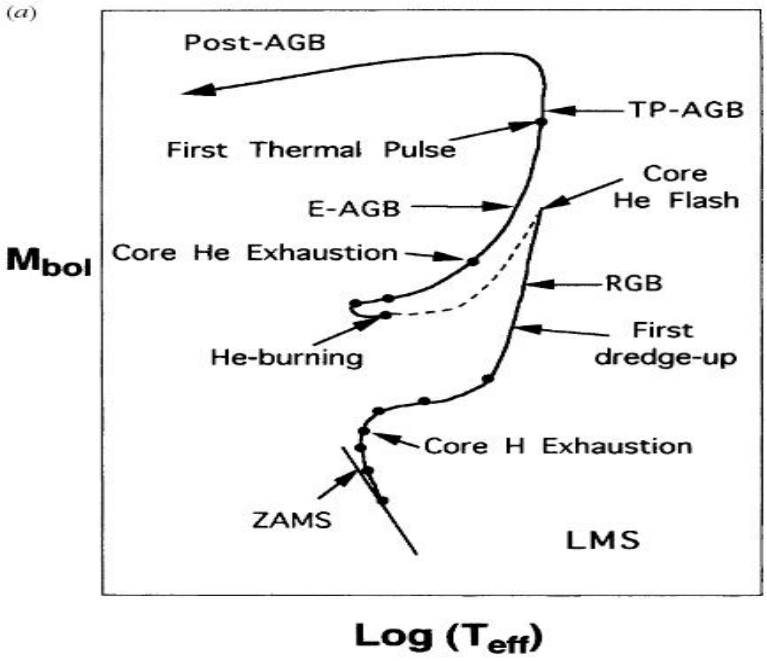

Figure 1.2: Schematic evolution in the H-R diagram of a 1 M⊙ stellar model and solar metallicity. All of the major evolutionary phases discussed in the section 1.2 are indicated (Busso et al. 1999).

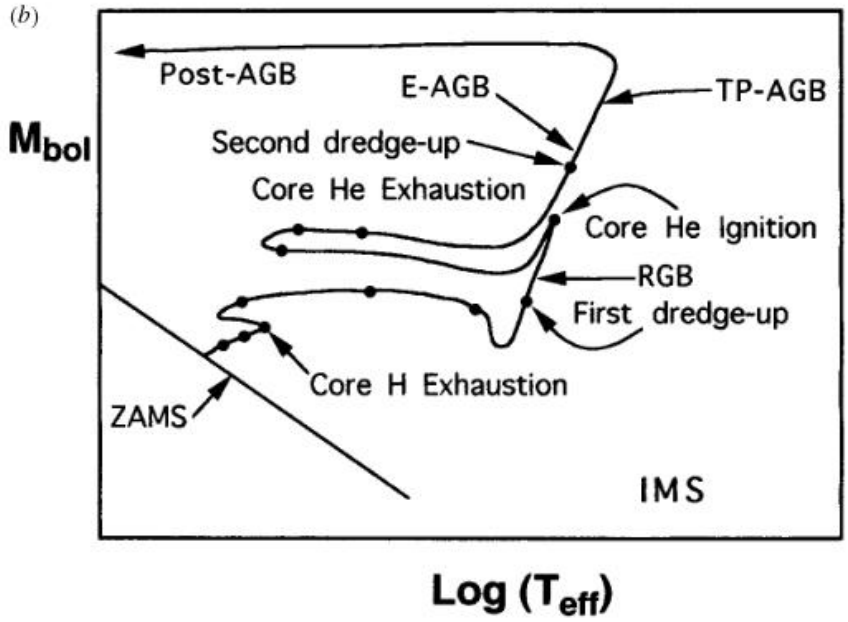

Figure 1.3: Same as in Figure 1.2, for a 5 M⊙ stellar model and solar metallicity (Busso et al. 1999).

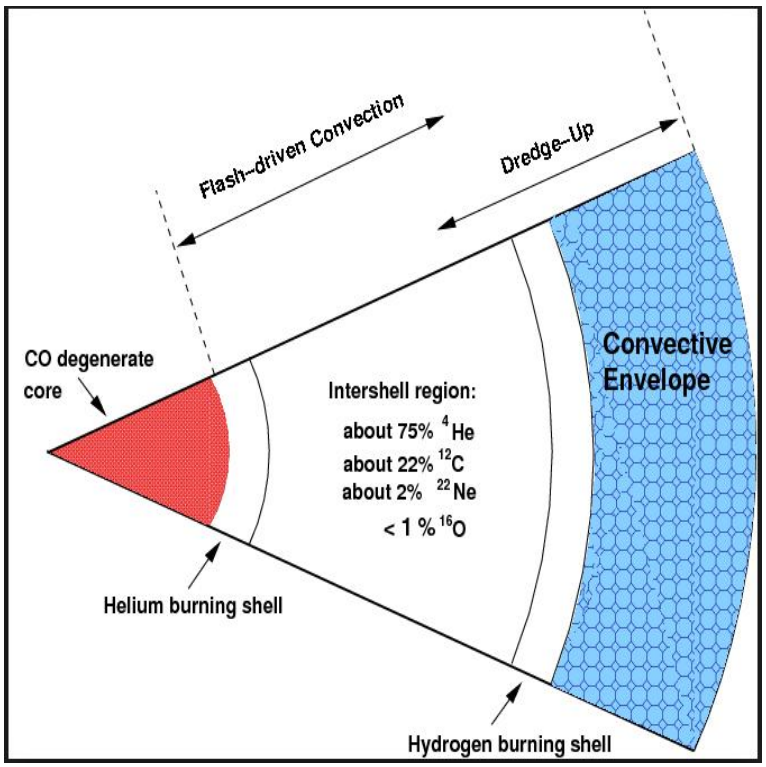

Figure 1.4: Schematic structure of an AGB star (Karakas 2010)

The core continues to contract which makes the free electrons in the core tightly packed and they became degenerate. Due to the very large border gravity associated at this stage, the hydrogen burning in the shell becomes furious making the star to move to the tip of red-giant branch. At this stage temperature of the core reaches 10^8 K which is enough to burn helium into carbon via triple alpha process.

Since the helium burning occurs at the degeneracy conditions, a slight increase in temperature causes an increase in pressure. Hence, the increase in core temperature lead to overproduction of nuclear energy without compensating the pressure increase and expansion. This helium burning occurs in a star as a thermal flash which occurs in some intervals. This causes the removal of the degeneracy in the shell. After the helium flash is completed the core contains ordinary helium plasma fusing helium into carbon and surrounded by a hydrogen burning shell. This state is called Horizontal Branch (HB) and also called as the helium main-sequence.

When the helium in the core of the horizontal branch star is exhausted, the core must contract similar to the case of hydrogen exhaustion in a main-sequence star. At this stage helium ignites in a shell outside the core and hydrogen burns in a shell above the helium burning shell. This double shell burning stage is called AGB stage (Figure 1.4). The

luminosity of the star increases very high at this stage. The core continues to contract making the free electrons degenerate and the envelop becomes convective. If the star is not very massive, its core temperature never gets hot enough for carbon to burn. At this stage the convective envelop penetrate through hydrogen burning shell transferring the products of helium burning material to the surface. This process is called Third Dredge Up (TDU). After the TDU we could find the carbon at the stellar photosphere and the C/O ratio of the object slowly increases. After many TDU episodes the star becomes a carbon star with C/O ratio greater than unity.

1.3 Intrinsic properties of carbon stars

A carbon star is a late type giant with strong bands of carbon compounds and no metallic oxide bands. Thus very intense bands of CH, CN, C_2 are visible. The interstellar medium is oxygen rich so the overwhelming majority of stars are formed with C/O ratio < 1. In case of carbon stars C/O ratio is found to be ≥ 1. The luminosity of the nearby carbon stars can be found from the Hipparcos parallax measurements and the values are found to be comparable with the luminosity values for giants. The masses of the carbon stars are generally observed between 1 - 3 $M_{\odot}$ (Wallerstein & Knapp 1998)

1.3.1 Spectral classification of carbon stars

Secchi (1868) classified the carbon stars as a group for the first time in his R−N system according to some spectral criteria, in which stars with relatively week C_2 and CN bands are put in the subclass from $R_0 - R_3$ and the stars with strong C_2 and CN bands are put in the classes $R_5 - R_8$. The stars in the R groups have well defined continuum at least down to 3900 Å. For the stars in the N class, even though they are showing strong carbon bands, continuum is very week in the regions below 4000 Å. Later Shane (1928) also did a detailed study on these R and N group stars. They revealed that temperature variations among these groups are very less and the branching is caused by the abundance variations in C and O. The modern system of classification of carbon stars was established by Keenan (1993), who subdivided them into three sequences C−R, C−N and CH corresponding to the old RN and CH star classifications. To indicate the temperature sequence, Keenan used the numerals from 1 - 9 e.g. from C−N1 to C−N9. Keenan described the spectra with the strengths of the C_2, CN and Merrill-Sanford bands as well as the $^{12}C/^{13}C$ ratio and the Li line strength. Wallerstein & Knapp (1998) had given a detailed description of their spectral characteristics. The next section describes the important spectral

characteristics of different groups of carbon stars.

1.3.2 C−R stars

C−R stars are the warmest of carbon stars. For them the blue part of the spectrum have appreciable flux and can be used for analysis. They have carbon rich atmospheres similar to CH stars. C−R stars show $^{12}C/^{13}C$ ratio between 4 to 9. The s-process elements are nearly solar in C−R stars (Dominy 1984) and they are not observed to be in binary systems.

1.3.3 C−N stars

Among the carbon stars, C−N stars have lowest temperatures and strong molecular bands. The C−N stars are easily detected in infrared surveys from their characteristic infrared colors. The majority of C−N stars show $^{12}C/^{13}C$ ratio of more than 30, ranging to nearly 100. The C−N stars show a weakening continuum below 4300 Å; the reason for this is assumed to be scattering by particulate matter.

1.3.4 C−J stars

The group of C−J stars show a very high ^{13}C abundance with $^{12}C/^{13}C$ value ≤ 13 (Lambert et al. 1986). C−J stars are not intrinsic. Abia & Isern (2000) showed that C−J type stars are less evolved objects than other types of carbon stars. They constitute about 10 - 15 per cent of the carbon stars in both our Galaxy and Magellanic clouds. There are many studies devoted to the understanding of the origin of these peculiar type of carbon stars (Ohnaka et al. 2008; Izumiura et al. 2008).

1.3.5 CH stars

CH stars were first described as a class of warm carbon stars by Keenan (1942). They have equivalent spectral types of G and K giants but show weak metallic lines. But features due to CH, C_2 and s-process elements are enriched relative to normal giants. In addition to being metal-poor they show large radial velocities indicating that they are halo objects. All these stars have relatively low effective temperatures (4000−4750 K) and high carbon abundances. CH stars are generally found in Galactic halo. A few are observed in globular clusters also.

Subgiant-CH stars

Bond (1974) discovered a class of stars with the enhancement of carbon and s-process elements but with a luminosity which place them near or above the main sequence. These class of objects were named as subgiant-CH stars. Many studies (Luck & Bond 1982; Sneden 1983; Sneden et al. 1985; Smith & Lambert 1986; Smith et al. 1993) indicated that most of them are moderately metal-deficient with [Fe/H] = −0.1 to −0.8. The atmospheric parameters of subgiant-CH stars are found to be typical of F- and G-type main-sequence stars (Luck & Bond 1991). They also show enhancement of s-process elements similar to Barium stars. Moderate velocities of subgiant-CH stars indicated their old disk behaviour rather than the halo. These objects are generally considered as the progenitors of metal-deficient Ba stars. Similar to CH and Ba stars most subgiant-CH stars are also found in a binary system. Smith & Demarque (1980) first suggested the mass transfer mechanisms to explain the anomalous abundance behaviour of these objects. Later in 1996, McClure confirmed the binary nature of subgiant-CH stars with radial velocity variations.

1.3.6 CH-like stars

Yamashita (1975) had given a detailed description of a group of stars whose spectra show close resemblance to those of CH stars, but their radial velocities and proper motions show no indication of high velocity and named these objects as CH-like stars. These stars also show a close similarity with the spectra of Ba II stars with enhanced carbon features. The spectra of CH-like stars show enhanced features of carbon and heavy elements. Even though the carbon is enhanced in CH like stars, C_2 bands are weakly detected. But the $^{12}C/^{13}C$ ratio is found similar to CH stars.

1.4 Metal-poor stars and carbon-enhancements

Metal-poor stars (whose metal contents are less compared to sun) in the Galactic halo are population II objects which are formed from the ejecta of the more massive population III objects and they provide an evidence of the chemical nature of the early universe. For the same reason, they are considered as the 'fossil record' of the early universe. The chemical abundance patterns in these objects help us to understand the formation and evolution of the elements and associated nucleosynthetic processes. Although the frequency of the metal-poor stars in the halo is high, due to the difficulties in detection these stars are found to be extremely rare in the solar neighborhood, only about 0.1 per

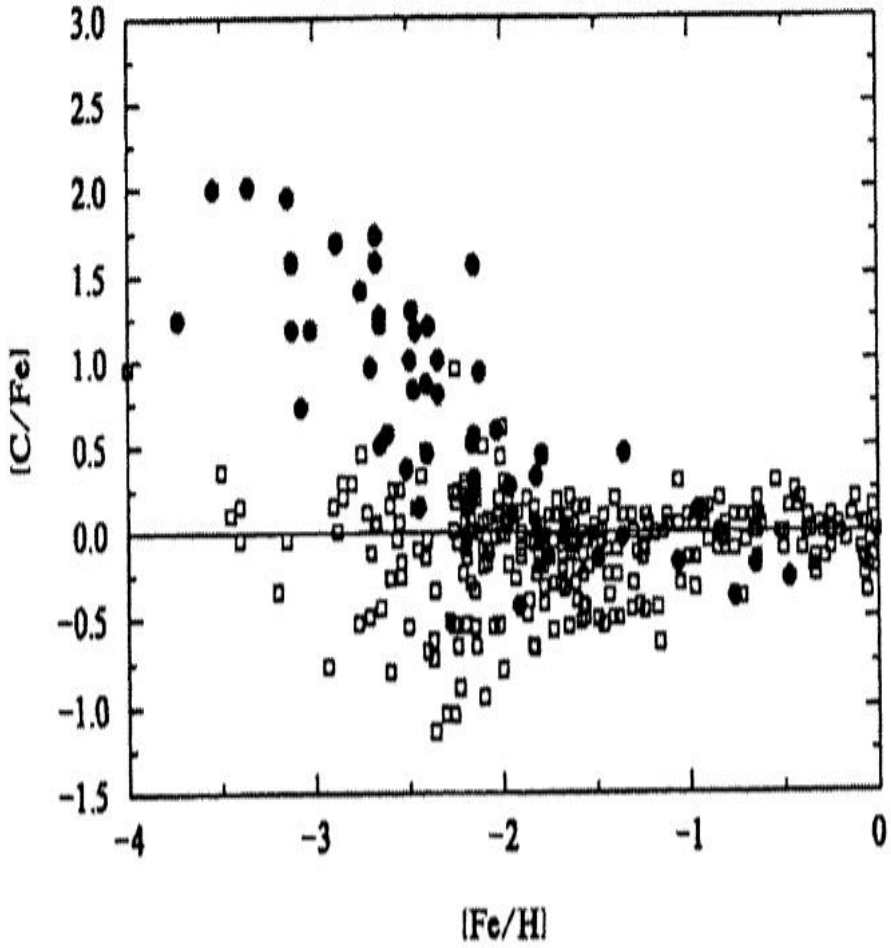

Figure 1.5: [C/Fe] versus [Fe/H] for a literature sample (open squares) including the metal-poor stars (solid circles) from Beers et al. (1992). Figure is from Rossi et al. (1999)

cent of stars within a kilo parsecs of the sun have [Fe/H] ≤ -2.0 . Despite the difficulty involved in finding the metal-poor stars much effort has been expended in search of them. Hamburg /ESO survey (Christlieb et al. 2001) and HK survey (Beers et al. 1992) are the two important ones among them. The most interesting results that came out from these surveys are, among the most metal-deficient stars there appears to be a high incidence of objects with enhanced carbon and neutron-capture elements (Rossi et al. 1999; Beers & Christlieb 2005; Frebel et al. 2006; Lucatello et al. 2006) called CEMP stars. The fraction of metal-poor stars that are also carbon-enhanced is much higher than the fraction of solar-metallicity stars exhibiting carbon enhancement. Approximately 20 per cent of metal-poor stars with [Fe/H] ≤ -2.0 are carbon-enhanced. The fraction increases with decreasing metallicity (Figure 1.5, Ref : Rossi et al. (1999)). This is further confirmed by different authors by the analysis of large number of metal-poor stars (Cohen et al.

2005; Lucatello et al. 2006). Frebel et al. (2006) show that the number of metal-poor stars increases with the distance from the Galactic plane. CEMP stars are not yet been understood fully and deserve more detailed analysis. As of now, two stars with [Fe/H] $\leq$ -5.0 called hyper metal-poor stars are detected (Christlieb et al. 2002; Frebel et al. 2005). The details about the origin and enhancement of the neutron-capture elements in CEMP stars are discussed in the next section.

1.4.1 Neutron-capture nucleosynthesis and production scenarios

With very high proton numbers, heavy elements with atomic numbers ≥ 56 inhibits the charged particle reactions (proton and α-capture) because of the electrostatic repulsion. Hence, the elements heavier than the iron peak are made through neutron addition on to the abundant Fe peak elements via two principal processes: the rapid neutron-capture process (r-process) and the slow neutron-capture process (s-process). The fundamental studies on these processes started with the work of Burbidge et al. (1957) (hereafter B^2FH). Production mechanisms of s- and r-process require not only two widely different astrophysical sites but also very different time scales and neutron flux. The s-process occurs at relatively low neutron densities ($N_n = 10^7 neutrons/cm^3$) and the time scale for neutron-capture by iron-seed elements for s-process is much longer than the time required for their β-decay. Hence the s-process produces elements along the valley of β-stability which include Sr, Y, Zr, Nb, Ba and La. Identification of an explicit stellar site for s-process nucleosynthesis started with the works of Weigert (1966) and Schwarzschild & Härm (1967) on the thermal pulse calculations. The free neutrons for the slow neutron-capture elements are produced mainly by two reactions,

$$^{12}C(p,\gamma)^{13}N(\beta)^{13}C(\alpha,n)^{16}O$$
$$^{14}N(\alpha,\gamma)^{18}F(\beta,\nu)^{18}O(\alpha,\gamma)^{22}Ne(\alpha,n)^{25}Mg$$

Since very high temperature is required for the operation of $^{22}Ne(\alpha,n)^{25}Mg$ reaction to occur, it is an efficient neutron source in massive AGB stars with initial masses $\geq 4\ M_\odot$. The main source of neutrons in the low-mass AGB stars is $^{13}C(\alpha,n)^{16}O$. The $^{13}C(\alpha,n)^{16}O$ reaction requires the operation of both proton and α-capture to occur in He shell, a region free of protons. During CNO cycle, there is some ^{13}C left over in the He intershell, which is not enough for the occurence of s-process in AGB stars (Gallino et al. 1998). Hence some mixing of protons from the convective envelop into the top layers of the He-intershell is required. The $^{13}C(\alpha,n)^{16}O$ reactions occur at low temperature T $\geq$ 90 $\times 10^6 K$, hence the ^{13}C burns under radiative conditions (Straniero et al. 1995). The s-

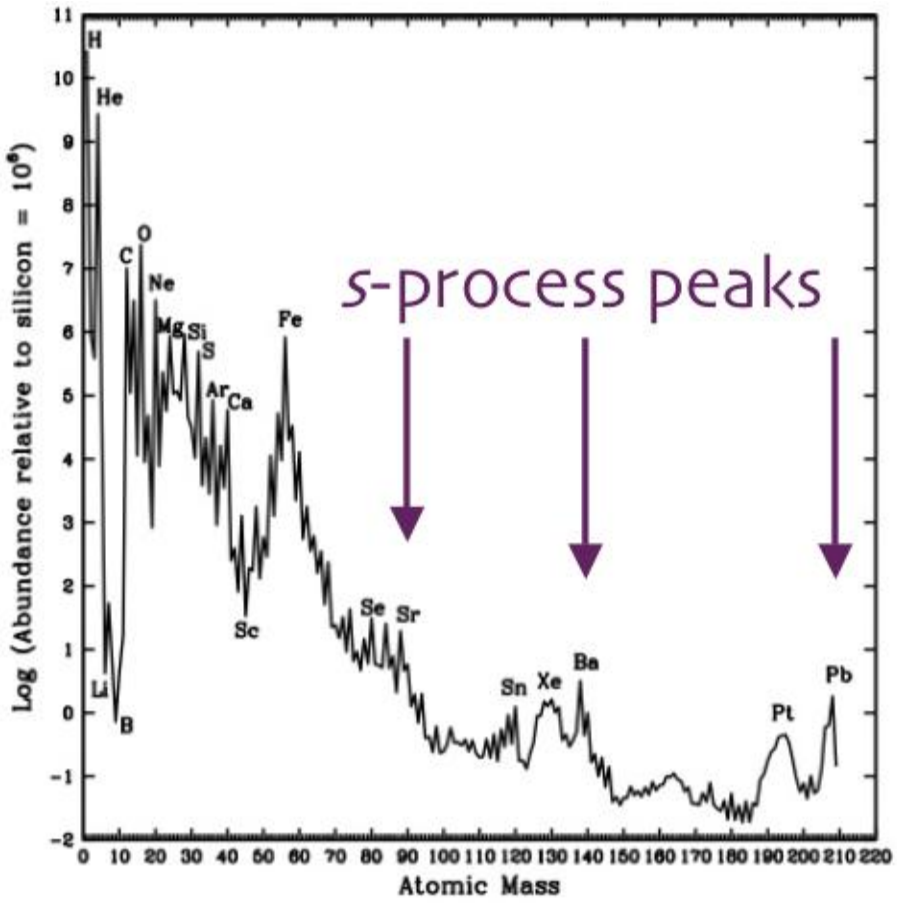

Figure 1.6: s-process peaks (Karakas 2010)

process occurs in the same layers where the ^{13}C was produced. The time scale for the neutron production during the interpulse are very long ($\geq 10^3 years$). This results a much lower neutron densities than the $^{22}Ne(\alpha, n)^{25}Mg$ reaction.

Clayton & Ward (1974) explained three components of s-process namely, weak, main and strong responsible for the production of heavy elements (see Figure 1.6 for different s-process peaks). The weak component of s-process is responsible for the production of elements with mass number upto 88. The main component is responsible for the production of elements with 88 ≤ A ≤208. The strong component of s-process is responsible for the production of 50 per cent of Pb^{208}. Busso et al. (1999) explained the various sites for the occurrence of these three components. The double shell burning phase of the AGB star is the preferred site for the main component of the s-process. While strong s-process occurs in very low metallicity AGB stars, the weak component occurs during He and C burning in massive stars with M ≥ 12 $M_\odot$. Prantzos et al. (1990) show that massive stars produce Zn to Zr.

For r-process a very high neutron density of the order of $10^{25} neutrons/cm^3$ is required and the time scale is much shorter than the β-decay time scale. Due to the extreme conditions required for the r-process, it is expected to occur during supernova explosions. The elements Eu, Er, Hf, Th etc are mainly produced by r-process.

Insight into the astrophysical sites and the production mechanisms of neutron-capture processes can be obtained by studying chemical composition of stars that exhibit large enhancement of neutron-capture elements.

1.4.2 CEMP- sub-groups and origin of abundance patterns

The initial classification of Beers & Christlieb (2005) defined CEMP stars as stars with [C/Fe] ratio ≥ 1.0. Later many authors (Ryan et al. 2005; Aoki et al. 2007; Carollo et al. 2012) revised this definition suggesting that a classification is possible even with a low value of [C/Fe] (i.e., [C/Fe] ≥ 0.5). CEMP stars are classified as CEMP-s stars which exhibit the presence of strongly enhanced s-process elements and CEMP-r stars that exhibit strong enhancement of r-process elements. CEMP stars that show enhancement of both r- and s-process elements are called CEMP r/s stars and CEMP stars that does not show enhancement of any neutron-capture elements are called CEMP-no stars. Taking Ba as the representative s-process element and Eu, the r-process element, Beers & Christlieb (2005) have given the classification criteria for these objects as given in Table 1.1. The trend of [Ba/Fe] values with respect to [Eu/Fe] for a large number of stars in dif-

Table 1.1: Definition of sub-classes of CEMP stars

Neutron-capture-rich stars	
r-I	0.3 ≤ [Eu/Fe] ≤ +1.0 and [Ba/Eu] ≤ 0
r-II	[Eu/Fe]≥ 1.0 and [Ba/Eu] ≤ 0
s	[Ba/Fe] ≥ 1.0 and [Ba/Eu] ≥ 0.5
r/s	0.0 ≤ [Ba/Eu] ≤ +0.5
Carbon-enhanced metal-poor stars	
CEMP	[C/Fe] ≥ +1.0
CEMP-r	[C/Fe] ≥ +1.0 and [Eu/Fe] ≥ +1.0
CEMP-s	[C/Fe] ≥ +1.0, [Ba/Fe] ≥ +1.0, and [Ba/Eu] ≥ +0.5
CEMP-r/s	[C/Fe] ≥ +1.0 and 0.0≤ [Ba/Eu] ≤ +0.5
CEMP-no	[C/Fe] ≥+1.0 and [Ba/Fe]≤ 0

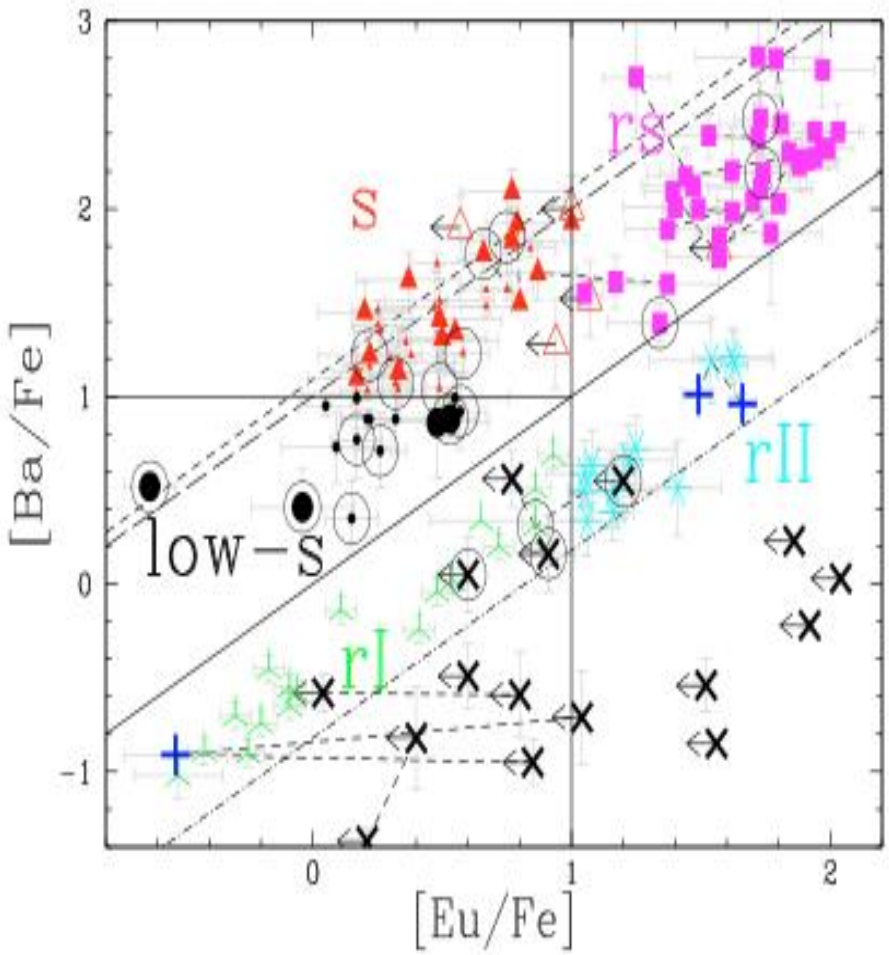

Figure 1.7: [Ba/Fe] versus [Eu/Fe] for the different group of CEMP classes mentioned in Table 1.1, where low-s stars are defined as CEMP stars with [Ba/Fe] < 1.0 and [Ba/Eu] > 0.0. Tiny black dots and tiny red triangles indicate Classical Ba stars and black crosses represents CEMP-no stars. Other classes are marked in the figure itself. Figure is taken from Masseron et al. (2010).

ferent CEMP- sub-groups are shown in Figure 1.7 (Masseron et al. 2010). The peculiar abundance patterns in CEMP-s star can be attributed to the mass transfer from an AGB companion since most of them are identified as binaries (Lucatello et al. 2005). Jonsell et al. (2006) presented various hypotheses to explain the anomalous abundance patterns in CEMP-r/s stars. There have been many discussions in the literature regarding the origin of CEMP-s and r/s stars. Tsangarides (2005) noted the similarity in [Ba/Eu] values for a few CEMP-s stars with that of some CEMP-r/s stars. This observations made him suggest that progenitors of both these classes may be thermally pulsing AGB stars. In the case of CEMP-r stars many studies (Preston & Sneden 2001; Hansen et al. 2011) suggest

that r-process enhancement is not coupled with the presence of a binary companion and it must have originated in separate pollution events of the molecular clouds from which they are formed. CEMP-no stars are very difficult to explain and Masseron et al. (2010) showed that number of CEMP-no stars are more in low metallicity but the carbon abundance in these objects is found to be decreasing with the decrease in metallicity of these objects. This trend could not be explained by any of the present theoretical models.

1.5 Abundance trends with metallicity in CEMP stars

Detailed abundance analysis of a large sample of CEMP stars is required to understand the behaviour of abundances of both lighter (Z $\leq$ 30) and heavier (Z $\geq$ 56) elements with metallicity. McWilliam et al. (1995) analysed thirty three stars with metallicity between -4.0 and -2.0. They have found that the α-elements (Mg, Ca, Si and Ti) which are produced by α-capture during various burning stages of late stellar evolution, show an enhancement of $\sim$ 0.4 dex with Fe. Ivans et al. (2003) found a few objects with poor α-elements. The abundance ratios of Cr and Mn are found to be decreasing with metallicity. [Sc/Fe] and [Ni/Fe] are found to be solar even at very low metallicity ([Fe/H] = -4). Heavy elements show larger scatter compared to light elements at low metallicities. Aoki et al. (2007) analysed a group of CEMP stars and confirmed the scatter in the abundances of heavy elements at lower metallicities. Sr shows large scatter compared to other heavy elements. Ba has less but still significant scatter at lowest metallicities (Ryan et al. 1996). These authors also proposed that the chemical yield of the early interstellar medium is primarily due to the explosion energies of the first supernovae (Frebel 2008). Allen et al. (2012) also described the anomalous abundance patterns in CEMP stars. They could see an increasing trend of [Ba/Fe] with [C/Fe] for their programme stars. For α-elements the observed trend is found to be similar to McWilliam et al. (1995).

1.6 [hs/ls]: An indicator to s-process efficiency

The ratio of the abundances of the heavy s-process elements (Ba, La, Ce, Pr, Nd, Sm) to the abundances of the light s-process elements (Sr, Y, Zr) can be used as an indicator of s-process efficiency. [hs/ls] ratio is a function of neutron irradiation and neutron-exposure (Luck & Bond 1991). As the metallicity decreases the number of seed nuclei decreases and more number of neutrons/seed nuclei is available. That favours the production of heavy s-process elements, increasing the [hs/ls] ratio with decreasing metallicity (Luck

& Bond 1991; Vanture 1992c). The [hs/ls] values for the extrinsic stars are expected to be lower compared to intrinsic stars. For the intrinsic stars, both ratios increase with the number of TDUs, but the [hs/ls] ratio after a relatively few TDUs approaches an asymptotic value. In the case of the extrinsic stars, [ls/Fe] and [hs/Fe] ratios are dependent on the values of these ratios in the AGB envelope during mass transfer and on the degree of dilution occurring in the extrinsic star on receipt of the mass or subsequently (Busso et al. 2001). A list of [hs/ls] values for stars in different evolutionary states are available in Busso et al. (2001). As the mass transfer from an AGB star to the companion is not expected to change the [hs/ls] ratios, many authors have suggested the possibility of an extra mixing and which could be the reason for the change in [hs/ls] ratios.

1.7 $^{12}C/^{13}C$ ratio as a probe of stellar evolution

Isotopic ratio of carbon is an important tool to understand the evolutionary status of the objects. When a star ascends Red Giant Branch (RGB), the $^{12}C/^{13}C$ ratio and the total carbon abundance decrease due to the convection which dredges up (FDU) the product of internal CNO cycle to the stellar atmosphere. A star in RGB has not yet reached the CNO equilibrium, hence ^{13}C is the main product in that region. After that if it reaches AGB stage, ^{12}C may be supplied from the internal He burning to stellar surface and the star may become a carbon star and $^{12}C/^{13}C$ ratio increases again. Which means intrinsic carbon stars (since they are in AGB stage) show very high $^{12}C/^{13}C$ value while extrinsic carbon stars show low ratios. Standard theoretical models predict that when an object ascends the giant branch $^{12}C/^{13}C$ ratio should decrease up to 20 to 30 (Vanture 1992a). This is in rough agreement with the observation for objects with masses above 2.5 $M_{\odot}$ (Lambert & Ries 1981; Luck & Bond 1982). There are objects mainly low−mass objects (population I giants) with this ratio as low as 10. Gilroy (1989) shows that some additional mixing from the bottom of the stellar envelop to the H−burning shell called the Hot Bottom Burning (HBB) which produces additional ^{13}C to lower the ratios to the observed level. Vanture (1992a) had explained the isotopic ratios found in a group of CH stars. They noticed a group of carbon stars with a $^{12}C/^{13}C$ ratio ~ 3 near the equilibrium value of CN cycle (early-type) and a second group with $^{12}C/^{13}C$ ratio ≥ 25 (late-type) similar to the value found for Population II giants and globular cluster stars. In extrinsic carbon stars, both mass transfer and internal mixing alters the surface abundances and hence, $^{12}C/^{13}C$ ratio for this objects could be used to study the nature of the observed star as well as the invisible companion.

1.8 Binary nature and mass transfer mechanisms

Various enrichment scenarios have been put forward to explain the observed chemical abundances of different types of carbon stars mainly the extrinsic carbon stars. CEMP-s stars are the most common and perhaps the most well-studied of the CEMP sub-classes; about 80 per cent of CEMP stars are s-process enhanced. They are believed to be low-mass members of a binary system that were polluted by mass transfer from a companion AGB star. In such a binary system, the more massive companion star undergoes AGB evolution and synthesize s-process elements in its core. Subsequently, material from the core (including carbon) was dredged up to the surface and blown off in stellar winds. A typical AGB star with mass 0.6 to 6 $M_\odot$ with radius of about 430 $R_\odot$ has a very low surface gravity of about 10 cm s^{-2}. This reults a small escape velocity of about 40 km s^{-1}, which makes it easier to escape the outer layers [†]. This material which is lost from the AGB star was accreted by the smaller binary companion and polluted the surface composition with the excess carbon and heavy elements. The AGB companion has since evolved into a faint white dwarf. This theory supported radial velocity measurements confirming binary membership. 68 per cent of CEMP-s stars are confirmed binaries, which is statistically compatible with a binary frequency of 100 per cent after correcting for factors such as inclination and long periods (Lucatello et al. 2005). CH stars, the high metallicity counterparts of CEMP-s, are also the result of a binary mass transfer scenario. McClure & Woodsworth (1990) and McClure (1997) confirmed the binary membership of a large number of CH stars and subgiant-CH stars by continous radial velocity monitoring. Hence binary mass transfer is the widely accepted reason for the enhancement of carbon and heavy elements in these objects. Most of the stars appear as binaries have periods ranging from 11 minutes to 10^6 yrs. Among these a large fraction of binary systems is close enough (with periods $\leq$ 10 yrs) to transfer mass from one star to the other. Binary stars surveys suggest around 30 - 50 per cent of the binary system to be close binaries. The mass transfer in these binary systems takes place either by Roche-Lobe Overflow (RLOF) or by wind mass transfer; depending on the orbital properties of the binary system.

[†]Vassiliadis & Wood (1993) derived an empirical relation which connects the period and mass-loss rate for AGB stars.

$$\log\left(\frac{dM}{dt}\right) = -11.4 + 0.0123 \times \mathrm{P}$$
$$\log\left(\frac{dM}{dt}\right) = -11.4 + 0.0123 \times \mathrm{P} - 100\left(\frac{M}{M_\odot} - 2.5\right) \quad \text{for } \mathrm{M} > 2.5\ \mathrm{M}_\odot$$

Where mass-loss rate is in $M_\odot$/yr and period, P in days. They have also found that $\frac{dM}{dt}$ increases exponentially with P until it reaches a very high value of 10^{-4} $M_\odot$/yr.

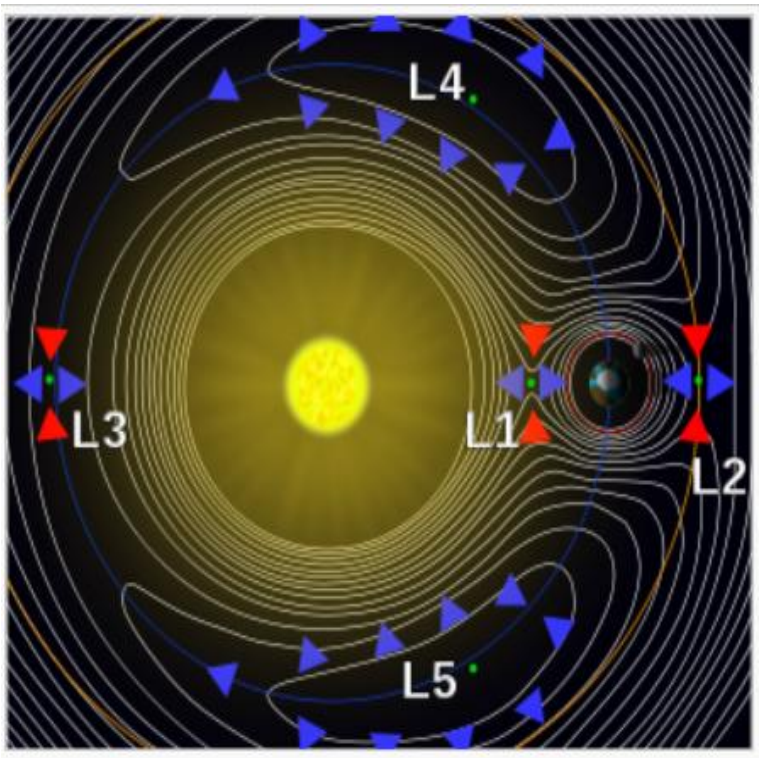

Figure 1.8: A contour plot of the effective potential due to gravity and the centrifugal force of a two-body system in a rotating frame of reference. The arrows indicate the gradients of the potential around the five Lagrange points. (http://pages.uoregon.edu)

1.8.1 Roche-lobe overflow and Wind mass transfer

A roche-lobe is defined as an effective potential in a co-rotating frame that includes the gravitational potential of the two stars and the centrifugal force. Also for this, the orbit of the binary is assumed as circular and coriolis force is neglected. This potential has five points, (as shown in Figure 1.8) called Lagrangian points where gradient of the effective potential is zero or in other words there exist no force in those points. Among these, L_1, the inner Lagrangian point is the most important one since the equipotential surface that passes through this point connects the gravitational spheres of the two star. If one star starts to fill its own roche-lobe (the part of the potential around the object), then matter can flow through the point L_1 to the other star (refer Figure 1.9). This is called RLOF. This depends on the orbital separation and mass ratio of the binary system. If the radii of the two stars are less compared to the individual roche-lobes, then RLOF does not happen. Another important mass transfer method is wind mass transfer. In this case one star has a very strong stellar wind and this matter can be accreted by the other object. Many studies (Mohamed & Podsiadlowski 2007; Abate et al. 2013) are devoted

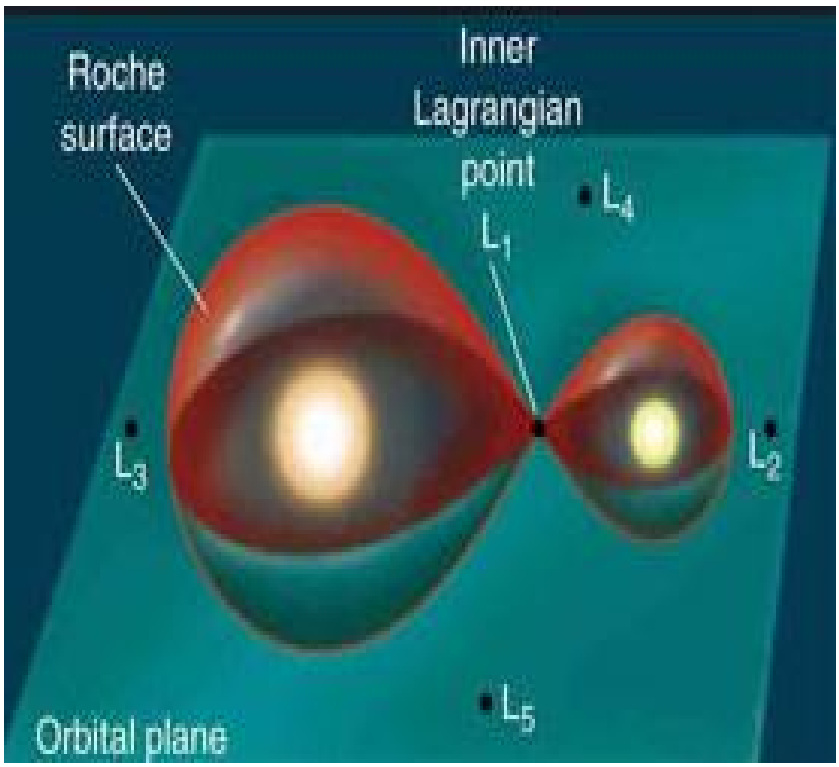

Figure 1.9: Roche-lobe overflow. (http://www.daviddarling.info/encyclopedia/R/Roche-lobe.html)

to understand the mass transfer mechanism taking place in CEMP or CH-binary systems. A star with convective envelop tends to expand rather than shrink when it loses mass very rapidly and also, due to mass transfer, the roche-lobe radius shrinks. The mass transfer becomes unstable if the accretor could not accrete all of the material transferred from the donor star. This leads to a common envelop evolution since the accretor expands due to the piled up mass and finally it overflows its roche-lobe (Paczyński 1965). In case of CEMP or CH-binary systems the companions are known as AGB stars and thus the mass transfer via RLOF may lead to common envelop evolution. In the case of binary system with wind velocity $\leq$ orbital velocity of accreting star, the wind mass transfer does not take place (Bondi & Hoyle 1944). For AGB stars, observed results indicate that the wind velocity is lower compared to the orbital velocity. Detailed description of wind mass transfer scenarios are given in Höfner (2009) and Bladh & Höfner (2012) . Recent hydro dynamical simulations by Mohamed & Podsiadlowski (2007) suggested a new mode of mass transfer called Wind Roche-Lobe Overflow (WRLOF). Abate et al. (2013) had found out the CEMP/VMP ratio from the population synthesis by considering WRLOF as an effective mode of mass transfer and the results are found to be consistent

with the ratio obtained by Lucatello et al. (2006).

1.9 Evolutionary link between CH and Ba stars

CH and Ba stars are known to show enhanced abundances of carbon and heavy elements. Barium stars are generally believed to be the metal-rich population I analogues of CH stars and also have the s-process signatures of AGB stars similar to CH stars (Allen & Barbuy 2006a,b). Abundances of heavy elements observed in barium stars are the result of a mass transfer process and can be explained with the help of a binary picture including low-mass AGB stars (Jorissen & van Eck 2000). The $^{12}C/^{13}C$ ratios of Ba stars are generally found to be in the range of 15 to 20, a value typical of population I giants. This also supports the Ba stars as the population I counter part of CH stars. Luck & Bond (1991) and Smith et al. (1993) have identified subgiant-CH stars as the progenitors of Ba stars. The isotopic ratios of subgiant-CH stars are found to be lower compared to Ba stars (Smith et al. 1993). From our analysis, even though the number of subgiant-CH stars are small, we could see a similar abundance trends in subgiant-CH stars and Ba stars. The studies on the evolutionary connection between CH and Ba stars by Luck & Bond (1991) suggest that Ba stars are a part of the evolutionary link; subgiant CH − Ba stars − CH giants. The degree of s-process enhancements and s-process neutron-exposure show similar ranges in these objects (Luck & Bond 1991). Moreover, most of the subgiant-CH stars, Ba stars and CH stars are identified as binaries with white dwarf companions, this also strongly support the evolutionary connection between these objects.

1.10 Outline of the thesis

The thesis consists of the following chapters

CHAPTER 1: **Introduction**

This chapter gives a brief introduction of the thesis work and its importance.

CHAPTER 2: **Data and Methodology**

This chapter describes the source of data and the methodology used for this study. The observation and data reduction techniques are described. The specifications and the properties of the instruments used are also explained.

CHAPTER 3: **Low-resolution spectroscopic analysis of CEMP (CH) stars**

In this chapter we have discussed the low-resolution spectroscopic analysis of eighty nine objects observed with 2 meter Himalayan Chandra Telescope at the Indian Astronomical

Observatory (IAO), Hanle. The objects are classified into different groups of carbon stars, i.e., CH, C−R, C−N, C−J etc. based on spectral criteria discussed in Goswami (2005). The primary spectral characteristics considered are:

1. The strength (band depth) of the CH band around 4300 Å.
2. Prominance of the secondary P-branch head near 4342 Å.
3. Strength/weakness of the Ca I feature at 4226 Å.
4. Isotopic band depths of C_2 and CN, in particular the Swan bands of $^{12}C^{13}C$ and $^{13}C^{13}C$ near 4700 Å.
5. Strengths of the other C_2 bands in the 6000 − 6200 Å region.
6. The ^{13}CN band near 6360 Å, and the other CN bands across the wavelength range.
7. Presence/absence of the Merrill-Sandford bands around 4900 − 4977 Å region.
8. Strength of the Ba II features at 4554 Å, and 6496 Å.

Along with these objects, the low resolution spectral analysis of twenty two CH stars from the CH star catalogue of Bartkevicius (1996) are also presented.

CHAPTER 4: **Spectroscopic analysis of CH stars I: basic observational properties**

In this chapter we have presented the detailed high resolution spectroscopic analysis of twenty two CH stars for which the low resolution analysis are already finished and presented in chapter 2. The basic data for the program stars along with the radial velocities and photometric temperatures are presented. The objects are classified in to group I (confirmed binaries), group II (objects for which radial velocity variations exist) and group III (no informations on radial velocity variations). The details of the linelist used for the calculation of stellar atmospheric stellar parameters and chemical abundances are also presented .

CHAPTER 5: **Spectroscopic analysis of CH stars II: Atmospheric parameters and elemental abundances**

In this chapter we have presented the atmospheric parameters and chemical abundances of the objects presented in chapter 4. The abundance patterns and abundance ratios observed in group I, group II and group III are critically analysed for the characteristic abundance patterns of CH stars.

CHAPTER 6: **Summary and Conclusions:**

This chapter gives the summary of the research work highlighting the important results. A brief description of the future work and a direction to proceed further is also discussed.

CHAPTER 2

DATA AND ANALYSIS

2.1 Introduction

Spectroscopy is an important tool to understand the properties of distant stars and Galaxies, such as their chemical composition, temperature, density, mass, distance, luminosity, and relative motion. Stars emit radiations at different wavelengths in the electromagnetic spectrum. Based on the wavelength coverage, astronomical spectroscopy can be devided into different branches; ultra violet, optical, infrared, radio and X-ray spectroscopy. Different characteristics properties of the astronomical objects can be studied using different branch of astronomical spectroscopy. The study in this thesis is mainly based on optical stellar spectroscopic observations and techniques. In this chapter, we describe low and high resolution spectroscopic observations and reduction procedures. We also discuss in brief the computational methods and analysis techniques involved in the study of spectra.

2.2 Astronomical techniques

Spectra of the distant objects are the only tool to study the behaviour of these objects. The main instrument used for the collection of electromagnetic radiations from the distant objects are telescopes. Based on the character of light gathering element used in the telescope they are classified as refracting telescopes which uses lenses and reflecting telescopes which uses mirrors. All the new generation telescopes are of reflecting type in which the light gathering element is a mirror. The gathered light is further studied using different astronomical instruments like imagers, photometers and spectrographs. Imagers are used to study the spatial distribution of photons from the source; the photometers will measure the brightness by measuring the number of photons collected from the source.

Spectrogragh helps us to understand the wavelength distribution of light. Since our analysis is mainly based on the wavelength distribution of light, we have to understand the functions of a spectrograph in detail.

2.2.1 Spectrograph

An astronomical spectrograph splits the light from a source into its component wavelengths. Prisms were used in old spectrograph as a dispersing element. If we use a prism as a dispersive element, light of different wavelengths get refracted by different amounts, with blue light being refracted more than red light; and thus, the dispersion is non-linear. In recent days, prisms are replaced by diffraction gratings as dispersing element. It consist of a large number of parallel lines marked on a transparent glass plate so that light can pass between the lines. This is called transmission grating. If the glass plate used is of reflective type the grating is called a reflection grating. Most of the spectrographs have the same design. Basic spectrograph design is shown in Figure 2.1. The five basic components of an astronomical spectrograph are the slit, collimator, grating, camera and detector.

Slit

The slit is a narrow rectangular aperture to select the region of interest we need to observe in the sky. Light falling only on the slit can enter the spectrograph. Slit helps to reduce the contamination in the target spectrum by allowing to enter only useful light. They also help us to get a stable spectral resolution.

Collimator

The collimator in an astronomical spectrograph is used to collimate the diverged light from the slit towards the grating. If the beam is not collimated, the incident angle of the diverged light on the grating is different which in turn makes the diffracted angle also different. Hence, the diffracted beams get imaged on to different positions in the detector, which will blurr the resulting spectrum. With a collimator, however, all angles of incidence on the grating are equal and no such blurring would result. Collimators can be either lenses or mirrors and must have the same focal ratio as the telescope and be positioned at a distance equal to its focal length from the telescope focal plane.

Grating

The diffraction grating is used as the dispersive element in the spectrograph, which splits the light into its component wavelengths and can be of either transmission or reflection type. The grating is usually positioned in the collimated beam from the collimator, which in turn helps to use a minimum-sized grating to collect light from all angles incident on

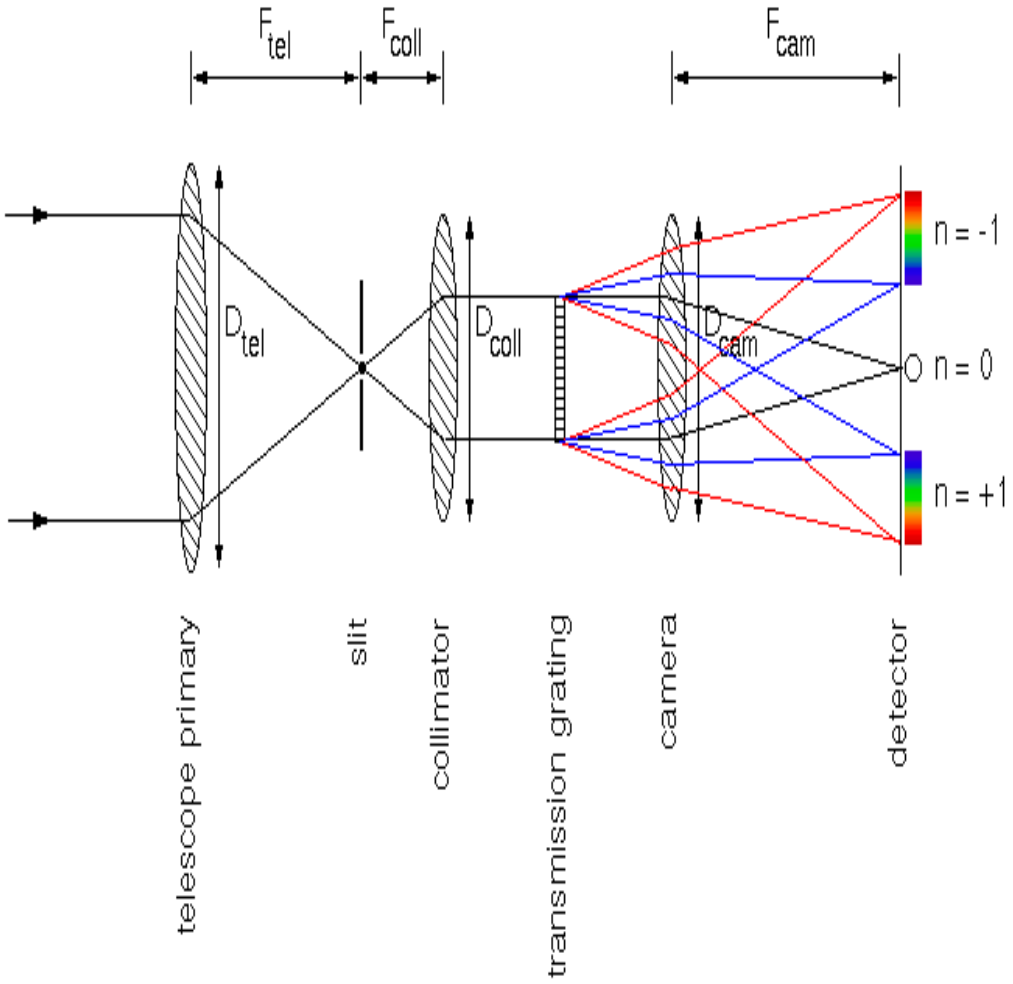

Figure 2.1: schematic of an astronomical spectrograph incorporating a transmission grating (http://www.vikdhillon.staff.shef.ac.uk/teaching)

the primary mirror. As per the grating equation,

$$n\lambda = d(sin\theta + sin\phi) \tag{2.1}$$

(where n is the order, d is the grating spacing, θ is the angle between the wavefront and the plane of the slits, ϕ is the angle between the incident beam and grating) changing the angle of the grating with respect to the incident beam, changes the angle of the diffracted beam. Hence most spectrographs have gratings that can be tilted in order to adjust the start and end wavelengths of the spectrum at desired order which in turn determines the wavelength coverage. These types of gratings are called blazed grating or echelle grating which

also allows most of the light to fall into the desired order. Echelle gratings are mostly manufactured with larger line spacing but are optimized for higher diffraction orders. For high resolution spectrographs, normal gratings are replaced by echelle gratings. The resolution of the spectrograph is given by

$$R = Nn = \frac{Wn}{d} \tag{2.2}$$

where N is the total number of lines in the grating and W is the width of the grating. Hence to increase the resolution, only possible and cheapest method is to increase n by increasing the angle of incidence and diffraction.

Camera

The camera is used to collect the spectrally dispersed beams from the grating. The camera can be either a lens, mirror, or catadioptric system.

Detector

The light collected by the camera is collimated and focussed to a detector. Then the spectrum gets imaged on the detector. We can define the direction along the slit as the spatial axis, and the direction along the spectrum (i.e. the horizontal direction) as the dispersion axis. In order to record the amount of light at each wavelength, a detector composed of an array of pixels is used. Mainly in all the spectrogrpahs, a two-dimensional ccd detector is used.

2.2.2 Factors affecting the quality of a spectrum

The light collected from the astronomical objects has to travel long distance through the atmosphere. Hence there are some changes from the light emitted by the objects and that collected by a detector. The reasons for this are mainly

Sky background: Due to the presence of scattered light in the sky, it acts as a noisy background to the light received from astronomical objects, making the detection of faint targets particularly difficult.

Atmospheric extinction: Dust and molecules in the atmosphere scatter and absorb the light from astronomical objects, dimming the images obtained by astronomical telescopes. The amount of dimming depends on the angle of the object above the horizon and the local conditions in the atmosphere at the time of observation.

Transparency variations: Similar to atmospheric extinction, clouds (i.e. water droplets) can absorb and scatter the light from astronomical objects. The amount of absorption tends to be much more variable than that due to extinction, as the clouds are blown across

the field of view of the telescope by the wind. The resulting variations in the amount of light received from an astronomical object range from partial attenuation due to thin cloud, or complete loss by thick cloud.

Seeing: Blurring of images caused by the turbulence in the atmosphere are referred as atmospheric seeing. The turbulence causes the refractive index to vary from layers to layers. Hence some rays of light bend more compared to others and the images are blurred. The brightness of the stars also fluctuate due to this.

2.3 Observations and Data

2.3.1 Low resolution spectroscopy

The Hamburg/ESO survey (Christlieb et al. 2001) and HK survey (Beers, Preston and Shectman) are two important surveys for the identification of CEMP stars in the halo of the Galaxy. We have carried out low resolution spectroscopy on some selected objects from these surveys to identify potential CH stars according to some specified spectral criteria. Programme stars are mainly chosen from the Hamburg/ESO survey which covers 6400 degree^2 limited by the declination, $\delta \leq +2.5^0$ and the Galactic longitude, $|b| \geq 30^0$. The magnitude limit of the sample is V $\sim$ 16.5. The wavelength range of these spectra is 3200 to 5200 Å, at a resolution of 15 Å, at H_γ. Christlieb et al. found a total of 403 FHLC stars in this survey by application of an automated procedure to the digitized spectra.

The identification of these objects as FHLC stars was based on a measure of line indices - i.e. ratios of the mean photographic densities in the carbon molecular absorption features and the continuum band passes. The primary consideration is the presence of strong C_2 and CN molecular bands shortward of 5200 Å; CH bands were not considered. We have carried out observations of the selected stars using the 2m Himalayan Chandra Telescope, Hanle. The camera and Grism combinations used for the observation provided a spectral resolution of 1330 and a wavelength coverage of 3800 - 6800 Å.

Himalayan Chandra Telescope

The 2 meter Himalayan Chandra telescope is located at Indian astronomical observatory, Digpa-ratsa Ri, Hanle. The latitude, longitude and altitude of the location are respectively 32d46m46s N, 78d57m51s E and 4500. Hanle Faint Object Spectrograph Camera (HFOSC), an optical imager cum spectrograph is used for the low and medium resolution spectroscopy. A collimator with same F number as that of the telescope and a camera are

used so that the focal length of the telescope can be reduced there by increasing the field coverage for a given CCD detector. Also it allows low resolution grism spectroscopy by inserting a dispersion element between the collimator and the camera. Using different slits (67 μ - 1340 μ) and grism combinations we can obtain a wavelength coverage from 3300 - 10500 Å and a resolution from 200 - 4500.

2.3.2 High resolution spectroscopy

The objects are selected from the CH star catalog of (Bartkevicius 1996) and the spectra are taken from the ELODIE archive. The details are given in the next section. CH95 catalogue of (Bartkevicius 1996) consist of 244 field stars and 17 globular cluster objects. We have considered only those CH stars for which high resolution spectra are available with S/N ratio $\geq$ 20. Optimal extraction and wavelength calibration of data are automatically performed by the online reduction software TACOS. The spectra recorded in a single exposure as 67 orders on a 1K CCD have a resolution of R $\sim$ 42000. The wavelength range spans from 3900 to 6800 Å.

Observatoire de Haute Provence (OHP)

The Observatoire de Haute-Provence (OHP) is situated in southeast France at an altitude of 650 meters and at +44 latitude and 5.7 East longitude. ELODIE is a cross-dispersed echelle spectrograph used at the 1.93 m telescope of OHP. Details about the spectrograph and reduction procedures are given in Baranne et al. (1996). This spectrograph was mainly used for extra solar planet detection and also for the high resolution spectroscopy of comparatively bright objects. In one single exposure a spectrum at a resolution of 42000 ($\frac{\lambda}{\delta\lambda}$) ranging from 3906 Å to 6811 Å is recorded on a 1024 $\times$ 1024 CCD. This performance is achieved by using a tan $\theta = 4$ echelle grating and a combination of a prism and a grism as cross-disperser. An automatic on-line data reduction techniques called TACOS reduces the ELODIE echelle spectra just after the exposures. Due to the use of fibres to feed the spectrograph, the shape of the orders are relatively stable on the CCD. All the images coming from the spectrograph are saved on a disk for security purposes. The CCD frames are then processed for correction of bad pixels, offset and dark current subtraction etc. After the extraction Wavelength calibrations are done using Thorium lamps. The ELODIE archive contains all the data taken with Elodie spectrograph.

2.3.3 Data reduction

This section describes the standard procedures for the extraction of CCD data with IRAF (Image Reduction and Analysis Facility). IRAF is a general image reduction and analysis facility providing a wide range of image processing tools for the users to process the raw two dimensional data into a one dimensional data for further analysis. IRAF is owned by the National Optical Astronomy Observatories (NOAO). The main steps for reducing the data are same in both low resolution and high resolution spectroscopy. The basic procedures to start with the reduction of the CCD data are zero correction and flat field correction. These steps are done using CCDPROC task in CCDRED package. Before doing these corrections we have to trim the section into an area which contains only useful data. Bias frames or zero frames, which are taken with zero exposure time for correcting the zero of the CCD are then combined to a master bias. This is done using ZERO COMBINE task in IRAF. We have to substract this master bias from all the other frames for zero correction. The next error which have to be removed from the data is the dark current which is due to heat. This is also additive to the useful data. The removal of the dark current is done using the dark exposures i.e., long integrations with shutter closed. Dark correction is not always needed. Some CCDs are cryogenically cooled to liquid nitrogen temperature (-77 K). They are not affected by dark current. CCDs which are cooled but not up to this temperature need to be corrected for dark currents. There are some multiplicative errors that also exist in CCD data. This is caused by the pixel to pixel variations of the light sensitivity of the CCDs. These types of errors are removed by taking calibration frames with a uniform source like halogen lamps called flat frames. For improving the quality we have to take many flat frames and then combine them in to a master flat. Master flat is then normalised and by dividing the object frames by the normalised master flat helps to reduce the multiplicative error in the data. These steps are done using the tasks FLAT COMBINE and RESPONSE in IRAF. Next step is the extraction of data using APALL in apextract. The extracted spectra contain counts vs pixels. The pixels have to be converted to wavelengths by using an arc spectrum for which the rest wavelengths are known. Bias subtracted arc frame is also extracted using task APALL. The spectral lines in the arc spectrum are identified using the task IDENTIFY (for single order spectra) or ECIDENTIFY (for echelle spectra) with the help of available identification charts. Then these arc frames are given as the reference to the object frames for the wavelength calibration using the task REFSPEC. The wavelength calibrated images are then corrected for dispersion using the task DISPCOR and continuum fitted for the further analysis.

2.4 Data analysis

The stellar atmospheric parameters like effective temperature (T_{eff}) and surface gravity (log g) are the pre-requisites to any detailed abundance analysis as well as defining the physical conditions in the stellar atmosphere. They are directly related to the physical properties of the star; mass (M), radius (R) and luminosity (L). The following sections give the details of the important terms involved in the calculation of stellar atmospheric parameters.

2.4.1 Bolometric magnitudes

Bolometric magnitude is the collective measure of all the radiations emitted by the objects at all the wavelengths. The corrections required to reduce visual magnitudes to bolometric magnitudes are large for very cool stars and very hot ones but are relatively small for stars such as the Sun. We measure the energy radiated by a star from earth using a detector. But the detectors are made such that it can measure only some part of the radiation. Very cool and very hot objects emit radiations at far infrared and ultraviolet regions of the electro magnetic spectrum, which can not be detected from earth. Hence we have to apply corrections to the absolute magnitudes of the stellar objects to find the bolometric magnitudes. The absolute magnitude and Bolometric magnitude are related by the following expression

$$M_{bol} = M_v + BC \tag{2.3}$$

where $M_v = V - 5logd + 5$ and d (distance)= $\frac{1}{\pi}$, where π is the parallax, V = absolute visual magnitude, BC is the bolometric corrections.

2.4.2 Luminosity

The luminosity L is the total energy output of a star per unit time. Bolometric magnitudes and luminosities are related by Pogson's equation as

$$M_{bol\odot} - M_{bol} = 2.5log(L/L_{\odot}) \tag{2.4}$$

2.4.3 Effective temperature

The effective temperature (T_{eff}) of an object is related to the total radiant power/unit area at stellar surface. It is also defined as the temperature of an equivalent black body that

gives the same total power per unit area, and is directly given by stellar luminosity and radius. By Steffan's law

$$\sigma T_{eff}^4 = \int F_\nu d_\nu = \frac{L}{4\pi R^2} \tag{2.5}$$

Radius (R) is taken as the depth of formation of the continuum, which in the visible region is approximately constant for most stars (Gray 1992).

2.4.4 Surface gravity

Surface gravity (g) of the object at its surface is the acceleration due to gravity on the surface. The pressure in a stellar surface is controlled by the surface gravity and are related with the gas pressure as, $P_g = Const.g^{2/3}$ and with the electron pressure as $P_e = Const.g^{1/3}$. The surface gravity is related to mass M and radius R of the object as

$$log\ g = log\ M - 2log\ R + 4.437 \tag{2.6}$$

From this equation it is clear that a star with higher mass but lower radius will be denser and also have higher pressure. This leads to larger number of atoms per unit area leading to a stronger spectral line, which implies an ionic line decreases in strength with increase in surface gravity since more and more free electrons will get chance to combine with ions since the density is very high.

2.4.5 Micro-turbulence

Micro-turbulence is the small scale motions of particles with its characteristic dimension less compared to unit optical depth. It has a high effect on the shape of a spectral line, because increase in the motion of atoms broadens line profiles without affecting the chemical abundance. This implies that strength of the line or equivalent width does not have any correlation with the abundances. This fact is used to determine the micro-turbulent velocity (ζ).

2.4.6 Equiwalent width

The equivalent width (W) of a spectral line is a measure of the area of the line on a plot of intensity versus wavelength (Figure 2.2). It is found by considering a rectangle with a height equal to that of continuum, and finding the width such that the area of the rectangle is equal to the area in the spectral line. Equivalent width measures the strength

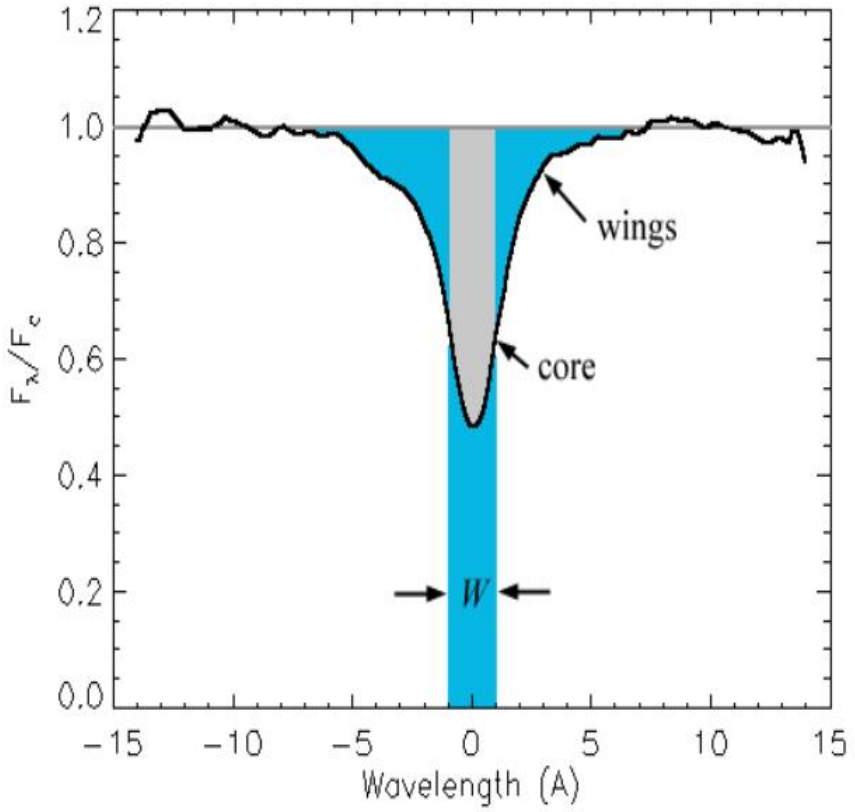

Figure 2.2: Equivalent width (W) of an absorption line is the total area inside the absorption line, if we create a rectangular box of the same area, extending from the continuum to the 0 flux line, the width of this box is the equivalent width. This measurement is used to describe the strength of the line (the higher the value, the stronger the line)(http://www.bdnyc.org/2012/03/02)

of a spectral feature and it is given by the equation

$$W = \int \frac{F_c - F_\lambda}{F_c} \tag{2.7}$$

where F_λ is the radiant flux and F_c is the continuum flux. The equivalent width is used as a quantitative measure of the strength of spectral features because the shapes of spectral features can vary depending upon the configuration of the system which is producing the lines. Another measure of width of spectral line is full width at half maximum and it is given by

$$\delta_{\lambda(1/2)} = \frac{F_c - F_\lambda}{F_c - F_{\lambda_0}} \tag{2.8}$$

We have measured the equivalent width of absorption lines in our programme stars spectra by fitting a Gaussian to the absorption lines.

2.4.7 Optical depth and opacity

When a beam of light travels through a medium, some photons get absorbed. The intensity I_λ decreases by an amount dI_λ. This value entirely depends on the composition, density and temperature of the medium. So the equation can be written as

$$dI_\lambda = -\kappa_\lambda \rho I_\lambda ds \tag{2.9}$$

where ds is the distance travelled and ρ is the density. The quantity κ_λ is called the absorption coefficient or opacity. It is defined as the cross-section for the absorbing photons of wavelength λ per unit mass of stellar material or it is the capacity of the material to absorb photons. Integrating this equation within the limits s=0 to s=s, then I_λ is given by

$$I_\lambda = I_{\lambda,0} e^{-\int \kappa_\lambda \rho ds} \tag{2.10}$$

where $-\kappa_\lambda \rho ds$ is defined as optical depth $d\tau_\lambda$. The intensity of light declines exponentially by a factor of e^{-1} for a mean free path $l = \frac{1}{\kappa_\lambda \rho}$. Then the optical depth can be defined as number of mean free paths from the rays original position to the surface. The optical depth entirely depend on the wavelength.

2.4.8 Model atmospheres

The chemical analysis of a spectrum is done by comparing the observed features with the theoretical predictions. For the purpose, a model atmosphere of the star is assumed which could reproduce the observed quantities. Model atmospheres are constructed by solving the equation for hydrostatic equilibrium which relates pressure and optical depth and is given as

$$dF = \rho g dA dx \tag{2.11}$$

$$\frac{dF}{dA} = dP \tag{2.12}$$

$$dP = \rho g dx \tag{2.13}$$

where ρ is the density, dAdx is the volume, g is surface gravity, dP is the pressure. To construct the model photosphere the following assumptions are made.

1. Plane parallel geometry, making all physical variables a function of only one space coordinate.

2. Hydrostatic equilibrium, meaning that the photosphere is not undergoing large scale accelerations comparable to the surface gravity.

3. Structures such as starspots and granulations are neglected.
4. Magnetic fields are not considered.

A model atmosphere consists of a table of numbers giving the pressure as a function of optical depth for an assumed chemical composition. Depending upon the purpose of usage some model contains intensity, absorption coefficient, electron pressure etc also. Usually photosphere is assumed to have seventy two layers and the model atmosphere contains seventy two rows each representing each layer of atmosphere. It is very difficult to establish a perfect thermodynamic equilibrium in stars. The temperature of the star varies with location. However, the thermodynamic equilibrium can be assumed in a small region of unit optical depth and is called the Local Thermodynamic Equilibrium (LTE). At LTE, photosphere can be represented by one temperature and optical depth. Also, only collisionally induced transition occurs at LTE.

2.4.9 Estimation of radial velocity

Radial velocities of our programme stars are calculated using a selected set of clean unblended lines in the spectra using the equation

$$V_r = \frac{\lambda_{obs} - \lambda_{lab}}{\lambda_{lab}} * c \tag{2.14}$$

Application of this formula requires laboratory measurements of the rest wavelength to high accuracy. When an object moves towards us, the transition is shifted to shorter wavelengths and it is called blue shifted. Similarly, when an object moves away from us the transition is towards a longer wavelengths and therefore called redshifted.

2.4.10 Calculation of photometric temperature

The effective temperature of an object can be derived by using their angular diameter and bolometric fluxes. But this direct method has very limited use. Alonso et al. (1996) had derived an indirect method called Infrared flux method to determine the temperatures of stellar dwarfs and sub-dwarfs, which is extended to main-sequence stars and giants and the results are presented in Alonso et al. (1996, 1999). They have used a theoretical model atmospheres flux distributions developed by Kurucz (1991, 1993). The infrared flux method uses the ratio between bolometric flux and monochromatic flux at the infrared wavelength of the continuum. This ratio is called observational R factor, which is then compared with the theoretically calculated R_{thoe}. Monochromatic fluxes are determined

observationally using IR photometry. The calibrations relate T_{eff} with Stromgren indices as well as [Fe/H] and colours (V−B), (V−K), (J−H) and (J−K) and hold within a temperature and metallicity range $4000 \leq T_{eff} \leq 7000$ K and $-2.5 \leq$ [Fe/H] ≤ 0. The Alonso et al. calibrations use Johnson photometric systems for UBVRI and use TCS (Telescopio Carlos Sanchez) system for IR colours, J−H and J−K. We have used colour-temperature calibrations of Alonso et al. (1996) that relate T_{eff} with various optical and near-IR colours. Estimated uncertainty in the temperature calibrations is ~ 100 K. Although the difference between 2MASS infrared photometric system and photometry data measured on the TCS system used by Alonso et al. to derive the T_{eff} scales is very small, the necessary transformations between these photometric systems are performed using transformation relations from Ramírez & Meléndez (2004) and Alonso et al. (1996, 1999). V−K is the preferred temperature indicator since both pass-bands are only marginally affected by the presence of the strong molecular lines in the temperature range of carbon stars. The B−V colour of a star with strong molecular carbon absorption features depends not only on T_{eff}, but also on the metallicity of the star and on the strength of its molecular carbon absorption features, due to the effect of CH molecular absorption in the B band. B−V colour often gives a much lower value than the actual surface temperature of the star due to the effect of CH molecular absorption in the B band. We have assumed that the effects of reddening on the measured colours are negligible. The equations used for the calculations are as follows.

$$J_{TCS} = J_{2MASS} + 0.001 - 0.049(J_{2MASS} - K_{2MASS})$$

$$H_{TCS} = H_{2MASS} - 0.018 + 0.003(J_{2MASS} - K_{2MASS})$$

$$K_{TCS} = K_{2MASS} - 0.014 + 0.034(J_{2MASS} - K_{2MASS})$$

$$K_J = K_{TCS} + 0.042 - 0.019(((J_{TCS} - K_{TCS}) - 0.008)/0.910)$$

$$(V - K)_{TCS} = 0.050 + 0.993(V - K_J)$$

$$\theta_{JK} = 0.582 + 0.799(J_{TCS} - K_{TCS}) + 0.085(J_{TCS} - K_{TCS})^2$$

$$\theta_{JH} = 0.587 + 0.922(J_{TCS} - H_{TCS}) + 0.218(J_{TCS} - H_{TCS})^2 + 0.016(M)(J_{TCS} - H_{TCS})$$

$$\theta_{VK} = 0.555 + 0.195(V-K)_{TCS} + 0.013(V-K)^2_{TCS} - 0.008(V-K)_{TCS}(M) + 0.009(M) - 0.002M^2$$

$$\theta_{BV}(M) = 0.541 + 0.533(B-V) + 0.007(B-V)^2 - 0.019(B-V)(M) - 0.047(M) - 0.011M^2$$

$$T_{EFF(xy)} = 5040/\theta_{(xy)} \tag{2.15}$$

M indicates the metallicity value. XY indicates J−K, J−H, V−K and B−V. The visible

magnitude (V) is in Johnson system, hence we have to convert 2MASS-K magnitude to Johnson system. we used Alonso et al. (1994) calibration equation.

$$(J-K)_{TCS} = 0.008 + 0.910(J-K)_J \tag{2.16}$$

We have determined the photometric temperatures for all the programme stars and the results are tabulated in Tables 3.4 and 4.3.

2.4.11 Stellar Atmospheric parameters

In a stars atmosphere under LTE conditions, there is a direct correlation between the effective temperature of the star and the excitation temperature determined from the analysis of spectral line strength of a given atomic species. Thus measurements of atomic lines with differing excitation potentials can be used to determine the effective temperature of stars. Another important factor at LTE is that abundances predicted from individual lines using an LTE atmosphere should not show any correlation to the excitation potential of the lines. We have used a set of Fe I and Fe II lines with excitation potential in the range 0.0 - 5.0 eV and equivalent width 20 Å to 180 Å to find the stellar atmospheric parameters. Throughout our analysis we have assumed LTE. The effective temperature is determined by making the slope of the abundance versus excitation potential of Fe I lines to be nearly zero. The initial value of temperature is taken from the photometric estimates and arrived at a final value by an iterative method with the slope nearly equal to zero. The micro-turbulent velocity was estimated at a given effective temperature by demanding that there be no dependence of the derived Fe I abundance on the equivalent width of the corresponding lines. Abundances derived from equivalent width are very sensitive to the adopted micro-turbulent velocity. Micro-turbulent velocity is fixed at a value which gives zero slope for the plot of equivalent width versus abundances of Fe lines.

The surface gravity is fixed at a value that gives the same abundances for Fe I and Fe II lines. Clean Fe II lines are more difficult to detect than Fe I lines, so we were limited to 4-10 Fe II lines for the abundance analysis in most cases.

Knowing the strength of a spectral line which depends on the number of atoms undergoing transition gives the abundance of the element involved in the transition.

2.4.12 Calculation of Chemical abundances

The method used to determine the abundances in stellar atmospheres are based on intensity of spectral lines. This is done by comparing the observed values with theoretical

predictions. The observed high resolution spectrum can be compared with a calculated spectrum. The results are entirely depend on the model atmospheres and the line formation mechanisms. The two methods used are

1) Fine analysis method : The fine analysis method consists in comparing the measured equivalent width with the equivalent widths calculated on the basis of selected model photosperes. Weak lines (20 - 180 Å) are generally used for the calculation because their equivalent widths are not affected by micro-turbulence and damping constants. For the accurate measurement of equivalent widths we need very high resolution spectra (R $\geq$ 20000) with a very high S/N ($\geq$ 20) ratio. Although LTE is assumed for the calculation, for some elements like Na, LTE abundance analysis does not give accurate results since they are affected by NLTE conditions. We have used lines with equivalent width $\leq$ 180 mÅ and they are not much affected by NLTE effects.

2) The spectrum synthesis method: In this method, a line profile is compared with a theoretically computed line profile instead of comparing equivalent widths. All the line broadening mechanisms have to be taken into account for calculating the theoretical profiles. An extensive line list for each element in the different ionisation states with known laboratory wavelengths, log gf and excitation potential are required for the accurate determination of the abundances. Spectrum synthesis method is generally applied to crowded regions with severe line blending. This method is also used to confirm the results obtained by the standard equivalent width method.

MOOG

MOOG is a FORTRAN code used to find the chemical abundances of objects. This code was developed by Chris Sneden in 1973 for his PhD thesis and subsequently revised by him. It uses the LTE conditions for the analysis. Moog needs a model photosphere together with a list of atomic or molecular transitions as inputs for the analysis. The detailed description of these codes and methods can be found in Chris Sneden's thesis and in a review article by Castelli & Hack (1990). For fine analysis method the subroutine ABFIND is used, which will fit the theoretically calculated equivalent widths to the observed equivalent widths. With respect to the corresponding atmospheric model selected, a numerous iterations are carried out by the program ABFIND, varying the abundances until the computed equivalent width matches the observed equivalent width. For the synthesis, the program SYNTH is used to fit the observed spectrum to the theoretically calculated spectrum. In this case also, a set of synthetic spectra are formed to match the observed one.

2.4.13 Hyperfine splitting and chemical abundances

Hyperfine splitting is the splitting in atomic energy levels caused by the interaction between the nucleons and electrons in an atom due to their non zero spins. When the spin angular momentum of the nucleus interacts with the total angular momentum of the electrons, the splitting of energy level occurs. This in turn broadens the width of a spectral line due to the transition between different levels. Abundances determined using these broadened lines lead to wrong conclusions. Hence it is very important to consider the hyperfine correction while doing the abundance analysis. We have synthesised the elements Sc, Mn, V, La and Eu with odd atomic numbers and Ba with even atomic number but odd number of neutrons, considering the hyperfine splitting of levels and their contributions to the total abundances.

2.5 Parametric model based study

Heavy element abundances in the solar system have contribution from both s- and r-process. Identification of the major process contributing to the elemental abundances is likely to provide clues to the nucleosynthetic mechanisms taking place in the objects which in turn can give clues to their evolutionary states. There have been several efforts to explain the solar system abundances of elements associated with slow neutron-capture processes. The model created by Howard et al. (1986) could reproduce the observed solar system σN curve, where σ is the neutron-capture cross-section and N is the abundance of the elements, with good agreement. This model used an exponential distribution of neutron exposures via sequential irradiations since s-process is a long term process and the neutron flux there by neutron exposure will vary time to time. This model was used by Aoki et al. (2001) to study the observed abundances in metal-poor stars. Zhang et al. (2006) also used this model to study the double enhancement in metal-poor stars. We have conducted a parametric model based study to understand the contribution of these neutron-capture processes to the observed abundances of the programme stars. The detailed methodology used for the parametric model study along with the results are explained in section 5.5.

2.6 Luminosities and Masses

We have determined the luminosities of the programme stars using the equation 2.4. Masses of the programme stars are determined using their positions in the Hertzsprung-

Russel diagram using the evolutionary tracks given by Girardi et al. (2000). The tracks are available for different initial compositions and initial masses from $0.6M_{\odot}$ to $120M_{\odot}$, which are calculated using updated opacities and equations of state considering all the physical changes like dredge-up mechanisms, mass loss episodes and convective over-shooting taking place in the stellar objects. These evolutionary tracks starts from Zero age main-sequence and ends either at thermally pulsing AGB stage or carbon ignition. We have selected the model for the initial composition with Y = 0.23 and Z = 0.019, 0.004, 0.008 etc, where Y represent the He mass fraction and Z is the global metallicity for all the other metals.

2.7 Error Analysis

We have calculated the error in the presented abundance results as described by Ryan et al. (1996). The errors in the elemental abundances have contributions from the uncertainty in measurement of atmospheric parameters and equivalent widths. The errors in the equivalent width have an affect on the measurement of surface gravity and micro turbulent velocities also. Inaccurate gf-values also contribute to the error in the elemental abundances. The elements, for which we have measured the abundances using spectrum synthesis method, the error is uniformly taken as 0.2 dex by considering the fitting error of 0.1 dex and error in gf-values as 0.1 dex. Similarly for a few objects we have calculated the elemental abundance using a single line, then the errors are expected to be from the measurement of atmospheric parameters. In that case, to find the minimum error for each star, we have considered the respective standard deviation of the iron abundances for each object which is approximately 0.1 in all the objects, along with the uncertainties in temperature, micro-turbulent velocities and surface gravities. We have assumed an error of 100 K in effective temperature corresponding to 0.1 dex in abundances. Similarly 0.03 dex in gravity and 0.06 in micro-turbulence corresponding to a $\Delta\zeta$ of 0.5 km/s. These values as typically accepted for the minimum error in giants and subgiants. Then the total minimum error is calculated using the following equation, and the value is found as 0.12.

$$E_r = \sqrt{{E_{r1}}^2 + {E_{r2}}^2 + {E_{r3}}^2 + {E_{r4}}^2 + {E_{r5}}^2 ..... + {E_{rn}}^2} \tag{2.17}$$

When a large number of lines are used for the calculation of abundances, the standard deviation of the abundances derived using individual lines is taken as the error.

CHAPTER 3

LOW RESOLUTION SPECTROSCOPIC STUDY OF CEMP (CH) STARS

Goswami A., Karinkuzhi D., Shantikumar N. S., 2010b, MNRAS, 402, 1111

3.1 Introduction

An accurate assessment of the fraction of CH stars can significantly aid our understanding of formation and evolution of heavy elements at low metallicity. Our objective in this study has been to identify the CH stars (as well as different type of stellar objects) in a selected sample of high Galactic latitude field stars. As explained in section 1.3.1, Morgan−Keenan system of carbon star classification (Keenan 1993) divided stars into C−R, C−N and CH sequence, with sub classes running to C−R6, C−N6 and CH6 according to the temperature of the stars. Wallerstein & Knapp (1998) had given a detailed description of the spectra of different groups of carbon stars. In this chapter we describes the classification of a large number of faint high Galactic latitude carbon stars into different groups based on spectral characteristics as discussed in Goswami (2005).

3.2 Selection of programme stars

The programme stars belong to the list of 403 Faint High Latitude Carbon (FHLC) stars presented by Christlieb et al. (2001) from the database of Hamburg/ESO Survey (HES) described by Wisotzki et al. (2000). The details of observations and data reduction procedures are explained in section 2.3. A sample of CH stars from the CH star catalogue of

Bartkevicius (1996) are also observed for a detailed studies of these objects.

3.3 Different types of carbon stars and their spectral characteristics

Spectral characteristics of different groups of carbon stars are explained in section 1.3. CH stars are mainly characterized by the presence of CH bands in their spectra. Using low resolution spectra it is very difficult to distinguish the CH and C−R stars. Both show strong CH bands in their spectra. In such cases the secondary P-branch head near 4342 Å is used as a more useful indicator. P-branch head are distinctly seen in CH stars spectra. Another important criteria is the strength or weakness of Ca I at 4226 Å. While in CH stars this feature is weakened by the overlying CH band, in C−R stars this feature is quite strong and strength will be similar to CN band strength. Enhanced lines of s-process elements and various strength of C_2 bands are also important criteria to distinguish CH stars from other groups of carbon stars. But as the narrow atomic lines are blended with contributions from the molecular bands, the classifications based on the elemental abundances derived from the medium resolution spectra may not be accurate. We have classified the spectra according to the following spectral characteristics.
1. The strength (band depth) of the CH band around 4300 Å.
2. Prominence of the secondary P-branch head near 4342 Å.
3. Strength/weakness of the Ca I feature at 4226 Å.
4. Isotopic band depths of C_2 and CN, in particular the Swan bands of $^{12}C^{13}C$ and $^{13}C^{13}C$ near 4700 Å.
5. Strengths of the other C_2 bands in the 6000 − 6200 Å region.
6. The ^{13}CN band near 6360 Å and the other CN bands across the wavelength range.
7. Presence/absence of the Merrill−Sandford bands around 4900 − 4977 Å region.
8. Strength of the Ba II features at 4554 Å and 6496 Å.

To assign a star in a particular group, we have compared the spectra of the programme stars with the spectra of known carbon stars available in the low resolution spectral atlas of Barnbaum et al. (1996). We have also acquired the spectra of some of the objects from this atlas using the same observational set up. The objects with prominent C_2 molecular bands are listed in Table 3.1 and those without prominent C_2 bands are listed in Table 3.2. The potential CH star candidates identified from this survey are presented in Table 3.3.

Table 3.1: HE stars with prominent C_2 molecular bands observed during 2007 − 2009

Star	RA (2000)[a] hh mm ss	DEC (2000)[a] dd mm ss	l	b	B_J^a	V^a	$B-V^a$	$U-B^a$	J	H	K	Dt of Obs
HE 0008−1712	00 11 19.2	−16 55 34	78.5866	−76.2106	16.5	15.2	1.78	1.64	13.630	13.069	12.975	06.12.2008
												11.09.2008
HE 0009−1824	00 12 18.5	−18 07 55	75.8376	−77.2654	16.5	15.7	1.09	0.58	14.080	13.724	13.665	12.09.2008
HE 0037−0654	00 40 02.0	−06 38 13	114.8865	−69.3303	16.4	15.5	1.19	0.58	14.146	13.708	13.724	11.09.2008
HE 0052−0543	00 55 00.0	−05 27 02	125.3316	−68.3057	16.5	15.0	1.95	1.74	12.952	12.241	12.086	12.09.2008
HE 0100−1619	01 02 41.6	−16 03 01	136.7651	−78.6185	15.9	14.7	1.54	1.28	13.114	12.537	12.476	21.11.2008
												12.09.2008
HE 0136−1831	01 39 01.8	−18 16 43	176.4932	−75.9157	16.9	15.6	1.72	1.43	14.216	13.679	13.532	12.09.2008
HE 0237−0835	02 40 13.6	−08 22 18	181.9346	−58.1620	16.8	15.6	1.67	1.42	13.706	13.136	12.987	19.12.2012
HE 0217+0056	02 20 23.5	+01 10 39	163.6094	−54.5125	16.3	14.6	2.35	2.25	11.276	10.271	9.833	22.11.2008
HE 0225−0546	02 28 19.4	−05 32 58	174.1738	−58.4222	16.5	15.2	1.79	1.51	13.347	12.707	12.528	06.12.2008
HE 0228−0256	02 31 15.5	−02 43 07	171.5942	−55.8545	16.2	14.7	1.99	1.52	12.506	11.813	11.531	18.01.2009
HE 0420−1037	04 22 47.0	−10 30 26	205.0454	−37.7176	15.2	14.7	1.38	0.99	12.341	11.815	11.695	21.11.2008
HE 0507−1430	05 10 07.6	−14 26 32	215.0951	−28.8440	13.2	14.4	1.66	1.40	12.325	11.717	11.575	20.12.2012
HE 0954+0137	09 57 19.2	+01 23 00	237.1030	41.0018	16.6	15.7	1.18	0.32	–	–	–	21.11.2008
HE 1045−1434	10 47 44.1	−14 50 23	263.5905	38.4049	15.5	14.6	1.23	0.96	12.935	12.449	12.244	09.04.2007
HE 1051−0112	10 53 58.8	−01 28 15	253.5294	49.7900	17.0	16.0	1.44	0.94	14.347	13.794	13.703	06.12.2008
HE 1102−2142	11 04 31.2	−21 58 29	272.5241	34.5071	16.0	14.9	1.44	0.98	13.275	12.714	12.601	16.03.2009
HE 1110−0153	11 13 02.7	−02 09 28	261.1493	52.4883	16.5	15.5	1.47	1.29	12.912	12.205	12.063	04.04.2009
HE 1116−1628	11 19 03.9	−16 44 50	273.2181	40.7347	16.6	15.6	1.28	1.41	13.241	12.614	12.482	06.02.2009
HE 1119−1933	11 21 43.5	−19 49 47	275.7342	38.2583	12.8	14.6	1.34	0.87	13.043	12.571	12.422	18.03.2009
HE 1120−2122	11 23 18.6	−21 38 33	277.1276	36.7743	12.9	–	–	–	9.573	8.902	8.788	17.03.2009
HE 1123−2031	11 26 08.7	−20 48 19	277.4490	37.8097	16.8	15.8	1.33	1.19	13.513	12.940	12.800	18.03.2009

Table 3.1 – continued from previous page

Star	RA (2000)[a] hh mm ss	DEC (2000)[a] dd mm ss	l	b	B_J^a	V^a	$B-V^a$	$U-B^a$	J	H	K	Dt of Obs
HE 1127−0604	11 29 36.8	−06 20 51	269.3427	51.1090	16.8	15.9	1.23	0.87	14.594	14.087	14.027	18.01.2009
HE 1142−2601	11 44 52.9	−26 18 29	284.8485	34.2157	13.9	13.0	1.28	1.07	11.218	10.675	10.539	04.04.2009
HE 1145−1319	11 48 21.4	−13 36 38	280.3756	46.4800	16.4	15.4	1.37	1.32	13.466	12.934	12.790	17.03.2009
												05.04.2009
HE 1146−0151	11 49 02.3	−02 08 11	273.2807	57.0990	14.9	14.2	0.96	0.97	12.929	12.400	12.262	16.03.2009
HE 1157−1434	12 00 11.5	−14 50 50	284.8854	46.2211	16.1	13.8	1.62	1.41	11.792	11.178	11.019	06.06.2007
												07.06.2007
HE 1205−0521	12 07 53.	−05 37 51	283.5026	55.5893	15.2	14.4	1.09	0.48	12.434	11.988	11.806	04.04.2009
HE 1205−2539	12 08 08.1	−25 56 38	290.8957	35.9137	13.6	15.4	1.91	1.72	12.313	12.665	12.540	17.03.2009
HE 1210−2636	12 12 59.7	−26 53 22	292.4334	35.1974	13.8	12.6	1.65	1.52	–	–	–	06.05.2009
HE 1228−0417	12 31 12.5	−04 33 40	293.4045	57.9360	14.8	14.0	1.17	0.96	12.406	11.969	11.818	04.04.2009
HE 1230−0327	12 33 24.1	−03 44 28	294.2159	58.8251	13.7	15.1	1.02	0.80	13.683	13.224	13.100	17.03.2009
HE 1238−0836	12 41 02.4	−08 53 06	298.5709	53.8987	13.1	–	–	–	9.189	8.503	8.154	08.04.2007
HE 1253−1859	12 56 38.4	−19 15 32	304.6277	43.5957	13.7	12.9	1.09	1.22	10.604	9.972	9.850	16.03.2009
HE 1315−2035	13 17 57.4	−20 50 53	311.2275	41.5961	16.7	15.7	1.35	0.93	13.678	13.236	13.047	06.05.2009
HE 1318−1657	13 21 19.4	−17 13 40	313.0578	45.0556	13.3	14.4	1.42	1.26	12.509	11.997	11.814	02.06.2010
HE 1331−2558	13 34 20.1	−26 13 38	314.7873	35.6550	13.9	16.0	1.53	1.10	10.998	10.394	10.240	18.03.2009
HE 1344−0411	13 47 25.7	−04 26 04	328.2429	55.6614	16.3	14.9	2.02	2.29	11.708	10.848	10.467	05.04.2009
HE 1358−2508	14 01 12.3	−25 22 39	322.8426	34.4322	13.2	12.3	1.25	0.84	9.521	8.802	8.532	18.01.2009
HE 1400−1113	14 03 39.8	−11 28 04	329.7145	47.6129	16.0	15.2	1.19	0.75	13.838	13.411	13.276	17.03.2009
HE 1400−0229	14 03 12.4	−02 44 16	335.8219	55.4831	16.5	15.5	1.37	0.85	13.456	12.847	12.693	23.05.2010
HE 1404−0846	14 06 55.1	−09 00 58	332.3876	49.4897	15.3	14.2	1.52	1.29	12.435	11.783	11.681	07.06.2007
HE 1405−0346	14 07 58.3	−04 01 03	336.5341	53.7853	14.7	13.5	1.68	1.28	11.608	11.068	10.903	16.03.2009
HE 1410−0125	14 13 24.7	−01 39 54	340.6313	55.0908	–	–	–	–	10.360	9.770	9.651	16.03.2009

Table 3.1 – continued from previous page

Star	RA (2000)[a] hh mm ss	DEC (2000)[a] dd mm ss	l	b	B_J^a	V^a	$B-V^a$	$U-B^a$	J	H	K	Dt of Obs
												11.06.2008
HE 1418−0306	14 20 57.1	−03 19 54	341.7366	52.6618	–	13.0	1.66	1.11	10.505	9.767	9.505	09.04.2007
HE 1428−1950	14 30 59.4	−20 03 42	332.6046	37.0083	–	–	–	–	9.988	9.469	9.318	06.02.2009
HE 1430−0919	14 33 12.9	−09 32 53	340.3560	45.7983	14.9	13.8	1.46	0.75	12.476	11.971	11.862	18.03.2009
												09.05.2007
HE 1431−0755	14 34 32.7	−08 08 37	341.8828	46.7820	14.6	13.5	1.51	1.44	11.283	10.605	10.422	08.05.2007
HE 1432−2138	14 35 47.6	−21 51 37	332.7735	34.8934	17.1	16.3	1.14	0.37	14.402	13.989	13.885	02.06.2010
HE 1439−1338	14 42 26.4	−13 51 18	339.7039	40.9588	14.5	13.5	1.39	0.97	10.810	10.112	9.836	25.07.2008
												09.04.2007
HE 1440−1511	14 43 07.1	−15 23 48	338.737	39.5765	14.6	13.8	1.13	0.87	12.238	11.757	11.606	09.05.2007
HE 1442−0058	14 44 48.9	−01 10 56	351.4558	50.6883	17.8	16.2	2.15	1.80	12.287	11.268	10.751	06.06.2007
HE 1447+0102	14 50 15.1	+00 50 15	355.2263	51.2262	15.6	15.0	0.90	0.14	13.207	12.760	12.682	12.09.2008
												08.04.2007
HE 1525−0516	15 27 52.2	−05 27 04	358.1110	40.1019	16.8	15.8	1.29	1.14	13.972	13.479	13.314	11.09.2008
												07.06.2007
												08.06.2007
HE 2114−0603	21 17 20.8	−05 50 48	45.5467	−34.9459	16.7	15.4	1.80	1.58	12.472	11.786	11.615	11.09.2008
												09.05.2007
HE 2157−2125	22 00 25.5	−21 11 23	32.0715	−50.7274	16.8	15.9	1.29	1.02	14.389	13.980	13.742	08.06.2007
												12.09.2008
HE 2211−0605	22 13 53.5	−05 51 06	55.3066	−46.9505	16.0	15.1	1.21	1.01	13.383	12.875	12.727	24.07.2008
HE 2213−0017	22 15 37.1	−00 02 59	62.3019	−43.8276	16.4	14.6	2.38	2.52	10.860	9.832	9.351	24.07.2008
												27.05.2007
HE 2216−0202	22 18 47.5	−01 47 36	61.0859	−45.5370	17.2	16.4	1.01	0.43	14.571	14.165	14.028	06.12.2008

Table 3.1 – continued from previous page

Star	RA (2000)[a] hh mm ss	DEC (2000)[a] dd mm ss	l	b	B_J^a	V^a	$B-V^a$	$U-B^a$	J	H	K	Dt of Obs
												11.09.1008
												24.07.2009
HE 2222−2337	22 25 38.8	−23 22 44	31.2015	−56.9371	17.1	15.7	1.93	1.84	13.535	12.837	12.664	12.09.2008
HE 2228−0137	22 31 26.2	−01 21 42	64.4957	−47.7030	15.8	14.7	1.56	1.20	12.301	11.715	11.589	11.09.2008
												25.07.2009
HE 2246−1312	22 49 26.4	−12 56 35	53.2930	−58.1569	17.0	15.9	1.56	1.60	14.101	13.472	13.303	11.09.2008
												25.07.2008
HE 2255−1724	22 58 06.8	−17 08 19	47.9045	−62.0030	16.1	15.1	1.45	1.05	12.931	12.374	12.310	11.09.2008
												25.07.2008
HE 2305−1427	23 08 10.9	−14 11 27	55.9986	−62.6875	16.4	15.3	1.41	0.80	13.269	12.762	12.744	25.07.2008
												10.10.2008
HE 2334−1723	23 37 03.7	−17 06 34	59.3241	−70.1108	16.1	15.1	1.38	1.48	13.583	13.119	12.977	10.10.2008
												25.07.2008
HE 2347−0658	23 49 56.3	−06 41 55	84.5844	−64.8865	16.9	16.0	1.30	0.69	14.568	14.145	14.158	11.09.2008
												24.07.2008
HE 2353−2314	23 55 44.0	−22 58 09	48.1281	−76.7257	16.5	15.2	1.82	1.53	13.064	12.403	12.199	25.07.2008

[a] From Christlieb et al. (2001)

Table 3.2: HE stars without prominent C_2 molecular bands observed during 2007 – 2009

Star	RA (2000)[a] hh mm ss	DEC (2000)[a] dd mm ss	l	b	B_J^a	V^a	B−V[a]	U−B[a]	J	H	K		Dt of Obs
HE 0201−0327	02 03 49.0	−03 13 05	161.9430	−60.4861	14.1	13.4	1.02	0.95	11.671	11.223	11.099	CH	05.10.2012
HE 0417−0513	04 19 46.8	−05 06 17	198.6595	−35.8232	14.6	13.7	1.31	1.21	11.169	10.524	10.386	CH	20.12.2012
HE 0419+0124	04 21 40.4	+01 31 46	192.1715	−31.9177	15.7	13.0	1.44	1.37	10.910	10.342	10.158	CH	05.10.2012
HE 0422−2518	04 24 38.5	−25 12 10	223.2761	−42.4854	13.9	–	–	–	–	–	–	CH, CN	22.11.2008
HE 0443−2523	04 45 17.7	−25 17 48	224.9946	−38.0024	13.8	–	–	–	10.704	10.169	10.012	CH, CN	06.12.2008
HE 0926−0417	09 29 10.3	−04 30 44	237.9142	31.8488	14.1	13.3	1.20	1.09	11.631	11.107	10.999	CH	19.12.2012
HE 1033−0059	10 36 34.0	+00 43 39	246.4726	48.2458	12.9	13.0	1.10	1.29	10.709	10.138	9.951	CH, CN	09.04.2007
HE 1036−2615	10 38 25.9	−26 30 50	269.3336	27.5445	14.6	13.7	1.21	1.49	–	–	–	CH, CN	17.01.2009
HE 1037−2644	10 40 02.3	−27 00 36	269.9776	27.3253	14.3	13.4	1.33	1.38	11.360	10.776	10.662	CH, CN	06.02.2009
HE 1105−2736	11 07 44.7	−27 52 35	276.5372	29.6271	14.1	13.2	1.30	1.23	11.314	10.742	10.551	CH, CN	17.03.2009
HE 1112−2557	11 15 14.1	−26 13 28	277.4416	31.8419	14.5	13.6	1.29	1.45	11.548	11.006	10.849	CH, CN	06.05.2009
HE 1150−2546	11 53 15.5	−26 03 41	286.9462	34.9979	15.6	–	–	–	–	–	–		18.03.2009
HE 1152−2432	11 54 35.0	−24 48 44	286.8824	36.2813	–	–	–	–	9.413	8.833	8.686	CH, CN	18.03.2009
HE 1229−1857	12 31 46.8	−19 14 02	296.5412	43.3938	14.6	14.0	0.85	0.73	12.124	11.569	11.459	CH, CN	04.04.2009
HE 1236−0036	12 39 25.4	−00 52 58	296.5586	61.8402	16.5	13.5	0.92	0.94	11.679	11.176	11.104	CH, CN	08.05.2007
HE 1406−2016	14 09 44.1	−20 30 57	326.6476	38.7233	15.1	14.2	1.28	1.22	12.092	11.558	11.423	CH, CN	16.03.2009
HE 1420−1659	14 23 03.1	−17 12 51	332.7845	39.8992	13.1	–	–	–	9.871	9.226	9.067	CH, CN	18.01.2009
HE 2115−0709	21 17 42.1	−06 57 11	44.4121	−35.5571	15.1	16.2	1.68	1.70	12.673	12.000	11.808	CH, CN	07.06.2007
HE 2124−0408	21 27 06.8	−03 55 22	49.0907	−36.0859	14.8	13.9	1.26	1.15	11.578	10.986	10.848	CH, CN	24.07.2008
HE 2319−1534	23 22 11.1	−15 18 16	58.0867	−66.1356	15.3	13.8	2.09	2.16	10.866	9.937	9.367	CH,CN	19.12.2012
HE 2331−1329	23 33 44.5	−13 12 34	66.5535	−67.120	16.2	14.5	2.29	2.19	11.841	10.990	10.652	CH,CN	20.12.2012

[a] From Christlieb et al. (2001)

Table 3.3: Potential CH star candidates

Star	RA (2000)[a] hh mm ss	DEC (2000)[a] dd mm ss	l	b	B_J^a	V^a	$B-V^a$	$U-B^a$	J	H	K	Dt of Obs
HE 0008−1712	00 11 19.2	−16 55 34	78.5866	−76.2106	16.5	15.2	1.78	1.64	13.630	13.069	12.975	06.12.2008
												11.09.2008
HE 0052−0543	00 55 00.0	−05 27 02	125.3316	−68.3057	16.5	15.0	1.95	1.74	12.952	12.241	12.086	12.09.2008
HE 0100−1619	01 02 41.6	−16 03 01	136.7651	−78.6185	15.9	14.7	1.54	1.28	13.114	12.537	12.476	21.11.2008
												12.09.2008
HE 0136−1831	01 39 01.8	−18 16 43	176.4932	−75.9157	16.9	15.6	1.72	1.43	14.216	13.679	13.532	12.09.2008
HE 0225−0546	02 28 19.4	−05 32 58	174.1738	−58.4222	16.5	15.2	1.79	1.51	13.347	12.707	12.528	06.12.2008
HE 0237−0835	02 40 13.6	−08 22 18	181.9346	−58.1620	16.8	15.6	1.67	1.42	13.706	13.136	12.987	19.12.2012
HE 0420−1037	04 22 47.0	−10 30 26	205.0454	−37.7176	15.2	14.7	1.38	0.99	12.341	11.815	11.695	21.11.2008
HE 0507−1430	05 10 07.6	−14 26 32	215.0951	−28.8440	13.2	14.4	1.66	1.40	12.325	11.717	11.575	20.12.2012
HE 1027−2501	10 29 29.5	−25 17 16	266.6832	27.4163	13.9	12.7	1.73	1.51	10.627	9.896	9.722	22.11.2008
HE 1045−1434	10 47 44.1	−14 50 23	263.5905	38.4049	15.5	14.6	1.23	0.96	12.935	12.449	12.244	09.04.2007
HE 1051−0112	10 53 58.8	−01 28 15	253.5294	49.7900	17.0	16.0	1.44	0.94	14.347	13.794	13.703	06.12.2008
HE 1102−2142	11 04 31.2	−21 58 29	272.5241	34.5071	16.0	14.9	1.44	0.98	13.275	12.714	12.601	16.03.2009
HE 1110−0153	11 13 02.7	−02 09 28	261.1493	52.4883	16.5	15.5	1.47	1.29	12.912	12.205	12.063	04.04.2009
HE 1119−1933	11 21 43.5	−19 49 47	275.7342	38.2583	12.8	14.6	1.34	0.87	13.043	12.571	12.422	18.03.2009
HE 1120−2122	11 23 18.6	−21 38 33	277.1276	36.7743	12.9	–	–	–	9.573	8.902	8.788	17.03.2009
HE 1123−2031	11 26 08.7	−20 48 19	277.4490	37.8097	16.8	15.8	1.33	1.19	13.513	12.940	12.800	18.03.2009
HE 1142−2601	11 44 52.9	−26 18 29	284.8485	34.2157	13.9	13.0	1.28	1.07	11.218	10.675	10.539	04.04.2009
HE 1145−1319	11 48 21.4	−13 36 38	280.3756	46.4800	16.4	15.4	1.37	1.32	13.466	12.934	12.790	17.03.2009
												05.04.2009
HE 1146−0151	11 49 02.3	−02 08 11	273.2807	57.0990	14.9	14.2	0.96	0.97	12.929	12.400	12.262	16.03.2009
HE 1157−1434	12 00 11.5	−14 50 50	284.8854	46.2211	16.1	13.8	1.62	1.41	11.792	11.178	11.019	06.06.2007
												07.06.2007
HE 1205−2539	12 08 08.1	−25 56 38	290.8957	35.9137	13.6	15.4	1.91	1.72	13.313	12.665	12.540	17.03.2009

Table 3.3 – continued from previous page

Star	RA (2000)[a]	DEC (2000)[a]	l	b	B_J^a	V^a	$B-V^a$	$U-B^a$	J	H	K	Dt of Obs
	hh mm ss	dd mm ss										
HE 1210−2636	12 12 59.7	−26 53 22	292.4334	35.1974	13.8	12.6	1.65	1.52	–	–	–	06.05.2009
HE 1228−0417	12 31 12.5	−04 33 40	293.4045	57.9360	14.8	14.0	1.17	0.96	12.406	11.969	11.818	04.04.2009
HE 1253−1859	12 56 38.4	−19 15 32	304.6277	43.5957	13.7	12.9	1.09	1.22	10.60	9.972	9.850	16.03.2009
HE 1318−1657	13 21 19.4	−17 13 40	313.0578	45.0556	13.3	14.4	1.42	1.26	12.509	11.997	11.814	02.06.2010
HE 1331−2558	13 34 20.1	−26 13 38	314.7873	35.6550	13.9	16.0	1.53	1.10	10.998	10.394	10.240	18.03.2009
HE 1400−0229	14 03 12.4	−02 44 16	335.8219	55.4831	16.5	15.5	1.37	0.85	13.456	12.847	12.693	23.05.2010
HE 1404−0846	14 06 55.1	−09 00 58	332.3876	49.4897	15.3	14.2	1.52	1.29	12.435	11.783	11.681	07.06.2007
HE 1405−0346	14 07 58.3	−04 01 03	336.5341	53.7853	14.7	13.5	1.68	1.28	11.608	11.068	10.903	16.03.2009
HE 1410−0125	14 13 24.7	−01 39 54	340.6313	55.0908	–	–	–	–	10.360	9.770	9.651	16.03.2009
												11.06.2008
HE 1431−0755	14 34 32.7	−08 08 37	341.8828	46.7820	14.6	13.5	1.51	1.44	11.283	10.605	10.422	08.05.2007
HE 1432−2138	14 35 47.6	−21 51 37	332.7735	34.8934	17.1	16.3	1.14	0.37	14.402	13.989	13.885	02.06.2010
HE 1440−1511	14 43 07.1	−15 23 48	338.737	39.5765	14.5	13.5	1.13	0.87	12.238	11.757	11.606	09.05.2007
HE 1447+0102	14 50 15.1	+00 50 15	355.2263	51.2262	15.6	15.0	0.90	0.14	13.207	12.760	12.682	08.04.2007
HE 1525−0516	15 27 52.2	−05 27 04	358.1110	40.1019	16.8	15.8	1.29	1.14	13.972	13.479	13.314	11.06.2008
												07.06.2007
HE 2114−0603	21 17 20.8	−05 50 48	45.5467	−34.9459	16.7	15.4	1.80	1.58	12.472	11.786	11.615	11.09.2008
												09.05.2007
HE 2211−0605	22 13 53.5	−05 51 06	55.3066	−46.9505	16.0	15.1	1.21	1.01	13.383	12.875	12.727	24.07.2008
HE 2228−0137	22 31 26.2	−01 21 42	64.4957	−47.7030	15.8	14.7	1.56	1.20	12.301	11.715	11.589	11.09.2008
												25.07.2009
HE 2246−1312	22 49 26.4	−12 56 35	53.2930	−58.1569	17.0	15.9	1.56	1.60	14.101	13.472	13.303	11.09.2008
												25.07.2008

[a] From Christlieb et al. (2001)

3.3.1 Location of the candidate CH stars on (J−H) vs (H−K) plot

We have used JHK photometry as supplementary diagnostics for stellar classification. Figure 3.1 shows the locations of the candidate CH stars listed in Table 3.3 on the (J−H) vs (H−K) plot. 2MASS JHK measurements of the stars are available online at http://www.ipac.caltech.edu/. The thick box on the lower left represents the location of CH stars and the thin box on the upper right represents the location of C−N stars (Totten et al. 2000). Except two lying outside (shown with open squares in Figure 3.1), the locations of the candidate CH stars (shown with open circles) are well within the CH box. This supports their identification with the class of CH stars. Location of the comparison CH stars HD 26, HD 5223 and HD 209621, C−R star RV Sct, C−N stars V460 Cyg and Z PSc, are shown by solid squares on the (J−H) vs (H−K) plot.

3.3.2 Effective temperatures of the programme stars

As described in section 2.4.10, we have used 2MASS JHK photometry to determine the effective temperatures of the objects.

Semi empirical temperature calibrations offered by Alonso et al. (1994, 1996, 1998) are used to derive preliminary temperature estimates of the programme stars. These values are listed in Table 3.4.

Table 3.4: Estimated effective temperatures from semi empirical relations, T_{eff} from (J−H), (V−K) and (B−V) for metallicity −0.5, −1.0, −1.5, −2.0, −2.5 from top to bottom

Star	T_{eff} (K) (J−K)	T_{eff} (K) (J−H)	T_{eff} (K) (V−K)	T_{eff} (K) (B−V)
HE 0008−1712	4556.51	4378.94	4770.97	3941.10
		4395.62	4757.96	3857.84
		4412.42	4749.49	3793.67
		4429.36	4745.52	3746.85
		4446.43	4746.02	3716.18
H E0009−1824	5530.27	5377.40	4993.57	5038.84
		5393.67	4982.96	4926.30
		5410.04	4977.31	4844.15
		5426.51	4976.59	4789.60
		5443.08	4980.78	4760.87
HE 0037−0654	5496.71	4912.74	5331.46	4774.22

Table 3.4 – continued from previous page

Star	T_{eff} (K) (J−K)	T_{eff} (K) (J−H)	T_{eff} (K) (V−K)	T_{eff} (K) (B−V)
		4929.47	5325.16	4668.96
		4946.30	5324.49	4591.13
		4963.26	5329.45	4538.21
		4980.33	5340.08	4508.58
HE 0052−0543	3924.81	3831.70	4073.39	3622.64
		3847.73	4054.99	3547.42
		3863.90	4040.00	3488.49
		3880.20	4028.33	3444.39
		3896.64	4019.94	3414.06
H E0100−1619	4615.21	4305.94	4771.83	4121.59
		4322.56	4758.83	4033.68
		4339.32	4750.37	3966.54
		4356.21	4746.41	3918.28
		4373.23	4746.92	3887.60
HE 0136−1831	4459.39	4493.10	4957.87	3941.10
		4509.84	4946.85	3857.84
		4526.71	4940.73	3793.67
		4543.70	4939.46	3746.85
		4560.81	4943.03	3716.19
HE 0217+0056	2794.61	3053.31	2825.70	3350.55
		3067.42	2805.35	3282.04
		3081.66	2786.83	3227.60
		3096.03	2770.08	3185.98
		3110.53	2755.03	3156.25
HE 0225−0546	4051.68	4086.82	4299.33	3941.10
		4103.22	4282.32	3857.84
		4119.76	4269.07	3793.67
		4136.44	4259.49	3746.85
		4153.25	4253.55	3716.18
HE 0228−0256	3655.89	3916.81	3855.61	3622.64
		3932.98	3836.19	3547.42

Table 3.4 – continued from previous page

Star	T_{eff} (K) (J−K)	T_{eff} (K) (J−H)	T_{eff} (K) (V−K)	T_{eff} (K) (B−V)
		3949.28	3819.85	3488.49
		3965.72	3806.53	3444.39
		3982.30	3796.15	3414.05
HE 0420−1037	4587.42	4534.65	3990.16	6037.74
		4551.40	3971.34	5896.46
		4568.28	3955.79	5798.10
		4585.29	3943.45	5738.69
		4602.42	3934.26	5715.91
HE 1011−0942	3417.52	3646.14	3210.10	4121.59
		3661.82	3189.36	4033.68
		3677.63	3170.88	3966.54
		3693.58	3154.58	3918.28
		3709.66	3140.41	3887.60
HE 1015−2050	5262.83	6529.13	5305.13	6037.74
		6542.25	5298.47	5896.46
		6555.41	5297.38	5798.10
		6568.63	5301.87	5738.69
		6581.90	5311.95	5715.91
HE 1027−2501	8484.79	8338.23	–	4121.59
		8340.33	–	4033.68
		8342.43	–	3966.54
		8344.53	–	3918.28
		8346.63	–	3887.60
HE 1037−2644	–	–	–	4774.22
		–	–	4668.96
		–	–	4591.12
		–	–	4538.21
		–	–	4508.57
HE 1045−1434	4436.49	4738.21	4624.39	4774.22
		4754.98	4609.98	4668.96
		4771.88	4599.85	4591.13

Table 3.4 – continued from previous page

Star	T_{eff} (K) (J−K)	T_{eff} (K) (J−H)	T_{eff} (K) (V−K)	T_{eff} (K) (B−V)
		4788.89	4593.96	4538.21
		4806.03	4592.25	4508.58
HE 1051−0112	4594.34	4411.69	4689.00	4535.43
		4428.39	4675.19	4436.62
		4445.22	4665.77	4362.69
		4462.17	4660.71	4311.38
		4479.26	4659.95	4281.16
HE 1102−2142	4492.47	4383.27	4687.26	4318.88
		4399.95	4673.43	4225.81
		4416.76	4664.00	4155.43
		4433.70	4658.91	4105.67
		4450.77	4658.13	4075.13
HE 1104−1442	4260.54	4037.36	4766.79	–
		4053.71	4753.73	–
		4070.18	4745.22	–
		4086.79	4741.19	–
		4103.54	4741.62	–
HE 1110−0153	3969.89	3842.74	3643.12	4535.43
		3858.79	3622.98	4436.62
		3874.97	3605.64	4362.69
		3891.29	3591.02	4311.38
		3907.75	3579.06	4281.16
HE 1116−1628	4224.43	4125.85	3895.27	4535.43
		4142.30	3876.01	4436.62
		4158.89	3859.89	4362.69
		4175.61	3846.84	4311.38
		4192.46	3836.80	4281.16
HE 1119−1933	4675.25	4790.28	4824.99	–
		4807.05	4812.53	–
		4823.93	4804.71	–
		4840.94	4801.49	–

Table 3.4 – continued from previous page

Star	T_{eff} (K) (J−K)	T_{eff} (K) (J−H)	T_{eff} (K) (V−K)	T_{eff} (K) (B−V)
		4858.06	4802.85	–
HE 1120−2122	4148.01	3961.56	–	–
		3977.80	–	–
		3994.17	–	–
		4010.68	–	–
		4027.32	–	–
HE 1123−2031	4365.86	4339.84	3995.37	4535.44
		4356.50	3976.57	4436.62
		4373.28	3961.06	4362.69
		4390.19	3948.76	4311.38
		4407.23	3939.62	4281.17
HE 1127−0604	4875.50	4604.60	5203.67	4774.22
		4621.37	5195.65	4668.96
		4638.26	5192.99	4591.13
		4655.28	5195.70	4538.21
		4672.42	5203.77	4508.58
HE 1142−2601	–	–	–	4774.22
		–	–	4668.96
		–	–	4591.13
		–	–	4538.21
		–	–	4508.58
HE 1146−0151	4515.88	4525.81	5120.79	5333.73
		4542.56	5111.71	5212.91
		4559.44	5107.84	5125.96
		4576.44	5109.15	5069.76
		4593.57	5115.64	5042.37
HE 1157−1434	4182.98	4181.08	4194.24	–
		4197.59	4176.55	–
		4214.24	4162.44	–
		4231.02	4151.85	–
		4247.93	4144.71	–

Table 3.4 – continued from previous page

Star	T_{eff} (K) (J−K)	T_{eff} (K) (J−H)	T_{eff} (K) (V−K)	T_{eff} (K) (B−V)
HE 1205−0521	4650.36	4927.12	4373.76	5038.84
		4943.84	4357.29	4926.30
		4960.67	4344.68	4844.15
		4977.61	4335.88	4789.60
		4994.67	4330.83	4760.87
HE 1210−2636	–	–	–	4121.59
		–	–	4033.68
		–	–	3966.54
		–	–	3918.28
		–	–	3887.60
HE 1228−0417	4795.85	4964.09	4819.73	5038.84
		4980.79	4807.22	4926.30
		4997.59	4799.34	4844.15
		5014.52	4796.04	4789.60
		5031.55	4797.31	4760.87
HE 1230−0327	4814.60	4846.74	5040.33	–
		4863.49	5030.27	–
		4880.35	5025.26	–
		4897.34	5025.27	–
		4914.44	5030.29	–
HE 1238−0836	3521.23	3954.13	–	–
		3970.35	–	–
		3986.72	–	–
		4003.21	–	–
		4019.85	–	–
HE 1253−1859	4239.41	4104.99	3952.74	5038.84
		4121.42	3933.74	4926.30
		4137.98	3917.96	4844.15
		4154.68	3905.33	4789.60
		4171.51	3895.80	4760.87
HE 1315−2035	4639.76	4949.26	4315.21	4535.43

Table 3.4 – continued from previous page

Star	T_{eff} (K) (J−K)	T_{eff} (K) (J−H)	T_{eff} (K) (V−K)	T_{eff} (K) (B−V)
		4965.96	4298.31	4436.62
		4982.78	4285.20	4362.69
		4999.71	4275.78	4311.38
		5016.76	4270.02	4281.16
HE 1331−2558	4227.41	4218.84	2380.29	–
		4235.39	2361.42	–
		4252.07	2343.93	–
		4268.89	2327.77	–
		4285.84	2312.90	–
HE 1344−0411	3118.34	3414.55	3001.50	3775.37
		3429.69	2980.86	3696.32
		3444.97	2962.25	3634.87
		3460.38	2945.59	3589.44
		3475.93	2930.81	3558.90
HE 1358−2508	–	–	–	4774.22
		–	–	4668.96
		–	–	4591.13
		–	–	4538.21
		–	–	4508.58
HE 1400−1113	4894.81	5010.94	5136.86	5038.84
		5027.60	5127.98	4926.30
		5044.38	5124.34	4844.15
		5061.27	5125.91	4789.60
		5078.27	5132.71	4760.87
HE 1404−0846	4239.41	4027.25	4452.00	4318.88
		4043.58	4436.13	4225.81
		4060.05	4424.25	4155.43
		4076.64	4416.30	4105.67
		4093.38	4412.24	4075.13
HE 1405−0346	4391.31	4484.40	4371.89	4121.59
		4501.13	4355.41	4033.68

Table 3.4 – continued from previous page

Star	T_{eff} (K) (J−K)	T_{eff} (K) (J−H)	T_{eff} (K) (V−K)	T_{eff} (K) (B−V)
		4517.99	4342.79	3966.54
		4534.98	4333.96	3918.28
		4552.09	4328.89	3887.60
HE 1410−0125	4378.56	4266.53	–	–
		4283.12	–	–
		4299.85	–	–
		4316.70	–	–
		4333.69	–	–
HE 1428−1950	4505.82	4573.18	–	–
		4589.94	–	–
		4606.83	–	–
		4623.84	–	–
		4640.98	–	–
HE 1429−1411	3057.76	3302.55	–	3775.37
		3317.39	–	3696.32
		3332.37	–	3634.87
		3347.49	–	3589.44
		3362.74	–	3558.90
HE 1430−0919	4700.39	4625.81	5119.78	4318.88
		4642.58	5110.69	4225.81
		4659.48	5106.80	4155.43
		4676.50	5108.09	4105.67
		4693.64	5114.56	4075.13
HE 1431−0755	3937.98	3950.23	3930.24	4318.88
		3966.45	3911.13	4225.81
		3982.81	3895.22	4155.43
		3999.30	3882.42	4105.67
		4015.93	3872.68	4075.13
HE 1432−2138	5074.95	5075.25	4557.66	5038.84
		5091.87	4542.66	4926.30
		5108.60	4531.83	4844.15

Table 3.4 – continued from previous page

Star	T_{eff} (K) (J−K)	T_{eff} (K) (J−H)	T_{eff} (K) (V−K)	T_{eff} (K) (B−V)
		5125.43	4525.11	4789.60
		5142.38	4522.47	4760.87
HE 1440−1511	4636.24	4747.85	4806.48	5038.84
		4764.62	4793.83	4926.30
		4781.51	4785.79	4844.15
		4798.53	4782.31	4789.60
		4815.66	4783.37	4760.87
HE 2114−0603	3948.57	3919.97	3395.16	3941.10
		3936.14	3374.54	3857.84
		3952.45	3356.40	3793.67
		3968.90	3340.66	3746.85
		3985.48	3327.27	3716.18
HE 2157−2125	4583.97	5135.81	4848.98	4774.22
		5152.37	4836.77	4668.96
		5169.04	4829.25	4591.13
		5185.82	4826.37	4538.21
		5202.71	4828.12	4508.58
HE 2211−0605	4553.10	4621.90	4605.25	4774.22
		4638.67	4590.67	4668.96
		4655.57	4580.34	4591.13
		4672.59	4574.20	4538.21
		4689.73	4572.22	4508.58
HE 2213−0017	2701.10	3005.84	2597.34	3228.85
		3019.80	2577.62	3163.29
		3033.88	2559.49	3110.86
		3048.10	2542.89	3070.40
		3062.45	2527.78	3041.04
HE 2216−0202	4969.46	5122.16	4604.51	5038.84
		5138.74	4589.92	4926.30
		5155.42	4579.58	4844.15
		5172.21	4573.44	4789.60

Table 3.4 – continued from previous page

Star	T_{eff} (K) (J−K)	T_{eff} (K) (J−H)	T_{eff} (K) (V−K)	T_{eff} (K) (B−V)
		5189.12	4571.45	4760.87
HE 2222−2337	3911.73	3879.01	3966.25	3775.36
		3895.12	3947.31	3696.31
		3911.36	3931.61	3634.87
		3927.74	3919.09	3589.44
		3944.26	3909.67	3558.89
HE 2228−0137	4369.03	4284.05	3900.54	4318.88
		4300.66	3881.31	4225.81
		4317.40	3865.22	4155.43
		4334.27	3852.21	4105.67
		4351.28	3842.21	4075.13
HE 2246−1312	4110.70	4125.95	4373.28	4318.88
		4142.40	4356.81	4225.81
		4158.99	4344.20	4155.43
		4175.70	4335.39	4105.67
		4192.56	4330.33	4075.13
HE 2255−1724	4675.26	4388.73	4183.68	4535.43
		4405.42	4165.93	4436.62
		4422.23	4151.74	4362.69
		4439.18	4141.05	4311.38
		4456.25	4133.80	4281.16
HE 2305−1427	5042.06	4594.23	4410.60	4318.88
		4611.00	4394.41	4225.81
		4627.89	4382.14	4155.43
		4644.91	4373.74	4105.67
		4662.05	4369.15	4075.13
HE 2334−1723	4729.39	4827.13	4889.88	4535.43
		4843.89	4878.12	4436.62
		4860.76	4871.11	4362.69
		4877.75	4868.82	4311.38
		4894.87	4871.24	4281.16

Table 3.4 – continued from previous page

Star	T_{eff} (K) (J−K)	T_{eff} (K) (J−H)	T_{eff} (K) (V−K)	T_{eff} (K) (B−V)
HE 2347−0658	5554.47	4989.70	5241.78	4774.22
		5006.38	5234.26	4668.96
		5023.17	5232.18	4591.13
		5040.08	5235.54	4538.21
		5057.10	5244.36	4508.58
HE 2353−2314	3927.45	4014.92	3996.47	3941.10
		4031.24	3977.67	3857.84
		4047.68	3962.17	3793.67
		4064.26	3949.88	3746.85
		4080.98	3940.74	3716.18

3.3.3 Isotopic ratio $^{12}C/^{13}C$ from molecular band depths

Carbon isotopic ratios $^{12}C/^{13}C$, widely used as mixing diagnostics provide an important probe of stellar evolution. These ratios measured on low resoltuion spectra do not give accurate results but provide a fair indication of evolutionary states of the objects.

We have estimated these ratios, whenever possible, using the molecular band depths of (1,0) $^{12}C^{12}C$ λ4737 and (1,0) $^{12}C^{13}C$ λ4744. For a majority of the candidate CH stars, the ratios $^{12}C/^{13}C$ are found to be ≤ 10. These ratios for HD 26, HD 5223 and HD 209621 are respectively 5.9, 6.1 and 8.8 (Goswami 2005).

Our estimated ratios of $^{12}C/^{13}C$ indicate that most of the candidate CH stars belong to the 'early−type' category. Low isotopic ratios (≤ 30) are typical of stars on their first ascent of the giant branch (section 1.7).

3.4 Spectral characteristics of the candidate CH stars

The spectra for the comparison stars obtained from the same observational set up are shown in Figure 3.2. In Figure 3.3 we show one example of HE stars spectra from the present sample corresponding to each comparison star's spectrum in Figure 3.2. **HE 0037−0654, 0420−1037, 1102−2142, 1142−2601, 1146−0151, 1210−2636, 1253−1859, 1447+0102.**

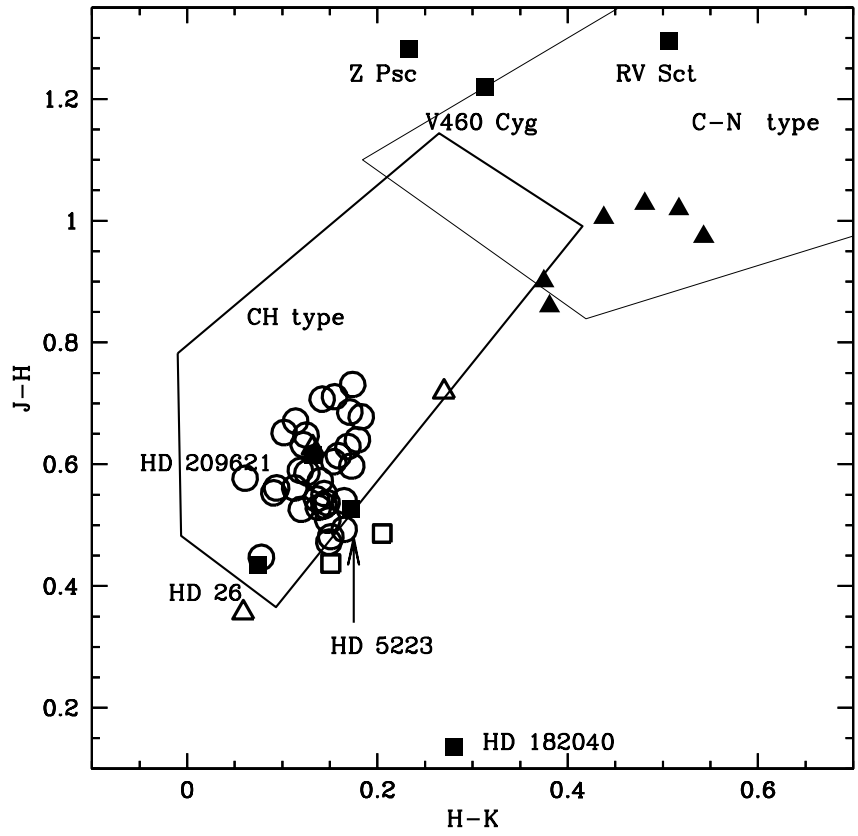

Figure 3.1: A two colour J−H versus H−K diagram of the candidate CH stars. The thick box on the lower left represents the location of CH stars and the thin box on the upper right represents the location of C−N stars (Totten et al. 2000). Majority of the candidate CH stars listed in Table 3.3 (represented by open circles) fall well within the CH box. The positions of the two outliers are shown with open squares. C−N stars found in our sample are represented by solid triangles. The location of the comparison stars are labeled and marked with solid squares. Location of the three dwarf carbon stars are indicated by open triangles.

The spectra of these objects resemble closely the spectrum of HD 26. HD 26 is a known classical CH star with effective temperature 5170 K and log g = 2.2 (Vanture 1992b). The temperatures of these objects as measured using JHK photometric data range from 4200 to 5000 K. The locations of these objects are well within the CH box in Figure 3.1. In Figure 3.4, we show as an example, a comparison of the spectra of three objects HE 0420−1037, HE 1142−2601 and HE 1146−0151 with the spectrum of HD 26.

With marginal differences in the strengths of the molecular features, the spectra of these three objects show more or less a good match with their counterparts in HD 26. The

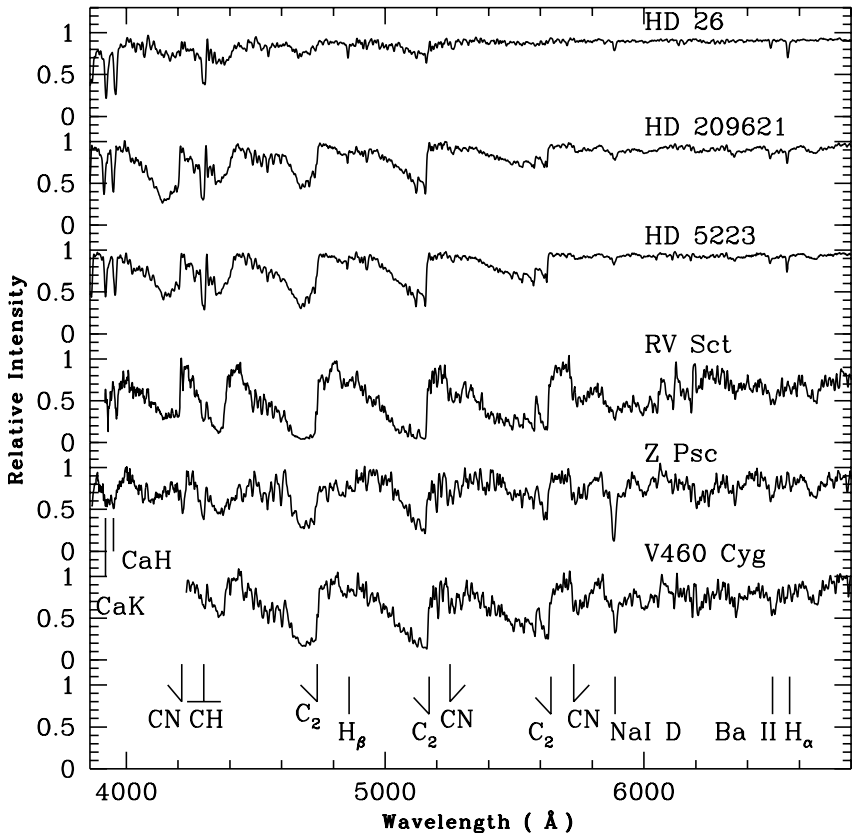

Figure 3.2: The spectra of the comparison stars in the wavelength region 3860 – 6800 Å. Prominent features seen on the spectra are indicated.

CN band around 4215 Å and the C_2 band around 5165 Å in the spectra of HE 0420−1037 and HE 1146−0151 are marginally stronger; the Na I D feature also appears stronger. The features due to Ca K and H appear with similar strengths. In the spectrum of HE 1142−2601, the CN band depth around 4215 Å and Ca II K and H line depths are deeper than their counterparts in HD 26. The Ca I line at 4226 Å is detected with line depth weaker than the band depth around 4215 Å. In HD 26, the Ca I 4226 Å feature is not detected. The object HE 1253−1859 also have very similar spectrum with that of HD 26. The CN band around 4215 Å and carbon isotopic band around 4730 Å are stronger, but the CH band, Ca II K and H features are of similar strengths. The molecular bands around 5165 Å and 5635 Å show an exact match. The lines due to Na I D, Ba II at 6496 Å and H_α are seen equally strongly as in HD 26. The Ca I feature at 4226 Å could not be detected and the secondary P-branch head around 4342 Å seems to be marginally weaker. In the spectrum of HE 1102−2142 the molecular C_2 bands around

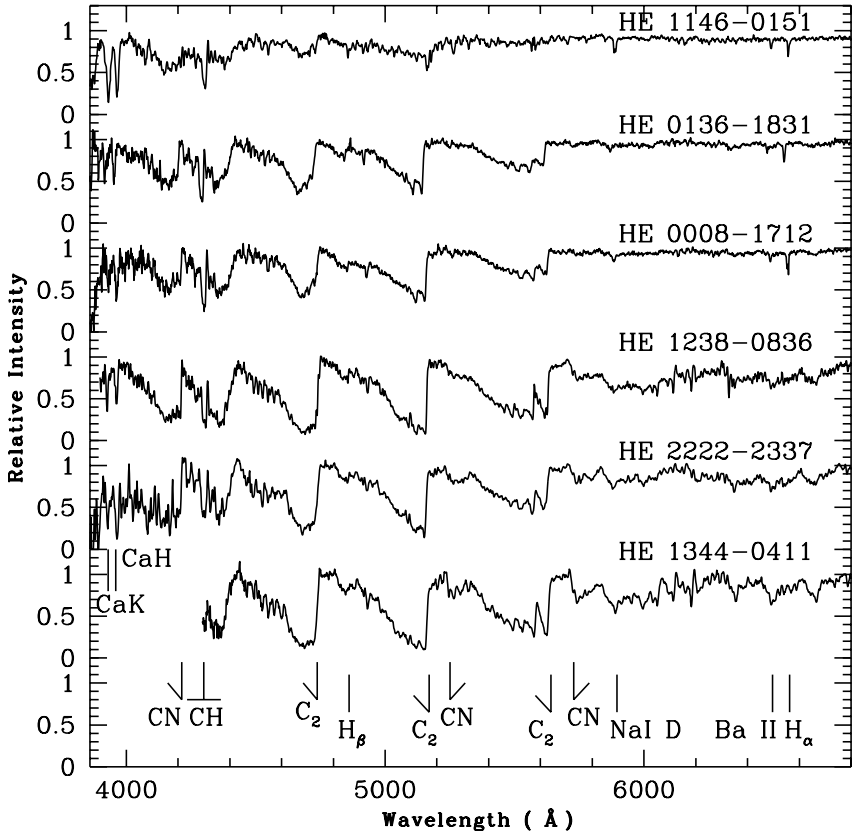

Figure 3.3: An example of each of the HE stars corresponding to the comparison stars presented in Figure 3.2, in the top to bottom sequence, in the wavelength region 3860 – 6800 Å. The locations of the prominent features seen in the spectra are marked on the figure.

4735, 5165 and 5635 Å are slightly deeper than those in HD 26. The CN band around 4215 Å and the CH band around 4310 Å also appear marginally stronger in the spectrum of HE 1102−2142. The H_α feature and the Ba II line at 6496 Å are marginally weaker; the feature due to Na I D appears with similar strength as in HD 26. H_β at 4856, is clearly seen. The Ca I line at 4226 Å is weakly detected. In the spectrum of HE 1210−2636, the CN band around 4215 Å and the secondary P-branch head around 4342 Å appear slightly stronger than in HD 26. The C_2 molecular band around 5165 Å is also slightly weaker. The carbon isotopic band around 4733 Å is marginally detectable. Ca I line at 4226 Å could not be detected. Features due to Ca II K and H and H_α are clearly detected. In the spectrum of HE 1447+0102, the CN band around 4215 Å is almost absent. Strong well defined features due to Ca II K and H are seen. Molecular bands around 4733, 5165, and 5635 Å are distinctly seen to be stronger than their counterparts in HD 26. In the redward

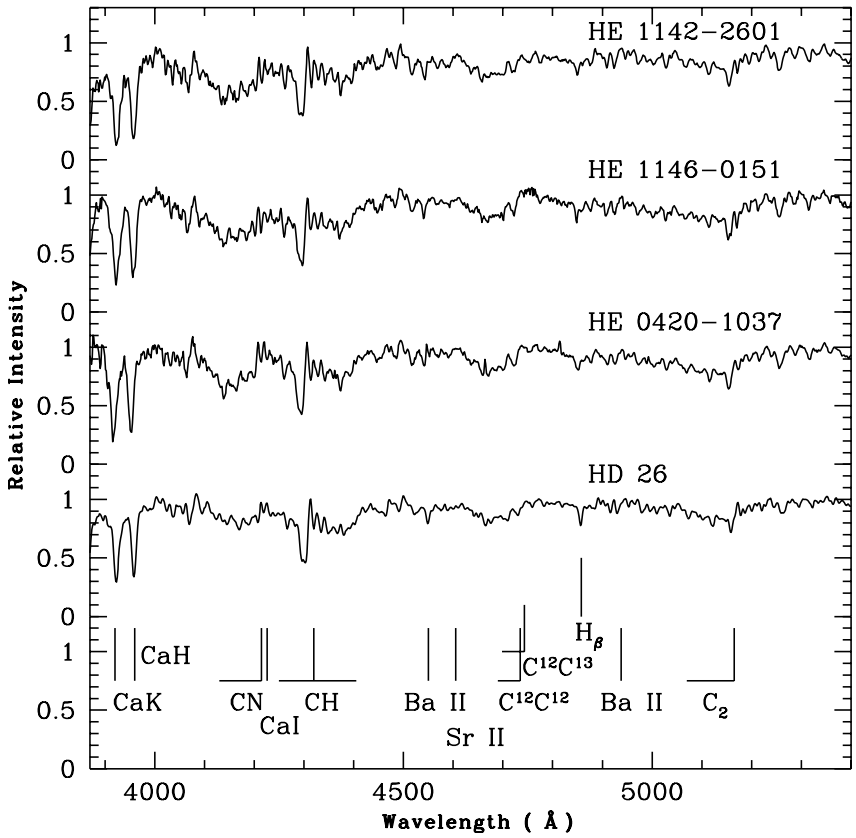

Figure 3.4: A comparison of the spectra of three HE stars in the wavelength region 3870 − 5400 Å with the spectrum of the comparison star HD 26. Prominent features noticed in the spectra are marked on the figure.

of 5700 Å no molecular bands are detected. We assign these objects to the CH group.

HE 0037−0654, 2216−0202

The spectrum of HE 0037−0654 looks very similar to the spectrum of HD 26; however, molecular bands of C_2 around 4730, 5165 and 5635 Å are marginally stronger than their counterparts in HD 26. The CN band around 4215 Å is barely detected, much weaker than in HD 26. Ba II line at 6496 Å is clearly detected. Strong lines of H_α and Na I D are distinctly noticed. Except for the features of Ca II K and H which are much weaker, the spectrum of HE 2216−0202 is very similar to the spectrum of HD 26. The secondary P-branch head around 4342 Å is much stronger than in HD 26. The CN band around 4215 Å is not observed. The CH band at 4305 Å is not as strong as in HD 26. The molecular bands around 4733 Å and 5236 Å are of similar depths. The carbon molecular band around 5635 Å is weaker than the band around 5165 Å. No molecular bands longward of

5700 Å are detectable.

HE 0136−1831, 1027−2501, 1051−0112, 1119−1933, 1120−2122, 1123−2031, 1145−1319, 1205−2539, 1331−2558, 1404−0846, 1525−0516, 2114−0603, 2211−0605, 2228−0137, 2246−1312.

The spectra of these objects resemble closely the spectrum of HD 209621, a classical CH star with effective temperature ∼ 4400 K (Tsuji et al. 1991). The effective temperatures estimated for this set of objects using JHK photometry range from 3948 K (HE 2114−0603) to 4675 K (HE 1119−1933). Their locations on the J−H vs H−K plot are well within the CH box in Figure 3.1. Three examples, HE 0136−1831, HE 1027−2501 and HE 2228−0137 from this set are shown in Figure 3.5 together with the spectrum of HD 209621. In the spectrum of HE 0136−1831, the CN band around 4215 Å is marginally weaker and the carbon molecular bands around 4733 and 5635 Å are marginally stronger than those in HD 209621. All other features show a good match. The spectrum of HE 1027−2501 also shows a close match with the spectrum of HD 209621. Except for the molecular bands around 4733, 5165 and 5635 Å that appear marginally weaker in the spectrum of HE 2228−0137 the spectrum of this object bears a close resemblance with the spectrum of HD 209621. The spectrum of HE 1051−0112 shows a weaker CN band around 4215 Å. The G-band of CH appears with almost the same strength as in HD 209621. The secondary P-branch head around 4342 Å and the bands around 4730 and 5635 Å are relatively stronger. Features due to Ca II K and H are barely detectable in the spectrum of this object. The molecular band around 5165 Å shows an exact match with its counterpart in HD 209621. The features due to H_α and Na I D are detected distinctly; the Ba II feature at 6496 Å is marginally detected.

In the spectrum of HE 1119−1933, Ca II K and H appear marginally stronger. The molecular band around 5365, appears marginally weaker than in HD 209621. The spectra of HE 1120−2122 and HE 1123−2031 are very similar, both exhibit a weaker CN band around 4215 Å. All other features show a good match with their counterparts in the spectrum of HD 209621. Ca II K and H appear with almost the same strength in the spectrum of HE 1120−2122 as in HD 209621. Ca I line at 4226 Å is not detectable. The spectra of HE 1123−2031, HE 1145−1319, HE 1205−2539, HE 1331−2558 are noisy shortward of 4100 Å and the lines due to Ca II K and H could not be clearly detected. Ca I line at 4226 Å is not detectable in these spectra. Features due to Na I D, H_α, and Ba II at 6496 Å are detected. In the spectrum of HE 1145−1319, C_2 molecular bands around 5635 and 4733 Å are marginally deeper than those in HD 209621. The features redward of 4200 Å in the spectrum of HE 1205−2539 show a good match with those in

HD 209621. The molecular features in the spectrum of HE 1331−2558 are also of similar strengths with those in HD 209621. Except for the G-band of CH, all other molecular features are weaker in the spectrum of HE 1404−0846. The features due to Ca II K and H are marginally stronger. The spectrum of HE 1404−0846 is noisy at the blue end. In the spectrum of HE 1525−0516, H_α and Na I D features are detected with almost equal strength as in HD 209621. The spectrum of HE 2114−0603 shows a remarkably close match with the features in HD 209621 including those longward of 5700 Å. However the features due to Ca II K and H that are seen very distinctly in the spectrum of HD 209621 could not be detected in the spectrum of HE 2114−0603; the spectrum is noisy blueward of 4000 Å. In the spectrum of HE 2211−0605 the molecular features are weaker than their counterparts in HD 209621 but stronger than those in HD 26. The CH band matches exactly with the one in HD 209621. Ca II K and H appear with almost equal strengths as in HD 209621. The spectrum of HE 2246−1312 shows a weaker molecular band around CN 4215 Å. Other molecular bands appear with almost of equal strengths as their counterparts in HD 209621. The spectrum blueward of 4100 Å is noisy and Ca II K and H features could not be detected as well defined features.

HE 0954+0137, 1230−0327, 1315−2035, 1400−1113, 1430−0919, 1447−0102, 2157−2125, 2216−0202, 2255−1724, 2305−1427, 2334−1723, 2347−0658, 2353−2314. The spectra of these objects are characterized by a weak (or absent) CN band around 4215 Å. Apart from this feature the spectra are somewhat similar to the spectrum of HD 209621.

The spectrum of HE 1230−0327 shows a strong G-band of CH and a distinct secondary P-branch head near 4342 Å. Ca I feature at 4226 Å is not detected. The CN band around 4215 Å is almost absent. While atomic lines of Ca II K, H , H_α, Na I D are distinctly seen, Ba II line at 6496 Å is marginally detected. The spectra of HE 0954+0137, HE 1400−1113, HE 1430−0919, HE 2255−1724 and HE 2347−0658 look very similar to the spectrum of HE 1230−0327. In the spectra of these objects the feature due to the CN band around 4215 Å is marginally detectable. Weak molecular bands noticed in the spectrum of HD 209621 upward of 5700 Å are not observable in these spectra. Compared to HD 209621, the molecular bands around 4733, 5165, and 5635 Å are slightly weaker in the spectra of these objects. Ca II K and H are detected almost with equal strength as in HD 209621. In the spectrum of HE 1430−0919 the secondary P-branch head near 4342 Å is marginally weaker than in HD 209621. While the molecular band around 5165 Å shows a good match, the bands around 4733 and 5635 Å are marginally stronger. The spectrum in the redward of 5700 Å resembles the spectrum of HD 209621. Features due

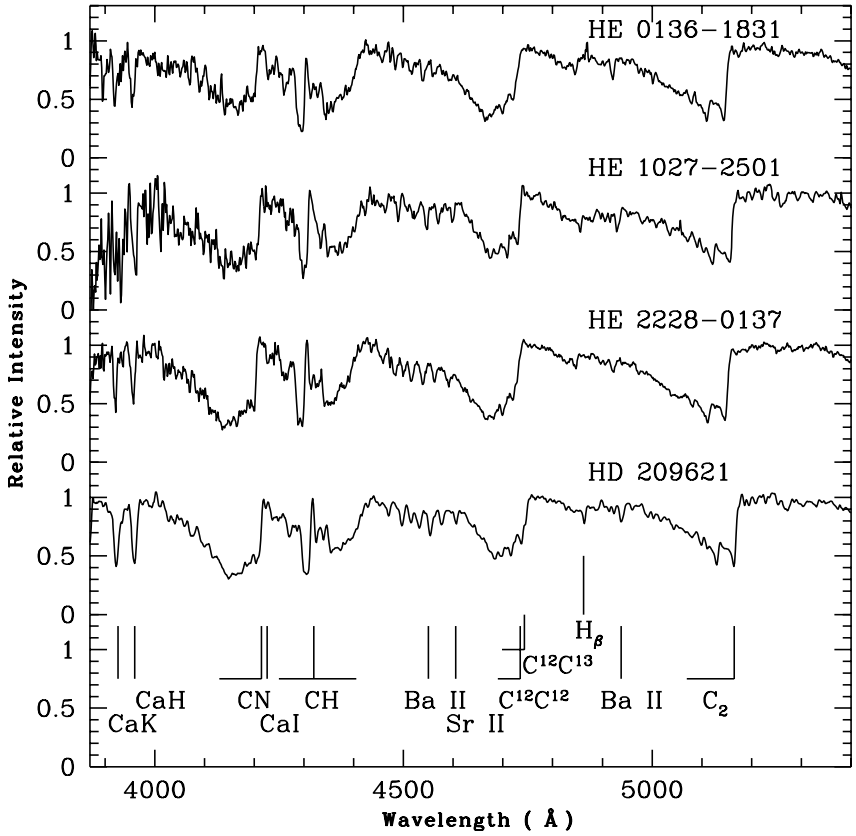

Figure 3.5: A comparison of the spectra of three HE stars in the wavelength region 3870 – 5400 Å with the spectrum of the comparison star HD 209621. Prominent features noticed in the spectra are marked on the figure.

to Na I D, H_α and Ba II line at 6496 Å are detected. In the spectrum of HE 1447+0102, the CN band around 4215 Å is almost absent. Strong well defined features of Ca II K and H are seen. The C_2 molecular bands around 4733, 5165, 5635 Å are distinctly present. No other molecular bands are noticed longward of 5700 Å. The spectra of HE 2305−1427 and HE 2334−1723 show the CN band around 4215 Å with band depth almost half of that in HD 209621. All other molecular features match well with their counterparts in the spectrum of HD 209621. Weak molecular bands that are noticed in the spectrum of HD 209621 upward of 5700 Å are not noticeable in the spectra of these two objects. The features due to Na I D, H_α and Ba II at 6496 Å could be detected. The secondary P-branch head at 4223 Å is seen as distinctly as in HD 209621.

In the spectrum of HE 2353−2314, the CH band around 4300 Å as well as the CN band around 4215 Å are marginally detected. The carbon molecular band around 5165 Å

is clearly detected; the band around 5635 Å is much weaker. No other molecular bands or atomic lines are detectable. In the spectrum of HE 2255−1724, the CN band around 4215 Å is much weaker than that in HD 209621. The CH band and Ca II K and H are of similar depths. The molecular bands around 4733, 5165, 5635 Å are slightly weaker in this object. Features of Na I D, Ba II line at 6496 Å, and H_α are distinctly seen. The molecular bands longward of 5635 Å are not detectable. The spectrum acquired on Sep 11, 2008 have a better signal. In the spectrum of HE 2334−1723, the CN band around 4215 Å is much weaker than in HD 209621; all other molecular bands show a good match. The features due to Ca II K and H also show a good match. No molecular bands are detectable upward of 5700 Å. In the spectrum of HE 2347−0658 the CN band around 4215 Å is almost absent. Ca II K and H features and carbon molecular bands around 4733, 5165, 5635 Å show a good match. Molecular bands seen in HD 209621 upward of 5700 Å are not detectable in the spectrum of this object.

The spectrum of HE 1400−1113 is noisy below about 4220 Å. The CN band around 4215 Å could be marginally detected. Ca II K and H are detected as weak features. A strong CH band around 4300 Å and the secondary P-branch head near 4342 Å are distinctly seen. Other molecular features have band depths marginally weaker than their counterparts in HD 209621. Except for Na I D, Ba II at 6496 Å and H_α no other atomic lines are detected redward of 5670 Å.

The spectrum of HE 1430−0919 also shows a very weak CN band around 4215 Å. The features due to Ca II K and H are not detected. The G-band of CH around 4300 Å is however very strong in the spectrum. The spectrum of HE 2157−2125 shows the CH band around 4300 Å with almost equal strength to its counterpart in HD 209621. Features due to Ca II K and H and other molecular features are also seen with equal intensities. However, the CN band around 4215 Å is much weaker than that in HD 209621.

The spectrum of HE 1315−2035 is noisy blueward of 4200 Å. The G-band of CH and the carbon molecular bands near 4733, 5165 and 5635 Å are detected in the spectrum. The H_α feature is clearly detected. The effective temperature of this object is 4639 K as estimated from J−K colour calibration.

HE 0008−1712, 0052−0543, 0100−1619, 0225−0546, 0237−0835, 0507−1430, 1045−1434, 1110−0153, 1157−1434, 1228−0417, 1318−1657, 1405−0346, 1400−0229, 1410−0125, 1431−0755, 1432−2138, 1440−1511.

The spectra of these objects closely resemble the spectrum of HD 5223, a well−known classical CH star with effective temperature ∼ 4500 K, log g = 1.0 and metallicity [Fe/H] = −2.06 (Goswami et al. 2006). The effective temperatures of these objects derived from

J−K colour range from about 3924 K (HE 0052−0543) to 4795 K (HE 1228−0417). Except for the two outliers HE 1045−1434 and HE 1228−0417 (represented with open squares) the locations of this set of objects are well within the CH box in Figure 3.1.

A comparison of the spectra of HE 0008−1712, HE 0100−1619 and HE 1405−0346 with the spectrum of HD 5223 is shown in Figure 3.6. The Ca I line at 4226 Å is not detectable in any of these spectra. The CH band as well as other molecular bands show a very good match. The features due to Ca II K and H are seen with equal strength as in HD 5223. The CN band around 4215 Å in HE 0100−1619 is slightly deeper. The bands longward of 5635 Å are also marginally deeper. This object HE 0100−1619 is also mentioned as a CH star in (Totten et al. 2000). Heliocentric radial velocity of HE 0100−1619 as reported by Bothun et al. (1991) is −142 km s^{-1}.

The spectra of HE 0052−0543 and HE 1110−0153 show stronger molecular bands than their counterparts in HD 5223. In the spectrum of HE 0225−0546 the molecular bands are marginally stronger than in HD 5223. The molecular features above 5700 Å seen in these two spectra are barely noticed in the spectrum of HD 5223. The spectrum of HE 1157−1434 also show a good match with the spectrum of HD 5223 except for the molecular band around 5635 Å which is distinctly weaker in its spectrum. The molecular features redward of 5700 Å are also noticed weakly in the spectrum of this object. The spectrum of HE 1405−0346 shows a stronger CN band around 4215 Å as well as a stronger carbon molecular band around 5635 Å. The secondary P-branch head near 4342 Å is also stronger than its counterpart in HD 5223. Other molecular bands around 4733 and 5165 Å show a good match. Ca II K and H are seen as strongly as in HD 5223. The effective temperature of the object from J−K colour is 4391 K, slightly lower than the effective temperature of HD 5223. In the spectrum of HE 1410−0125 the molecular features are slightly shallower than their counterparts in HD 5223. The CH band depth is however of similar strength. The feature at Ca I 4226 Å is absent; the features due to Ca II K and H are of similar strengths. The CN band around 4215 Å matches well with the CN feature in HD 5223. The radial velocity of this object as quoted by (Frebel et al. 2006) is +80 Km s^{-1}. The effective temperature estimated using J−K calibration returns a value 4378 K for this object.

The spectrum of HE 1431−0755 is noisy blueward of 4000 Å; the features of Ca II K and H could not be detected. The CH band around 4310 Å and the CN band around 4215 Å appear slightly stronger than their counterparts in HD 5223. Other C_2 molecular bands present in the spectrum are narrower than their counterparts in HD 5223. The spectrum redward of 5700 Å shows molecular features that are barely noticed in the spectrum of

HD 5223. The spectrum of HE 1440−1511 shows molecular bands with almost equal depths with those in HD 5223. Ca II K and H features are however stronger than their counterparts in HD 5223. The spectrum shows a distinctly stronger feature due to Na I D. Features of H_α and Ba II at 6496 Å are of equal strengths. The spectrum redward of 5700 Å shows a good match.

In the spectrum of HE 1228−0417 the Ba II feature at 6496 Å and H_α are seen with equal strengths as in HD 5223. The part of the spectrum redward of 5700 Å shows a very good match. The Ca I line at 4226 Å is not detected. The feature due to Na I D is clearly detected. Other carbon molecular features around 4730, 5165, and 5635 Å appear marginally weaker than their counterparts in HD 5223. The G-band of CH appears with almost equal strength but the CN band around 4215 Å is marginally weaker than its counterpart in HD 5223. The effective temperature of the object estimated using J−K colour calibration is 4795 K, higher than the effective temperature of HD 5223 ∼ 4500 K (Goswami et al. 2006). The location of this object outside the CH box is not obvious from its low resolution spectra.

The spectra of the objects HE 0237−0835, HE 0507−1430, HE 1318−1657, HE 1400−0229, HE 1432−2138 closely resemble the spectra of HD 5223. The G-band of CH is visible at about 4300 Å and of almost equal strength in all the objects including HD 5223. The Ca I line at 4226 Å is weakly detected in HE 1318−1657. The C_2 molecular bands of HE 1318−1657 is also weak compared to HD 5223. H_β line is clearly visible and of equal strength to HD 5223. The Ba II features at 4554 and 6496 Å are marginally weaker in HE 1318−1657. The Na I D feature is weakly detected.

The spectra of HE 0507−1430 and HE 1400−0229 show very close resemblances to the spectrum of HD 5223. CH and C_2 bands are strongly detected and are seen with equal strengths as in HD 5223. The Ca I feature at 4226 Å is very weakly detected. The C_2 molecular bands around 4730, 5165, 5635 Å are also very strong similar to HD 5223. In HE 0237−0835 and HE 1432−2138 the C_2 bands at 4737 and 5165 Å are found to be similar in strength to HD 5223. But the C_2 band at 5635 Å is slightly weak compared to HD 5223. The H_α line at 6563 Å and Ba II line at 6496 Å are seen in all the objects except HE 1432−2138 with similar strength to HD 5223. In HE 1432−2138, these lines are weakly detected. The H_β line is clearly visible in case of HE 1400−0229 and 0237−0835 but slightly weak and broad in HE 0507−1430, 1432−2138. The Ba II line at 4554 Å is stronger in HE 0237−0835, 0507−1430 moderately strong in HE 1400−0229 and very weak in HE 1432−2138. The Na I D feature is shallow and weak in all of these stars and the individual contributions are not visible.

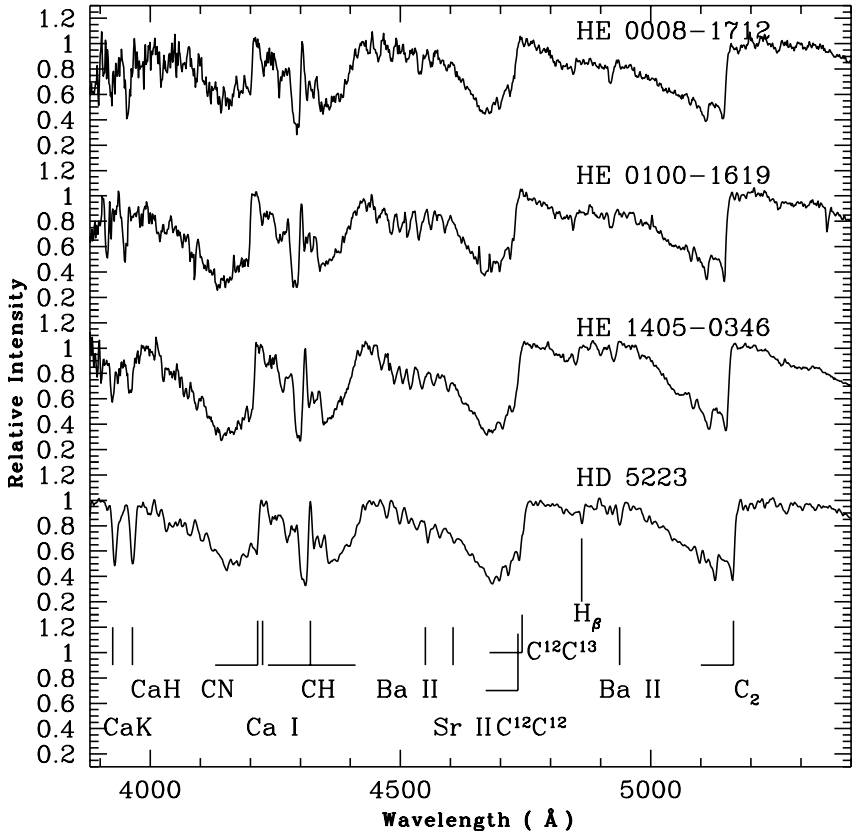

Figure 3.6: A comparison of the spectra of three HE stars in the wavelength region 3880 − 5400 Å with the spectrum of the comparison star HD 5223. Prominent features noticed in the spectra are marked on the figure.

HE 0009−1824, 1116−1628, 1358−2508.

The spectra of these objects are illustrated in Figure 3.7. These three objects are known dwarf carbon stars. The effective temperatures of HE 0009−1824, HE 1116−1628, HE 1358−2508 as estimated from J−K calibration are respectively 5530 K, 4224 K and 3623 K. As expected, the molecular band depths are the strongest in HE 1358−2508, the coolest of the three objects; and weakest in HE 0009−1824. In the spectrum of HE 0009−1824 the CN band around 4215 Å is completely missing. The features due to Ca II K and H as well as the CN band near 3880 Å are detected. The G-band of CH is strong but not as strong as it appears in CH stars. The secondary P-branch head near 4342 Å is seen distinctly. Apart from the absence of the CN band around 4215 Å the spectrum of this object looks somewhat similar to the spectrum of HD 209621. The distance of this object as reported by Mauron et al. (2007) is 300 pc. The spectra of HE 1116−1628 and

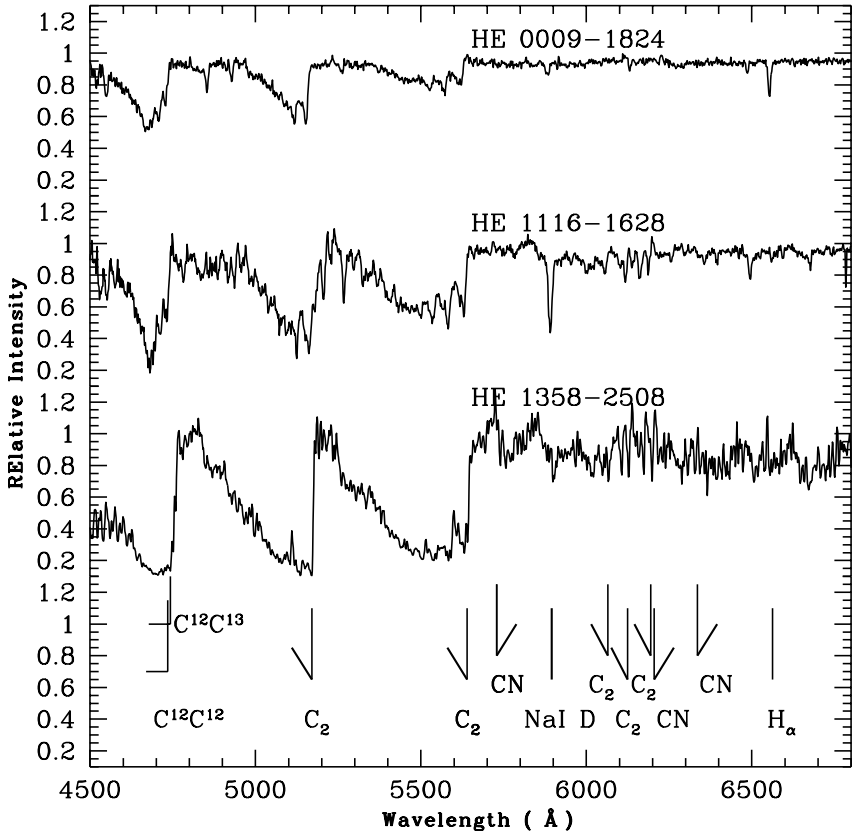

Figure 3.7: The spectra of three dwarf carbon stars in the wavelength region 4500 – 6800 Å. Prominent features noticed in the spectra are marked on the figure.

HE 1358−2508 show characteristics of C−R star RV Sct with marginal differences in the molecular band depths. In the spectrum of HE 1358−2508, the CH band is marginally stronger than in RV Sct. The C_2 molecular bands are stronger in the spectrum of this object. The CN band around 4215 Å is clearly detected. Ratnatunga, in his PhD thesis (1983) first proposed this object HE 1116−1628 to be a dwarf carbon star. This object is also present in the list of dwarf carbon stars of Lowrance et al. (2003). Mauron et al. (2007) reported the proper motions in α and δ and their respective 1σ errors in mas yr^{-1} as −23.5 ± 6.7 and +29.8 ± 4.6. The distances of HE 1116−1628 and HE 1358−2508 as reported by Mauron et al. (2007) are 170 pc and 270 pc respectively. Totten & Irwin (1998) reported a radial velocity of −69 km s^{-1} for the object HE 1116−1628. All the three objects have total proper motion $\mu \geq 30$ mas yr^{-1} (Mauron et al. 2007).

The locations of the three dwarf carbon stars are indicated by open triangles in Figure 3.1. Location of HE 0009−1824 is on the left below the CH box, the location of

HE 1358−2508 is on the right edge of the CH box and the location of HE 1116−1628 is found to be well inside the CH box. Dwarf carbon stars have anomalous infrared colours (Green et al. 1992; Westerlund et al. 1995). In the conventional two colour JHK diagram the locus of dwarf carbon stars colours is away from the normal carbon star locus. The locus defined by dwarf carbon stars is bounded by (J−H) ≤ 0.75 and (H−K) ≥ 0.25 (Westerlund et al. 1995). This condition is satisfied by HE 1358−2508; however HE 0009−1824 and HE 1116−1628 both have (H−K) colours less than the lower limit of 0.25 mag set for dwarf carbon stars.

3.5 Candidate C−R stars

HE 0201−0327, 0417−0513, 0419+0124, 0926−0417, 1011−0942, 1127−0604, 1205−0521, 1238−0836, 1319−2340, 1418−0306, 1428−1950, 1439−1338, 2222−2337. The spectra of these objects show characteristics of C−R stars. The spectra of HE 1011−0942, HE 1205−0521, HE 1238−0836 match closest to the spectrum of RV Sct. The effective temperatures of the objects estimated using J−K calibration range from 3521 K (HE 1238−0836) to 4875 K (HE 1127−0604).

In the spectra of HE 1238−0836 and HE 1428−1950 the CH band around 4300 Å is slightly deeper than in RV Sct. The molecular features in the redward of 5700 Å appear marginally weaker. The spectrum of HE 2222−2337 has low flux below about 4100 Å. The CH band does not appear as strong as it should be in C−R star's spectrum. The CN band around 4215 Å is marginally detected. Other molecular bands are of similar strengths. The molecular features redward of 5635 Å are slightly weaker. We place these objects in the C−R group.

The spectra of the objects HE 0201−0327, HE 0417−0513, HE 0419+0124, HE 0926−0417, HE 1319−2340 closely resemble the spectra of C−R stars. The Na I D line is very strongly detected in all these star's spectra which is a well known characteristic of C−R stars. The Ca I line at 4226 Å is also strong and of equal strength in all these spectra. The CH band is weakly detected. The secondary P-branch head is not visible. The C_2 molecular bands around 4730 and 5635 Å are very weak in all the spectra. The C_2 band at 5165 Å is moderately strong in HE 0201−0327, HE 0417−0513 and HE 0419+0124. The CN band (4215 Å) is strong for HE 0926−0417. In HE 0201−0327 the CN band is appeared very weak but for HE 0417−0513 and HE 0419+0124 it appeared moderately strong. While the H_β line in all these spectra, is broad and blended with molecular lines, the H_α line is clearly visible. The Ba II line at 4554 Å is very weak in all the objects. Similarly Ba II

line at 6496 Å is clearly visible though not strong. H_α and Ba II line at 6496 Å are seen with similar strengths.

3.6 Candidate C−N stars

HE 0217+0056, 0228−0256, 1019−1136, 1344−0411, 1429−1411, 1442−0058, 2213−0017, 2319−1534, 2331−1329

The spectra of these objects show a close resemblance with the spectrum of the C−N star Z PSc with similar strengths of CN and C_2 molecular bands across the wavelength regions. In Figure 3.1, the objects HE 0217+0056, HE 1344−0411, HE 1429−1411, HE 1442−0058 and HE 2213−0017 represented by solid triangles lie well within the CN box. The spectra have low flux below about 4400 Å. The spectrum of HE 1429−1411 is similar to that of Z PSc's spectrum, except that the CN band around 4215 Å is marginally weaker in this star. The CH band is weakly detected in the spectrum of HE 1116−1628. The molecular bands near 4735, 5135 and 5635 Å are noticed distinctly. The feature due to Na I D is strongly detectable. The Ba II line at 6496 Å is detectable but the H_α feature could not be detected. HE 1127−0604 has low flux below about 4200 Å. The CH band and C_2 molecular bands around 4735, 5165, 5635 Å are detected. All the features in the spectrum are weaker than their counterparts in Z Psc. While features of Ca II K and H are detected, the CN band around 4215 Å is not clearly seen. The spectra of the objects HE 2213−0017, HE 1442−0058, HE 1344−0411 compare closest to the spectrum of C−N star V460 Cyg as illustrated in Figure 3.8.

The objects HE 0217+0056, HE 1442−0058 and HE 2213−0017 are also mentioned as N−type stars in the APM survey of cool carbon stars in the Galactic halo (Totten & Irwin 1998). Totten et al. (2000) have provided proper motion measurements for these objects. The distances measured by these authors assuming an average $M_R = -3.5$ for these objects lies in the range 16 to 43 kpc. Heliocentric radial velocities estimated by Totten & Irwin (1998) for these objects are respectively −142 ± 3, 126 ± 4, 37 ± 4, −44 ± 3, and −113 ± 5 km s^{-1}. Heliocentric radial velocity of HE 0228−0256 is −72 km s^{-1} (Bothun et al. 1991).

The spectra of the objects HE 2319−1534, HE 2331−1329 show a strong depression in the bluer side of the spectra. In HE 2319−1534 the spectrum is noisy blueward from 4400 Å and in HE 2331−1329 spectrum is noisy from 4200 Å. All C_2 bands appears to be strong except the C_2 band at 5635 Å in HE 2319−1534. The Na I D line is very broad in both the spectra and appear strong in HE 2331−1329 compared to HE 2319−1534.

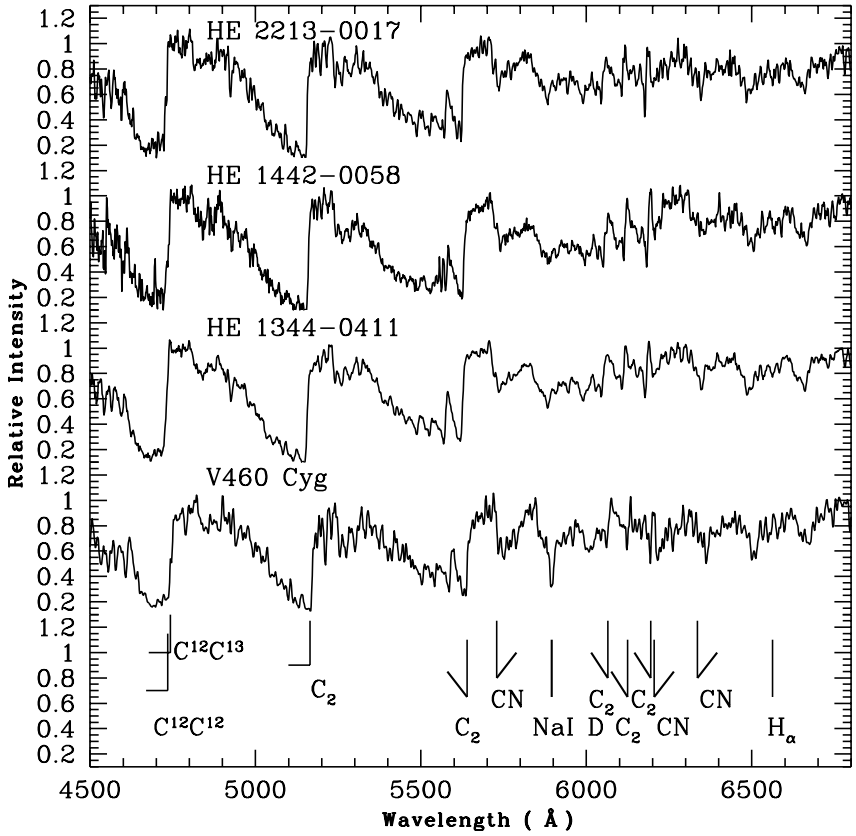

Figure 3.8: A comparison of the spectra of the candidate C−N stars with the spectrum of V460 Cyg in the wavelength region 4500 − 6800 Å. The bandheads of the prominent molecular bands, Na I D and H_α are marked on the figure.

The strong Ca I line (4226 Å) can be seen in HE 2331−1329 but is not visible in HE 2319−1534 due to the depression in the spectrum. The H_α line is not visible in these spectra and H_β line appears very broad and weak. The Ba II feature at 4554 Å is strong for both these stars. Similarly the Ba II at 6496 Å line is also broadened in the spectra of HE 2331−1329 while in HE 2319−1534 it appears narrow. These objects lie well within the C−N box in J−H and H−K plot. All these features strongly support these stars to be the members of C−N group.

HE 1015−2050. The spectra of HE 1015−2050 do not show the presence of any carbon molecular bands. The features due to Ca II K and H are not detected. The G-band of CH is seen as a weak feature. Features due to Ca I at 4226 Å and Na D I are seen as strong features. Ba II line at 6496 Å and H_α feature are detected. 2MASS JHK photometry is not available for this object. A careful inspection reveals the star to exhibit

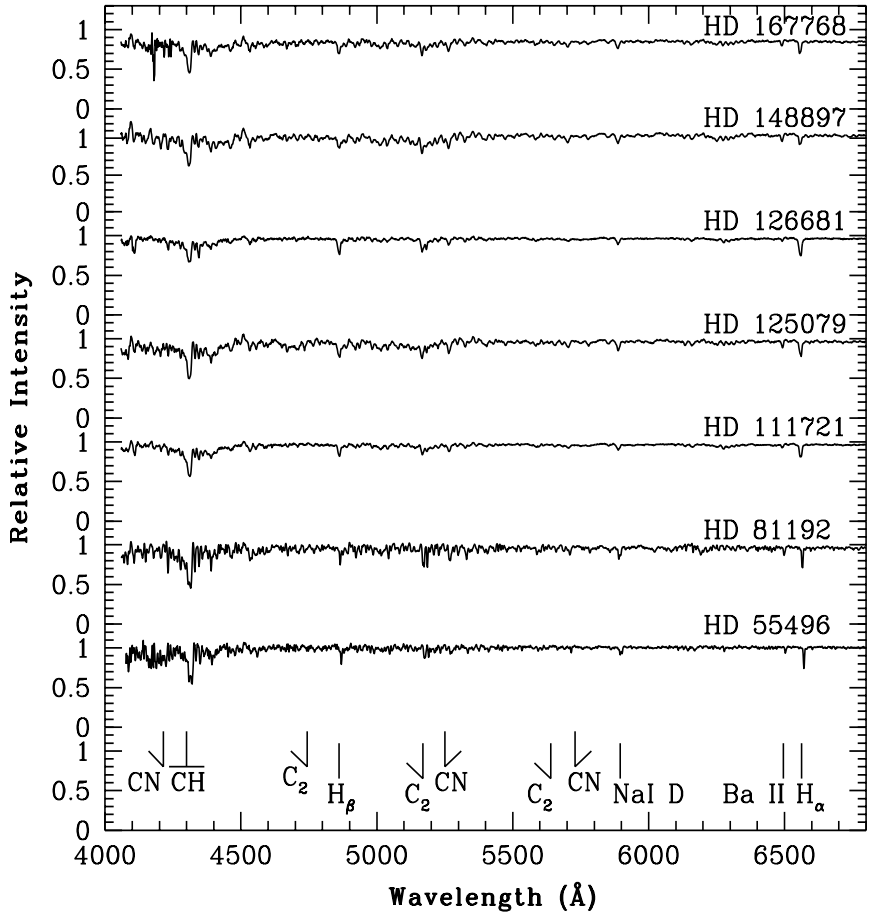

Figure 3.9: Spectra for the CH stars from the catalogue of Bartkevicius (1996)

spectral characteristics of cool HdC stars.

3.7 Low resolution spectroscopy of stars from the CH star catalogue of Bartkevicius (1996)

We have conducted low resolution as well as high resolution spectroscopic study for twenty two stars from the CH star catalogue of Bartkevicius (1996) Low resolution spectra of a sample of these objects obtained with 2m HCT at IAO are presented in Figures 3.9 and 3.10. The detailed studies of these objects based on high resolution Elodie spectra; analyses and results; are discussed in chapter 4 and 5.

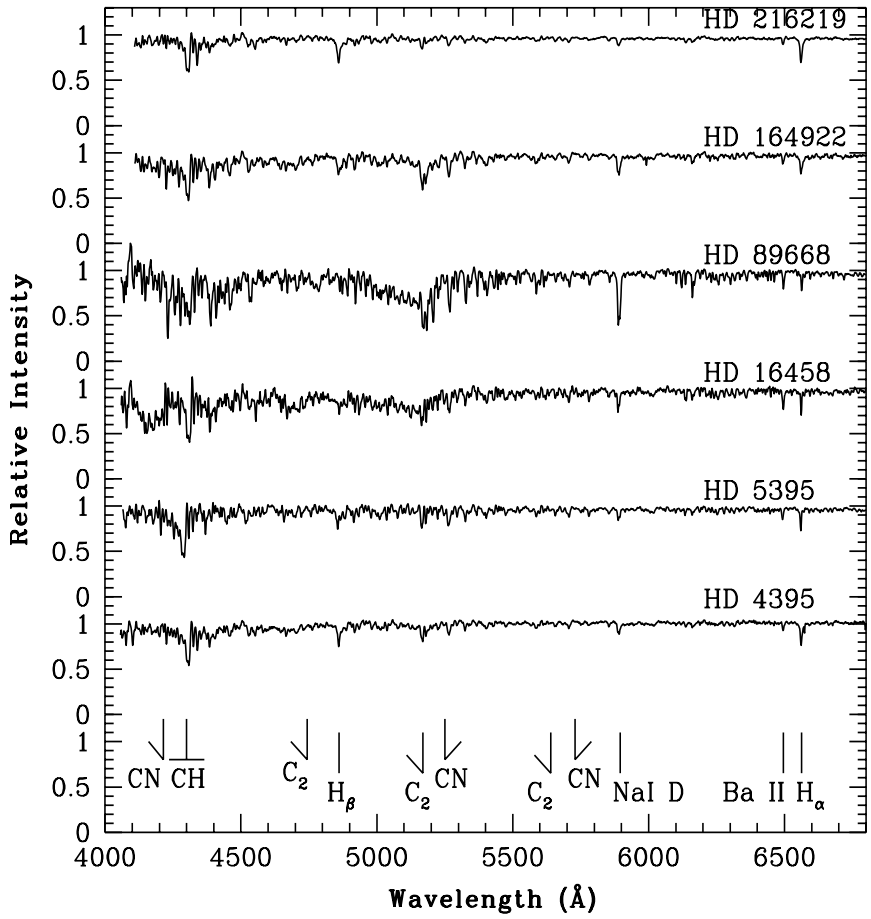

Figure 3.10: Same as Figure 3.9

3.8 Conclusion

We have analysed a total of hundred and eleven objects including twenty two objects from the CH star catalogue of Bartkevicius (1996). Among these, the spectra of sixty eight objects are characterized by the presence of strong C_2 molecular bands. The spectra of twenty two objects from the CH95 catalogue are also characterized by a weak or moderate G-band of CH. The spectral analysis led to the detection of thirty eight potential CH star candidates. Their locations on the two color J−H versus H−K diagram are in support of their classification with this class of objects. This set of objects will make important targets for subsequent chemical composition studies based on high resolution spectroscopy and for confirmation of these objects with this class of identification.

While identification of C−N and C−J type stars are relatively easy, separating C−R stars from CH stars is not so straightforward. The two main properties, presence or ab-

sence of s-process elements and binarity that differentiate early−R stars from CH stars, can be known only through detailed abundance studies that require high resolution spectroscopy and from long−term radial velocity monitoring. The faintness of these objects makes high resolution spectroscopic studies very difficult. As such, the method described in Goswami (2005) to distinguish a C−R from a CH star proved quite useful. Abia et al. (2002) have shown that CH stars cannot be formed above a threshold metallicity, around $Z \sim 0.4Z_{\odot}$. According to Dominy (1984), the metallicities of C−R stars are either solar or slightly sub-solar. C−R stars are believed to be Core Helium Burning (CHeB) counterparts of CH stars in which s-process elements are either absent or not detectable (Izzard et al. 2007). These authors have predicted an early−R/CH ratio $\sim$ 7 per cent, at [Fe/H] = −2.3, a metallicity typical of the Galactic halo. This ratio is derived considering only CHeB CH stars, if CH giants and dwarfs are also considered, this ratio is likely to get much lower.

Westerlund et al. (1995) defined dwarf carbon stars as having J−H $\leq$ 0.75, H−K $\geq$ 0.25 mag. Among the three dwarf carbon stars in our sample the objects HE 1358−2508 occupies a region defined by these limits on J−H, H−K plane. HE 0009−1824 and HE 1116−1628 however do not follow the JHK definition of dwarf carbon stars offered by Westerlund et al. (1995). It seems, these limits on J−H and H−K may not be very tight. Proper motions of these objects have been estimated by Mauron et al. (2007) and have placed them as dwarf carbon stars.

CHAPTER 4

SPECTROSCOPIC ANALYSIS OF CH STARS I: BASIC OBSERVATIONAL PROPERTIES

Karinkuzhi D, & Goswami A, 2014, MNRAS, 440, 1095
Karinkuzhi D, & Goswami A, 2015, MNRAS, 446, 2348

4.1 Introduction

In this chapter we have presented the observational properties of the programme stars from the CH star catalogue of Bartkevicius (1996) for which we have carried out detailed abundance analysis in chapter 5. CH stars characterized by iron deficiency, enhanced carbon and s-process elements are known to be post-mass-transfer binaries (McClure & Woodsworth 1990) in which the companion (primary) has evolved to white dwarf passing through an AGB stage of evolution. The chemical composition of CH stars (secondaries) bear the signature of the nucleosynthesis processes occurring in the companion AGB stars due to mass transfer. Two suggested mass transfer mechanisms include RLOF and wind accretion (section 1.8.1). Recent hydrodynamical simulations have shown in the case of the slow and dense winds, typical of AGB stars, that efficient wind mass transfer is possible through a mechanism called wind Roche-lobe overflow (WRLOF) (Abate et al. (2013) and references therein). CH stars (secondaries) thus form ideal targets for studying the operation of s-process occurring in AGB stars. Chemical abundances of key elements such as Ba, Eu etc. and their abundance ratios could provide insight in this regard. How-

ever, literature survey shows that detailed chemical composition studies of many for the objects belonging to the CH star catalogue of Bartkevicius (1996) are currently not available. A few studies that exist are either limited by resolution or wavelength range. We have therefore undertaken to carry out chemical composition studies for a selected sample of CH stars from this catalogue using high resolution spectra. In our previous studies along this line (see chapter 3) we have considered the sample of faint high latitude carbon stars of Hamburg/ESO survey (Christlieb et al. 2001) and based on medium resolution spectroscopy found about 33 per cent of the objects to be potential CH star candidates (Goswami 2005; Goswami et al. 2007, 2010b). Chemical composition of two objects from this sample based on high resolution Subaru spectra are discussed in Goswami et al. (2006).

CH stars (with $-0.2 <$ [Fe/H] < -2) and the class of carbon-enhanced metal-poor (CEMP)-s stars of the CEMP stars classification of Beers & Christlieb (2005) are believed to have a similar origin as far as their chemical composition is concerned and that, the CEMP-s stars are thought to be more metal-poor counterparts of CH stars. High resolution spectroscopic analyses of CEMP stars have established that the largest group of CEMP stars are s-process rich (CEMP-s) stars and accounts for about 80 per cent of all CEMP stars (Aoki et al. 2007). Chemical composition studies of carbon-enhanced metal-poor stars (Barbuy et al. 2005; Norris et al. 1997a,b, 2002; Aoki et al. 2001, 2002; Goswami et al. 2006; Goswami & Aoki 2010) also have suggested that a variety of production mechanisms are needed to explain the observed range of elemental abundance patterns in them; however, the binary scenario of CH star formation is currently considered as the most likely formation mechanism also for CEMP-s stars. This idea has gained further support with the demonstration by Lucatello et al. (2005), that the fraction of CEMP-s stars with detected radial-velocity variations is consistent with the hypothesis of all being members of binary systems.

The sample of programme stars includes five confirmed binaries, HD 16458, HD 122202, HD 201626, HD 204613 and HD 216219. Six objects in this sample, HD 4395, HD 48565, HD 55496, HD 92545, HD 104979 and HD 107574 are known to show radial velocity variability, and for the rest, none of these two information is available. In the following text, for convenience, we will refer the objects that are confirmed binaries as group I objects, those with limited radial velocity information as group II objects and the objects for which none of these information are available as group III objects. One of our primary objectives is to estimate the abundances of heavy elements and critically examine the abundance patterns and abundance ratios if they exhibit characteristic abundance patterns

of CH stars and if there exist any correlation between the group I, group II and group III objects.

4.2 High resolution spectra of the programme stars

Programme stars are selected from the CH star catalogue of Bartkevicius (1996); the basic data of these objects are listed in Table 4.1. The spectra are taken from the ELODIE archive (Moultaka et al. 2004). We have considered only those CH stars for which high resolution spectra are available in the archive with S/N ratio > 20. ELODIE is an echelle spectrograph used at the 1.93 m telescope of Observatoire de Haute Provence (OHP). The spectra recorded in a single exposure as 67 orders on a 1K CCD have a resolution of R $\sim$ 42000. Details about the telescope and ELODIE spectrograph are explained in section 2.3.2. The wavelength range spans from 3900 to 6800 Å. A few sample spectra are shown in Figures 4.1 and 4.2.

4.3 Radial velocity

Radial velocities of the programme stars are calculated using a selected set of clean unblended lines in the spectra. Estimated mean radial velocities along with the standard deviation from the mean values are presented in Table 4.2. The literature values are also presented for a comparison. Radial velocity variations are reported in McClure (1984, 1997) and McClure & Woodsworth (1990) for four stars, HD 16458, HD 201626, HD 216219 and HD 4395. McClure (1997) has reported the radial velocity variations and orbital parameters for two subgiant-CH stars HD 122202 and HD 204613. Except HD 4395, other five objects are confirmed binaries. Radial velocity variations in HD 4395 is found to be very small. Our radial velocity estimate for HD 48565 shows a difference of $\sim$ 6 km s^{-1} from the literature value. Variation in radial velocity for this object was also reported by North et al. (1994) and Nordstroem et al. (2004). For the remaining stars we note smaller differences from the literature values. Except for HD 55496 (315 km s^{-1}) HD 201626 ($-$141.6 km s^{-1}) and HD 81192 ($-$136.5 km s^{-1}), the programme stars are low-velocity objects. Although radial velocity variations are noticed in HD 55496, it is not confirmed as a binary. Our estimate also shows a difference of 7 km s^{-1} from the literature value. Mild radial velocity variations are noticed in HD 92545 and HD 107574 (North & Duquennoy 1992) also. Our radial velocity estimates of HD 104979 and HD 164922 show a difference of $\sim$ 15 km s^{-1} from the literature values.

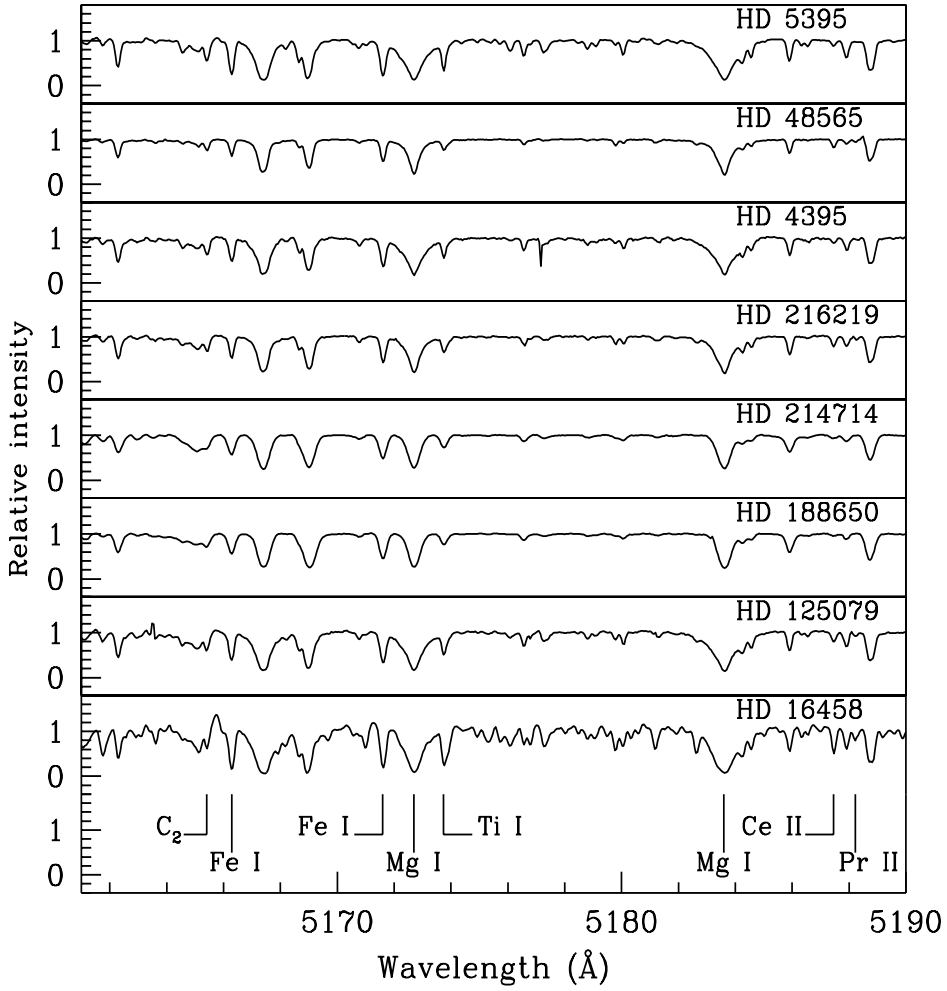

Figure 4.1: Sample spectra of a few programme stars in the wavelength region 5161 to 5190 Å

4.4 Temperatures from photometric data

The estimates of photometric temperatures at metallicity values from −0.5 to −1.5 of the programme stars are presented in Table 4.3. The equations used and the details about the calculations performed are explained in section 2.4.10. The temperature calibrations from the (J−H) and (V−K) relations involve a metallicity ([Fe/H]) term. Adopted [Fe/H] values are shown in parenthesis in table 4.3.

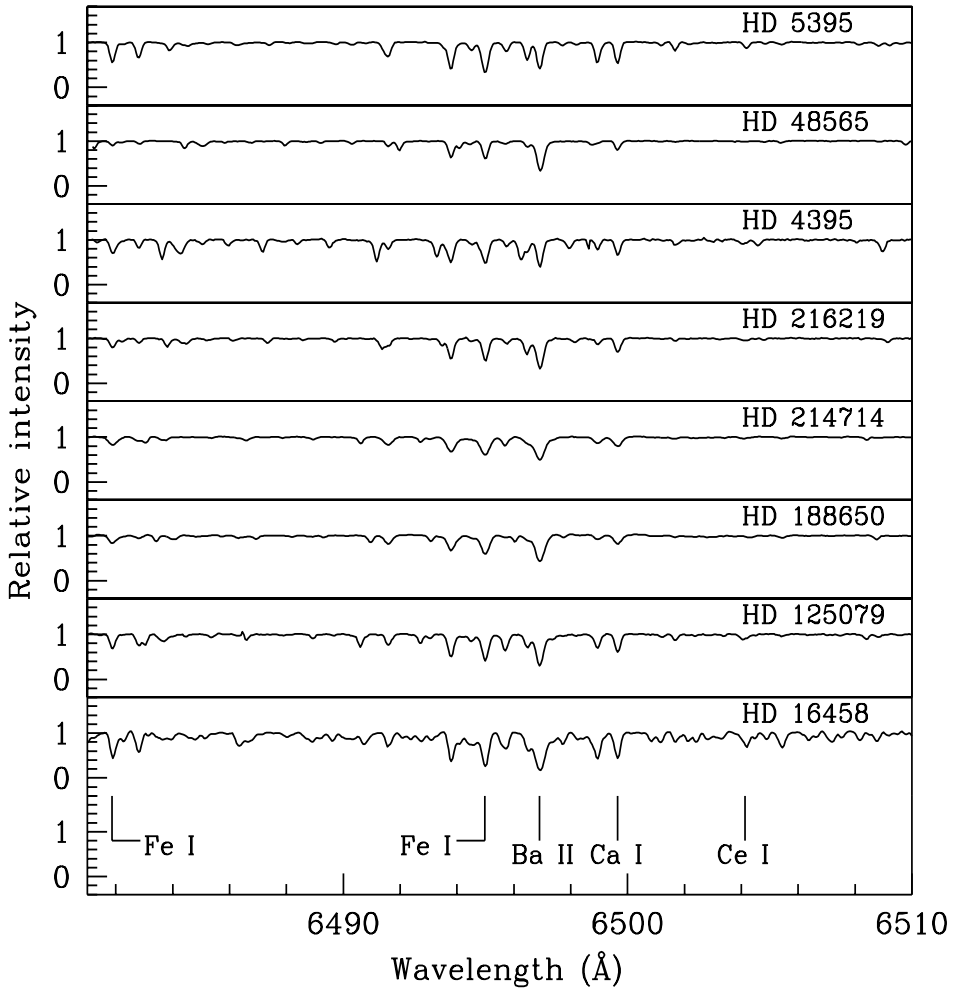

Figure 4.2: Spectra showing the wavelength region 6481 to 6510 Å, for the same stars as in Figure 4.1.

Table 4.1: Basic data for the programme stars

Star	RA (2000) h m s	DEC (2000) d m s	B	V	J	H	K
Group I							
HD 16458	02 47 47.70	+81 26 54.51	7.12	5.79	3.840	3.343	3.032
HD 122202	14 00 18.96	+04 51 25.06	9.85	9.36	8.506	8.358	8.252
HD 201626	21 09 59.27	+26 36 54.92	9.20	8.13	6.315	5.838	5.736
HD 204613	21 27 42.96	+57 19 18.86	8.86	8.22	7.100	6.824	6.788
HD 216219	22 50 52.15	+18 00 07.58	8.06	7.44	6.265	6.034	5.935
Group II							
HD 4395	00 46 13.74	-11 27 08.56	8.39	7.70	6.394	6.099	5.972
HD 48565	06 44 54.92	+20 51 38.35	7.73	7.20	6.122	5.884	5.806
HD 55496	07 12 11.37	−22 59 00.61	9.30	8.40	6.590	6.043	5.931
HD 92545	10 40 57.70	−12 11 44.23	9.07	8.56	7.548	7.347	7.282
HD 104979	12 05 12.54	+08 43 58.74	5.10	4.13	2.459	1.987	1.869
HD 107574	12 21 51.86	−18 24 00.15	8.99	8.54	7.660	7.460	7.415
Group III							
HD 5395	00 56 39.90	+59 10 51.80	5.57	4.63	3.123	2.680	2.468
HD 81192	09 24 45.33	+19 47 11.86	7.45	6.53	4.846	4.282	4.119
HD 89668	10 20 43.40	−01 28 11.38	10.50	9.41	7.443	6.908	6.760
HD 111721	12 51 25.19	−13 29 28.17	8.78	7.97	6.347	5.898	5.786
HD 125079	14 17 20.71	-04 15 57.81	9.57	8.67	7.136	6.759	6.610
HD 126681	14 27 24.91	−18 24 40.43	9.93	9.32	8.044	7.709	7.631
HD 148897	16 30 33.54	+20 28 45.07	6.50	5.25	2.950	2.248	1.966
HD 164922	18 02 30.86	+26 18 46.80	7.79	6.99	5.553	5.203	5.113
HD 167768	18 16 53.10	−03 00 26.64	6.89	6.00	4.376	3.906	3.789
HD 188650	19 54 48.25	+36 59 44.43	6.52	5.79	4.626	4.111	4.114
HD 214714	22 39 34.33	+37 35 34.14	6.86	6.03	-	-	

Table 4.2: Radial velocities for the programme stars

Star	V_r (km s^{-1}) our estimates	V_r (km s^{-1}) literature	References
Group I			
HD 16458	18.2 ± 0.5	18	1
HD 122202	−7.40 ± 0.97	−10.5	2
HD 201626	−141.6 ± 1.2	−145.7	6
HD 204613	−89.53 ± 0.33	−90.96	7
HD 216219	−6.8 ± 0.7	−7.5	4
Group II			
HD 4395	−0.8 ± 0.8	−1.3	6
HD 48565	−25.7 ± 0.4	−19.4	6
HD 55496	315.28 ± 0.80	322.00	8
HD 92545	−17.51 ± 0.65	−16.65	12
HD 104979	−45.40 ± 0.42	−29.62	9
HD 107574	−16.33 ± 0.72	−29.40	8
Group III			
HD 5395	−47.8 ± 0.9	−47.0	9
HD 81192	136.5 ± 0.3	135.3	1
HD 89668	22.84 ± 0.70	23.0	10
HD 111721	20.59 ± 0.67	21.40	8
HD 125079	−4.5 ± 0.2	−4.3	3
HD 126681	−45.36 ± 0.46	−45.58	11
HD 148897	17.55 ± 0.71	18.40	8
HD 164922	34.86 ± 0.91	20.29	5
HD 167768	1.39 ± 0.42	1.60	8
HD 188650	−24.6 ± 0.4	−23.8	1
HD 214714	−7.0 ± 0.5	−6.8	1

1. Wilson (1953), 2. Luck & Bond (1991), 3. Smith et al. (1993), 4. de Medeiros & Mayor (1999), 5. Nidever et al. (2002), 6.Nordstroem et al. (2004), 7. Pourbaix et al. (2004), 8. Gontcharov (2006), 9. Massarotti et al. (2008), 10. Soubiran et al. (2008), 11. Santos et al. (2011), 12. Siebert et al. (2011).

Table 4.3: Photometric temperatures of the programme stars

Star HD	T_{eff} (K) (J-K)	T_{eff} (K) (J-H) (−0.5)	T_{eff} (K) (V-K) (−0.5)	T_{eff} (K) (J-H) (−1.0)	T_{eff} (K) (V-K) (−1.0)	T_{eff} (K) (J-H) (−1.5)	T_{eff} (K) (V-K) (−1.5)	T_{eff} (K) (B-V) (−0.5)	T_{eff} (K) (B-V) (−1.0)	T_{eff} (K) (B-V) (−1.5)
Group I										
16458	4082.41	4713.82	4216.43	4730.59	4198.88	4747.49	4184.9	3886.55	3804.68	3741.41
122202	6417.84	6878.47	6890.04	6901.64	6370.16	6382.14	6402.28	6329.12	6179.09	6076.03
201626	4829.70	4754.07	4581.24	4770.85	4566.44	4787.74	4555.8	4381.70	4286.98	4215.57
204613	6070.18	5869.04	5841.82	5884.32	5843.53	5899.68	5852.03	5494.19	5368.80	5279.24
216219	5969.13	6209.69	5723.41	6223.98	5723.10	6238.33	5729.3	5595.08	5466.79	5375.59
Group II										
4395	5496.71	5776.28	5398.05	5791.79	5392.69	5518.56	6854.3	5365.08	5243.37	5155.90
48565	6047.46	6150.12	5891.51	6164.60	5894.11	6179.15	5903.61	5928.43	5790.39	5693.80
55496	4542.90	4441.94	4502.61	4458.65	4487.14	4475.49	4475.76	4774.22	4668.96	4591.12
92545	6343.00	6422.81	6088.75	6436.34	6095.01	6449.92	6108.68	6159.33	6014.42	5914.10
104979	5025.77	5056.49	4896.90	5073.13	4885.21	5089.87	4878.30	4604.59	4503.92	4428.86
107574	6605.48	6892.23	6774.10	6903.73	6795.30	6915.27	6825.87	6847.21	6681.19	6569.80

Table 4.3 – continued from previous page

Star HD	T_{eff} (K) (J-K)	T_{eff} (K) (J-H) (−0.5)	T_{eff} (K) (V-K) (−0.5)	T_{eff} (K) (J-H) (−1.0)	T_{eff} (K) (V-K) (−1.0)	T_{eff} (K) (J-H) (−1.5)	T_{eff} (K) (V-K) (−1.5)	T_{eff} (K) (B-V) (−0.5)	T_{eff} (K) (B-V) (−1.0)	T_{eff} (K) (B-V) (−1.5)
Group III										
5395	4556.52	4950.59	4842.04	4967.30	4829.76	4984.11	4822.10	4666.20	4563.87	4487.80
81192	4321.94	4382.20	4555.65	4398.88	4540.63	4415.69	4529.70	4734.38	4630.20	4553.02
89668	4462.68	4502.02	4518.76	4535.63	4318.91	4302.05	4288.96	4339.6	4246.01	4175.29
111721	-	4601.48	6451.12	4618.25	6464.85	4635.14	6486.97	5011.10	4899.33	4817.63
125079	5037.98	5285.39	4964.79	5301.79	4953.86	5318.29	4947.83	4774.22	4668.96	4591.13
126681	5539.93	5508.00	5524.06	5540.22	5452.94	5448.38	5449.71	5629.53	5500.24	5408.49
148897	3635.13	3885.78	3762.86	3901.90	3743.08	3918.15	3726.27	4015.00	3929.84	3864.45
164922	5412.07	5422.44	5191.94	5438.65	5183.77	5454.94	5180.94	5038.84	4926.30	4844.15
167768	4841.08	4060.94	4910.98	4077.32	4899.44	4093.83	4892.70	4799.45	4693.50	4615.26
188650	5095.69	4553.41	5469.31	4570.17	5464.99	4587.06	5466.60	5226.76	5108.96	5023.75
214714	–	–	–	–	–	–	–	4964.61	4854.13	4773.19

The numbers in the parenthesis indicate the metallicity values at which the temperatures are calculated.

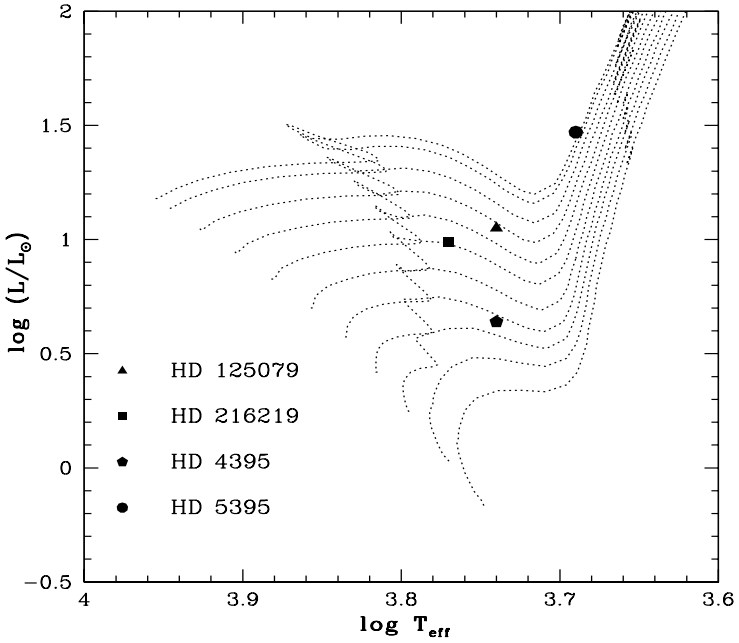

Figure 4.3: The location of HD 125079, HD 216219, HD 4395 and HD 5395 are indicated in the H-R diagram. The masses are derived using the evolutionary tracks of Girardi et al. (2000). The evolutionary tracks for masses 1, 1.1, 1.2, 1.3 1.4, 1.5, 1.6 1.7, 1.8, 1.9 and 1.95 $M_{\odot}$ from bottom to top are shown in the Figure.

4.5 Stellar masses

We have derived the mass of the programme stars from their locations in the Hertzsprung-Russel diagram (Figures 4.3 to 4.7), using Girardi et al. (2000) database of evolutionary tracks in the mass range of 0.15 $M_{\odot}$ to 7.0 $M_{\odot}$ and the Z values from 0.0004 to 0.03. These evolutionary tracks are available at http://pleiadi.pd.astro.it/. Since [Fe/H] of our target stars are near solar, we have selected an initial composition of Z = 0.0198, Y = 0.273. The masses derived are presented in Table 4.4. For the objects that have metallicities < -0.5 we have also used evolutionary tracks for Z = 0.008, however the masses obtained are found to be similar to those obtained using the evolutionary tracks with Z = 0.019. In general the masses are found to lie within a range of 0.6 $M_{\odot}$ − 2 $M_{\odot}$, except for HD 188650 and 214714, for which our estimated stellar masses are 3.5 and 4 $M_{\odot}$ respectively. Stellar masses could not be estimated for the rest of the objects as the parallax estimates are not available in the literature.

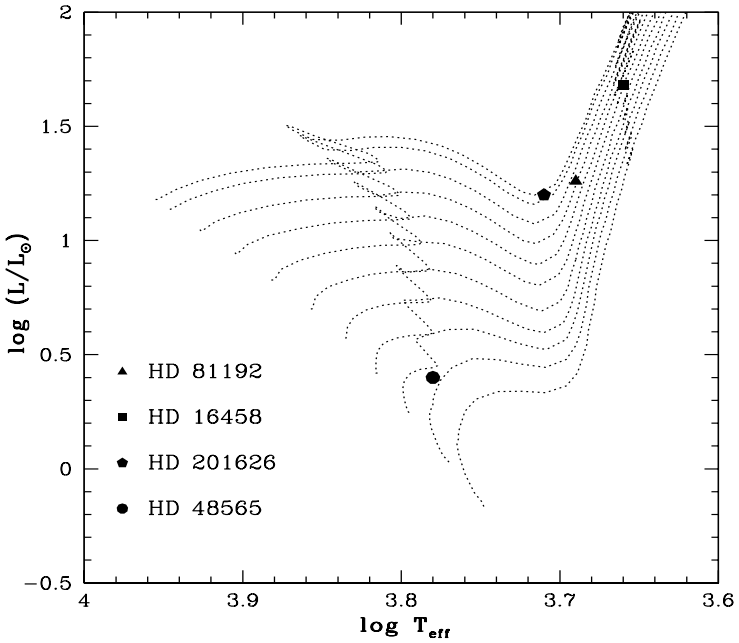

Figure 4.4: Same as Figure 4.3, but for objects HD 81192, HD 16458, HD 201626 and HD 48565.

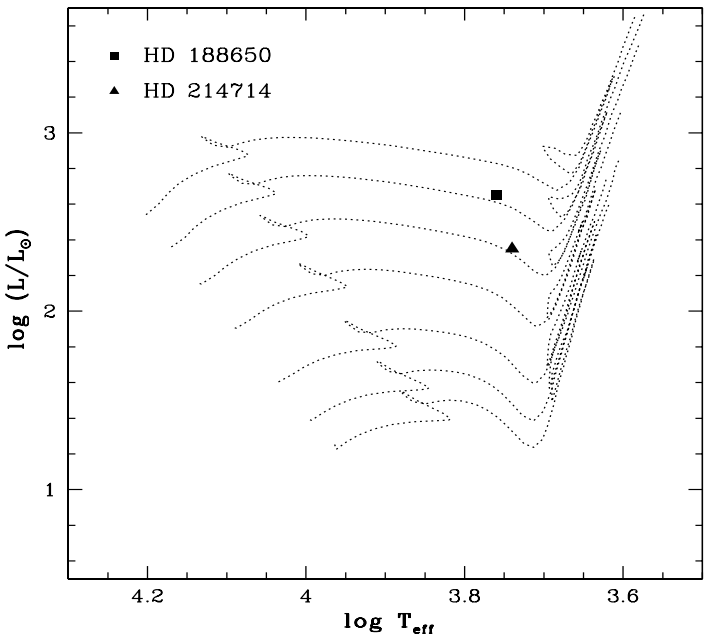

Figure 4.5: The location of HD 188650, and HD 214714 are indicated in the H-R diagram. The evolutionary tracks of Girardi et al. (2000) are shown for masses 2, 2.2, 2.5, 3.0, 3.5, 4.0 and 4.5 $M_\odot$ from bottom to top.

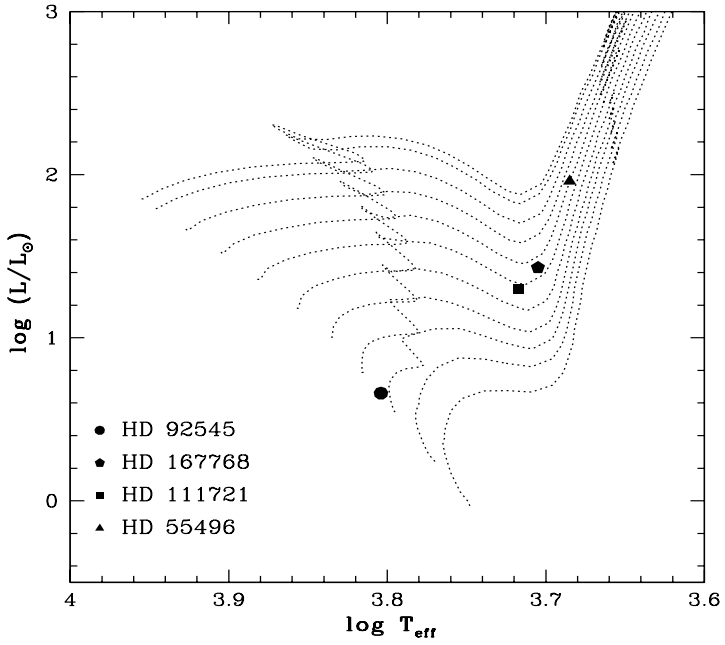

Figure 4.6: Same as figure 4.3, but for the objects HD 92545, HD 167768, HD 111721 and HD 55496.

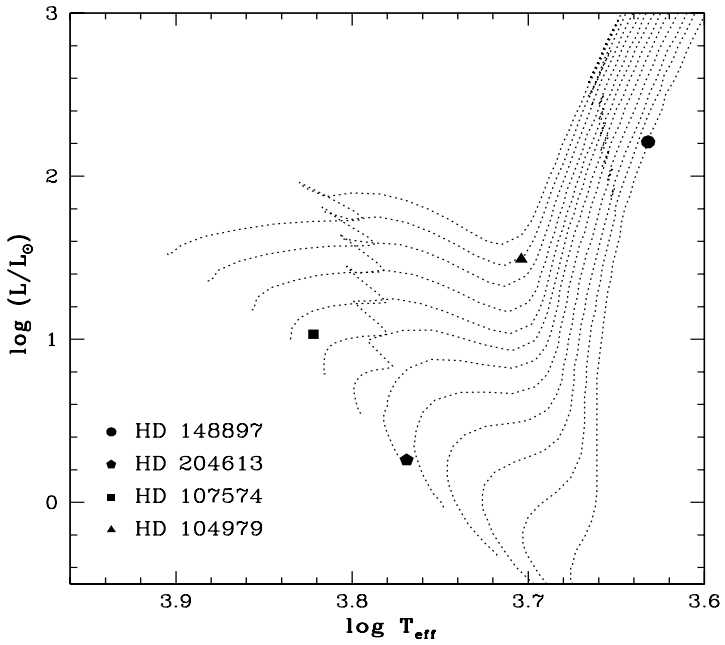

Figure 4.7: The location of HD 148897, HD 204613, HD 107574 and HD 104979 are indicated in the H-R diagram. The masses are derived using the evolutionary tracks of Girardi et al. (2000). The evolutionary tracks are shown for masses 0.6, 0.7, 0.8, 0.9, 1.0, 1.1, 1.2, 1.3 1.4, 1.5, 1.6 1.7, 1.8, 1.9 and 1.95 $M_{\odot}$ from bottom to top.

Table 4.4: Stellar masses

Star	M_v	$\log(L/L_\odot)$	Mass ($M_\odot$)
Group I			
HD 16458	0.1	1.68	1.50
HD 201626	1.3	1.20	1.90
HD 204613	3.9	0.26	1.10
HD 216219	2.1	0.99	1.60
Group II			
HD 4395	2.8	0.64	1.35
HD 48565	3.7	0.40	1.15
HD 55496	-0.16	1.96	1.60
HD 92545	3.1	0.66	1.20
HD 104979	0.63	1.49	1.60
HD 107574	2.1	1.03	1.45
Group III			
HD 5395	0.70	1.47	1.95
HD 81192	1.20	1.26	1.70
HD 111721	1.2	1.30	1.50
HD 125079	1.80	1.05	1.75
HD 148897	2.3	2.21	0.60
HD 167768	2.1	1.43	1.55
HD 188650	-2.70	2.65	4.00
HD 214714	-1.30	2.35	3.50

4.6 Linelist and Equivalent widths

The set of Fe I and Fe II lines that are generated and used in the present analysis to find the stellar atmospheric parameters are listed in Tables A.1 – A.3. The equivalent width of a spectral line is measured by fitting a gaussian to the line as explained in section 2.4.6. The excitation potential of the lines are in the range 0.0 - 5.0 eV and equivalent width in the range 20 Å to 180 Å. We have also presented the list of lines used for the determination of chemical abundances for the programme stars in Tables A4 – A6. A master line list including all the elements is generated comparing the spectra of the programme stars with

the spectrum of Arcturus and equivalent widths are measured for all the lines wherever possible. The presented line lists contain only those lines which are used for abundance calculation. In most of the spectra we could get very few usable clean lines. The log gf values for the atomic lines were adopted from various sources (Aoki et al. 2005, 2007; Goswami et al. 2006; Jonsell et al. 2006; Luck 1991; Sneden et al. 1996), and also from Kurucz atomic line database (Kurucz 1995b,a). The log gf values for a few La lines are taken from Lawler et al. (2001).

4.7 Conclusions

In this chapter, we have presented the basic observational properties of the programme stars namely radial velocities, photometric temperatures, mass and luminosities. In general, CH stars are known as high velocity objects. Our sample includes three high-velocity ($V_r \geq \pm$ 100 km s^{-1}) and nineteen low-velocity ($V_r \leq \pm$ 50 km s^{-1}) CH stars. Five of our programme stars are confirmed binaries (group I). Among these, the objects HD 122202, HD 204613 and HD 216219 with periods 1290, 878 and 3871 days respectively (McClure & Woodsworth 1990; McClure 1997) are known subgiant-CH stars. Other two stars HD 16458 and HD 201626 have periods 2018 and 1465 days respectively (McClure 1984, 1997; McClure & Woodsworth 1990). Long-term radial velocity monitoring ($\sim$ 10 years) for the subgiant-CH star HD 4395 shows a radial velocity variation of -4 km s^{-1} indicating its binarity (McClure 1983, 1984, 1997). Our radial velocity estimate differs by 6 km s^{-1} from the literature value. Other six objects from the sample are known to show radial velocity variations (group II). Our estimates also suggest that these are possible binary objects. Among the group III objects that have no information on radial velocity variations, we find HD 164922 showing a variation of 15 km s^{-1} from the literature value. Long term radial velocity monitoring is required for confirming its binarity.

We have calculated the photometric temperatures for these objects. The temperature estimates of the programme stars derived using JHK-temperature calibration relations (Alonso et al. 1994, 1996, 1999) although varying over a wide range, provide a preliminary temperature check for the programme stars and can be used as starting values in deriving atmospheric parameters using model atmospheres.

CH stars are low-mass objects. Sixteen objects in our sample for which we could estimate stellar masses are found to be low-mass objects with masses in the range 0.6 $M_\odot$ to 1.95 $M_\odot$. Two objects HD 188650 and HD 214714 have masses 4.0 $M_\odot$ and 3.5 $M_\odot$ respectively. Stellar masses could not be estimated for the rest four objects as the parallax

estimates are not available in the literature.

In the next chapter we have presented the stellar atmospheric parameters and elemental abundance ratios for these objects. A parametric model based analysis are also carried out to understand the origin of the neutron-capture elements observed in these objects.

CHAPTER 5

SPECTROSCOPIC ANALYSIS OF CH STARS II: ATMOSPHERIC PARAMETERS AND CHEMICAL ABUNDANCES

Karinkuzhi D, & Goswami A, 2014, MNRAS, 440, 1095
Karinkuzhi D, & Goswami A, 2015, MNRAS, 446, 2348

5.1 Introduction

CH stars provide an important means to study the production and distribution of heavy elements arising from AGB nucleosynthesis. Inspite of their usefulness, literature survey reveals that detailed chemical composition studies are not available for many CH stars. Many of the objects listed in Bartkevicius (1996) catalogue have no information on binary status. We have carried out the detailed chemical analysis of twenty two objects from this catalogue, some of them are known binaries, others with no information on binary status. Basic data for these objects along with the radial velocities and photometric temperatures are presented in chapter 4. This chapter describes the details of the chemical analysis of these objects.

Elements heavier than iron are mainly produced by two neutron-capture processes, the slow neutron-capture process (s-process) and the rapid neutron-capture process (r-process), see section 1.4.1. They require entirely different astrophysical environments,

different time-scales and different neutron fluxes. While slow neutron-capture elements are believed to be produced in the inter pulse phases of low mass AGB stars, the rapid neutron-capture process requires very high temperatures and neutron flux and are expected to be produced during supernova explosions. As mentioned in chapter 1, based on the abundances of representative elements of the s-process and r-process, CEMP stars are classified into different sub groups (Table 1.1). To understand the contribution of these two processes to the chemical abundance of the neutron-capture elements we have conducted a parametric model based study. Our study indicates seven objects in our sample to have abundances of heavy elements with major contributions coming from the s-process.

Estimation of stellar atmospheric parameters and elemental abundances are discussed in this chapter. A discussion on the parametric model based analysis of heavy element abundances is also presented.

5.2 Stellar Atmospheric parameters

The set of Fe I and Fe II lines used for the present analysis to find the stellar atmospheric parameters are listed in Tables A1, A2 and A3 . The excitation potential of the lines are in the range 0.0 - 5.0 eV and equivalent width in the range 20 Å to 180 Å. We have assumed LTE for our calculations. A recent version of MOOG of Sneden (1973) is used. Model atmospheres (available at http: //cfaku5.cfa.harvard.edu/ and labelled with a suffix odfnew) were selected from the Kurucz grid of model atmospheres with no convective over shooting. Solar abundances are taken from Asplund et al. (2005).

The effective temperature is determined by making the slope of the abundance versus excitation potential of Fe I lines to be nearly zero. The initial value of temperature is taken from the photometric estimates and arrived at a final value by an iterative method with the slope nearly equal to zero (Figure 5.1).

The microturbulent velocity is estimated at a given effective temperature by demanding that there be no dependence of the derived Fe I abundance on the equivalent width of the corresponding lines (Figure 5.2). The surface gravity is fixed at a value that gives same abundances for Fe I and Fe II lines. Derived atmospheric parameters are listed in Table 5.1.

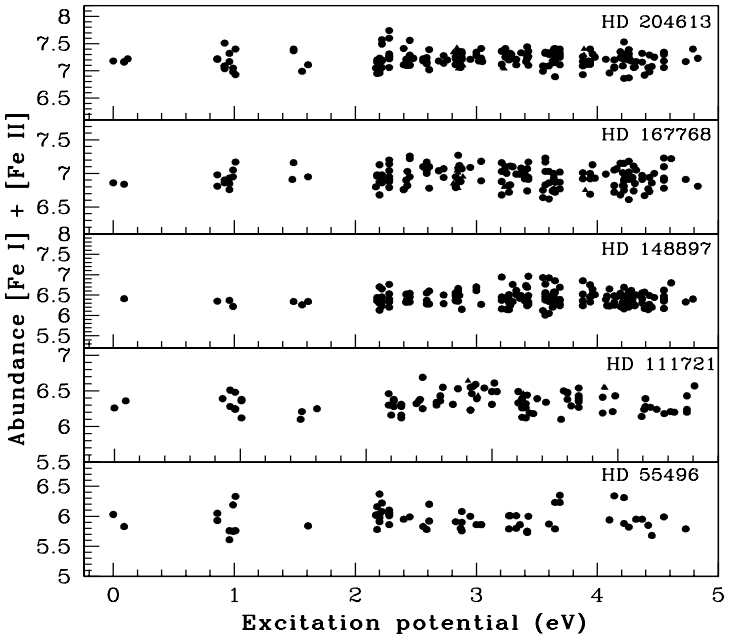

Figure 5.1: The iron abundances of stars are shown for individual Fe I and Fe II lines as a function of excitation potential. The solid circles indicate Fe I lines and solid triangles indicate Fe II lines.

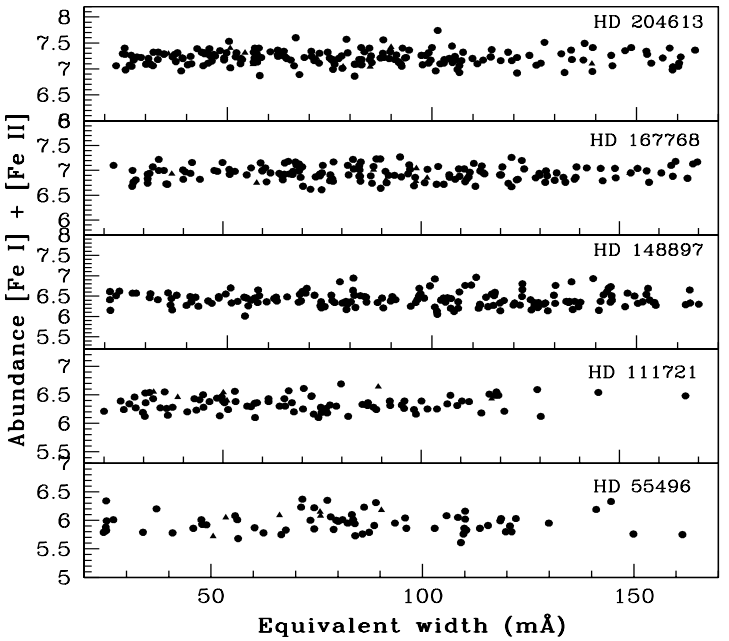

Figure 5.2: The iron abundances of stars are shown for individual Fe I and Fe II lines as a function of equivalent width. The solid circles indicate Fe I lines and solid triangles indicate Fe II lines.

Table 5.1: Derived atmospheric parameters and carbon isotopic ratios for the programme stars

Star	T_{eff} (K)	log g	ζ km s^{-1}	[Fe I/H]	[Fe II/H]	$^{12}C/^{13}C$
Group I						
HD 16458	4550	1.8	1.92	−0.65	−0.66	
HD 122202	6430	4.0	2.08	−0.63	−0.65	13.2
HD 201626	5120	2.25	1.02	−1.39	−1.41	
HD 204613	5875	4.2	1.22	−0.24	−0.24	11.1
HD 216219	5950	3.5	1.31	−0.17	−0.18	
Group II						
HD 4395	5550	3.66	0.93	−0.16	−0.19	
HD 48565	6030	3.8	1.13	−0.59	−0.59	
HD 55496	4850	2.05	1.52	−1.49	−1.41	4
HD 92545	6380	4.65	1.45	−0.21	−0.22	-
HD 104979	5060	2.67	1.55	−0.26	−0.31	9.9
HD 107574	6250	2.9	1.35	−0.65	−0.60	-
Group III						
HD 5395	4860	2.51	1.21	−0.24	−0.24	
HD 81192	4870	2.75	1.08	−0.50	−0.51	
HD 89668	5400	4.35	2.35	−0.13	−0.19	19.1
HD 111721	5212	2.6	1.30	−1.11	−1.11	-
HD 125079	5520	3.3	1.25	−0.18	−0.18	
HD 126681	5760	4.65	0.9	−0.90	−0.92	-
HD 148897	4285	0.6	1.83	−1.02	−0.99	13
HD 164922	5400	4.3	0.09	0.22	0.23	12
HD 167768	5070	2.55	1.49	−0.51	−0.56	-
HD 188650	5700	2.15	2.33	−0.46	−0.44	
HD 214714	5550	2.41	1.96	−0.35	−0.36	

5.3 Abundance analysis

Abundances for most of the elements are determined from the measured equivalent widths of lines (listed in Tables A4 - A6) due to neutral and ionized elements using a recent version of MOOG of Sneden (1973) and the adopted model atmospheres.

We have determined abundances for Na, Mg, Ca, Sc, Ti, V, Cr, Mn, Co, Ni, Zn and for heavy elements Sr, Y, Zr, Ba, La, Ce, Pr, Nd, Sm, Eu and Dy. For the elements Sc, V, Mn, Ba, La and Eu, spectrum synthesis was used to find the abundances considering hyperfine structure. The results are shown in Tables A.7 - A.9 along with the errors. The line lists for each region that is synthesized were generated from Kurucz atomic line list (http://www.cfa.harvard.edu/amdata/ampdata/kurucz23/sekur.html). Atomic line databases like NIST, VALD etc were also consulted. As an example, spectrum synthesis calculations for Sc, Ba and La are shown in Figures 5.3, 5.4 and 5.5.

Derived abundance ratios with respect to iron are listed in Tables 5.2 and 5.3. In Table 5.4, we have presented [ls/Fe], [hs/Fe] and [hs/ls] values, where ls represents light s-process elements Sr, Y and Zr and hs represents heavy s-process elements Ba, La, Ce, Nd and Sm.

5.3.1 Carbon

We have derived the carbon abundance for our objects using the synthesis of C I line at 5380.337 Å. We have determined a carbon abundance of 8.65 dex and $^{12}C/^{13}C$ ratio of 12 for the object HD 16458 while Smith (1984) reported a carbon abundance of 8.70 dex and $^{12}C/^{13}C \sim 15$. For the three subgiant-CH stars in our sample, HD 4395, HD 125079 and HD 216219 we have found carbon abundance of 8.09, 8.39 and 8.55 dex respectively. Carbon abundances and isotopic ratios are also available in the literature for these objects (Smith et al. 1993; Luck & Bond 1982). Smith et al. (1993) gave carbon abundances of 8.65 dex, 9.05 dex and 9.02 dex for HD 4395, HD 125079 and HD 216219 respectively. Luck & Bond (1982) determined a [C/Fe] value of 0.4 and 1.2 for HD 216219 and HD 4395 respectively. For HD 201626, we have calculated a carbon abundance of 8.22 dex and a [C/Fe] value of 1.22. Vanture (1992a,b) reported a carbon abundance of 8.4 dex and $^{12}C/^{13}C \sim 25$ for the object HD 201626. Due to severe line distortions we could not find $^{12}C/^{13}C$ ratio in this object. While Luck (1991) gives a [C/H] ~ -0.16 and $^{12}C/^{13}C \sim 25$ for HD 214714 we could a find [C/H] value of -0.30 and [C/Fe] of 0.05. We have calculated the [C/Fe] value of 0.16 in HD 188650. Baird et al. (1975) also noticed an enhancement of carbon in HD 188650 and HD 214714 with respect to β Aqr. Because of the carbon deficiency in β Aqr they concluded that these two stars show normal carbon abundances. For HD 81192, Cottrell & Sneden (1986) reported a C/N ratio of 11.2 and Shetrone et al. (1993) gave $^{12}C/^{13}C \sim 35$. We could not find carbon abundance in HD 81192. For the objects HD 5395 and HD 48565 the calculated [C/Fe] values are -0.06 and 0.59 respectively.

We could not detect a C I line for HD 89668, HD 111721 and HD 126681 due to noise and line distortions through out the spectra. For HD 148897, we could find a very weak C I line but it is not useful for spectrum synthesis. For HD 148897 and HD 111721 we have found out the carbon abundance by synthesising CH band at 4300 Å. For HD 126681 we could not determine C abundance due to severe line distortion and blending throughout the spectrum. The [C/Fe] ratio determined for all the objects are listed in Table 5.2. Although the isotopic shifting of ^{12}CH and ^{13}CH lines is very small we have estimated the ^{12}C/^{13}C ratio using the synthesis of CH band. The initial ^{12}C/^{13}C is fixed at solar value and then varied to fit the observed spectrum for the determined carbon abundances. The values are given in Table 5.1 along with the atmospheric parameters. We could determine the isotopic ratios for seven objects and the values are in the range 4 - 19. The line list for the synthesis of CH band is taken from the Kurucz database for molecular lines. We have derived a [C/H] value of −0.23 and −1.23 for two cyanogen-weak giants HD 104979 and HD 148897. For these objects Luck (1991) reported the [C/H] value for as −0.38 and −0.94 respectively. We have determined a carbon abundance of 8.68 dex for HD 204613 while Smith et al. (1993) reported a carbon abundance of 8.91 dex for the same object. North et al. (1994) has given the [C/H] ratio of −0.07 and −0.03 respectively for HD 92545 and HD 107574. We have derived slightly lower [C/H] values for these objects. For HD 92545 we have obtained [C/H] value of −0.37 and for HD107574, we found a value of −0.18. Masseron et al. (2010) listed the [C/Fe] ratio of these objects as 0.32 and 0.39 respectively. Carbon abundance for HD 122202 is not available in the literature. We have derived a [C/H] value of −0.13 and [C/Fe] value of 0.50 for this object. We could get a [C/H] value of −0.48 and [C/Fe] value of 0.03 in HD 167786, which is in good agreement with the value of [C/H] = −0.63 and [C/Fe] = −0.02 in from Luck & Heiter (2007).

5.3.2 Na and Al

The sodium (Na) abundance is calculated using the lines at 5682.65 Å and 5688.22 Å for most of the programme stars. For HD 48565 a single line at 5682.65 Å is used. As these lines could not be used for HD 5395 and HD 81192, the resonant doublet lines at 5890.9 and 5895.9 Å are used. For HD 201626 the line at 5895.9 Å is used which is observed as a broad line with an equivalent width of 214 mÅ. We have used LTE analysis for the abundance determination. However, the resonance lines are sensitive to non-LTE effects (Baumueller & Gehren 1997; Baumueller et al. 1998; Cayrel et al. 2004). Derived Na abundances from LTE analysis range from −0.23 to 0.76 in the present sample. We note

that Na in HD 5395, HD 81192, HD 104979, HD 148897 and HD 164922 are found to be underabundant with respect to Fe while the other stars show near solar or mild over abundances.

Even though we could measure a few Aluminium (Al) lines in our programme stars spectra, they are blended and could not be used for abundance determination.

5.3.3 Mg, Si, Ca, Sc, Ti, V

We could measure several lines due to these elements. Except for HD 201626 and HD 148897, that show an overabundance for magnesium (Mg) with [Mg/Fe] $\geq$ 0.63, all other stars show mild enhancement or near-solar value of Mg. [Mg/Fe] in HD 148897 and HD 201626 (both with metallicity < -1.0) are $\sim$ 0.63 and $\sim$ 0.69 respectively, slightly higher than as expected for classical enhancement of α-elements in stars with [Fe/H] ~ -1.0 (Goswami & Prantzos 2000).

Abundance of silicon (Si) could not be estimated as none of the Si lines are found usable for abundance determination. Calcium (Ca) shows a near solar value or mild enhancement in most of the programme stars. HD 89668 and HD 201626, show an overabundance of Ca with [Ca/Fe] $\sim$ 0.60.

Scandium (Sc) abundance is determined using spectrum synthesis calculation of Sc II line at 6245.637 Å considering hyperfine structure from Prochaska & McWilliam (2000). While Sc is found to be mildly underabundant in ten objects with [Sc/Fe] ≥ -0.54, other stars show nearly solar values. HD 81192 and HD 204613 show a [Sc/Fe] value of 0.25 and 0.17 respectively.

Mild overabundance or near-solar abundance for titanium (Ti) is noticed in all the programme stars except for HD 89668. More than ten good lines of Ti are used for abundance determination. HD 201626 shows an overabundance of Ti with [Ti/Fe] $\sim$ 0.74.

We have detected more than 16 vanadium (V) lines but only one or two are usable for the determination of V abundance; other lines appear either blended or distorted in the spectra. Abundance of V is estimated for fifteen programme stars, from spectrum synthesis calculation of V I line at 5727.048 Å taking into account the hyperfine splitting. The log gf values of these lines are taken from Kurucz database. V abundance could not be estimated for other objects due to severe line blending. While HD 16458 and HD 164922 show [V/Fe] $\sim$ 0.25 and 0.40 respectively all other programme stars show mild under abundance or nearly solar values.

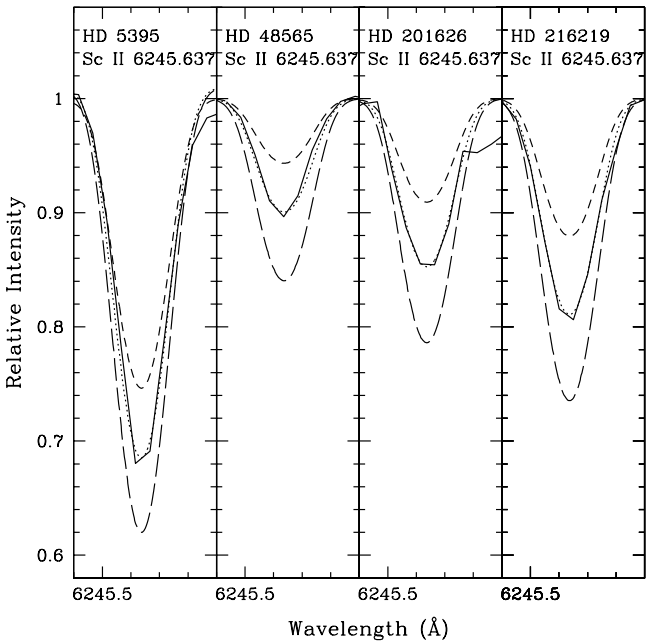

Figure 5.3: Spectral-synthesis fits of Sc II line at 6245.637 Å. The dotted lines indicate the synthesized spectra and the solid lines indicate the observed line profiles. Two alternative synthetic spectra for [X/Fe] = +0.3 (long-dashed line) and [X/Fe] = −0.3 (short-dashed line) are shown to demonstrate the sensitivity of the line strength to the abundances.

5.3.4 Cr, Co, Mn, Ni, Zn

HD 16458 shows a mild overabundance of cromium (Cr) relative to Fe. HD 4395, HD 107574, HD 122202, HD 125079, HD 148897, HD 188650, HD 164922 and HD 216219 show near-solar abundances. The rest of the stars in our sample are mildly underabundant in Cr. HD 55496 and HD 201626 however shows a larger underabundance with [Cr/Fe] = −0.35 and −0.59 respectively. Cr abundances measured using Cr II lines whenever possible also show similar trends.

Manganese (Mn) abundance is calculated using spectrum synthesis of 6013.51 Å line considering hyperfine structures from Prochaska & McWilliam (2000). Except for HD 16458, HD 89668 and HD 164922, with a mild overabundance of Mn with [Mn/Fe] ∼ 0.06, 0.34 and 0.14 respectively, the rest of the objects show underabundance with [Mn/Fe] ≤ −0.33. Except for HD 16458 and HD 92545, with [Co/Fe] ∼ 0.49 and 0.80 all other stars in our sample show near-solar values or mild underabundance for cobalt (Co). Abundances of nickel (Ni) measured from Ni I lines give near-solar values for all the stars. HD 5395, HD 16458 and HD 122202 show mild overabundance with [Zn/Fe] ∼ 0.29, 0.43 and 0.50 respectively. The rest of the objects show near-solar values.

Table 5.2: Elemental abundance ratios: Light elements

Star	[C/Fe]	[Na I/Fe]	[Mg I/Fe]	[Ca I/Fe]	[Sc II/Fe]	[Ti I/Fe]	[Ti II/Fe]	[V I/Fe]	[Cr I/Fe]	[Cr II/Fe]	[Mn I/Fe]	[Co I/Fe]	[Ni I/Fe]	[Zn I/Fe]
Group I														
*HD 16458	0.91	0.65	0.04	0.28	0.10	0.31	0.41	0.25	0.29	-	0.06	0.49	0.15	0.43
#HD 122202	0.50	-	0.32	0.33	-	-	0.36	-	0.11	-	-	-	0.14	0.59
HD 201626	1.22	0.41	0.69	0.65	0.04	0.74	0.81	-	−0.59	-	-	0.00	−0.11	−0.04
#HD 204613	0.49	0.08	0.11	0.13	0.17	0.26	0.41	−0.01	−0.06	0.08	−0.33	−0.19	0.04	-
#HD 216219	0.33	0.32	0.15	0.14	−0.18	0.11	0.29	−0.13	−0.09	0.12	−0.32	0.03	0.00	0.16
Group II														
#HD 4395	−0.14	0.23	0.12	0.01	−0.09	0.04	0.22	−0.14	0.01	0.15	−0.23	−0.19	−0.02	0.18
*HD 55496	1.01	0.4	0.33	0.46	-	−0.1	−0.16	0.19	−0.35	−0.21	-	-	−0.18	0.02
*HD 48565	0.59	0.18	0.15	0.11	−0.11	0.04	0.30	−0.21	−0.19	−0.32	−0.42	−0.15	−0.17	−0.18
HD 92545	0.68	0.01	−0.09	−0.05	-	0.03	0.6	-	−0.15	-	-	0.8	0.01	-
HD 104979	0.03	−0.01	0.07	0.05	−0.01	0.14	0.32	0.05	−0.02	0.06	−0.23	0.28	0.04	−0.03
HD 107574	0.47	0.49	-	0.19	−0.13	0.32	0.34	-	0.1	−0.26	-	-	0.01	-

Table 5.2 – continued from previous page

Star	[C/Fe]	[Na I/Fe]	[Mg I/Fe]	[Ca I/Fe]	[Sc II/Fe]	[Ti I/Fe]	[Ti II/Fe]	[V I/Fe]	[Cr I/Fe]	[Cr II/Fe]	[Mn I/Fe]	[Co I/Fe]	[Ni I/Fe]	[Zn I/Fe]
Group III														
*HD 5395	−0.06	−0.39	0.12	0.04	0.04	0.08	0.18	−0.24	−0.19	0.0	−0.5	0.20	−0.09	0.29
HD 81192	-	−0.29	0.29	0.18	0.25	0.25	0.25	0.10	−0.33	−0.23	−0.40	0.28	0.08	−0.14
HD 89668	0.05	0.08	0.28	0.63	0.0	−0.26	−0.38	-	−0.09	−0.27	0.34	−0.23	−0.12	
HD 111721	0.08	0.07	0.46	0.41	-	0.46	0.03	-	−0.21	−0.31	-	-	−0.07	-
HD 125079		0.34	0.05	0.03	0.02	0.0	0.45	−0.12	−0.06	-	−0.22	0.03	0.07	0.11
HD 126681	-	−0.26	0.44	0.07	-	0.52	0.60	-	0.1	-	-	-	−0.08	-
HD 148897	−0.21	−0.29	0.63	0.19	−0.33	0.11	0.46	−0.18	−0.22	0.0	−0.54	0.06	−0.13	−0.26
HD 164922	−0.15	−0.02	0.36	−0.07	−0.47	0.25	0.05	0.40	0.04	0.06	0.14	0.13	0.06	0.19
HD 167768	0.03	0.04	0.17	0.22	−0.04	0.17	0.41	0.2	−0.09	−0.21	−0.56	−0.03	−0.09	0.18
HD 188650	0.16	0.76	0.27	−0.02	−0.49	0.24	0.24	−0.24	−0.04	0.01	−0.24	0.06	−0.16	−0.05
HD 214714	0.05	0.47	0.00	0.17	−0.54	−0.19	0.32	−0.44	−0.32	−0.23	−0.49	−0.06	−0.26	−0.13

subgiant-CH stars

* Objects are also included in Ba star catalogue of Lu (1991)

5.3.5 Sr, Y, Zr

The strontium (Sr) abundance is derived from Sr I line at 4607.327 Å for fourteen stars. HD 16458, HD 4395, HD 48565, HD 89668, HD 125079, HD 204613 and HD 216219 show overabundances with [Sr/Fe] ≥ 1.0. The objects HD 5395, HD 55496, HD 81192, HD 104979, HD 148897, HD 164922 and HD 167768 give [Sr/Fe] ratios in the range 0.28 to 0.99. For the remaining objects the Sr abundance could not be measured as the line at 4607.327 Å appears distorted. None of the Sr II lines detected in the spectra are usable for abundance estimates.

The abundance of yttrium (Y) is derived for all the stars except for HD 201626. HD 16458, HD 48565, HD 122202, HD 125079, HD 204613 and HD 216219 show an overabundance with [Y/Fe]≥ 1.0. In the case of HD 4395, HD 89668, HD 104979 and HD 167768 [Y/Fe] ≤ 0.71. Also HD 204613 and HD 55496 show [Y/Fe] values of 0.97 and 0.85 respectively. The remaining stars HD 92545, HD 5395, HD 81192, HD 111721, HD 126681, HD 148897, HD 164922, HD 188650 and HD 214714 show near-solar values.

We could derive zirconium (Zr) abundance for eleven stars. Five stars show an overabundance with [Zr/Fe] ≥ 1.0. HD 148897 and HD 214714 show an underabundance with [Zr/Fe] ≤ −0.28 and HD 81192 gives a near-solar value. HD 4395 and HD 104979 show overabundance with [Zr/Fe] ∼ 0.58 and 0.85 respectively. The rest show mild enhancement with [Zr/Fe] ≥ 0.2.

5.3.6 Ba, La, Ce, Pr, Nd, Sm, Eu, Dy

As many lines due to Ce, Pr, Nd, Sm and Dy could be measured on our spectra, the standard abundance determination method using equivalent width measurements are used for the abundance determination of the elements Ce, Pr, Nd, Sm and Dy. Spectrum synthesis calculation are carried out for Ba, La and Eu. We could determine the abundances for Ba and Ce for all the stars.

Barium (Ba): We have determined Ba abundances by synthesising Ba II line at 5853.67 Å considering hyperfine components from McWilliam (1998). Nine of our programme stars HD 16458, HD 48565, HD 92545, HD 104979, HD 107574, HD 125079, HD 204613, HD 201626 and HD 216219 show over abundance of Ba with [Ba/Fe] ≥ 1.0. HD 4395 shows an overabundance with [Ba/Fe] ∼ 0.79. The objects HD 5395, HD 81192 and HD 188650 show near solar values. HD 55496, HD 122202 and HD 126681 show only a mild overabundance. Five objects HD 89968, HD 111721, HD 148897, HD 167768 and

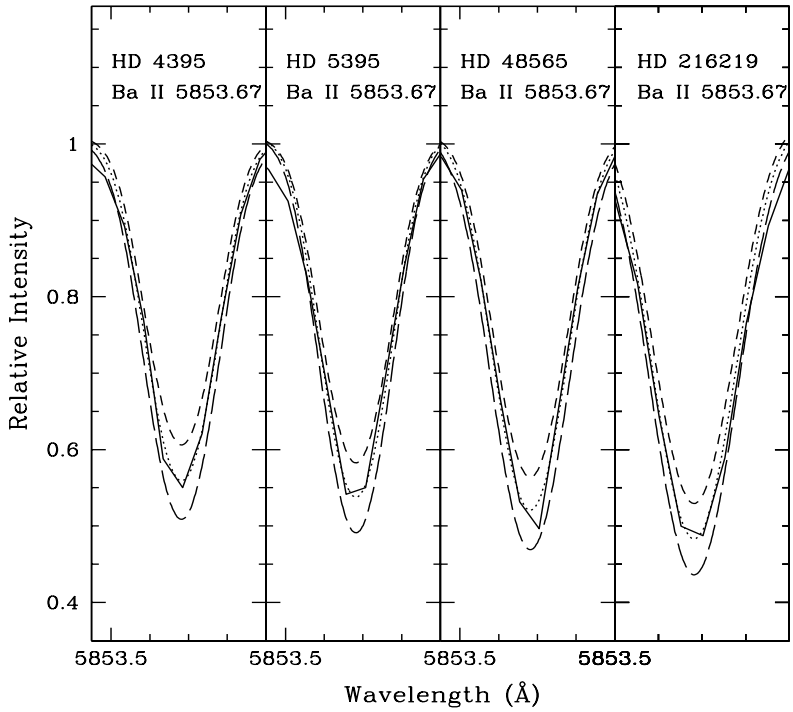

Figure 5.4: Spectral-synthesis fits of Ba II line at 5853.67 Å. The dotted lines indicate the synthesized spectra and the solid lines indicate the observed line profiles. Two alternative synthetic spectra for [X/Fe] = +0.3 (long-dashed line) and [X/Fe] = −0.3 (short-dashed line) are shown to demonstrate the sensitivity of the line strength to the abundances.

HD 214714 show underabundance with [Ba/Fe] in the range −0.09 to −0.65 (Table 5.3).

Lanthanum (La): We have derived La abundance for the programme stars from spectrum synthesis calculation of La II line at 4921.77 Å considering hyperfine components from Jonsell et al. (2006). Except for HD 81192, HD 5395, HD 111721, HD 148897, HD 164922 and HD 167768, La in all other stars is found to be overabundant relative to Fe with [La/Fe] ≥ 0.9. HD 5395, HD 81192, HD 111721, HD 148897, HD 164922 and HD 167768 show [La/Fe] of 0.24, −0.13, 0.31, 0.29, 0.15 and −0.54 respectively.

Cerium (Ce): We have derived Ce abundance for all the programme stars. In HD 125079 [Ce/Fe] ∼ 0.93. While three stars HD 5395, HD 188650 and HD 214714, show almost near-solar values, HD 16458, HD 48565, HD 201626, HD 216219 give 1.47, 1.42, 1.89 and 1.03 respectively for [Ce/Fe]. Six of the programme stars, HD 89668, HD 92545, HD 104979, HD 111721, HD 122202 and HD 204613 also show overabundance with [Ce/Fe] ≥ 1.0. Estimated [Ce/Fe] for HD 4395 and HD 107574 is ∼ 0.42 and 0.6 respectively. While two stars HD 55496 and HD 167768 show almost near-solar values for [Ce/Fe], HD 81192, HD 148897 and HD 164922 show mild underabundance with

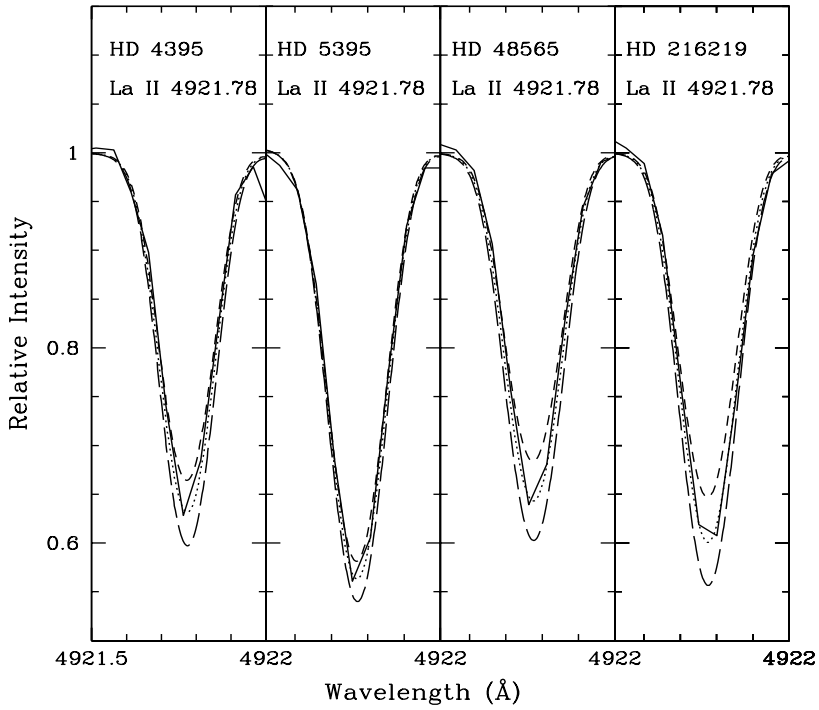

Figure 5.5: Spectral-synthesis fits of La II line at 4921.78 Å. The dotted lines indicate the synthesized spectra and the solid lines indicate the observed line profiles. Two alternative synthetic spectra for [X/Fe] = +0.3 (long-dashed line) and [X/Fe] = −0.3 (short-dashed line) are shown to demonstrate the sensitivity of the line strength to the abundances.

[Ce/Fe] ∼ −0.10.

Praseodymium (Pr): We could derive Pr abundance in the programme stars mainly using the Pr II line at 5292.619 Å. A mild over enhancement of Pr is seen in HD 4395, HD 55496 and HD 188650 with [Pr/Fe] ∼ 0.53, 0.43 and 0.57 respectively. In all the other stars Pr shows an overabundance with values 0.79 ≥ [Pr/Fe] ≥ 1.0.

Neodymium (Nd): Abundance of Nd is estimated for seventeen programme stars. Two stars HD 148897 and HD 167768 give [Nd/Fe] values ∼ 0.13 and 0.65 respectively. HD 188650 and HD 214714 show mild overabundance with [Nd/Fe] ∼ 0.39 and 0.36 respectively. Two stars HD 4395 and HD 5395 give [Nd/Fe] ∼ 0.8 and 0.74 respectively. While HD 16458, HD 48565, HD 81192 HD 125079 and HD 216219 show an overabundance with [Nd/Fe] ≥ 1.0, HD 111721 and HD 201626 show a large overabundance with [Nd/Fe] ≥ 2.1.

Samarium (Sm): Except for HD 125079, we have used at least two clean lines for deriving the Sm abundance. HD 188650 shows a mild underabundance with [Sm/Fe] ∼ −0.12. This value is found to be 0.85, 0.56, 0.58, 0.90, 0.46 and 0.91 respectively in

HD 81192, HD 125079, HD 148897, HD 167768, HD 214714 and HD 216219. Abundance of Sm is derived from a single Sm II line at 4577.690 Å in HD 125079. Four objects HD 16458, HD 4395, HD 48565 and HD 201626 show an overabundance with [Sm/Fe] ~ 1.87, 1.08, 1.18 and 1.63 respectively. Similarly HD 89668, HD 104979, HD 122202, HD 126681 and HD 204613 show overabundance with [Sm/Fe] ≥ 1.0. We could not estimate Sm abundance in HD 5395.

Europium (Eu): The abundance of Eu is derived for HD 5395 and HD 16458 using spectrum synthesis of Eu II lines at 6437.640 Å and 6645.130 Å by considering the hyperfine components from Worley et al. (2013). Eu shows an overabundance with [Eu/Fe] ~ 0.34 and 0.67 respectively. In HD 48565 we have used the Eu II line at 4129.700 Å and hyperfine components are taken from Mucciarelli et al. (2008). Eu is found to be slightly overabundant with [Eu/Fe] ~ 0.29. In case of HD 216219 we note that the above Eu II lines are marginally asymmetric on the right wings. These lines however, return a near solar value with [Eu/Fe] ~ 0.07 for this object. Eu shows mild overabundance in HD 89668, HD 92545 and HD 167768 with [Eu/Fe] ~ 0.38, 0.40 and 0.26 respectively. HD 204613 shows a near-solar value with [Eu/Fe] ~ 0.06.

Dysprosium (Dy): We could derive Dy abundance for six objects using the Dy II lines at 4103.310 Å and 4923.167 Å. For, HD 5395, HD 81192, HD 167768, HD 201626 and HD 204613 Dy shows an overabundance with [Dy/Fe] ≥ 1.0. HD 148897 shows a near-solar value of ~ 0.02.

Table 5.3: Elemental abundance ratios : Heavy elements

Star	[$\frac{\text{Sr I}}{\text{Fe}}$]	[$\frac{\text{Y II}}{\text{Fe}}$]	[$\frac{\text{Zr II}}{\text{Fe}}$]	[$\frac{\text{Ba II}}{\text{Fe}}$]	[$\frac{\text{La II}}{\text{Fe}}$]	[$\frac{\text{Ce II}}{\text{Fe}}$]	[$\frac{\text{Pr II}}{\text{Fe}}$]	[$\frac{\text{Nd II}}{\text{Fe}}$]	[$\frac{\text{Sm II}}{\text{Fe}}$]	[$\frac{\text{Eu II}}{\text{Fe}}$]	[$\frac{\text{Dy II}}{\text{Fe}}$]
Group I											
*HD 16458	1.37	1.46	1.17	1.18	1.42	1.47	1.82	1.55	1.87	0.66	-
#HD 122202	-	1.44	-	0.33	0.9	1.62	1.26	-	1.77	-	-
HD 201626	-	-	-	2.12	1.76	1.89	2.09	2.24	1.63	-	0.97
#HD 204613	1.71	0.97	1.14	1.04	1.21	1.24	1.52	1.02	1.61	0.06	1.77
#HD 216219	1.8	1.00	0.98	1.10	1.04	1.03	1.14	0.99	0.91	0.07	-
Group II											
#HD 4395	1.08	0.65	0.58	0.79	1.03	0.42	0.53	0.80	1.08	-	-
*HD 48565	1.73	1.08	0.9	1.52	1.46	1.42	1.29	1.51	1.18	0.29	-
*HD 55496	0.82	0.85	0.52	0.57	-	0.13	0.43	-	-	-	-
HD 92545	-	0.23	-	0.91	0.95	1.6	-	-	-	-	-
HD 104979	0.99	0.71	0.85	0.94	1.11	1.06	1.04	1.13	1.17	0.40	-
HD 107574	-	1.02	-	0.97	1.04	0.6	-	-	-	-	-

Table 5.3 – continued from previous page

Star	[Sr I/Fe]	[Y II/Fe]	[Zr II/Fe]	[Ba II/Fe]	[La II/Fe]	[Ce II/Fe]	[Pr II/Fe]	[Nd II/Fe]	[Sm II/Fe]	[Eu II/Fe]	[Dy II/Fe]
Group III											
*HD 5395	0.26	0.05	-	0.03	0.24	0.06	0.79	0.74	-	0.34	1.38
HD 81192	0.58	0.10	0.12	0.13	−0.13	−0.15	-	1.01	0.85	-	1.21
HD 89668	1.06	0.55	-	−0.24	1.87	1.52	1.66	1.44	1.23	0.38	-
HD 111721	-	0.05	-	−0.09	0.31	1.6	-	2.1	-	-	-
#HD 125079	1.59	1.05	-	1.06	-	0.93	1.00	1.16	0.56	-	-
HD 126681	-	0.02	-	0.27	-	0.67	-	1.2	1.07	-	-
HD 148897	0.31	0.03	−0.47	−0.65	0.29	−0.16	-	0.13	0.58	-	0.02
HD 164922	0.79	0.14	-	0.28	0.15	−0.09	-	-	-	-	-
HD 167768	0.77	0.56	0.2	−0.36	−0.54	0.06	-	0.65	0.9	0.26	1.04
HD 188650	-	−0.03	-	−0.01	-	−0.03	0.57	0.39	−0.12	-	-
HD 214714	-	0.22	−0.28	−0.31	-	0.05	0.93	0.36	0.46	-	-

subgiant-CH stars

* Objects are also included in Ba star catalogue of Lu (1991)

Table 5.4: [ls/Fe], [hs/Fe] and [hs/ls] for the programme stars

Star	[Fe/H]	[ls/Fe]	[hs/Fe]	[hs/ls]	Remarks
Group I					
HD 16458	−0.65	1.34	1.50	0.16	1
HD 122202	−0.63	1.44	1.16	−0.28	1
HD 201626	−1.39	-	1.93	-	1
	−1.30	1.10	1.60	0.50	2
HD 204613	−0.24	1.27	1.16	−0.11	1
HD 204613	−0.35	1.0	0.6	−0.4	2
HD 216219	−0.17	1.26	1.01	−0.25	1
	−0.32	1.00	0.9	−0.10	2
Group II					
HD 4395	−0.18	0.77	0.82	0.05	1
	−0.33	0.70	0.50	−0.2	2
HD 48565	−0.59	1.24	1.47	0.23	1
HD 55496	−1.49	0.73	0.38	−0.35	1
HD 92545	−0.21	0.23	1.15	0.92	1
HD 104979	−0.26	0.85	1.03	0.18	1
HD 104979	−0.47	0.6	1.0	0.4	2
HD 107574	−0.48	1.02	0.87	−0.15	1
Group III					
HD 5395	−0.24	0.16	0.27	0.11	1
HD 81192	−0.50	0.26	0.34	0.08	1
HD 89668	−0.13	0.81	1.16	0.35	1
HD 111721	−1.11	0.05	0.98	0.93	1
HD 125079	−0.18	1.32	0.93	−0.39	1
HD 126681	−0.90	0.02	0.80	0.78	1
HD 148897	−1.02	−0.13	0.01	0.14	1

Table 5.4 – continued from previous page

Star	[Fe/H]	[ls/Fe]	[hs/Fe]	[hs/ls]	Remarks
HD 164922	0.22	0.47	0.10	−0.37	1
HD 167768	−0.51	0.51	0.14	−0.37	1
HD 188650	−0.45	−0.03	0.23	0.26	1
HD 214714	−0.35	−0.03	0.14	0.17	1

1. Our work; 2: Busso et al. (2001)

5.4 Discussion on individual stars

Comparisons of our estimated atmospheric parameters and elemental abundance ratios with literature values whenever available, are presented in Tables 5.5 and 5.6 respectively. In the case of HD 201626 the author gave absolute abundances (logϵ(x)), rather than abundance ratios; hence in Table 5.6, calculated abundance ratios are presented using solar Fe values from Asplund et al. (2005).

Information on the circumstellar environment of these objects are not available in the literature. Information on polarization estimates is limited to only eight objects (Goswami & Karinkuzhi 2013) in this sample. Estimated percentage polarization in B, V, R, I bands are found to be low with < 0.2 per cent in all the four bands for HD 81192 and < 0.4 per cent for HD 125079 (Goswami & Karinkuzhi 2013). Among these, three objects show percentage V-band polarization at a level ∼ 0.2 per cent (HD 55496 (p_v% ∼ 0.18), HD 111721 (p_v% ∼ 0.22, and HD 164922 (p_v% ∼ 0.28)) indicating presence of circumstellar dust distribution in non-spherically symmetric envelopes. The other three objects, HD 92545, HD 107574 and HD 126681, show V-band percentage polarization at a level < 0.1%.

HD 125079, **HD 4395**, **HD 216219**: These three low-velocity CH stars are identified as subgiant-CH stars by Bond (1974). Spectral characteristics of subgiant-CH stars are similar to giant CH stars. With lower temperatures and luminosities the subgiant-CH stars occupy a position below the giants in H-R diagram. High resolution spectroscopic analyses of subgiant-CH stars by Sneden & Bond (1976) and Luck & Bond (1982) have confirmed the enhancement of heavy elements and a metal-deficiency in the range −0.2 to −0.5 for these objects. As in the case of CH giants, abundance peculiarities of

subgiant-CH stars are also explained as due to mass transfer mechanisms from their binary companions (Luck & Bond 1991). Smith et al. (1993) have reported the abundances for elements Y, Zr, Ba and Nd. The effective temperature adopted by us is about 250 K larger than what they have considered for these three stars. The estimated metallicity values are about 0.15 dex lower than their estimates. For HD 125079, our estimated abundances for Y is about 0.3 dex higher and for Ba and Nd, the values are about 0.2 dex higher. In addition, we have also estimated the abundances of Ce, Pr and Sm in these objects. For the other two stars we have derived almost similar abundances for Y. For Zr, Ba and Nd, our estimated abundances are slightly higher than their values.

HD 122202, **HD 204613**: These two objects are also subgiant-CH stars. Luck & Bond (1991) have studied the object HD 122202 and reported abundances for a few s-process elements. HD 204613 was studied by Smith (1984); these authors gave the abundances for Y, Zr, Ba and Nd in this object. In addition to these elements we estimated the abundances for Sr, La, Ce, Pr, Sm, Eu and Dy in HD 204613 and La, Pr and Sm in HD 122202. The object HD 122202 shows a large enhancement in Ce, Pr and Nd. However, Ba is only mildly enhanced with [Ba/Fe] $\sim$ 0.33. HD 204613 shows a large enhancement in all the elements except Eu. According to Beers and Christlieb (2005) classification, this object fall into the group of CEMP-s stars with [Ba/Fe] $\sim$ 1.04 and [Ba/Eu] $\sim$ 0.98. McClure (1997) have confirmed these objects as binaries and also provided the information on the orbital elements. While HD 122202 shows radial velocity variations in the range -14.81 to -7.64 with an orbital period of 1290 $\pm$ 9 days; HD 204613 exhibits radial velocity variations from -95.07 to -87.85 with period 878 $\pm$ 4 days.

HD 55496: Bond (1974) has classified this high velocity object as a subgiant-CH star. MacConnell et al. (1972) included this in the category of weak lined metal-deficient Ba II star. Being a high velocity object with lower metallicity ([Fe/H] = -1.45), HD 55496 seems to show the extreme halo kinematics. Luck & Bond (1991) has studied this object and reported abundances for a few elements (Table 5.6). Estimated Ba abundance ([Ba/Fe] = 0.57) does not qualify the object to be a typical CH star. Light s-process elements Sr, Y and Zr are more abundant in this star than the heavy s-process elements Ba, Ce, and Pr.

HD 16458: This star is included both in the Ba star catalogue of Lu (1991) and CH star catalogue of Bartkevicius (1996). Estimated radial velocity is about 18.24 km s^{-1}. Chemical composition studies of this object with respect to the abundances of a standard giant star β Gem by Tomkin & Lambert (1983) reported the enhancement of heavy ele-

ments in this object. Smith (1984) also studied this star and reported the enhancement of heavy elements. Our abundance estimates are slightly higher compared to those of Smith (1984). With [Ba/Fe] value ∼ 1.18 and [Ba/Eu] ∼ 0.52, this star satisfies the conditions for CEMP-s stars (Beers & Christlieb 2005). Long-term radial velocity monitoring of HD 16458 by McClure & Woodsworth (1990) have confirmed it to be a binary star.

HD 5395: HD 5395 is included both in the Ba star catalogue of Lu (1991) and CH star catalogue of Bartkevicius (1996). McWilliam (1990) provided the elemental abundances for Sr, Zr, Y, La and Nd. We present updates on these abundances along with the first estimates of abundances for Ba, Ce, Pr and Eu. While Y, Ba and Ce show almost near-solar values, Sr, La and Eu show mild enhancement with [Sr/Fe] = 0.26, [La/Fe] = 0.24 and [Eu/Fe] = 0.38. Pr, Nd and Dy show larger enhancement with respect to Fe. As far as the chemical abundances are concerned this object does not seem to belong to the group of CH stars if we stick to the definition that CH stars are those that show high abundance of s-process elements with [Ba/Fe] > 1.

HD 214714, **HD 188650**: The spectra of HD 214714 and 188650 show a close resemblance. Bidelman (1953) first noticed strong bands of CH and moderate CN bands in the spectra of these stars and called them as low-velocity CH stars. Our estimated radial velocities for these two objects are −7.04 and −24.6 km s^{-1} respectively. Strong ionized lines of elements seen in their spectra indicate high luminosity. However, following Morgan et al. (1943), Luck (1991) referred to these objects as a cyanogen-weak giants as their spectrum is characterized by weak violet CN bands. Using a curve of growth method in comparison with β Aqr, Baird et al. (1975) estimated chemical abundances for these objects and reported a high lithium abundance for HD 214714. Our chemical analysis with respect to solar values indicates a mild enhancement of heavy elements. Ba is found to be underabundant in this object. We present first-time estimates of chemical abundances for HD 188650 based on high-resolution spectrum. The abundance of Eu could not be estimated for this object. Light s-process element Y, and heavy s-process elements Ba, Ce and Sm show near-solar values in this object. Pr and Nd also show mild enhancement with [Pr/Fe] ∼ 0.57 and [Nd/Fe] ∼ 0.39 respectively. This object does not seem to represent the characteristic properties of CH stars as far as the heavy element abundances are concerned.

HD 104979, **HD 148897**: Luck (1991), identified these objects as cyanogen-weak giants and reported elemental abundances for Y, Zr, Ce, Nd and Eu. Our results closely match with their values. In addition to these elements we could measure abundances for Sr, Ba, La, Sm, Pr and Dy. Similar to the two cyanogen-weak giants HD 188650 and

HD 214714, the object HD 148897 also does not show large enhancement in heavy elements. These three objects are of the same spectral type. The object HD 104979 shows enhancements in Ba with [Ba/Fe] = 0.94. Estimated metallicities of these objects are −0.26 and −1.02 respectively.

HD 201626 : This object was first identified as a CH star by Wallerstein & Greenstein (1964); its spectrum closely resembles the spectrum of the well-known CH star HD 26. This is a high velocity object with a radial velocity of −141.6 km s^{-1} and metallicity [Fe/H] ∼ −1.4. Abundances of heavy elements Ba, La, Ce, Pr, Nd, Sm and Dy with respect to Fe are found to be highly enhanced in this object. Our estimates of heavy element abundances are in good agreement with the estimates of Vanture (1992c).

HD 48565: The object HD 48565 is known to show abnormally strong Sr line at 4077 Å North et al. (1994). Bidelman (1981) classified these type of objects as F Str λ 4077 stars. They exhibit enhancement of light and heavy s-process elements but abundances of iron-peak elements are similar to those generally seen in F type stars. Allen & Barbuy (2006a) have given the abundance estimates for heavy elements in this star. Our results are slightly higher than their results, with [X/Fe] values > 1 for all the heavy elements (Table 5.3). Our estimated radial velocity (−25.74 km s^{-1}) is about 6 km s^{-1} lower than the literature value. This object is showing a large radial velocity variations (North et al. 1994; Nordstroem et al. 2004) giving indications of the object being a binary system.

HD 92545, **HD 107574**: North & Duquennoy (1992) have categorized these objects as F str λ 4077 stars following the classification of Bidelman (1981). Allen & Barbuy (2006a,b) have reported chemical abundances for these objects (Table 5.6). For HD 92545, our Ce abundance is higher than their estimates. Other elements show a close similarity and within the error limits. For HD 107574, our results are fairly in good agreement with their estimates.

HD 81192: Except for Sr, Nd and Sm this object shows almost near-solar values for Y, Zr, Ba, La, and Ce with respect to Fe. Morgan et al. (1943) have noted weaker CN bands in HD 81192 compared to other stars of same temperature and luminosity. Weakening of CN band is most common in stars with high space velocities. Estimated radial velocity of this object is 136 km s^{-1}. Cottrell & Sneden (1986) have studied the kinematics and elemental abundances of this object. Estimated heavy element abundances by Luck & Bond (1985) are found to be in close agreement with our estimates. We present first-time estimates of abundances for Sr, Sm and Dy for this object. With [Ba/Fe] = 0.13, this object too does not seem to belong to the group of CH stars.

HD 89668: We present first time detailed abundances for this object. This object

shows large enhancements in La, Ce, Pr, Nd and Sm with [X/Fe], where X represents the heavy elements, values ≥ 1; however, Ba is slightly underabundant with [Ba/Fe] ∼ −0.24.

HD 111721: Gratton & Sneden (1994) have studied this object and reported abundances for a few heavy elements. From our analysis and also from Gratton & Sneden (1994) this object does not show enhancement in heavy elements. The metallicity of this object is −1.11. Estimated [C/Fe] ratio is 0.08 for this object.

HD 126681: We have presented the first time abundance estimates for the elements Ce, Nd and Sm in this object. Fulbright (2000) has studied this object and reported abundances for Y and Ba. This object shows a large enhancement in Nd and Sm but other heavy elements are only mildly enhanced.

HD 164922: The object HD 164922 is listed as a CH star by Bartkevicius (1996), however, this object does not seem to show the characteristics of CH stars. Mishenina et al. (2013) have studied this object and reported abundances for a few heavy elements that show almost near-solar values for Zr, Ba, Ce, Nd, Sm and Eu. Our estimated Ba and Ce abundances give [Ba/Fe] ∼ 0.28 and [Ce/Fe] ∼ −0.09 for this object.

HD 167768: Luck & Heiter (2007) has studied this object and reported abundances for Y, Ba, Ce, Pr, Nd, Eu. In addition to these elements, we have estimated abundances for Sr, Zr, La and Sm. This object does not show large enhancement of heavy elements.

Table 5.5: Atmospheric parameters from literature

Star	Vmag	T_{eff} (K)	log g	[Fe/H]	Reference
Group I					
HD16458	5.78	4550	1.80	−0.65	1
		4582	2.00	−0.32	5
		4582	2.00	−0.43	5
		4800	1.80	−0.30	6
		4500	1.40	−0.36	17
HD 122202	9.37	6430	4.0	−0.63	1
		6600	3.0	−0.09	19
HD 201626	8.13	5120		−1.39	1
HD 204613	8.21	5875	4.2	−0.24	1
		5718	3.88	−0.38	39
		5650	3.80	−0.35	35

Table 5.5 – continued from previous page

Star	Vmag	T_{eff} (K)	log g	[Fe/H]	Reference
		5650	3.80	−0.35	23
		5600	3.5	−0.70	14
		5600	3.5	−0.65	16
		5663	3.75	−0.54	12
HD216219	7.40	5950	3.5	−0.17	1
		5478	2.80	−0.55	7
		5600	3.25	−0.39	12
		5600	3.20	−0.32	23
Group II					
HD4395	7.50	5550	3.66	−0.17	1
		5478	3.40	−0.31	7
		5478	3.30	−0.38	12
		5450	3.30	−0.33	23
		5467	3.32	−0.35	34
HD48565	7.07	6030	3.80	−0.59	1
		5910	4.27	−0.56	25
HD 55496	8.40	4850	2.05	1.45	1
		4858	2.05	−1.48	39
		4935	2.33	−1.44	37
		4800	2.8	−1.55	19
HD 92545	8.56	6380	4.65	−0.21	1
		6240	4.23	−0.26	25
HD 104979	4.13	5060	2.67	−0.26	1
		4842	2.9	−0.51	33
		4996	2.86	−0.33	32
		4825	2.34	−0.33	18
		4870	3.23	−0.51	16
		4893	2.6	−0.29	11
		4990	2.65	−0.11	3

Table 5.5 – continued from previous page

Star	Vmag	T_{eff} (K)	log g	[Fe/H]	Reference
		5250	3.25	−0.29	2
HD 107544	8.55	6250	2.9	−0.65	1
		6340	3.87	−0.36	24
Group III					
HD5395	4.63	4860	2.51	−0.24	1
		4800	2.20	−1.00	17
		4770	2.90	−0.51	16
		4764	2.36	−0.44	34
HD 81192	6.54	4870	2.75	−0.50	1
				−0.61	4
		4755	2.40	−0.60	8
		4582	2.75	−0.70	9
HD 89968	9.41	5400	4.35	−0.13	1
		4811	4.45	−0.11	40
HD 111721	7.97	5212	2.6	−1.11	1
		5120	2.90	−1.27	37
		4995	2.52	−1.26	30
		4825	2.2	−1.54	29
		4800	3.00	−1.68	28
		5164	3.27	−0.98	27
		4940	2.40	−1.34	26
		5103	3.06	−1.22	24
		5000		−1.34	22
		5103	2.87	−1.25	20
HD125079	8.60	5520	3.30	−0.18	1
		5305	3.50	−0.30	12
		5300	3.50	−0.16	23
HD 126681	9.32	5760	4.65	−0.90	1
		5507	4.45	−1.17	38

Table 5.5 – continued from previous page

Star	Vmag	T_{eff} (K)	log g	[Fe/H]	Reference
		5561	4.71	−1.14	40
		5577	4.25	−1.12	39
		5475	4.65	−1.38	36
		5533	4.28	−1.14	31
		5450	4.5	−1.25	29
		5625	4.95	−1.09	27
HD 148897	5.25	4285	0.6	−1.02	1
		4293	1.01	−1.11	39
		4100	0.09	−1.16	19
		4345	1.5	−0.62	10
HD 167768	6.00	5070	2.55	−0.51	1
		4953	2.29	−0.69	39
		5102	2.76	−0.61	32
HD188650	5.76	5700	2.15	−0.46	1
HD214714	6.03	5550	2.41	−0.36	1
		5400	2.38	−0.36	18

References.1. Our work, 2. Lambert & Ries (1981), 3. Sneden et al. (1981), 4. Luck & Bond (1983), 5. Tomkin & Lambert (1983), 6. Smith (1984), 7. Krishnaswamy & Sneden (1985), 8. Luck & Bond (1985), 9. Cottrell & Sneden (1986), 10. Kyrolainen et al. (1986), 11. Tomkin & Lambert (1986), 12. Smith & Lambert (1986), 13. Abia et al. (1988), 14. Rebolo et al. (1988), 15. Abia et al. (1988), 16.McWilliam (1990), 17. Fernandez-Villacanas et al. (1990) 18. Luck (1991), 19. Luck & Bond (1991), 20. Gratton & Sneden (1991), 21. Tomkin et al. (1992), 22.Pilachowski et al. (1993), 23. Smith et al. (1993), 24. Gratton & Sneden (1994), 25. North et al. (1994), 26. Ryan & Lambert (1995), 27. Gratton et al. (1996), 28.Cavallo et al. (1997), 29. Fulbright (2000), 30. Gratton et al. (2000), 31. Nissen et al. (2000), 32. Luck & Heiter (2007), 33. Massarotti et al. (2008), 34. Soubiran et al. (2008), 35.Frasca et al. (2009), 36. Sozzetti et al. (2009), 37. Koleva & Vazdekis (2012), 38. Nissen & Schuster (2011), 39. Prugniel et al. (2011), 40. Sousa et al. (2011).

Table 5.6: Literature values of heavy element abundances

Star	[$\frac{\text{Sr I}}{\text{Fe}}$]	[$\frac{\text{Y II}}{\text{Fe}}$]	[$\frac{\text{Zr II}}{\text{Fe}}$]	[$\frac{\text{Ba II}}{\text{Fe}}$]	[$\frac{\text{La II}}{\text{Fe}}$]	[$\frac{\text{Ce II}}{\text{Fe}}$]	[$\frac{\text{Pr II}}{\text{Fe}}$]	[$\frac{\text{Nd II}}{\text{Fe}}$]	[$\frac{\text{Sm II}}{\text{Fe}}$]	[$\frac{\text{Eu II}}{\text{Fe}}$]	[$\frac{\text{Dy II}}{\text{Fe}}$]	Reference
Group I												
HD 16458	1.37	1.46	1.17	1.18	1.42	1.47	1.82	1.55	1.87	0.66	-	1
	1.25	1.06	0.95	1.03	0.96	0.89	0.68	0.97	-	0.35	-	3
HD 122202	-	1.44	-	0.33	0.90	1.62	1.26	-	1.77	-	-	1
	-	0.74	0.15	-	0.79	0.74	-	0.75	0.44	-	-	7
HD 201626	-	-	-	2.12	1.76	1.89	2.09	2.24	1.63	-	0.97	1
	-	0.09	-	-	1.6	1.62	2.09	1.55	1.6	-		8
HD 204613	1.71	0.97	1.14	1.04	1.21	1.24	1.52	1.02	1.61	0.06	1.77	1
	-	1.22	1.00	0.71	-	-	-	0.77	-	-	-	9
HD 216219	1.80	1.00	0.98	1.10	1.04	1.03	1.14	0.99	0.91	0.07	-	1
	-	1.10	0.85	0.87	-	0.95	-	-	-	-	-	9
	1.30	0.96	-	-	0.72	0.70	-	0.83	0.53	-	-	2
Group II												
HD 4395	1.08	0.65	0.58	0.79	1.03	0.42	0.53	0.80	1.08	-	-	1
	-	0.70	0.61	0.53	-	-	-	0.39	-	-	-	9
	1.08	0.10	1.01	−0.20	-	-	-	−0.20	-	−0.55	-	2

Table 5.6 – continued from previous page

Star	[Sr I/Fe]	[Y II/Fe]	[Zr II/Fe]	[Ba II/Fe]	[La II/Fe]	[Ce II/Fe]	[Pr II/Fe]	[Nd II/Fe]	[Sm II/Fe]	[Eu II/Fe]	[Dy II/Fe]	Reference
HD 55496	0.82	0.85	0.52	0.57	-	0.13	0.43	-	-	-	-	1
	-	-	0.72	-	0.52	0.32	-	0.52	0.33	-	-	7
HD 48565	1.73	1.08	0.9	1.52	1.46	1.42	1.29	1.51	1.18	0.29	-	1
	0.97	1.01	1.19	1.29	1.39	1.60	1.09	1.31	0.95	0.35	-	10
HD 92545	-	0.23	-	0.91	0.95	1.6	-	-	-	-	-	1
	0.67	0.64	0.75	1.04	0.72	0.60	0.44	0.42	0.24	0.32	0.09	10
HD 104979	0.99	0.71	0.85	0.94	1.11	1.06	1.04	1.13	1.17	0.40	-	1
	-	0.52	0.40	-	-	0.48	-	0.82	0.51	0.61	-	6
HD 107574	-	1.02	-	0.97	1.04	0.6	-	-	-	-	-	1
	0.67	0.64	0.75	1.04	0.72	0.6	0.44	0.42	0.24	0.14	0.09	10
Group III												
HD 5395	0.26	0.05	-	0.03	0.24	0.06	0.79	0.74	-	0.34	1.38	1
	1.44	0.27	−1.04	-	0.17	-	-	0.38	-	-	-	5
HD 81192	0.58	0.10	0.12	0.13	−0.13	−0.15	-	1.01	0.85	-	1.21	1
	-	−0.07	−0.34	−0.12	−0.51	−0.04	-	-	-	-	-	4
HD 89968	1.06	0.55	-	−0.24	1.87	1.52	1.66	1.44	1.23	0.38	-	1
HD 111721	-	0.05	-	−0.09	0.31	1.6	-	2.1	-	-	-	1

Table 5.6 – continued from previous page

Star	[Sr I/Fe]	[Y II/Fe]	[Zr II/Fe]	[Ba II/Fe]	[La II/Fe]	[Ce II/Fe]	[Pr II/Fe]	[Nd II/Fe]	[Sm II/Fe]	[Eu II/Fe]	[Dy II/Fe]	Reference
	−0.13	0.14	−0.45	0.08	0.04	0.03	0.28	0.17	0.22	0.36	-	12
	-	0.02	-	0.27	-	0.67	-	1.2	1.07	-	-	1
HD 125079	1.59	1.05	-	1.06	-	0.93	1.00	1.16	0.56	-	-	1
	-	1.36	0.98	0.89	-	-	-	0.99	-	-	-	9
HD 126681	-	0.02	-	0.27	-	0.67	-	1.2	1.07	-	-	1
	-	0.23	-	0.14	-	-	-	-	-	-	-	14
HD 148897	0.31	0.03	−0.47	−0.65	0.29	−0.16	-	0.13	0.58	-	0.02	1
	-	0.04	−0.29	-	-	0.07	-	0.01	-	−0.13	-	6
HD 164922	0.79	0.14	-	0.28	-	−0.09	-	-	-	-	-	1
	-	−0.15	0.04	−0.10	-	0.08	-	0.03	0.01	0.10	-	16
HD 167768	0.77	0.56	0.2	−0.36	−0.54	0.06	-	0.65	0.9	0.26	1.04	1
	-	0.03	-	−0.03	-	−0.04	−0.10	−0.14	-	0.45	-	15
HD 188650	-	−0.03	-	−0.01	-	−0.03	0.57	0.39	−0.12	-	-	1
HD 214714	-	0.22	−0.28	−0.31	-	0.05	0.93	0.36	0.46	-	-	1
	-	0.24	0.72	-	-	0.36	-	-	-	-	-	6

[#] Objects from the CH star catalogue of Bartkevicius (1996)

[*] Objects are also included in Ba star catalogue of Lü (1991)

1. Our work, 2. Luck & Bond (1982), 3. Smith (1984), 4. Luck & Bond (1985), 5. McWilliam (1990), 6.Luck (1991), 7. Luck & Bond (1991), 8. Vanture (1992c), 9. Smith et al. (1993), 10.Allen & Barbuy (2006a), 11. Luck (1991), 12. Gratton & Sneden (1994), 13. Fulbright (2000), 14. Allen & Barbuy (2006a), 15.Luck & Heiter (2007), 16. Mishenina et al. (2013)

5.5 Parametric model based study

Elements heavier than iron are mainly produced by two neutron-capture processes, the s-process and the r-process. Observed abundances of heavy elements estimated using model atmospheres and spectral synthesis techniques do not provide direct quantitative estimates of the relative contributions from s- and/or r- process nucleosynthesis. Identification of the dominant processes contributing to the heavy element abundances in the stars is likely to provide clues to their origin. We have investigated ways to delineate the observed abundances into their respective r- and s-process contributions in the framework of a parametric model using an appropriate model function. The origin of the neutron-capture elements is explored by comparing the observed abundances with predicted s- and r-process contributions following Goswami et al. (2010a), (and references there in). The ith element abundance can be calculated as

$$N_i(\mathrm{Z}) = A_s N_{is} + A_r N_{ir}\ 10^{[Fe/H]}$$

where Z is the metallicity of the star, N_{is} indicates the abundance from s-process in AGB star, N_{ir} indicates the abundance from r-process; A_s indicates the component coefficient that correspond to contributions from the s-process and A_r indicates the component coefficient that correspond to contributions from the r-process.

We have utilized the solar system s- and r-process isotopic abundances from stellar models of Arlandini et al. (1999) . The observed elemental abundances are scaled to the metallicity of the corresponding CH star and are normalised to their respective Ba abundances. Elemental abundances are then fitted with the parametric model function. The best fit coefficients and reduced chi-square values for a set of CH stars are given in Table 5.7. The best fits obtained with the parametric model function $log\epsilon_i = A_s N_{is} + A_r N_{ir}$ for HD 16458, HD 48565, HD 92545, HD 104979, HD 107574, HD 204613 and HD 216219 are shown in Figures 5.6 - 5.13. The errors in the derived abundances play an important role in deciding the goodness of fit of the parametric model functions. From the parametric model based analysis we find HD 16458 to fall in the group of CEMP r/s stars . The objects HD 48565, HD 92545, HD 104979, HD 107574, HD 125079, HD 204613 and HD 216219 belong to the group of CEMP-s stars.

Table 5.7: Best fit coefficients and reduced chi-square values

Star Name	A_s	A_r	χ^2
HD 16458	0.490 ± 0.09	0.600 ± 0.09	1.6
HD 48565	0.835 ± 0.09	0.112 ± 0.08	1.15
HD 92545	0.560 ± 0.33	0.503 ± 0.33	2.15
HD 104979	0.514 ± 0.16	0.493 ± 0.15	0.50
HD 107574	0.823 ± 0.01	0.171 ± 0.01	1.22
HD 125079	0.832 ± 0.16	0.182 ± 0.15	0.50
HD 204613	0.739 ± 0.08	0.291 ± 0.08	1.65
HD 216219	0.859 ± 0.14	0.169 ± 0.13	1.22

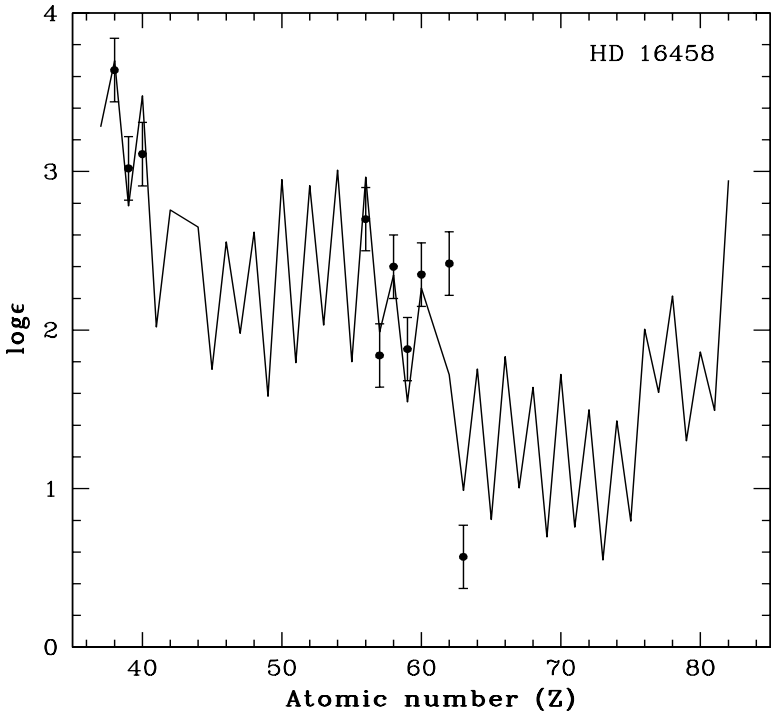

Figure 5.6: Solid curve represent the best fit for the parametric model function logϵ = $A_s N_{si}$ + A_r N_{ri}, where N_{si} and N_{ri} represent the abundances due to s- and r-process respectively (Arlandini et al. (1999), Stellar model, scaled to the metallicity of the star). The points with errorbars indicate the observed abundances in HD 16458.

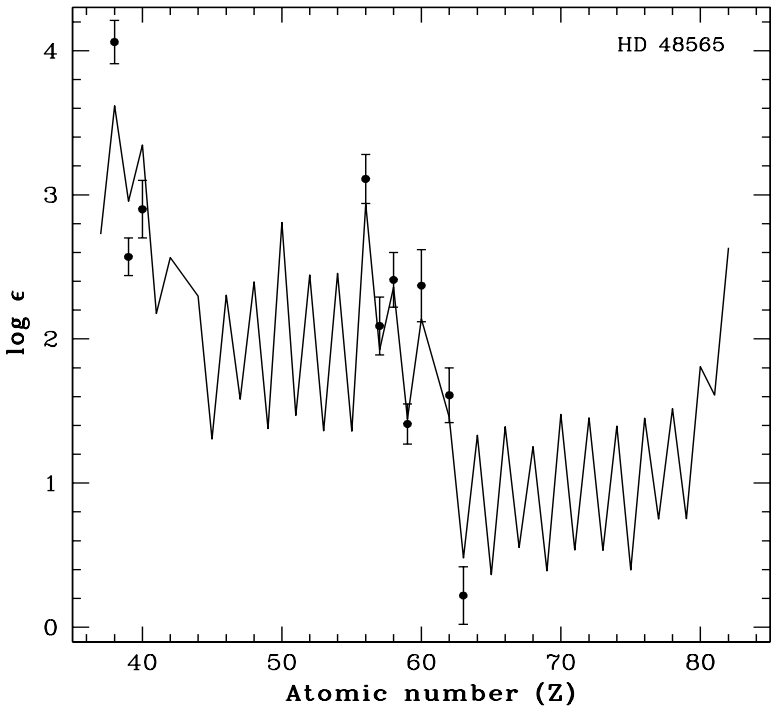

Figure 5.7: Same as Figure 5.6, but for HD 48565.

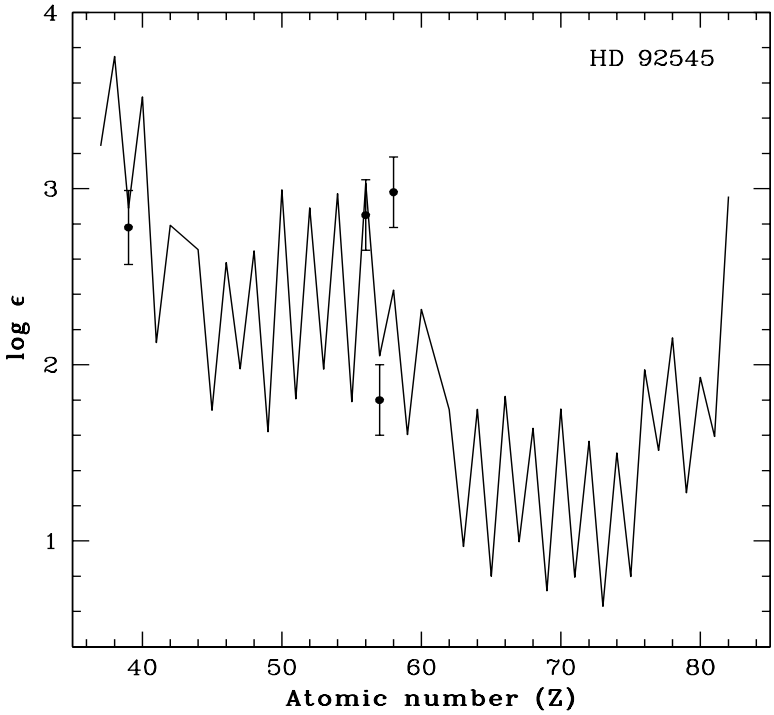

Figure 5.8: Same as Figure 5.6, but for HD 92545.

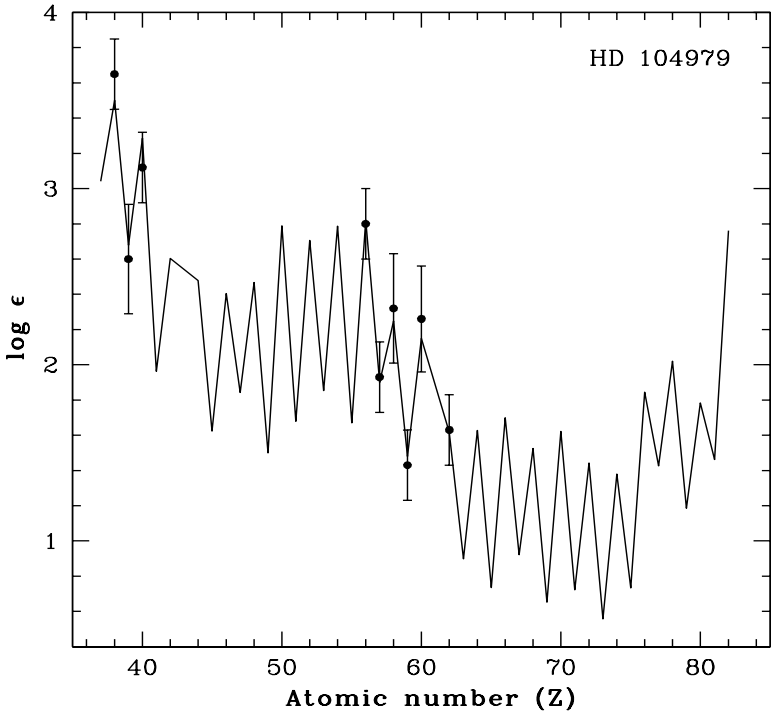

Figure 5.9: Same as Figure 5.6, but for HD 104979.

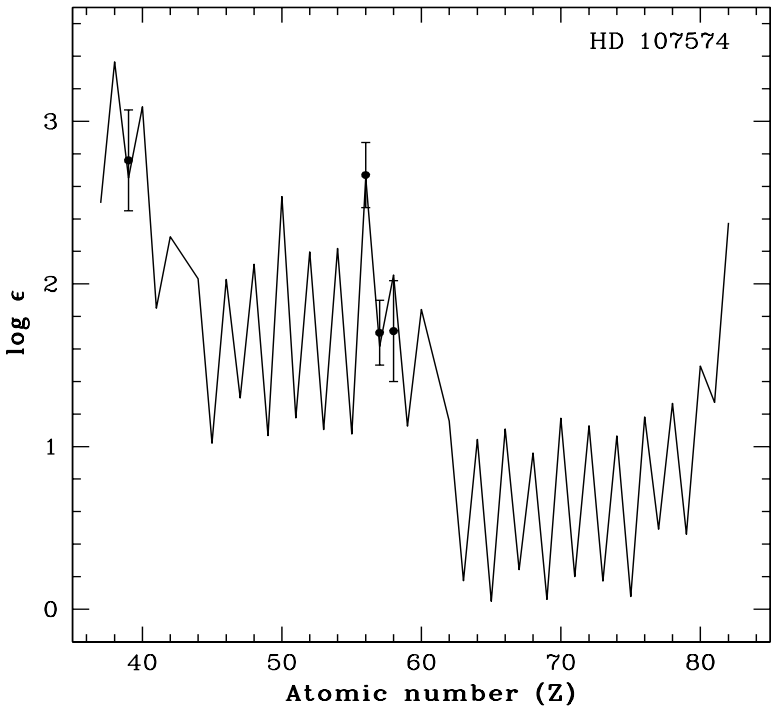

Figure 5.10: Same as Figure 5.6, but for HD 107574

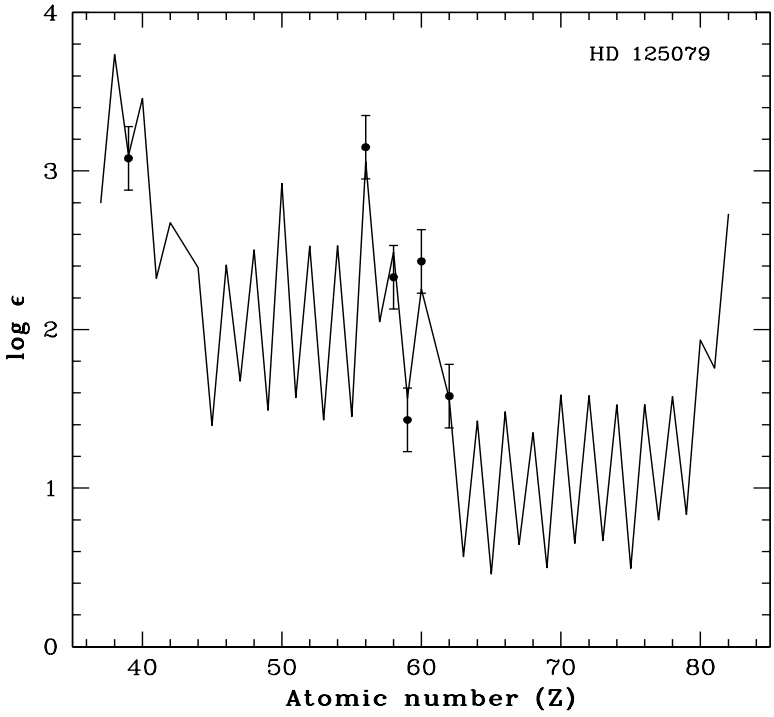

Figure 5.11: Same as Figure 5.6, but for HD 125079.

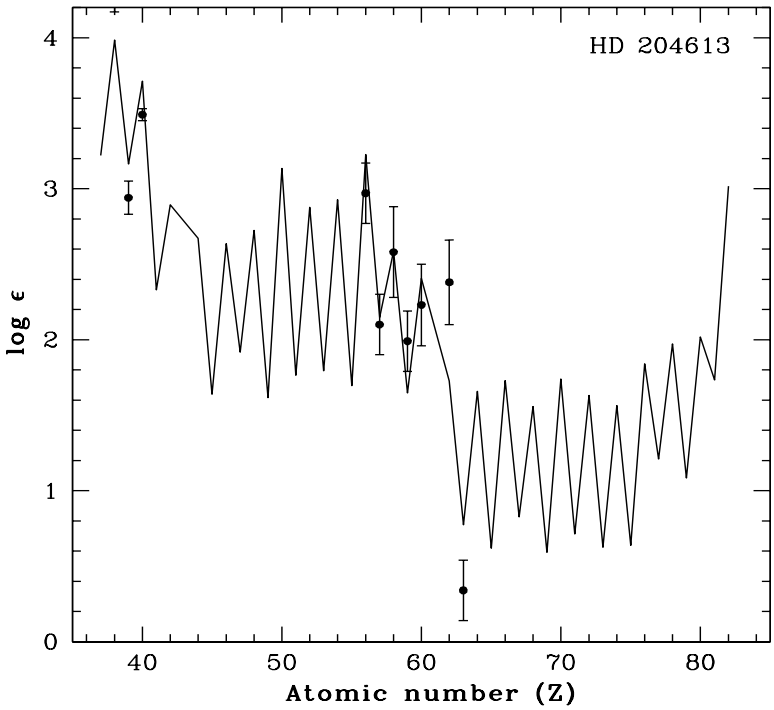

Figure 5.12: Same as Figure 5.6, but for HD 204613.

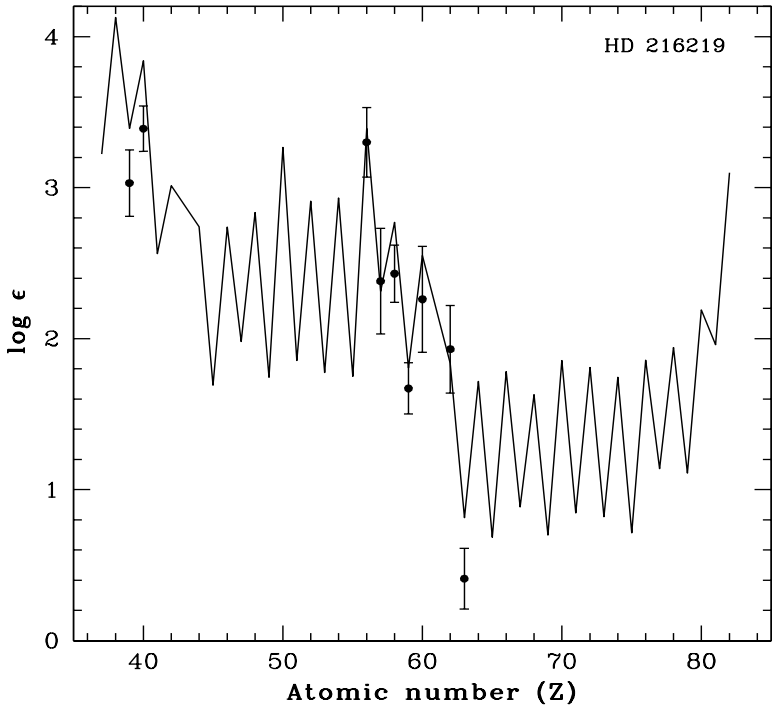

Figure 5.13: Same as Figure 5.6, but for HD 216219.

5.6 Conclusion

Results from our analyses of a group of twenty two stars from the CH star catalogue of Bartkevicius (1996) are presented. Abundances for 22 elements are estimated. The high velocity object, HD 55496 with radial velocity 315.2 km s^{-1}, is also listed in the Ba star catalogue of Lu (1991). This object with a metallicity of −1.49 and [C/Fe] ratio of 1.01 shows a mild enhancement in neutron-capture elements. Estimated [Ba/Fe] for this object is ∼ 0.57. Metallicity [Fe/H] of the other two high-velocity stars HD 81192 and HD 201626 (with V_r = 136.5, −141.6 km s^{-1} respectively) are found to be −0.5 and −1.4 respectively. For the low-velocity stars ($V_r \leq 100$), metallicity ranges from −0.18 to −0.66. The derived T_{eff} from V−K is ∼ 400 K, and from J−H is ∼ 300 K lower than the adopted spectroscopic T_{eff} derived by imposing Fe I excitation equilibrium. For two objects temperature derived from both spectroscopic method and photometric method are similar.

The estimated [C/Fe] ratio for the objects, except for HD 55496 and HD 201626, are less than 1.0. Thus, if we follow the CEMP stars classification of Beers and Christlieb (2005), only HD 55496 and HD 201626 fit well in the CEMP star group with [Fe/H] ≤

−1.0 and [C/Fe] ≥ 1.0. Several authors have adopted a value for [C/Fe] ≥ 0.5 to define CEMP stars (Ryan et al. 2005; Carollo et al. 2012). In our sample six objects have [C/Fe] ≥ 0.5. HD 107574 shows a [C/Fe] value of 0.47. The rest show either solar or mildly under solar value for [C/Fe]. These objects also show nearly solar or underabundant [Ba/Fe] value. Although other heavy elements are mildly enhanced in these objects, these objects are unlikely to belong to the group of CEMP or classical CH stars.

We have estimated the Ba abundance for all the objects in our sample, however abundance of Eu could be measured only for eight objects. Following the abundance criteria of Beers & Christlieb (2005) based on Ba and Eu abundances five objects fall into the group of CEMP-s stars. These objects show enhancement in heavy elements. Two subgiant-CH stars HD 204613 ([Ba/Fe] = 1.04, [Ba/Eu] = 0.98) and HD 216219 ([Ba/Fe] = 1.10, [Ba/Eu] = 1.03) and three objects from the CH star catalogue, i.e. HD 16458 ([Ba/Fe] = 1.18, [Ba/Eu] = 0.52), HD 48565 ([Ba/Fe] = 1.52, [Ba/Eu] = 1.23), HD 104979 ([Ba/Fe] = 0.94, [Ba/Eu] = 0.54) satisfy the criterion for CEMP-s stars; among these HD 16458 and HD 48565 although listed in the Ba star catalogue are more likely CH stars. HD 201626 with [Ba/Fe] = 2.12 can also be considered in CEMP-s group. In HD 16458, HD 48565, HD 104979 the heavy s-process elements are more enhanced than the light s-process elements with [hs/ls] ≥ 0.16. In HD 204613 and HD 216219, light s-process elements are more enhanced than heavy s-process elements. The parametric model based analysis of HD 48565, HD 104979, HD 204613 and HD 216219 also indicate higher contribution from the s-process than that of r-process to the abundances of heavy elements observed in these objects.

For the objects, HD 89968, HD 126681 and HD 164922, we have [Ba/Fe] < 0.30 with HD 89968 giving a [Ba/Fe] estimate of ∼ −0.24. These objects do not qualify as CH stars. HD 89668 and HD 126681, La, Ce, Pr and Nd are found to be enhanced. HD 122202 with a [C/Fe] ratio 0.5, shows enhancements of heavy elements other than Ba. HD 107574 with a metallicity −0.48 and [C/Fe] value 0.47 show enhancements in light s-process elements. In HD 148897, the heavy elements are either underabundant or nearly solar. HD 111721 with a metallicity −1.11, shows near solar [C/Fe] ratio and enhancements in second peak s-process elements.

Two subgiant-CH stars HD 4395 ([Fe/H] = −0.16 and [C/Fe] = −0.14) and HD 125079 ([Fe/H] = −0.18) show enhancement in all the heavy elements. HD 4395, with known radial velocity variations, shows almost equal enhancements of light and heavy s-process elements with [hs/ls] ∼ 0.05. But in the case of HD 125079, light s-process elements are more enhanced. The abundance trends indicate these objects to be members of CH group.

HD 5395, with estimated [Ba/Fe] ~ 0.13, [Eu/Fe] ~ 0.34 and [Ba/Eu] ~ −0.31 also does not seem to belong either to the group of CH stars or CEMP-r/s stars. However, heavy elements Pr and Nd are found to be overabundant with [Pr/Fe] and [Nd/Fe] values of 0.79 and 0.74 respectively. Sr and La are also found to be mildly overabundant with [Sr/Fe] ~ 0.26 and [La/Fe] ~ 0.24. The abundance of HD 5395 is however consistent with one of the characteristic properties of CH stars, i.e. the 2nd peak s-process elements are more abundant than the first-peak s-process elements.

The chemical composition of HD 81192 with [Ba/Fe] = 0.13, is peculiar, (i.e., it is enriched) in heavy elements of Nd and Sm and shows near-solar abundances for Ba, La, and Ce. This object shows a mild enhancement of Sr with [Sr/Fe] = 0.58. For CH and CEMP-s stars estimated [hs/Fe] are in general ≥ 1, where hs represents the heavy s-process elements and ls represents the light s-process elements. This condition is also not satisfied by this object. The binary status of this object is not known; the object does not seem to represent a typical CH star as far as its chemical composition is concerned.

HD 167768, an object with no information on radial velocity variations, shows enhancements in a few heavy elements but Ba and La are found to be underabundant with [Ba/Fe] = −0.36 and [La/Fe] = −0.54. This indicate the object may not be a bonafide member of CH star group.

Estimated values of [Ba/Fe] for the two high mass objects in our sample HD 188650 and 214714 are respectively ~ −0.01 and −0.31. Abundance of Eu could not be estimated for these two objects from our spectra. Except for Pr ([Pr/Fe] = 0.57) and Nd ([Nd/Fe] = 0.39) all other heavy elements i.e., Y, Ce and Sm show near-solar values for HD 188650. Similarly, HD 214714 shows a near-solar value for Ce. While Y is overabundant with [Y/Fe] = 0.22, Zr is found to be underabundant with [Zr/Fe] = −0.28 in this object. Pr, Nd and Sm are overabundant with [Pr/Fe] = 0.93, [Nd/Fe] = 0.36 and [Sm/Fe] = 0.46. It is possible that the objects that show mild enhancement of heavy elements such as Pr, Nd etc., their origin could be from material that are pre-enriched with such heavy elements.

CEMP-s stars are believed to be the metal-poor counterparts of CH stars having same origin as CH stars. As in the case of CH stars, the observed chemical composition of CEMP-s stars is also explained considering a binary picture. The relationship between CEMP-s and CEMP-r/s stars are not clearly understood; there are however speculations that the progenitors of the CEMP-s and CEMP-r/s class may be one and the same (TP-AGB) (Tsangarides 2005). None of the four stars for which we could measure both Ba and Eu abundances are found to satisfy the criterion of Beers & Christlieb (2005) for CEMP-r/s stars.

Several authors have used [hs/ls] as a good indicator of s-process efficiency and used these values for classification of CH stars. For example Bisterzo et al. (2012) classified the stars with [hs/Fe] value $\geq$ 1.5 as S II stars and those with [hs/Fe] value $\leq$ 1.5 as S I stars. In our sample three objects belong to S II category according to these criteria. For subgiant-CH stars light s-process are enhanced compared to heavy s-process elements. For giant-CH stars heavy s-process elements are found to be more enhanced. The correlation between metallicity and [hs/ls] values (see section 1.6) are also clear from our analysis.

Abundance ratios of the sample stars show a large scatter with respect to [Fe/H] (Figure 5.14). [X/Fe] ratios of the heavy elements for most of the objects belonging to group III are distinctly lower than their counterparts observed in the stars of group I and II. Abundance ratios of Eu with respect to Fe observed in three stars of group III show similar values as those seen in two objects of group II. Population I Ba stars are believed to be metal-rich counter parts of CH stars. Both CH stars and Ba stars are known to show enhancement in heavy elements. A comparison of the abundance ratios of heavy elements with those observed in barium stars (solid squares) and CEMP stars from Masseron et al. (2010) (solid pentagons) within the metallicity range 0.2 to -2.2 show that the group III objects distinctly return lower [X/Fe] ([Zr/Fe], [Ba/Fe], [La/Fe] and [Ce/Fe]; Figure 5.15). These objects do not seem to belong to the group of CH stars as far as the chemical composition of heavy elements are concerned.

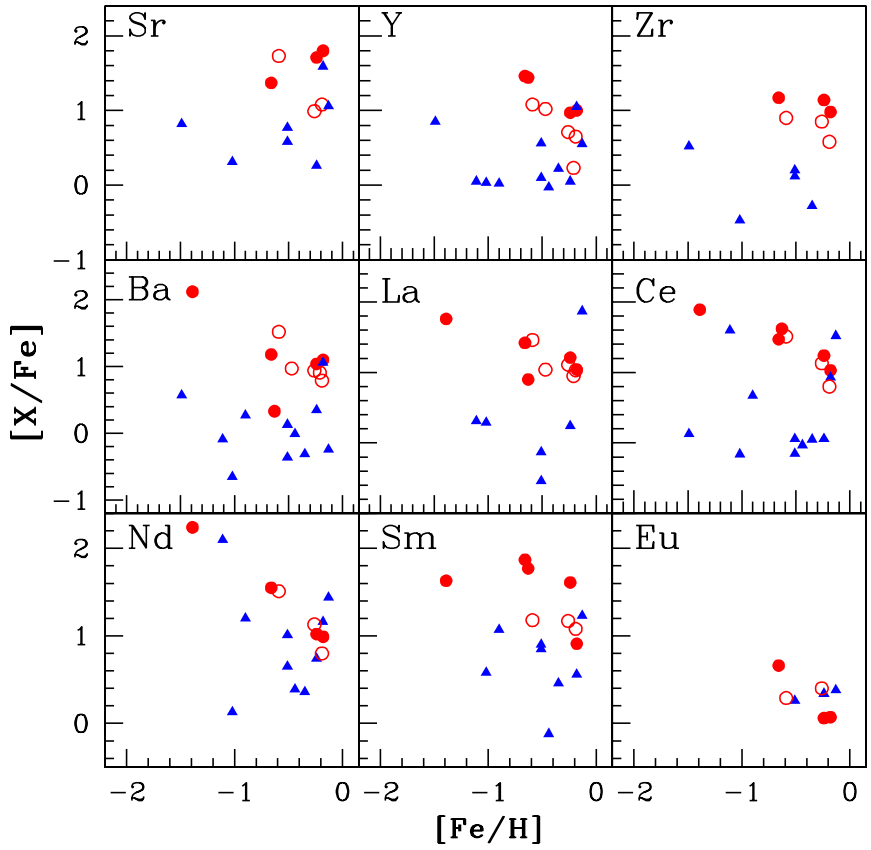

Figure 5.14: Abundance ratios of heavy elements observed in the programme stars with respect to [Fe/H]. The confirmed binaries are shown with solid circles, the objects with limited radial velocity information are shown with open circles, and the rest of the objects are indicated with solid triangles. The abundance ratios show a large scatter with respect to metallicity.

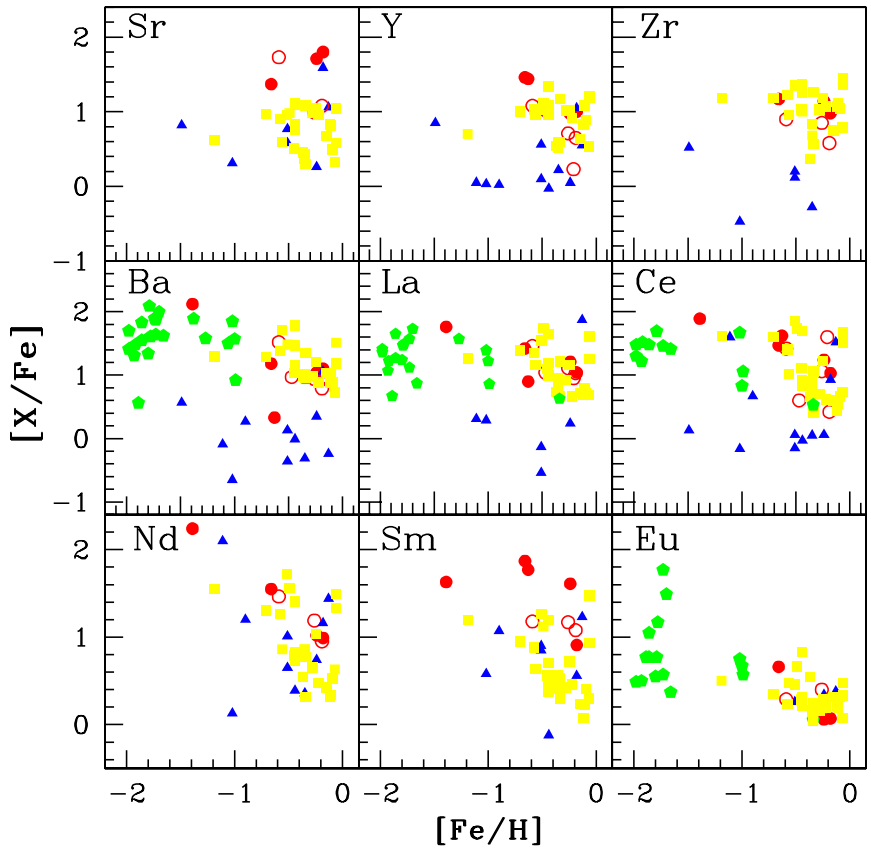

Figure 5.15: Same as figure 5.14. But the estimated abundance ratios of Ba, La, Ce and Eu with respect to Fe plotted in this figure are compared with the abundance ratios observed in CEMP stars (solid pentagons) from Masseron et al. (2010) and Ba stars (solid squares) from Allen & Barbuy (2006a).

CHAPTER 6

SUMMARY AND CONCLUSION

Studies on very metal-poor stars have progressed significantly over the past three decades. Detailed studies of a number of metal-poor stars have revealed a large fraction of them to possess a wide variety of elemental abundance patterns and overabundance of carbon (the CEMP stars and their sub-classes). Inspite of several efforts to understand their formation mechanisms (Qian & Wasserburg 2003; Zijlstra 2004; Wanajo et al. 2006) numerous questions still remain as to the nucleosynthetic histories and astrophysical sites associated with the production of these classes of objects. Although carbon-enhanced stars have several sub-classes, the majority are those showing large enhancement of heavy elements which are provided by AGB stars (CEMP-s and CEMP-r/s); being the largest group they could have major impacts on the Galactic chemical evolution.
An important aspect of this study is to obtain statistics of CEMP stars in addition to elemental abundances. These inputs are required to estimate the contribution of their progenitors (AGB stars) to the Galactic chemical evolution. Towards this end, we have undertaken a detailed spectroscopic studies of these objects. To summarize the important results,

1. A total of hundred and eleven objects from HES survey and CH star catalogue of Bartkevicius (1996) were classified into CH, C−R, C−N and C−J sub-classes based on low-resolution spectroscopy and using well-defined spectral criteria.
2. Conducted a detailed chemical composition study of a sample of 22 CH (CEMP-s) stars based on high resolution (R ~ 48000) spectra, dividing into three groups: group I (known binaries), group II (objects with limited radial velocity information) and group III (objects that have no information either on radial velocity or binarity).

- The **group I** objects show enhancement in carbon with two objects HD 16458 and

HD 201626 showing [C/Fe] values ≥ 0.9. The $^{12}C/^{13}C$ ratio in these objects are below 15. The other three objects show a [C/Fe] value ≤ 0.50. The group I objects, that include three subgiant-CH stars HD 122202, HD 204613, HD 216219 clearly show enhancement in heavy elements, in which, the light s-process elements are found to be more enhanced than the heavy s-process elements (Table 5.4). In HD 122202, while Ba is mildly enhanced with [Ba/Fe] = 0.33, other heavy elements are largely enhanced. Except HD 201626, with [Fe/H] = −1.39, the other objects are not so Fe-poor. For HD 201626, all the heavy s-process elements are highly enhanced.

• Among the **group II** objects, except HD 4395 with [C/Fe] = −0.14 and HD 104979 with [C/Fe] = 0.03, the other objects show mild or large enhancement with [C/Fe] in the range 0.47 to 1.01. All the six objects in this group exhibit enhancements in heavy elements. This group also includes a subgiant-CH star HD 4395, which show almost equal enhancements of light and heavy s-process elements with [hs/ls] ∼ 0.05. HD 48565 with metallicity −0.59, shows a large enhancement in Ba with [Ba/Fe] = 1.52, other heavy elements are also highly enhanced. For the other five objects although enhanced [Ba/Fe] estimates are ≤ 1.0. Estimated Eu gives [Eu/Fe] = 0.29. Four objects, HD 55496, HD 92545, HD 104979 and HD 107574 show the heavy s-process elements that are more enhanced than the light s-process elements. The metallicity of these objects are either solar or mildly metal poor except for HD 55496 for which [Fe/H] = −1.49. The abundance patterns in these objects suggest them to be members of binary systems. Long term radial velocity monitoring is required to understand the binary nature.

• **Group III** objects show near solar or mild underabundance of C. While HD 89668 and HD 125079 show large enhancements in heavy elements, other objects show mild enhancements. HD 125079, a subgiant-CH star, shows enhancement in all the heavy elements and HD 89668 shows enhancement in heavy elements other than Ba with [Ba/Fe] = −0.24. In the three cyanogen−weak giants HD 148897, HD 188650 and HD 214714, all the heavy elements are either solar or mildly underabundant. HD 164922 and HD 167768 show mild enhancements in light s-process elements. In general, group III objects show smaller enhancement in heavy element abundances compared to their counterparts in group II and group III objects with similar metallicities (Figures 5.14 and 5.15). Six objects in this group show underabundance in Ba. The origin of the heavy elements in these objects can be attributed to the interstellar clouds from which they have formed. Further studies are required for confirmation. The object, HD 164922, shows in radial velocity a difference of 15 km s^{-1} from the literature value indicating that the object could be a member of binary system. Long term radial velocity monitoring of these objects are

also required to understand the binary nature.

In summary,

• Enhancement of heavy elements, a well known characteristic of CH stars is evident for eleven objects (group I and II) from our analysis.

• Stars with radial velocity variations or binaries show more enhancements of heavy elements.

• The s-process enhancement in subgiant-CH stars are similar to Ba stars.

• High neutron-exposure index [hs/ls] favours lower metallicities.

• Light s-process elements are found to be enhanced than heavy s-process elements in subgiant-CH stars.

The spread in metallicity of our programme stars is not wide enough to make a critical analysis of the abundance trends with metallicity. In our sample, the abundances of the heavy elements appear scattered with respect to metallicity, suggesting that the enrichment may not be a function of only metallicity. Many studies (McClure 1983; Jorissen & Mayor 1992; Zacs 1991) have been conducted to find a possible correlation between the level of s-process enhancement and orbital parameters. McClure finds no correlation between the derived orbits and and Barium line strength in a sample of Barium stars. Zacs (1991) concluded that a correlation exists between s-process abundance anomalies and orbital periods for Barium star binaries. Most of the Ba stars are identified as wide binaries with long periods. Three objects in our sample are also listed in the Ba star catalogue of Lu (1991). Among the confirmed binaries with long periods $\geq$ 878 days, we could not find any correlation between the orbital parameters and abundances of heavy elements.

6.1 Future plans

Detailed chemical analysis of a large number of CH stars are required to draw a robust conclusion on their roles in the Galactic chemical evolution. We would like to extend this study to more number of CH stars and low metallicity carbon stars.

We have collected high resolution spectra for several carbon-enhanced metal-poor stars from the ESO-FEROS (Fiber-fed Extended Range Optical Spectrograph) covering the wavelength range 3500 – 9200 Å. Analysis of these data are in progress. We also plan to analyse medium resolution 4m LAMOST (The Large Sky Area Multi-Object Fibre Spectroscopic Telescope in China) spectra with a primary objective to search for metal-poor carbon-enhanced stars.

The data used for the present analysis cover a wavelength range 3800 – 6800 Å.

We would like to extend the analysis along the higher wavelength region and derive the nitrogen and oxygen abundances which would help to understand better the evolutionary stages. We also plan to extend our study based on theoretical models in order to get better ideas about the nature of binary companions and hence to understand the origin of the observed abundances.

The present analysis is based on optical spectroscopy, it would be worthwhile to carry out the investigation using IR spectroscopy to understand the nature and extent of the circumstellar envelop; this is expected to provide insight into the mass transfer mechanisms.

Appendix A

Linelists and equivalent widths

Table A.1: Fe lines used for deriving atmospheric parameters for HD 4395, HD 5395, HD 16458, HD 48565, HD 81192, HD 125079, HD 188650 , HD 201626, HD 214714 and HD 216219

Wavelength Å	Element	E_{low} eV	log gf	4395 mÅ	5395 mÅ	16458 mÅ	48565 mÅ	81192 mÅ	125079 mÅ	188650 mÅ	201626 mÅ	214714 mÅ	216219 mÅ
4114.440	Fe I	2.830	-1.300	-	-	-	57.9	91.4	-	-	-	115.5	-
4132.900		2.850	-1.010	-	-	-	72.2	-	-	-	-	-	96.4
4143.870		1.560	-0.510	-	-	-	147.1	-	-	-	-	-	-
4147.670		1.490	-2.100	-	-	-	89.1	120.9	-	-	-	-	-
4153.900		3.400	-0.320	-	-	-	76.9	-	-	-	-	-	-
4154.500		2.830	-0.690	-	-	-	79.6	-	-	-	-	-	-
4184.890		2.830	-0.870	113.7	-	-	-	-	-	143.5	-	134.7	104.5
4187.040		2.450	-0.550	-	-	-	100.0	-	-	-	-	-	137.7
4216.180		0.000	-3.360	-	-	-	88.4	-	-	-	-	-	-
4202.030		1.490	-0.710	-	-	-	-	-	-	-	130.2	-	-
4337.050		1.560	-1.700	124.3	-	-	-	-	-	-	-	-	125.5
4438.345		3.882	-1.630	-	-	-	-	-	-	29.2	-	42.7	-
4427.310		0.050	-2.920	-	-	-	117.9	-	-	-	-	-	-
4422.567		2.845	-1.110	-	-	-	-	123.5	-	-	-	-	-
4445.470		0.087	-5.380	-	-	122.4	-	-	-	39.8	-	-	-
4446.833		3.687	-1.330	-	-	-	34.1	77.0	-	-	-	-	51.5
4447.720		2.220	-1.340	-	-	-	98.9	138.0	-	141.6	38.5	-	-

Table A.1 – continued from previous page

Wavelength Å	Element	E_{low} eV	log gf	4395 mÅ	5395 mÅ	16458 mÅ	48565 mÅ	81192 mÅ	125079 mÅ	188650 mÅ	201626 mÅ	214714 mÅ	216219 mÅ
4454.380		2.832	-1.250	-	-	-	70.0	101.4	-	-	-	-	88.7
4461.653		0.087	-3.210	137.6	-	-	92.3	-	-	-	-	-	-
4466.551		2.832	-0.590	-	-	-	100.3	147.3	-	160.9	91.8	160.1	125.5
4484.220		3.602	-0.720	81.4	-	-	63.2	83.7	95.3	94.7	49.7	-	77.7
4489.739		0.121	-3.966	-	-	-	67.5	123.6	-	122.0	-	-	-
4531.150		1.490	-2.150	-	-	-	87.2	-	-	-	-	-	-
4547.846		3.546	-0.780	-	-	-	54.2	85.7	96.5	-	-	-	-
4566.514		3.301	-2.250	-	-	55.7	-	-	-	-	-	-	-
4574.215		3.211	-2.500	28.1	55.9	-	-	-	-	23.4	-	35.1	-
4587.128		3.573	-1.780	51.3	-	-	-	55.0	-	44.9	-	60.7	44.5
4595.358		3.301	-1.720	57.9	-	-	38.9	68.3	-	76.7	-	56.1	65.9
4596.060		3.602	-1.640	-	-	-	34.7	-	-	-	-	57.2	-
4619.287		3.602	-1.120	-	-	-	41.8	-	-	89.2	-	-	74.5
4625.044		3.241	-1.340	-	-	-	-	88.5	-	94.0	-	-	-
4630.121		2.278	-2.600	-	-	-	38.1	81.5	-	72.8	-	92.2	-
4632.911		1.608	-2.913	-	-	-	57.6	-	-	109.3	-	-	-
4635.846		2.845	-2.420	-	-	-	-	63.9	-	42.7	-	65.6	33.7
4643.463		3.654	-1.290	-	82.8	-	-	-	-	57.4	-	73.1	52.3

Table A.1 – continued from previous page

Wavelength Å	Element	E_{low} eV	log gf	4395 mÅ	5395 mÅ	16458 mÅ	48565 mÅ	81192 mÅ	125079 mÅ	188650 mÅ	201626 mÅ	214714 mÅ	216219 mÅ
4690.140		3.686	-1.640	-	67.5	-	23.0	53.9	-	-	-	-	44.4
4710.280		3.018	-1.610	-	-	-	57.3	-	-	94.5	-	-	-
4733.591		1.484	-2.710	-	-	-	57.3	-	-	-	-	114.0	92.5
4736.772		3.211	-0.740	-	-	-	89.0	125.8	-	139.6	-	-	-
4741.529		2.832	-2.000	71.2	-	-	-	83.7	-	65.8	-	67.2	-
4745.800		3.654	-0.790	-	-	-	48.2	87.2	-	-	-	-	-
4768.319		3.686	-1.109	-	-	102.7	45.9	-	-	72.2	-	88.3	-
4787.833		3.000	-2.770	-	-	-	-	-	-	24.2	-	30.5	-
4788.760		3.237	-1.760	63.0	87.3	-	31.6	-	-	57.6	-	-	57.9
4789.650		3.546	-0.910	87.7	-	-	-	84.7	-	-	-	-	-
4842.788		4.104	-1.560	41.1	-	-	-	45.4	-	-	-	-	-
4871.318		2.865	-0.360	-	-	-	108.8		-	-	-	-	145.2
4875.870		3.332	-2.020	53.2	71.4	-	25.5	63.8	-	32.9	-	44.3	45.9
4882.140		3.417	-1.640	-	80.2	107.2	31.7	75.9	-	-	-	63.8	51.3
4896.440		3.884	-2.050	- -		-	-		-	20.7	-	34.9	-
4903.310		2.883	-0.930	-	-	-	84.5	144.9	-	139.2	-	139.5	110.2
4907.737		3.430	-1.840	56.7	81.5	-	22.3	-	-	-	-	-	46.6
4908.029		4.217	-1.285	33.4	-	-	-	-	-	-	-	-	-

Table A.1 – continued from previous page

Wavelength Å	Element	E_{low} eV	log gf	4395 mÅ	5395 mÅ	16458 mÅ	48565 mÅ	81192 mÅ	125079 mÅ	188650 mÅ	201626 mÅ	214714 mÅ	216219 mÅ
4917.229		4.191	-1.180	58.4	55.0	-	28.5	-	-	49.9	72.8	65.6	142.4
4924.770		2.279	-2.256	92.1	-	151.4	54.2	-	-	106.1	-	108.6	-
4930.315		3.959	-1.350	-	-	-	29.4	69.9	-	53.2	-	69.4	-
4939.690		0.859	-3.340	-	147.5	-	63.1	127.2	122.1	119.4	-	131.7	88.5
4967.890		4.191	-0.622	70.8	89.1	108.1	43.4	-	80.4	-	-	73.9	63.5
4969.916		4.216	-0.710	69.5	90.2	-	38.9	-	-	-	-	-	61.9
4985.250		3.928	-0.560	91.9	110.2	109.8	57.4	93.5	-	-	-	-	-
5001.860		3.881	0.090	-	-	-	77.8	111.7	126.6	-	65.2	-	-
5005.711		3.883	-0.180	100.8	-	-	74.1	-	132.3	-	-	-	98.2
5006.119		2.833	-0.610	146.8	-	-	98.5	157.0	-	173.3	-	-	128.4
5007.728		4.294	-1.502	-	-	-	-	-	50.0	-	-	-	-
5022.235		3.984	-0.530	91.1	-	-	59.5		-	97.8	-	-	-
5028.126		3.573	-1.474	-	-	-	-		-	75.9	-	-	60.1
5031.915		4.372	-1.670	-	37.2	-	-		-	-	-	24.7	-
5044.210		2.851	-2.150	72.1	-	-	-	83.5	-	65.6	-	79.9	-
5049.820		2.279	-1.344	136.0	-	-	86.5	-	-	157.0	-	161.8	115.2
5051.635		0.915	-2.795	-	-	-	87.6	-	-	-	95.9	-	-
5054.640		3.639	-2.140	37.1	55.7	-	-		-	25.6	-	35.1	24.7

Table A.1 – continued from previous page

Wavelength Å	Element	E_{low} eV	log gf	4395 mÅ	5395 mÅ	16458 mÅ	48565 mÅ	81192 mÅ	125079 mÅ	188650 mÅ	201626 mÅ	214714 mÅ	216219 mÅ
5079.224		2.198	-2.067	-	-	-	70.1		-	-	-	-	-
5083.338		0.958	-2.958	104.3	157.2	-	74.6	147.6	-	136.3	-	-	98.6
5088.166		4.155	-1.780	-	-	-	-		-	-	-	26.62	-
5109.650		4.301	-0.980	59.8	-	-	35.2	-	-	52.7	-	-	-
5127.360		0.920	-3.310	94.6	148.6	-	64.7	117.0	120.4	107.3	-	-	-
5141.739		2.424	-2.150	87.1	114.1	-	48.1	93.71	-	80.6	-	102.8	76.4
5151.910		1.011	-3.320	-	-	-	63.0		-	118.5	-	-	-
5159.050		4.283	-0.820	52.3	79.2	83.2	32.8	-	-	46.6	-	67.1	57.6
5166.282		0.000	-4.195	111.9	-	-	72.0	133.8	-	112.9	79.1	129.0	-
5171.600		1.485	-1.790	156.3	-	-	108.5		-	178.4	103.1	164.4	135.1
5192.343		3.000	-0.420	-	-	-	108.8		-	164.6	-	163.2	-
5187.914		4.143	-1.260	53.8	-	-	19.6		-	25.02	-	38.5	-
5194.941		1.557	-2.090	119.9	170.0	-	83.3	146.8	-	151.8	-	142.7	114.4
5195.468		4.220	-0.020	89.1	111.2	-	62.0	-	-	-	-	-	89.1
5198.711		2.223	-2.135	98.3	-	-	57.5	121.5	-	103.5	-	113.0	83.3
5215.179		3.266	-0.933	-	131.9	148.2	69.8	-	-	108.8	-	119.6	98.3
5228.403		4.221	-1.290	-	-	-	-	59.3	-	40.9	-	53.13	-
5226.862		3.038	-0.667	-	-	-	103.0		-	-	-	-	-

Table A.1 – continued from previous page

Wavelength Å	Element	E_{low} eV	log gf	4395 mÅ	5395 mÅ	16458 mÅ	48565 mÅ	81192 mÅ	125079 mÅ	188650 mÅ	201626 mÅ	214714 mÅ	216219 mÅ
5232.939		2.940	-0.060	-	-	-	127.4	-	-	-	-	-	167.4
5250.645		2.198	-2.050	-	-	-	-		-	113.6	-	130.3	74.9
5247.050		0.087	-4.980	-	-	-	22.9	100.3	-	-	-	-	-
5242.490		3.630	-0.970	74.2	-	111.0	50.9	-	-	-	-	90.8	-
5253.461		3.283	-1.670	73.8	-	109.9	35.2	85.4	-	60.9	-	73.4	61.7
5263.305		3.265	-0.970	105.5	-	-	68.5		-	101.1	67.5	103.2	93.9
5266.555		2.998	-0.490	106.1		-	-		-	-	152.2	127.2	-
5281.800		3.040	-0.833	128.0	-	-	81.9	147.2	-	125.0	76.3	131.9	112.1
5283.630		3.240	-0.524	-	-	-	95.3		-	147.1	-	148.1	-
5324.178		3.211	-0.240	-	-	-	112.5	172.4	-	170.2	98.85	169.2	-
5307.370		1.610	-2.912	85.3	130.0	149.3	47.5	112.5	107.6	99.0	57.19	104.6	73.1
5321.110		4.434	-1.090	39.3	53.7	-	-	39.9	-	22.9	-	35.1	30.3
5322.040		2.279	-2.800	55.8	95.7	114.3	-	81.4	75.8	48.5	-	63.0	-
5328.040		0.915	-1.470	-	-	-	147.4		-	-	160.5	-	-
5339.928		3.266	-0.680	124.6	148.2	-	83.38	121.5	-	129.1	78.3	134.2	108.2
5364.858		4.446	0.220	107.0	120.8	-	71.3	100.0	119.1	111.0	-	109.2	99.9
5367.479		4.415	0.350	-	123.6	130.5	70.1	107.2	-	118.6	63.4	115.8	104.4
5369.958		4.371	0.350	124.2	136.2	-	84.0	107.7	-	131.5	66.5	134.9	109.6

Table A.1 – continued from previous page

Wavelength Å	Element	E_{low} eV	log gf	4395 mÅ	5395 mÅ	16458 mÅ	48565 mÅ	81192 mÅ	125079 mÅ	188650 mÅ	201626 mÅ	214714 mÅ	216219 mÅ
5373.698		4.473	-0.860	-	72.0	77.6	23.6	-	-	-	-	48.9	47.4
5379.574		3.694	-1.480	-	81.6	100.3	23.2	68.6	67.0	45.3	-	54.5	48.8
5383.369		4.312	0.500	132.6	148.6	163.9	92.7	134.4	143.5	136.3	-	139.4	125.2
5429.710		0.960	-1.881	-	-	-	141.7		-	-	140.4	-	-
5434.520		1.011	-2.130	159.5	-	-	102.8	-	-	-	128.4	-	132.5
5464.280		4.143	-1.400	38.6	53.9	-	18.2	-	55.0	-	-	-	36.9
5497.520		1.011	-2.830	-	-	-	-	163.1	-	166.5	-	-	-
5501.464		0.958	-2.950	116.8	-	-	77.1	148.3	151.0	144.2	-	156.8	106.7
5525.539		4.231	-1.330	45.3	66.6	50.0	-	-	46.3	33.2	-	37.4	37.3
5543.937		4.217	-1.140	56.3	75.0	-	25.5	60.1	66.2	45.9	-	-	44.9
5554.882		4.548	-0.440	-	-	97.0	-	79.1	-	69.4	-	-	-
5560.207		4.434	-1.190	41.5	-	42.5	17.4	42.3	49.0	29.6	-	40.4	35.93
5567.392		2.608	-2.800	-	-	-	21.7	81.2	-	51.9	-	68.2	49.9
5569.618		3.417	-0.540	124.3	-	-	85.7	128.3	-	127.9	-	124.5	112.0
5576.090		3.430	-1.000	102.3	-	133.1	67.3	106.6	111.5	110.0	-	-	-
5586.756		3.364	-0.210	-	-	-	114.3		174.9	159.8	90.70	153.2	138.2
5615.660		3.330	0.050	-	-	-	117.7		-	-	-	-	152.1
5617.186		3.252	-2.880	-	41.3	52.1	-		-	-	-	-	-

Table A.1 – continued from previous page

Wavelength Å	Element	E_{low} eV	log gf	4395 mÅ	5395 mÅ	16458 mÅ	48565 mÅ	81192 mÅ	125079 mÅ	188650 mÅ	201626 mÅ	214714 mÅ	216219 mÅ
5618.630		4.209	-1.270	43.2	61.7	-	-	41.8	-	28.1	-	36.9	32.28
5636.694		3.640	-2.610	-	34.0	26.3	-	25.2	21.5	-	-	-	-
5701.549		2.559	-2.216	-	-	136.7	42.6		-	-	-	-	-
5731.765		4.256	-1.300	52.2	-	-	21.8		-	38.0	-	46.7	-
5741.848		4.256	-1.730	22.5	45.3	-	-		-	-	-	-	-
5753.121		4.260	-0.760	75.2	90.2	87.6	37.8		79.5	65.5	-	73.7	65.23
5809.220		3.884	-1.610	45.8		82.8	-	70.1	60.2	-	18.9	36.9	33.2
5855.080		4.607	-1.480	25.3	-	-	-	-	24.7	-	-	-	-
5856.100		4.294	-1.560	28.7	-	66.5	-	32.7	40.1	-	-	-	20.1
5862.370		4.550	-0.250	79.4	93.3	106.3	44.7		86.2	68.7	-	75.3	70.5
5883.813		3.959	-1.360	57.8	81.4	104.2	30.9	66.8	-	-	-	-	49.1
5914.194		4.607	-0.050	-	-	-	-	-	-	105.1	-	116.2	-
5976.779		3.943	-1.310	-	106.6	-	22.7	62.1	-	-	21.2	-	51.1
6003.017		3.881	-1.120	-	82.0	97.7	37.8		88.6	71.9	24.0	72.9	67.8
6024.049		4.548	-0.102	61.7	-	119.5	56.8	92.1	107.3	97.9	39.7	98.0	81.1
6082.710		2.223	-3.550	-	-	90.0	35.6	76.0	50.8	-		-	31.0
6136.615		2.453	-1.400	137.6	-	-	86.2		-	-	-	-	-
6136.993		2.198	-2.950	75.5	-	125.3	26.9		150.6	-	-	-	-

Table A.1 – continued from previous page

Wavelength Å	Element	E_{low} eV	log gf	4395 mÅ	5395 mÅ	16458 mÅ	48565 mÅ	81192 mÅ	125079 mÅ	188650 mÅ	201626 mÅ	214714 mÅ	216219 mÅ
6137.694		2.588	-1.400	-	-	-	80.6		-	139.6	83.2	145.9	114.6
6151.620		2.176	-3.370	32.4	-	101.6	52.2	-	64.3	34.2		-	49.3
6165.360		4.143	-1.460	44.2	60.8	65.7	-	39.1	51.6	25.5	-	32.1	28.6
6180.205		2.727	-2.780	50.5	-	115.6	-	70.9	-	37.8	-	-	40.1
6173.343		2.223	-2.880	67.7	107.5	139.7	25.9		85.6	67.3	-	-	54.2
6219.280		2.197	-2.430	90.2	132.1	157.4	51.4	109.5	109.0	103.5	66.9	105.6	80.2
6232.639		3.653	-1.270	78.0	103.1	-	37.4	-	-	64.5	-	80.2	68.5
6230.736		2.559	-1.280	140.6	-	-	86.9		-	153.9	-	156.6	121.5
6246.327		3.602	-0.960	-	-	-	62.9		-	103.7	-	107.1	-
6240.650		2.223	-3.170	-	87.2	-	-		64.9	-	-	-	34.0
6252.550		2.404	-1.690	104.0	77.4	-	114.9	158.0	134.1	125.7	-	81.8	131.7
6254.250		2.278	-2.400	-	-	-	-		-	-	-	122.4	-
6265.130		2.176	-2.540	-	-	- 44.18	104.8	103.3	92.4	-	105.9	73.3	
6246.327		3.602	-0.960	-	-	120.6	-	-	-	-	-	-	-
6270.240		2.858	-2.710	49.2	-	-	-	62.3	-	-	-	-	36.9
6280.630		0.859	-4.390	-	118.2	140.4	-	-	89.4	-	-	-	-
6297.800		2.222	-2.740	-	-	-	33.2	-	86.7	73.4	-	82.6	68.8
6301.498		3.653	-0.740	99.6	-	-	63.6	-	118.1	101.1	-	-	91.1

Table A.1 – continued from previous page

Wavelength Å	Element	E_{low} eV	log gf	4395 mÅ	5395 mÅ	16458 mÅ	48565 mÅ	81192 mÅ	125079 mÅ	188650 mÅ	201626 mÅ	214714 mÅ	216219 mÅ
6318.018		2.453	-2.330	-	-	138.3	-	113.4	-	106.8	-	117.2	-
6322.690		2.588	-2.402	79.4	109.3	127.9	37.74	-	84.7	63.9	43.0	71.0	61.3
6335.340		2.197	-2.230	96.6	141.4	-	56.4	123.4	-	108.8	-	114.4	83.96
6336.823		3.686	-1.050	-	-	-	56.6		-	98.2	-	99.2	-
6408.016		3.686	-1.040	90.3	-	-	48.0		-	-	-	100.3	76.1
6411.650		3.653	-0.820	-	-	-	70.3	91.5	-	-	-	117.2	-
6419.980		4.733	-0.240	79.7	96.3	114.3	38.6	74.6	86.1	72.1	-	76.8	68.8
6421.350		2.278	-2.030	-	-	-	68.3	127.3	132.6	122.3	75.69	128.9	100.0
6481.869		2.278	-2.984	-	105.2	-	33.2	-	75.5	65.8	-	68.1	48.2
6494.980		2.404	-1.273	-	-	-	94.4	163.8	154.1	148.6	-	166.1	127.7
6574.240		0.990	-5.040	31.7	-	115.1	-	66.0	-	-	-	-	-
6575.022		2.588	-2.820	-	-	-	-		-	-	-	-	44.39
6593.880		2.432	-2.420	-	-	147.5	40.02	-	-	-	-	-	73.41
6597.557		4.796	-1.070	-	-	22.9	-	45.0	40.6	-	-	-	-
6627.540		4.548	-1.680	22.9	-	-	-		-	-	-	-	-
6677.989		2.692	-1.470	-	-	-	-	133.8	-	138.7	-	-	107.4
6713.750		4.795	-1.390	-	27.0	-	-	20.8	-	-	-	-	-
6725.360		4.103	-2.170	-	27.8	-	-		23.7	-	-	-	-

Table A.1 – continued from previous page

Wavelength Å	Element	E_{low} eV	log gf	4395 mÅ	5395 mÅ	16458 mÅ	48565 mÅ	81192 mÅ	125079 mÅ	188650 mÅ	201626 mÅ	214714 mÅ	216219 mÅ
6739.520		1.557	-4.790	-	-	58.4	-		23.7	-	-	-	-
6750.150		2.424	-2.620	-	113.5	-	33.9	74.2	81.5	-	-	-	61.1
6752.711		4.640	-1.200	-	-	-	-	-	34.0	-	-	27.0	23.4
6793.260		4.076	-2.330	-	21.2	22.3	-	-	-	-	-	-	-
4233.172	Fe II	2.580	-2.000	-	-	-	97.5	101.8	-	-	76.9	-	-
4491.405		2.855	-2.700	69.1	-	-	64.6		-	132.9	45.7	109.5	89.4
4515.339		2.840	-2.480	-	-	-	74.3		-	-	-	-	101.5
4520.224		2.810	-2.600	-	-	-	71.7	70.5	-	-	-	-	94.9
4620.510		2.830	-3.290	-	66.4	69.8	-	-	-	-	-	-	-
4629.340		2.807	-2.280	-	-	-	75.8		-	99.4	-	130.6	-
4923.930		2.891	-1.320	145.6	161.0	158.4	123.6	120.3	-	-	-	-	165.0
5197.577		3.230	-2.100	-	95.0	-	71.2	73.0	-	-	54.9	131.1	98.1
5534.834		3.245	-2.930	-	-	-	50.6		-	118.4	-	100.4	72.9
6247.550		3.891	-2.510	38.3	-	34.4	42.5	-	-	-	-	90.7	-
6369.460		2.891	-4.020	-	26.8	-	-	-	-	-	-	-	-
6416.919		3.891	-2.740	-	46.0	35.7	25.7	30.2	44.0	71.0	-	57.9	49.3
6456.383		3.903	-2.075	57.9	67.8	-	51.4	-	-	-	33.4	-	-

Table A.2: Fe lines used for deriving atmospheric parameters for HD 55496, HD 92545, HD 89668, HD 104979, HD 107574, HD 111721

Wavelength Å	Element	E_{low} eV	log gf	HD 55496 mÅ	HD 92545 mÅ	HD 89668 mÅ	HD 104979 mÅ	HD 107574 mÅ	HD 111721 mÅ
4062.440	Fe I	2.850	-0.860	-	-	110.3	-	-	-
4114.440		2.830	-1.300	-	-		-	-	-
4132.900		2.850	-1.010	-		-	-	-	-
4143.870		1.560	-0.510	-		-	-	-	-
4147.670		1.490	-2.100	-		-	-	-	-
4153.900		3.400	-0.320	-		-	-	-	-
4154.500		2.830	-0.690	-		-	-	-	-
4184.890		2.830	-0.870	-		151.2	143.1	-	-
4187.040		2.450	-0.550	-		56.1	-	-	-
4216.180		0.000	-3.360	-		-	-	-	-
4202.030		1.490	-0.710	-		-	-	-	-
4337.050		1.560	-1.700	-		-	-	-	-
4438.345		3.882	-1.630	-	-	-	67.9	-	-
4427.310		0.050	-2.920	-	-	-	-	-	-
4422.567		2.845	-1.110	-	-	-	-	-	-
4445.470		0.087	-5.380	-	65.4	-	82.2	-	-
4446.833		3.687	-1.330	-	106.5	-	93.3	-	-

Table A.2 – continued from previous page

Wavelength Å	Element	E_{low} eV	log gf	HD 55496 mÅ	HD 92545 mÅ	HD 89668 mÅ	HD 104979 mÅ	HD 107574 mÅ	HD 111721 mÅ
4447.720		2.220	-1.340	-	-	-	-	-	-
4454.380		2.832	-1.250	-	-	-	120.1	-	75.13
4461.653		0.087	-3.210	-	-	74.46	-	-	-
4466.551		2.832	-0.590	-	-	-	165.7	-	-
4484.220		3.602	-0.720	-	133.5	-	-	-	-
4489.739		0.121	-3.966	-	-	-	-	-	-
4531.150		1.490	-2.150	-	-	102.0	-	-	-
4547.846		3.546	-0.780	-	123.9	-	-	-	58.14
4566.514		3.301	-2.250	-	57.5	-	50.9	-	-
4574.215		3.211	-2.500	-	65.7	-	-	-	-
4587.128		3.573	-1.780	-	-	27.92	88.3	-	-
4595.358		3.301	-1.720	-	109.4	-	-	-	29.79
4596.060		3.602	-1.640	-	-	96.88	-	-	-
4619.287		3.602	-1.120	-	-	-	99.8	-	53.22
4625.044		3.241	-1.340	-	138.7	-	-	-	49.25
4630.121		2.278	-2.600	45.83	106.8	32.3	113.6	-	45.12
4632.911		1.608	-2.913	-	156.8	-	-	-	-
4635.846		2.845	-2.420	-	65.9	-	72.4	-	

Table A.2 – continued from previous page

Wavelength Å	Element	E_{low} eV	log gf	HD 55496 mÅ	HD 92545 mÅ	HD 89668 mÅ	HD 104979 mÅ	HD 107574 mÅ	HD 111721 mÅ
4643.463		3.654	-1.290	21.36	-	-	93.1	-	-
4690.140		3.686	-1.640	-	93.4	-	62.2	-	31.54
4710.280		3.018	-1.610	-	-	-		39.07	70.37
4733.591		1.484	-2.710	72.44	-	71.80	132.7	-	74.11
4736.772		3.211	-0.740	-	234.0	84.88	-	63.64	85.21
4741.529		2.832	-2.000	19.02	92.1	57.04	-	-	43.33
4745.800		3.654	-0.790	-	127.9	-	125.3	-	-
4768.319		3.686	-1.109	-	147.3	43.58	-	-	50.01
4787.833		3.000	-2.770	-	-	-	59.6	-	15.35
4788.760		3.237	-1.760	-	63.7	31.33	89.3	-	35.84
4789.650		3.546	-0.910	-	65.0	68.53	-	-	-
4842.788		4.104	-1.560	-	-	-	70.5	-	-
4871.318		2.865	-0.360	-	-	109.7	-	-	129.3
4875.870		3.332	-2.020	-	80.9	-	81.5	-	-
4882.140		3.417	-1.640	-	-	58.20	93.0	-	-
4896.440		3.884	-2.050	-	80.8	-	48.5	-	-
4903.310		2.883	-0.930	105.7	227.1	94.01	164.2	73.09	95.77
4907.737		3.430	-1.840	-	65.7	-	76.4	-	26.44

Table A.2 – continued from previous page

Wavelength Å	Element	E_{low} eV	log gf	HD 55496 mÅ	HD 92545 mÅ	HD 89668 mÅ	HD 104979 mÅ	HD 107574 mÅ	HD 111721 mÅ
4908.029		4.217	-1.285	-	38.6	-	-	-	-
4917.229		4.191	-1.180	-	67.8	-	-	-	-
4924.770		2.279	-2.256	78.28	134.3	-	-	-	65.68
4930.315		3.959	-1.350	-	-	47.19	-	-	-
4939.690		0.859	-3.340	108.4	159.6	-	142.6	38.83	92.12
4967.890		4.191	-0.622	-	158.5	57.97	89.4	-	36.15
4969.916		4.216	-0.710	-	-	-	82.0	-	37.32
4985.250		3.928	-0.560	-	-	-	98.6	-	-
5001.860		3.881	0.090	78.63	147.9	89.45	-	-	-
5005.711		3.883	-0.180	66.08	-	88.81	-	61.52	74.94
5006.119		2.833	-0.610	115.5	-	118.7	171.0	97.03	119.0
5007.728		4.294	-1.502	-	46.5	-	31.5	-	
5022.235		3.984	-0.530	-	-	-	114.3	-	65.49
5028.126		3.573	-1.474	-	-	-	108.7	27.32	44.98
5031.915		4.372	-1.670	-	-	-	44.8	-	-
5044.210		2.851	-2.150	-	109.1	44.81	101.4	-	53.04
5049.820		2.279	-1.344	118.6	-	-	170.9	-	98.69
5051.635		0.915	-2.795	100.5	-	100.7	-	70.43	117.2

Table A.2 – continued from previous page

Wavelength Å	Element	E_{low} eV	log gf	HD 55496 mÅ	HD 92545 mÅ	HD 89668 mÅ	HD 104979 mÅ	HD 107574 mÅ	HD 111721 mÅ
5054.640		3.639	-2.140	-	-	-	52.5	-	-
5079.224		2.198	-2.067	67.26	-	-	-	-	78.62
5083.338		0.958	-2.958	109.7	131.7	85.06	158.6	-	98.2
5088.166		4.155	-1.780	-	55.4	-	46.8	-	-
5109.650		4.301	-0.980	-	-	-	83.3	23.15	
5127.360		0.920	-3.310	-	175.0	70.38	-	32.36	88.05
5141.739		2.424	-2.150	-	145.3	-	114.3	-	67.43
5151.910		1.011	-3.320	-	-	-	144.6	35.53	86.64
5159.050		4.283	-0.820	-	-	-	64.2	-	-
5166.282		0.000	-4.195	122.1	-	66.62	157.4	95.68	
5171.600		1.485	-1.790	-	98.4	105.8	-	-	121.0
5192.343		3.000	-0.420	94.25	-	129.4	-	-	119.5
5187.914		4.143	-1.260	-	-	-	70.5	-	-
5194.941		1.557	-2.090	110.2	204.3	101.5	-	77.82	-
5195.468		4.220	-0.020	89.02	102.4	-	120.2	-	-
5198.711		2.223	-2.135	67.24	-	67.39	130.5	-	74.74
5215.179		3.266	-0.933	-	139.3	-	128.0	-	76.02
5228.403		4.221	-1.290	-	62.7	-	-	-	-

Table A.2 – continued from previous page

Wavelength Å	Element	E_{low} eV	log gf	HD 55496 mÅ	HD 92545 mÅ	HD 89668 mÅ	HD 104979 mÅ	HD 107574 mÅ	HD 111721 mÅ
5226.862		3.038	-0.667	102.9	-	-	-	-	107.4
5232.939		2.940	-0.060	-	-	191.9	-	121.7	144.7
5250.645		2.198	-2.050	-	160.0	95.16	-	-	-
5247.050		0.087	-4.980	67.72	110.2	95.34	123.9	-	58.65
5242.490		3.630	-0.970	-	109.2	70.84	97.9	45.81	57.08
5253.461		3.283	-1.670	-	115.8	-	92.7	-	48.5
5263.305		3.265	-0.970	83.63	-	87.37	139.3	56.01	77.01
5266.555		2.998	-0.490	113.6	-	139.6	-	-	109.1
5281.800		3.040	-0.833	96.19	210.3	110.2	154.6	-	-
5283.630		3.240	-0.524	79.58	-	-	195.2	81.25	100.1
5324.178		3.211	-0.240	97.73	-	147.4	-	-	118.7
5307.370		1.610	-2.912	78.97	134.2	69.03	124.6	-	70.24
5321.110		4.434	-1.090	-	60.9	-	54.5	-	-
5322.040		2.279	-2.800	47.71	83.2	-	92.4	-	30.32
5328.040		0.915	-1.470	176.1	-	-	-	-	193.2
5339.928		3.266	-0.680	87.37	-	87.27	145.5	66.41	81.57
5364.858		4.446	0.220	56.42	157.5	96.47	115.5	-	67.88
5367.479		4.415	0.350	74.43	183.1	91.11	119.8	-	75.82

Table A.2 – continued from previous page

Wavelength Å	Element	E_{low} eV	log gf	HD 55496 mÅ	HD 92545 mÅ	HD 89668 mÅ	HD 104979 mÅ	HD 107574 mÅ	HD 111721 mÅ
5369.958		4.371	0.350	82.33	-	-	126.1	-	76.30
5373.698		4.473	-0.860	-	-	34.77	68.8	-	
5379.574		3.694	-1.480	-	68.5	39.31	76.9	-	28.0
5383.369		4.312	0.500	112.5	-	114.2	141.9	97.05	88.71
5429.710		0.960	-1.881	162.3	-	-	-	128.8	166.7
5434.520		1.011	-2.130	149.9	-	137.1	-	112.6	130.2
5464.280		4.143	-1.400	25.18	50.2	-	67.7	-	-
5497.520		1.011	-2.830	144.6	-	119.3	-	-	112.1
5501.464		0.958	-2.950	109.1	-	79.34	167.6	55.93	104.0
5525.539		4.231	-1.330	-	85.2	-	64.3	-	
5543.937		4.217	-1.140	-	75.6	-	71.8	24.16	
5554.882		4.548	-0.440	-	115.9	-	103.0	41.99	42.76
5560.207		4.434	-1.190	-	52.8	33.54	58.9	16.59	
5567.392		2.608	-2.800	37.13		105.3	-	102.0	35.29
5569.618		3.417	-0.540	84.13	-	105.1	141.0	68.39	-
5576.090		3.430	-1.000	73.51	-	100.8	121.4	-	-
5586.756		3.364	-0.210	109.9	-	137.0	-	-	110.3
5615.660		3.330	0.050	121.1	-	144.5	-	106.9	115.2

Table A.2 – continued from previous page

Wavelength Å	Element	E_{low} eV	log gf	HD 55496 mÅ	HD 92545 mÅ	HD 89668 mÅ	HD 104979 mÅ	HD 107574 mÅ	HD 111721 mÅ
5617.186		3.252	-2.880	-	-	-	36.7	-	-
5618.630		4.209	-1.270	-	49.4	-	58.3	-	14.97
5636.694		3.640	-2.610	-	27.0	-	28.4	-	-
5701.549		2.559	-2.216	58.70	128.7	56.2	115.7	-	56.10
5731.765		4.256	-1.300	-	76.3	-	70.4	-	-
5741.848		4.256	-1.730	-	46.3	15.7	42.1	-	-
5753.121		4.260	-0.760	25.21	98.6	-	87.6	-	34.17
5809.220		3.884	-1.610	-	67.5	-	70.6	-	-
5855.080		4.607	-1.480	-	31.6	-	27.8	-	-
5856.100		4.294	-1.560	-	45.9	-	45.4	-	-
5862.370		4.550	-0.250	24.93	102.4	-	92.4	-	40.95
5883.813		3.959	-1.360	-	90.9	73.80	85.5	-	20.0
5914.194		4.607	-0.050	-	151.4	-	-	59.44	66.58
5976.779		3.943	-1.310	17.72	104.6	-	81.9	-	-
6003.017		3.881	-1.120	-	118.6	-	94.5	40.10	44.11
6024.049		4.548	-0.102	79.3	140.1	86.95	107.4	58.23	51.30
6082.710		2.223	-3.550	-	67.3	-	70.8	-	-
6136.615		2.453	-1.400	118.4	-	-	163.8	73.74	101.6

Table A.2 – continued from previous page

Wavelength Å	Element	E_{low} eV	log gf	HD 55496 mÅ	HD 92545 mÅ	HD 89668 mÅ	HD 104979 mÅ	HD 107574 mÅ	HD 111721 mÅ
6136.993		2.198	-2.950	71.58	117.3	-	106.6	-	-
6137.694		2.588	-1.400	91.47	-	111.6	168.6	77.24	-
6151.620		2.176	-3.370	26.90	77.5	-	83.0	-	27.71
6165.360		4.143	-1.460	-	50.3	-	54.3	-	-
6180.205		2.727	-2.780	-	-	-	88.4	-	30.41
6173.343		2.223	-2.880	55.67	100.4	45.06	103.7	-	46.56
6219.280		2.197	-2.430	80.12	127.0	-	119.2	-	-
6232.639		3.653	-1.270	33.87	125.2	66.45	94.7	25.63	-
6230.736		2.559	-1.280	110.4	-	102.5	-	87.74	106.6
6246.327		3.602	-0.960	60.30	174.8	-	122.2	-	72.33
6240.650		2.223	-3.170	16.99	76.7	-	82.5	-	30.54
6252.550		2.404	-1.690	-	181.8	102.3	152.8	69.90	95.11
6254.250		2.278	-2.400	83.28	134.7	78.26	136.9	-	-
6265.130		2.176	-2.540	62.39	134.1	54.91	124.5	-	64.32
6246.327		3.602	-0.960	-	174.1	-	122.2	-	72.43
6270.240		2.858	-2.710	-	74.7	-	81.1	-	-
6280.630		0.859	-4.390	-	-	-	-	-	-
6297.800		2.222	-2.740	74.39	108.0	-	107.6	-	-

Table A.2 – continued from previous page

Wavelength Å	Element	E_{low} eV	log gf	HD 55496 mÅ	HD 92545 mÅ	HD 89668 mÅ	HD 104979 mÅ	HD 107574 mÅ	HD 111721 mÅ
6301.498		3.653	-0.740	-	-	92.22	118.8	50.97	-
6318.018		2.453	-2.330	-	161.4	82.63	137.2	49.56	79.8
6322.690		2.588	-2.402	40.87	103.6	-	102.5	-	50.44
6335.340		2.197	-2.230	95.92	-	66.56	135.0	54.37	72.94
6336.823		3.686	-1.050	77.48	-	70.62	117.5	-	61.45
6408.016		3.686	-1.040	71.32	138.9	65.25	112.9	38.94	57.96
6411.650		3.653	-0.820	86.17	-	88.77	-	55.76	-
6419.980		4.733	-0.240	24.58	105.2	66.44	-	46.48	-
6421.350		2.278	-2.030	81.90	171.4	-		-	86.51
6481.869		2.278	-2.984	-	95.5	-	99.8	-	-
6494.980		2.404	-1.273	129.9	-	108.8	-	96.24	-
6574.240		0.990	-5.040	-	73.8	-	76.8	-	
6575.022		2.588	-2.820	-	109.4	-	97.8	-	32.38
6593.880		2.432	-2.420	-	122.4	-	122.2	-	61.45
6597.557		4.796	-1.070	-	-	-	44.2	-	-
6627.540		4.548	-1.680	-	36.7	-	36.6	-	-
6677.989		2.692	-1.470	-	-	-	157.4	-	92.24
6713.750		4.795	-1.390	-	20.0	-	44.41	-	-

Table A.2 – continued from previous page

Wavelength Å	Element	E_{low} eV	log gf	HD 55496 mÅ	HD 92545 mÅ	HD 89668 mÅ	HD 104979 mÅ	HD 107574 mÅ	HD 111721 mÅ
6725.360		4.103	-2.170	-	24.4	-	24.9	-	-
6739.520		1.557	-4.790	-	33.5	-	35.2	-	-
6750.150		2.424	-2.620	-	103.3	-	107.9	-	-
6752.711		4.640	-1.200	-	-	-	46.8	-	-
6793.260		4.076	-2.330	-	18.1	-	18.2	-	-
4233.172	Fe II	2.580	-2.000	-	-	-	-	-	-
4491.405		2.855	-2.700	53.50	-	-	91.8	-	-
4515.339		2.840	-2.480	66.22	-	-	-		49.69
4520.224		2.810	-2.600	-	-	116.5	100.5	-	-
4620.510		2.830	-3.290	-	-	-	66.8		-
4629.340		2.807	-2.280	75.87	110.3	88.28	120.2	112.7	89.17
4923.930		2.891	-1.320	121.3	75.5	16.06	163.3	160.2	117.8
5197.577		3.230	-2.100	43.95	-	80.14	99.6	100.6	51.03
5534.834		3.245	-2.930	-	-	62.77	77.6	57.18	38.64
6247.550		3.891	-2.510	-	10.7	73.73	56.0	59.54	32.52
6369.460		2.891	-4.020	-	-	70.79	27.3	-	-
6416.919		3.891	-2.740	-	30.9	-	41.0	-	-
6456.383		3.903	-2.075	-	-	-	69.9	68.85	50.06

Table A.3: Fe lines used for deriving atmospheric parameters for HD 122202, HD 126681, HD 148897, HD 164922, HD 167768, HD 204613

Wavelength Å	Element	E_{low} eV	log gf	HD 122202 mÅ	HD 126681 mÅ	HD 148897 mÅ	HD 164922 mÅ	HD 167768 mÅ	HD 204613 mÅ
4062.440	Fe I	2.850	-0.860	-	-	-	-	-	102.9
4114.440		2.830	-1.300	-	-	129.8	-	-	-
4132.900		2.850	-1.010	-	-	-	-	-	107.6
4143.870		1.560	-0.51	-	-	-	-	-	-
4147.670		1.490	-2.100	-	-	-	-	-	114.6
4153.900		3.400	-0.320	-	-	-	-	-	-
4154.500		2.830	-0.690	-	-	-	-	-	-
4184.890		2.830	-0.870	-	-	-	-	-	105.0
4187.040		2.450	-0.550	-	-	-	-	-	153.6
4216.180		0.000	-3.360	-	-	-	-	-	-
4202.030		1.490	-0.710	-	-	-	-	-	-
4337.050		1.560	-1.700	-	-	-	-	-	-
4438.345		3.882	-1.630	-	-	77.51	-	-	-
4427.310		0.050	-2.920	-	-	-	-	-	-
4422.567		2.845	-1.110	-	-	-	-	-	-
4445.470		0.087	-5.380	-	-	124.1	-	-	
4446.833		3.687	-1.330	-	-	96.9	81.7	-	60.45

Table A.3 – continued from previous page

Wavelength Å	Element	E_{low} eV	log gf	HD 122202 mÅ	HD 126681 mÅ	HD 148897 mÅ	HD 164922 mÅ	HD 167768 mÅ	HD 204613 mÅ
4447.720		2.220	-1.340	-	-	-	-	-	137.3
4454.380		2.832	-1.250	-	75.6	134.9	-	108.6	93.72
4461.653		0.087	-3.210	-	-	-	-	167.2	119.5
4466.551		2.832	-0.590	-	-	-	-	-	126.6
4484.220		3.602	-0.720	23.5	-	101.3	-	98.5	81.1
4489.739		0.121	-3.966	-	-	-	-	-	88.1
4531.150		1.490	-2.150	-	-	-	-	-	-
4547.846		3.546	-0.780	54.6	-	105.4	-	89.75	75.77
4566.514		3.301	-2.250	-	-	57.4	-	-	28.9
4574.215		3.211	-2.500	-	-	56.66	-	27.10	
4587.128		3.573	-1.780	-	29.9	-	-	68.33	43.68
4595.358		3.301	-1.720	-	-	108.1	-	81.50	
4596.060		3.602	-1.640	-	-	100.7	-	-	-
4619.287		3.602	-1.120	-	-	103.8	91.2	-	72.53
4625.044		3.241	-1.340	-	53.8	-	-	97.2	82.7
4630.121		2.278	-2.600	-	-	130.2	-	84.6	58.3
4632.911		1.608	-2.913	54.2	-	-	-	-	-
4635.846		2.845	-2.420	-	-	84.01	-	64.73	37.4

Table A.3 – continued from previous page

Wavelength Å	Element	E_{low} eV	log gf	HD 122202 mÅ	HD 126681 mÅ	HD 148897 mÅ	HD 164922 mÅ	HD 167768 mÅ	HD 204613 mÅ
4643.463		3.654	-1.290	-	-	86.7	-	73.42	56.7
4690.140		3.686	-1.640	-	-	67.9	-	-	44.4
4710.280		3.018	-1.610	-	-	-	-	-	-
4733.591		1.484	-2.710	-	-	170.8	108.1	119.9	
4736.772		3.211	-0.740	83.7	71.9	141.2	-	126.0	
4741.529		2.832	-2.000	-	-	113.2	85.5	-	
4745.800		3.654	-0.790	-	-	134.1	-	-	67.56
4768.319		3.686	-1.109	-	-	-	-	-	-
4787.833		3.000	-2.770	-	-	68.3	-	-	-
4788.760		3.237	-1.760	-	-	96.3	74.9	84.4	57.2
4789.650		3.546	-0.910	-	42.5	139.4	-	91.31	76.16
4842.788		4.104	-1.560	-	-	-	-	-	-
4871.318		2.865	-0.360	-	-	190.8	-	163.5	144.1
4875.870		3.332	-2.020	-	-	82.55	-	-	-
4882.140		3.417	-1.640	-	19.6	91.06	-	74.9	57.2
4896.440		3.884	-2.050	-	-	37.62	-	-	-
4903.310		2.883	-0.930	-	81.4	172.8	-	139.2	118.6
4907.737		3.430	-1.840	-	-	83.54	-	64.18	45.7

Table A.3 – continued from previous page

Wavelength Å	Element	E_{low} eV	log gf	HD 122202 mÅ	HD 126681 mÅ	HD 148897 mÅ	HD 164922 mÅ	HD 167768 mÅ	HD 204613 mÅ
4908.029		4.217	-1.285	-	-	36.50	55.48	-	-
4917.229		4.191	-1.180	-	-	67.66	-	65.59	48.16
4924.770		2.279	-2.256	45.6	45.2	141.9	-	113.3	79.4
4930.315		3.959	-1.350	-	-	80.66	-	69.16	-
4939.690		0.859	-3.340	-	-	-	128.1	124.1	88.14
4967.890		4.191	-0.622	-	-	81.3	103.4	70.15	70.6
4969.916		4.216	-0.710	-	-	79.3	-	74.5	64.07
4985.250		3.928	-0.560	-	-	-	-	-	82.2
5001.860		3.881	0.090	-	-	-	-	-	106.7
5005.711		3.883	-0.180	-	54.6	125.0	-	105.0	
5006.119		2.833	-0.610	-	97.9	-	145.8	143.8	
5007.728		4.294	-1.502	-	-	-	-	-	-
5022.235		3.984	-0.530	76.1	40.3	115.2	128.0	96.74	85.08
5028.126		3.573	-1.474	-	30.5	109.6	-	88.66	-
5031.915		4.372	-1.670	-	-	21.32	-	-	-
5044.210		2.851	-2.150	-	-	115.4	-	87.96	62.31
5049.820		2.279	-1.344	-	80.5	-	-	154.6	123.8
5051.635		0.915	-2.795	-	78.1	-	-	127.5	

Table A.3 – continued from previous page

Wavelength Å	Element	E_{low} eV	log gf	HD 122202 mÅ	HD 126681 mÅ	HD 148897 mÅ	HD 164922 mÅ	HD 167768 mÅ	HD 204613 mÅ
5054.640		3.639	-2.140	-	-	47.86	-	27.44	24.43
5079.224		2.198	-2.067	-	48.9	-	-	-	-
5083.338		0.958	-2.958	-	80.6	130.6	136.4	99.72	
5088.166		4.155	-1.780	-	-	31.00	-	32.30	
5109.650		4.301	-0.980	-	-	-	-	68.5	
5127.360		0.920	-3.310	-	56.1	111.2	-	129.9	82.78
5141.739		2.424	-2.150	-	47.4	133.4	105.6	-	74.98
5151.910		1.011	-3.320	-	51.3	-	-	-	
5159.050		4.283	-0.820	-	25.8	72.94	72.97	67.61	53.60
5166.282		0.000	-4.195	-	-	-	-	139.0	-
5171.600		1.485	-1.790	-	-	-	-	-	158.1
5192.343		3.000	-0.420	153.0	102.9	-		-	-
5187.914		4.143	-1.260	-	-	64.59	-	60.68	39.10
5194.941		1.557	-2.090	75.7	74.4	-	-	-	106.2
5195.468		4.220	-0.020	-	-	113.7	-	100.9	81.07
5198.711		2.223	-2.135	-	59.8	163.0	-	116.0	82.81
5215.179		3.266	-0.933	-	60.7	128.3	-	111.5	98.50
5228.403		4.221	-1.290	-	-	69.40	61.83	-	50.38

Table A.3 – continued from previous page

Wavelength Å	Element	E_{low} eV	log gf	HD 122202 mÅ	HD 126681 mÅ	HD 148897 mÅ	HD 164922 mÅ	HD 167768 mÅ	HD 204613 mÅ
5226.862		3.038	-0.667	-	92.9	-	-	-	-
5232.939		2.940	-0.060	-	-	-	-	-	-
5250.645		2.198	-2.050	-	55.4	-	-	-	-
5247.050		0.087	-4.980	-	-	178.3	81.04	-	49.23
5242.490		3.630	-0.970	-	40.8	104.6	96.82	87.56	75.79
5253.461		3.283	-1.670	-	21.4	94.80	-	77.61	62.28
5263.305		3.265	-0.970	-	65.3	143.9	-	105.7	99.18
5266.555		2.998	-0.490	-	111.4	-	-	-	152.4
5281.800		3.040	-0.833	72.7	-	154.7	-	131.8	114.3
5283.630		3.240	-0.524	-	94.7	-	-	134.0	
5324.178		3.211	-0.240	-	-	-	-	173.2	164.3
5307.370		1.610	-2.912	-	47.8	154.4	111.8	115.7	72.38
5321.110		4.434	-1.090	-	-	39.98 -	55.37	35.67	25.08
5322.040		2.279	-2.800	-	-	106.4 -	-	77.02	44.08
5328.040		0.915	-1.470	-	173.4	-	-	-	-
5339.928		3.266	-0.680	-	81.9	150.3	124.4	109.9	
5364.858		4.446	0.220	80.8	58.9	111.4	162.7	107.2	97.71
5367.479		4.415	0.350	-	68.1	116.7	164.9	111.1	106.7

Table A.3 – continued from previous page

Wavelength Å	Element	E_{low} eV	log gf	HD 122202 mÅ	HD 126681 mÅ	HD 148897 mÅ	HD 164922 mÅ	HD 167768 mÅ	HD 204613 mÅ
5369.958		4.371	0.350	102.9	73.8	98.07 127.3	181.6	120.2	116.8
5373.698		4.473	-0.860	-	-	61.39	-	59.99	46.98
5379.574		3.694	-1.480	-	-	73.78	73.79	60.96	45.32
5383.369		4.312	0.500	101.3	73.9	135.8	-	128.9	125.5
5429.710		0.960	-1.881	155.5	-	-	-	-	
5434.520		1.011	-2.130	113.0	108.1	-	-	185.4	132.4
5464.280		4.143	-1.400	-	-	42.85	50.31	-	26.55
5497.520		1.011	-2.830	-	80.9	-	157.9	169.7	
5501.464		0.958	-2.950	77.2	69.3	150.1 -	149.1		
5525.539		4.231	-1.330	-	-	54.08 -	-	48.63	37.78
5543.937		4.217	-1.140	-	21.6	62.15	-	55.99	46.74
5554.882		4.548	-0.440	39.4	32.5	83.87	-	-	70.53
5560.207		4.434	-1.190	-	11.44	47.85	-	41.79	34.45
5567.392		2.608	-2.800	-	-	106.7	-	75.18	45.60
5569.618		3.417	-0.540	78.8	83.3	147.2	122.0	114.4	
5576.090		3.430	-1.000	-	58.3	127.7	107.1	94.39	
5586.756		3.364	-0.210	107.6	114.2	177.8	-	156.9	
5615.660		3.330	0.050	-	-	-	-	-	160.4

Table A.3 – continued from previous page

Wavelength Å	Element	E_{low} eV	log gf	HD 122202 mÅ	HD 126681 mÅ	HD 148897 mÅ	HD 164922 mÅ	HD 167768 mÅ	HD 204613 mÅ
5617.186		3.252	-2.880	-	-	21.36	-	-	-
5618.630		4.209	-1.270	15.9	-	51.03	-	44.21	31.19
5636.694		3.640	-2.610	-	-	-	-	-	-
5701.549		2.559	-2.216	-	-	-	-	-	-
5731.765		4.256	-1.300	-	-	57.80	-	51.60	42.59
5741.848		4.256	-1.730	-	-	35.50	-	-	-
5753.121		4.260	-0.760	-	32.6	72.99	-	74.36	62.42
5809.220		3.884	-1.610	-	-	59.60	-	51.70	30.15
5855.080		4.607	-1.480	-	-	17.37	36.49	-	-
5856.100		4.294	-1.560	-	-	32.99	47.84	31.50	
5862.370		4.550	-0.250	-	34.6	79.08	104.7	66.79	66.29
5883.813		3.959	-1.360	-	-	81.05	-	-	49.83
5914.194		4.607	-0.050	-	-	122.1	-	-	-
5976.779		3.943	-1.310	-	-	99.45	-	65.55	-
6003.017		3.881	-1.120	28.6	40.6		-	84.50	63.62
6024.049		4.548	-0.102	-	60.2	102.2	128.7	91.81	88.03
6082.710		2.223	-3.550	-	-	87.75	56.40	53.00	19.45
6136.615		2.453	-1.400	-	86.2	-	-	152.9	111.1

Table A.3 – continued from previous page

Wavelength Å	Element	E_{low} eV	log gf	HD 122202 mÅ	HD 126681 mÅ	HD 148897 mÅ	HD 164922 mÅ	HD 167768 mÅ	HD 204613 mÅ
6136.993		2.198	-2.950	-	-	143.2	-	-	51.99
6137.694		2.588	-1.400	70.1	73.8	-	168.3	148.9	107.2
6151.620		2.176	-3.370	-	-	104.7	-	67.69	30.68
6165.360		4.143	-1.460	-	-	46.25	56.28	40.04	26.05
6180.205		2.727	-2.780	-	-	96.79	-	70.05	37.14
6173.343		2.223	-2.880	-	27.4	125.0	-	87.30	53.34
6219.280		2.197	-2.430	-	51.3	154.2	-	112.0	75.49
6232.639		3.653	-1.270	-	34.3	103.3	-	84.41	64.53
6230.736		2.559	-1.280	-	82.8	-	-	163.1	
6246.327		3.602	-0.960	-	-	126.0	-	110.9	
6240.650		2.223	-3.170	-	-	100.7	-	69.60	31.81
6252.550		2.404	-1.690	-	76.6	177.7	148.0	131.3	99.21
6254.250		2.278	-2.400	-	-	153.2	-	125.4	101.4
6265.130		2.176	-2.540	-	33.1	151.5	106.3	112.3	71.22
6246.327		3.602	-0.960	-	57.2	-	-	-	89.77
6270.240		2.858	-2.710	-	-	90.28	-	69.08	34.46
6280.630		0.859	-4.390	-	22.2	-	-	-	
6297.800		2.222	-2.740	-	35.1	136.3	-	-	79.08

Table A.3 – continued from previous page

Wavelength Å	Element	E_{low} eV	log gf	HD 122202 mÅ	HD 126681 mÅ	HD 148897 mÅ	HD 164922 mÅ	HD 167768 mÅ	HD 204613 mÅ
6301.498		3.653	-0.740	-	58.4 -	-	103.9	90.92	
6318.018		2.453	-2.330	-	-	152.4	-	122.8	88.10
6322.690		2.588	-2.402	-	-	121.5	-	-	56.39
6335.340		2.197	-2.230	-	60.9	165.2	-	113.7	78.12
6336.823		3.686	-1.050	44.2	39.8	117.6	-	101.6	84.69
6408.016		3.686	-1.040	-	-	111.8	109.8	95.03	77.94
6411.650		3.653	-0.820	-	72.6	132.8	-	-	100.0
6419.980		4.733	-0.240	-	31.2	78.10	105.8	77.14	65.45
6421.350		2.278	-2.030	65.1	64.5	-	153.6	134.2	97.43
6481.869		2.278	-2.984	-	-	116.6	-	81.67	66.65
6494.980		2.404	-1.273	-	87.8	-	-	157.5	148.7
6574.240		0.990	-5.040	-	-	-	-	57.09	-
6575.022		2.588	-2.820	-	-	-	-	84.85	41.05
6593.880		2.432	-2.420	-	40.4	144.0	104.0	109.5	68.84
6597.557		4.796	-1.070	-	-	-	-	-	-
6627.540		4.548	-1.680	-	-	23.57	-	22.37	-
6677.989		2.692	-1.470	-	72.5	-	158.4	145.3	103.0
6713.750		4.795	-1.390	-	-	-	31.45	-	-

Table A.3 – continued from previous page

Wavelength Å	Element	E_{low} eV	log gf	HD 122202 mÅ	HD 126681 mÅ	HD 148897 mÅ	HD 164922 mÅ	HD 167768 mÅ	HD 204613 mÅ
6725.360		4.103	-2.170	-	-	18.03	32.10	-	-
6739.520		1.557	-4.790	-	-	55.13	-	-	-
6750.150		2.424	-2.620	-	33.5	130.1	-	93.29	53.20
6752.711		4.640	-1.200	-	-	-	54.81	-	-
6793.260		4.076	-2.330	-	-	-	21.07	-	-
4233.172	Fe II	2.580	-2.000	-	-	-	-	-	-
4491.405		2.855	-2.700	-	38.4	90.32	-	87.95	71.78
4515.339		2.840	-2.480	106.3	46.5	-	98.81	90.04	
4520.224		2.810	-2.600	91.7	-	79.94	-	83.29	
4620.510		2.830	-3.290	-	-	-	-	-	-
4629.340		2.807	-2.280	85.7	-	-	99.58	101.5	
4923.930		2.891	-1.320	153.7	82.0	154.8	133.4	152.6	139.1
5197.577		3.230	-2.100	81.5	-	97.35	69.24	91.12	78.30
5534.834		3.245	-2.930	62.4	-	-	-	-	54.30
6247.550		3.891	-2.510	-	-	-	42.87	-	50.69
6369.460		2.891	-4.020	-	-	-	-	-	-
6416.919		3.891	-2.740	-	-	-	39.95	37.07	35.60
6456.383		3.903	-2.075	-	18.9	53.48	55.27	58.50	56.26

Table A.4: Lines used for the calculation of elemental abundances for HD 4395, HD 5395, HD 16458, HD 48565, HD 81192, HD 125079, HD 188650 , HD 201626, HD 214714 and HD 216219

Wavelength Å	Element	E_{low} eV	log gf	4395 mÅ	5395 mÅ	16458 mÅ	48565 mÅ	81192 mÅ	125079 mÅ	188650 mÅ	201626 mÅ	214714 mÅ	216219 mÅ
5682.650	Na I	2.100	-0.700	94.6	-	143.4	48.66	-	109.7	109.9	-	95.46	81.17
5688.220		2.100	-0.400	100.6	-	149.9	-	-	120.9	138.2	-	128.4	107.1
5889.950		0.000	0.100	-	411.5	-	-	411.5	-	-	-	-	358.0
5895.920		0.000	-0.200	347.2	378.6	536.7	242.5	378.6	-	-	214.0	-	284.4
4702.990	Mg I	4.350	-0.666	-	-	238.8	150.3	202.1	199.9	174.9	133.2	174.9	178.8
6318.720		5.108	-1.730	-	52.21	52.79	15.55	-	-	-	-	26.95	-
5528.400		4.350	-0.490	185.7	211.8	192.4	143.5	211.8	199.5	184.9	-	176.2	157.2
4098.520	Ca I	2.525	-0.540	-	-	-	47.8	-	-	66.2	63.5	95.4	85.3
4283.010		1.885	-0.224	-	-	-	109.8	-	-	-	-	-	149.9
4425.430		1.879	-0.385	136.8	-	102.2	99.6	144.0	-	132.1	-	-	114.5
4435.679		1.890	-0.520	133.6	-	-	109.5	141.0	-	-	-	137.3	122.1
4455.890		1.900	-0.510	137.6	-	-	104.3	137.7	165.7	132.9	107.8	113.2	133.7
4578.550		2.521	-0.560	64.2	-	-	47.19	102.6	98.7	47.52	-	-	67.2
5261.710		2.521	-0.730	90.9	112.4	146.6	55.70	-	102.7	80.50	52.2	92.9	79.5
5265.560		2.520	-0.110	-	-	-	-	-	-	-	160.	5 -	-
5512.990		2.932	-0.290	76.5	-	135.3	45.36	87.4	86.2	54.8	-	-	68.1
5581.980		2.523	-0.710	89.1	-	125.7	58.81	115.6	107.2	79.45	-	93.9	84.51

Table A.4 – continued from previous page

Wavelength Å	Element	E_{low} eV	log gf	4395 mÅ	5395 mÅ	16458 mÅ	48565 mÅ	81192 mÅ	125079 mÅ	188650 mÅ	201626 mÅ	214714 mÅ	216219 mÅ
5588.760		2.530	0.360	129.7	-	-	102.8	140.9	141.8	137.4	-	137.5	127.7
5590.130		2.521	-0.710	82.7	-	94.4	54.1	103.2	94.0	-	-	86.08	77.9
5594.470		2.520	0.100	108.9		-	-	-	156.0	-	164.6	-	-
5857.450		2.930	0.240	120.8	-	170.3	82.3	131.4	137.5	130.9	-	-	111.0
6162.170		1.900	-0.090	-	210.5	-	-	200.9	204.8	187.3	132.0	185.2	162.9
6439.070		2.530	0.390	141.8	168.0	185.2	106.8	161.3	162.8	162.6	-	161.8	140.0
6449.820		2.520	-0.550	78.5	-	-	60.7	-	-	-	-	118.8	88.7
6455.590		2.523	-1.350	53.9	-	111.0	-	79.7	-	-	-	-	45.5
6471.670		2.525	-0.590	93.7	-	134.8	52.3	-	98.8	81.1	54.5	86.4	79.6
6493.790		2.521	0.140	145.8	-	168.4	88.1	136.8	130.6	111.4	-	127.0	111.9
6499.650		2.523	-0.590	79.7	-	-	44.3	-	95.9	55.5	-	-	75.1
6717.690		2.709	-0.610	-	-	186.0	60.7	-	-	-	-	105.6	95.9
4431.110		6.035	-2.520	-	-	25.0	-	-	-	-	68.3	-	-
4400.389	Sc II	0.606	-0.510	-		-	-		-	-	-	158.5	-
5031.021		1.360	-0.260	79.5	-	-	61.9	-	119.3	131.7	-	-	-
6604.600		1.357	-1.480	-	-	-	22.7	-	60.41	-	-	65.85	-
6245.637		1.507	-1.030	-	73.1	74.5	21.7	61.4	56.9	69.3	34.3	72.7	46.9
4512.700	Ti I	0.836	-0.480	64.9	-	115.3	34.9	79.1	82.9	48.3	-	56.7	53.7

Table A.4 – continued from previous page

Wavelength Å	Element	E_{low} eV	log gf	4395 mÅ	5395 mÅ	16458 mÅ	48565 mÅ	81192 mÅ	125079 mÅ	188650 mÅ	201626 mÅ	214714 mÅ	216219 mÅ
4453.710		1.873	-0.010	52.9	-	-	18.1	66.57	-	-	-	-	-
4533.239		0.848	0.476	111.6	-	-	71.4	140.1	-	-	73.6	-	99.25
4617.250		1.748	0.389	-	88.4	-	29.3	83.5	-	35.31	-	-	-
4656.468		0.000	-1.345	56.2	-	150.1	30.4	104.7	85.8	37.8	-	46.8	-
4759.272		2.255	0.514	-	76.7	-	18.3	63.9	59.7	16.4	-	26.4	39.2
4820.410		1.502	-0.441	-	89.2	-	-	86.5	-	23.6	64.5	36.9	62.7
4840.880		0.899	-0.509	-	-	119.3	26.9	86.4	79.4	-	-	-	52.7
4778.250		2.236	-0.220	-	34.3	71.7	-	-	19.6	-	-	-	-
4999.500		0.830	0.310	101.0	-	-	-	136.7	-	-	-	131.2	-
4937.730		0.813	-2.230	117.1	35.1	74.1	-	-	-	-	-	-	-
5007.210		0.820	0.170	-	-	-	-	152.3	-	-	108.8	-	-
5039.960		0.020	-1.130	-	124.6	-	42.8	-	105.3	66.9	-	83.4	72.9
5064.650		0.050	-0.940	94.0	145.3	-	42.8	-	-	-	-	-	68.9
5087.060		1.429	-0.780	-	80.2	93.8	-	92.8	-	-	-	-	-
5210.390		0.048	-0.884	-	127.5	-	52.7	-	111.4	81.2	-	97.3	78.2
6556.060		1.460	-1.074	93.1	60.7	104.0	-	-	33.72	-	-	-	-
4161.530	Ti II	1.080	-2.160	66.2	-	- -	-		-	-	-	108.1	-
4417.710		1.160	-1.430	-	-	-	-	-	141.8	-	-	160.8	117.5

Table A.4 – continued from previous page

Wavelength Å	Element	E_{low} eV	log gf	4395 mÅ	5395 mÅ	16458 mÅ	48565 mÅ	81192 mÅ	125079 mÅ	188650 mÅ	201626 mÅ	214714 mÅ	216219 mÅ
4418.330		1.240	-1.990	-	-	140.0	67.5	98.3	-	-	-	112.7	83.42
4443.790		1.080	-0.700	138.1	175.3	179.7	123.4	124.6	181.5	196.8	128.6	-	145.3
4468.520		1.130	-0.600	-	-	-	-	-	186.8	-	-	-	-
4470.900		1.164	-2.280	-	88.9	-	53.8	-	-	115.7	71.01	-	75.79
4493.510		1.080	-2.730	-	-	84.4	32.04	52.10	-	62.26	60.59	79.18	60.06
4563.760		1.221	-0.960	131.2	-	210.7	110.4	150.6	-	-	121.9	193.6	141.6
4571.960		1.571	-0.530	139.1	-	-	118.5	-	-	-	68.33	-	165.1
4568.310		1.224	-2.650	-	-	94.1	-	66.1	-	56.8	15.3	-	35.8
4657.210		1.240	-2.320	51.7	-	47.41	46.81	64.6	-	-	-	-	-
4708.665		1.240	-2.370	-	83.6	-	-	-	-	-	-	-	66.7
4798.510		1.080	-2.670	-	-	-	32.8	-	-	-	-	-	65.8
4805.090		2.060	-1.100	101.1	-	134.3	75.2	108.5	-	154.6	100.8	147.1	108.2
5185.900		1.890	-1.350	-	-	- -	88.3		-	63.9	126.3	-	69.8
5226.530		1.570	-1.300	-	141.9	165.2	83.7	107.8	-	-	96.5	-	110.1
4090.570	V I	1.853	-2.099	-	-	- -	-		-	-	96.4	-	-
4379.230		0.300	0.580	119.3	-	215.3	57.40	110.8	124.3	84.8	-	-	87.3
4406.630		0.300	-0.190	-	-	220.7	47.2	122.9	-	73.4	-	-	68.1
4876.430		2.115	-2.714	-	-	-	-	-	-	-	-	99.8	-

Table A.4 – continued from previous page

Wavelength Å	Element	E_{low} eV	log gf	4395 mÅ	5395 mÅ	16458 mÅ	48565 mÅ	81192 mÅ	125079 mÅ	188650 mÅ	201626 mÅ	214714 mÅ	216219 mÅ
5727.653		1.051	-0.870	-	95.0	76.3	45.0	37.1	17.2	-	-	-	-
6531.420		1.218	-0.840	-	-	51.1	-	-	-	-	-	-	-
4274.800	Cr I	0.000	-0.230	200.8	-	-	147.4	-	-	-	-	-	161.6
4289.720		0.000	-0.360	-	-	-	86.5	-	-	-	88.4	-	-
4351.050		0.970	-1.450	55.1	-	-	-	48.6	-	-	-	-	45.31
4600.750		1.000	-1.260	-	-	-	-	-	-	-	-	-	47.8
4616.140		0.980	-1.190	87.4	115.9	202.5	54.7	-	110.1	99.9	32.8	116.4	74.0
4626.190		0.970	-1.320	80.9	106.9	111.6	43.8	94.8	97.7	86.3	-	100.9	62.25
4652.160		1.000	-1.030	103.1	-	184.1	57.6	113.2	122.2	110.8	-	117.4	94.59
4737.380		3.087	-0.099	59.9	75.8	109.8	-	-	-	24.3	-	-	68.6
4942.490		0.941	-2.294	-	-	163.5	29.2	-	-	64.8	-	72.1	-
5206.040		0.940	0.020	-	-	-	-	-	-	-	-	-	169.3
5247.570		0.961	-1.640	77.4	-	140.5	34.3	84.7	-	77.2	-	89.1	641
5345.810		1.003	-0.980	115.4	159.3	-	70.7	140.8	137.9	-	-	140.2	105.8
5348.312		1.003	-1.290	-	-	-	-	-	-	-	51.3	107.0	-
4588.190	Cr II	4.072	-0.630	66.6	73.5	-	57.7	49.3		131.1	-	99.9	84.2
4592.040		4.073	-1.220	33.2	48.6	-	33.2	27.3		81.9	-	64.2	52.7
4812.350		3.864	-1.800	-	-	-	19.8	40.9		-	-	42.5	41.67

Table A.4 – continued from previous page

Wavelength Å	Element	E_{low} eV	log gf	4395 mÅ	5395 mÅ	16458 mÅ	48565 mÅ	81192 mÅ	125079 mÅ	188650 mÅ	201626 mÅ	214714 mÅ	216219 mÅ
4634.070		4.073	-1.240	-	-	-	-	-	-	102.5	-	-	73.7
4848.250		3.864	-1.140	-	-	-	-	-	-	-	-	87.16	65.3
4030.750	Mn I	0.000	-0.470	-	-	-	-	-	-	-	115.1	-	-
4034.480		0.000	-0.810	-	-	-	125.3	-	-	176.0	-	-	183.0
4041.360		2.110	0.280	-	195.2	-	102.6	-	151.3	-	68.66	-	143.0
4451.580		2.890	0.280	-	-	131.7	73.42	73.69	116.5	95.92	-	98.18	97.47
4470.140		2.941	-0.444	37.5	56.8	59.4	11.5	41.4	63.6	41.2	23.1	23.8	28.00
4739.080		2.941	-0.490	44.2	80.9	124.6	17.9	-	73.4	48.3	-	56.2	36.9
4761.530		2.953	-0.138	67.8	100.0	105.9	25.3	-	90.2	62.8	-	68.3	59.6
4765.860		2.941	-0.080	68.4	100.8	95.9	32.8	-	82.8	63.5	-	67.0	57.0
4766.420		2.919	0.100	83.0	127.8	140.7	46.38	109.6	-	95.96	23.9	-	72.52
4783.430		2.300	0.040	125.6	159.3	200.9	75.8	-	137.9	136.8	-	138.1	107.2
5516.770		2.178	-1.847	-	93.2	141.6	-	-	-	26.2	-	43.52	20.2
6013.488		3.072	-0.250	75.8	108.3	148.9	23.9	84.9	98.9	66.9	-	74.8	54.3
4813.480	Co I	3.216	0.050	-	-	-	10.57	46.3	-	24.2	-	-	-
4121.320		0.920	-0.320	125.2	-	-	-	-	-	-	-	135.3	107.9
4118.770		1.050	-0.490	-		-	-		-	-	70.1	-	-
4749.660		3.053	-0.321	-	-	-	-	74.8	-	-	-	-	-

Table A.4 – continued from previous page

Wavelength Å	Element	E_{low} eV	log gf	4395 mÅ	5395 mÅ	16458 mÅ	48565 mÅ	81192 mÅ	125079 mÅ	188650 mÅ	201626 mÅ	214714 mÅ	216219 mÅ
4771.080		3.133	-0.504	-	59.0	72.4	-	-	-	-	-	-	-
4781.430		1.882	-2.150	-	33.8	73.7	-	-	-	-	-	-	-
4792.850		3.252	-0.067	29.3	52.6	-	-	-	-	-	-	-	-
5530.770		1.710	-2.060	-	52.9	98.5	-	46.1	-	-	-	-	-
5590.720		2.042	-1.870	-	47.3	92.1	-	-	25.2	-	-	-	-
5991.870		2.080	-1.850	-	59.7	97.7	7.483	-	-	-	-	-	-
6454.990		3.632	-0.233	-	-	40.2	-	-	-	-	-	-	-
6632.430		2.280	-2.000	-	29.3	59.6	-	-	-	-	-	-	-
4470.470	Ni I	3.699	-0.400	-	-	-	-	-	-	-	-	34.3	-
4714.420		3.380	0.230	-	-	-	83.4	132.7	164.4	-	-	-	126.4
4732.460		4.106	-0.550	33.18	-	-	11.5	29.5	-	-	-	-	-
4814.590		3.597	-1.680	-	-	54.4	-	16.3	49.7	-	-	-	-
4821.130		4.153	-0.850	-	-	60.1	-	32.8	-	15.4	-	-	-
4852.560		3.542	-1.070	32.5	-	-	-	46.8	52.1	24.4	-	32.7	28.3
4855.410		3.540	0.000	84.8	-	111.1	53.2	98.9	-	-	27.5	-	-
4857.390		3.740	-1.199	44.6	-	-	13.5	60.7	60.2	27.8	-	-	34.2
4953.200		3.740	-0.670	46.9	-	-	17.8	66.7	61.6	36.9	-	38.8	35.6
4937.340		3.606	-0.390	66.6	-	120.2	36.3	-	-	62.7	-	71.8	61.9

Table A.4 – continued from previous page

Wavelength Å	Element	E_{low} eV	log gf	4395 mÅ	5395 mÅ	16458 mÅ	48565 mÅ	81192 mÅ	125079 mÅ	188650 mÅ	201626 mÅ	214714 mÅ	216219 mÅ
4980.160		3.610	-0.110	94.5	-	-	57.5	92.2	-	-	40.1	92.6	87.8
5035.370		3.630	0.290	79.3	-	94.3	63.6	94.6	-	95.4	-	87.5	73.7
5081.120		3.847	0.300	84.3	102.9	97.3	58.2	81.5	92.3	83.9	-	80.6	69.5
5082.350		3.657	-0.540	62.5	76.6	-	30.0	-	75.1	42.3	-	58.9	47.3
5084.080		3.678	0.030	74.9	94.1	77.7	51.8	75.9	90.2	72.5	-	74.1	71.5
5099.930		3.678	-0.100	80.9	-	-	46.8	-	-	-	-	96.5	73.6
5102.960		1.676	-2.620	58.7	-	-	18.2	-	-	-	-	37.0	35.4
5259.470		3.740	-1.502	10.0	-	114.3	-	-	-	-	-	-	17.8
6086.280		4.266	-0.530	35.1	51.9	64.3	11.7	33.6	45.8	23.9	-	27.2	-
6111.070		4.088	-0.785	31.6	45.5	59.1	-	30.0	36.3	-	-	-	27.4
6176.810		4.088	-0.148	-	-	93.8	23.5	-	68.6	42.0	-	-	20.3
6186.710		4.106	-0.777	-	42.2	-	-	-	33.6	-	-	-	48.2
6204.600		4.088	-1.060	-	30.7	56.9	-	-	26.7	-	-	-	-
6643.640		1.676	-2.300	94.4	145.5	169.0	41.8	118.4	-	86.8	50.9	100.9	77.7
4722.150	Zn I	4.029	-0.370	76.0	-	-	52.6	51.6	-	89.5	152.3	91.2	85.9
4810.530		4.080	-0.170	-	-	90.7	51.3	68.1	87.5	101.2	47.1	89.5	76.7
4607.327	Sr I	0.000	-0.570	60.4	65.6	138.6	56.5	62.9	95.9	-	-	-	80.2
4854.863	Y II	0.992	-0.380		77.1		-	63.7	-	95.3	-	-	98.1

Table A.4 – continued from previous page

Wavelength Å	Element	E_{low} eV	log gf	4395 mÅ	5395 mÅ	16458 mÅ	48565 mÅ	81192 mÅ	125079 mÅ	188650 mÅ	201626 mÅ	214714 mÅ	216219 mÅ
4883.685		1.084	0.07	90.4	81.1	211.9	87.2	72.4	134.4	126.9	-	122.8	119.9
5087.416		1.080	-0.170	71.9	71.3		80.2	71.7	104.1	96.2	-		98.1
5119.112		0.992	-1.360		31.7	120.6	36.7	-	71.7	44.3	-	-	64.8
5205.724		1.033	-0.340		-		-	-	-	-	-	-	116.2
5289.815		1.033	-1.850	15.5	-	87.5	13.7	-	41.4	-	-	-	34.2
5544.611		1.738	-1.090		-		22.1	-	-	-	-	-	41.6
5546.009		1.748	-1.100	30.9	-	27.9	-	-	22.0	-	-	22.2	51.6
5662.925		1.944	0.160		-		63.8	-	-	-	-	-	-
6613.733		1.748	-1.11		42.6	119.5	22.3	-	-	-	-	-	45.5
4048.670	Zr II	0.800	-0.480		-		-	-	-	-	-	-	-
4208.990		0.710	-0.460	68.2	-		68.2	64.9	-	-	-	-	88.0
4317.321		0.713	-1.380		-		-	-	-	-	-	30.3	66.0
4554.036	Ba II	0.000	0.120	259.1	215.0	-	-	176.2	412.3	284.4	286.0	259.5	338.7
4130.650		2.720	+0.560	77.8	-	182.2	-	-	98.96	-	-	-	108.8
4934.076		0.000	-0.150		-		265.6	-	-	298.1	333.9	-	-
5853.668		0.604	-1.020		-	263.9	-	-	-	147.8	-	-	-
6141.727		0.704	-0.076		158.9	420.5	200.8	-	253.8	237.9	-	-	230.0
6496.897		0.604	-0.377	157.1	149.8	402.3	214.7	-	233.9	225.0	-	229.9	209.4

Table A.4 – continued from previous page

Wavelength Å	Element	E_{low} eV	log gf	4395 mÅ	5395 mÅ	16458 mÅ	48565 mÅ	81192 mÅ	125079 mÅ	188650 mÅ	201626 mÅ	214714 mÅ	216219 mÅ
4123.230	La II	0.320	+0.120		-		87.1	-	-	-	-	-	-
4238.380		0.400	-0.058	92.5	68.0		101.1	-	-	-	-	-	97.9
4322.510		0.170	-1.050	44.3	-		-	19.9	-	-	-	-	-
4333.760		0.170	-0.160	108.8	-		-	56.6	-	-	-	-	-
4619.874		1.754	-0.140	-	-		22.8	-	-	-	-	-	25.7
4748.726		0.927	-0.860	-	-	72.1	23.2	-	-	-	-	-	42.1
4921.776		0.244	-0.680	67.4	85.1	173.9	64.5	72.9	-	-	78.8	-	77.9
5808.313		0.000	-2.200	-	-	77.3	-	-	-	-	-	-	-
6320.376		0.170	-1.610	-	-		-	-		-	54.4	-	-
4073.470	Ce II	0.480	+0.320	-	-		60.5	-	58.5	-		-	61.5
4117.290		0.740	-0.450	-	-	39.2	-		-	-	36.8	-	27.9
4190.630		0.900	-0.390	-	-		19.1	-	-	-	-	-	-
4193.870		0.550	-0.400	-	-		33.5	-	-	-	-	-	-
4257.120		0.460	-1.116	-	-		-		-	-	31.8	-	-
4336.244		0.704	-0.564	-	-		-	-	-	-	-	-	34.9
4418.790		0.860	+0.310	-	-		-	-	-	28.8	-	30.6	55.3
4427.920		0.540	-0.380	-	-		-	-	-	-	-	22.1	39.7
4460.207		0.477	0.171	-	-		-	-	-	94.8	-	-	-

Table A.4 – continued from previous page

Wavelength Å	Element	E_{low} eV	log gf	4395 mÅ	5395 mÅ	16458 mÅ	48565 mÅ	81192 mÅ	125079 mÅ	188650 mÅ	201626 mÅ	214714 mÅ	216219 mÅ
4560.280		0.910	0.000	-	-		52.2	-	-	-		-	-
4562.359		0.478	0.081	-	-	132.0	60.6	34.1	74.9	48.6	78.6	69.8	73.3
4628.160		0.520	+0.260	-	46.3	135.4	64.5	-	-	44.4		-	76.08
4747.167		0.320	-1.246	-	-		14.3	-	-	-		-	-
4773.941		0.924	-0.498	-	24.7	20.5	-	34.9	-	47.4	12.3	30.5	
4873.999		1.107	-0.892	-	-	57.4	-	-	-	-	-		-
5274.230		1.044	0.323	25.3	23.6		37.0	-	-	-	-	23.9	45.2
5330.556		0.869	-0.760	12.7	-		22.4	-	-	-	48.9	12.4	28.2
5188.217	Pr II	0.922	-1.145		-	34.1	-	-	-	-	-	-	-
5259.740		0.630	-0.070	10.4	-	104.6	15.1	-	-	-	-	-	-
5219.045		0.795	-0.240	-	-	92.5	-	-	-	-	-	-	17.3
5292.619		0.648	-0.300	-	42.6	104.0	15.0	-	-	16.9	-	21.4	22.8
5322.772		0.482	-0.315	-	-	109.6	12.4	-	26.1	-	54.5	-	-
5892.251		1.439	-0.352	-	-	41.8	11.1	-	-	-	-	-	-
6278.676		1.196	-0.630	-	63.8		-	-	-	-	-	-	-
4021.327	Nd II	0.320	0.230		-	-	61.8	-	-	-	-	-	-
4059.951		0.205	-0.360		-	60.3	-	-	-	-	-	-	31.2
4061.080		0.471	0.550	64.0	56.6	123.2	67.1	-	-	-	-	-	-

Table A.4 – continued from previous page

Wavelength Å	Element	E_{low} eV	log gf	4395 mÅ	5395 mÅ	16458 mÅ	48565 mÅ	81192 mÅ	125079 mÅ	188650 mÅ	201626 mÅ	214714 mÅ	216219 mÅ
4069.270		0.060	-0.400	-	-		-	-	-	-	-	-	35.4
4109.448		0.320	+0.180	-	-	111.4	-	-	-	-	-	-	-
4446.390		0.200	-0.630	37.4	-	175.0	49.2	60.4	-	32.1	-	47.1	44.5
4451.563		0.381	-0.040	-	-		74.1	-	-	-	104.9	-	-
4451.980		0.000	-1.340	-	-	153.2	31.7	-	-	-	-	36.4	44.6
4556.133		0.064	-1.610	-	-	119.0	-	-	-	-	60.5	-	-
4797.153		0.559	-0.950	-	-	94.0	19.9	-	-	-	-	-	27.9
4811.342		0.063	-1.140	27.8	44.2	124.4	38.8	-	57.4	26.6	68.5	28.0	42.8
5089.832		0.204	-1.160	-	-		14.9	-	-	-	-	-	16.7
5130.590		1.300	+0.100	-	-		39.3	-	-	-	-	-	60.9
4859.039		0.320	-0.830	-	-	147.6	-	-	-	44.5	-	51.91	-
4947.020		0.559	-1.250	-	-	68.1	-	-	-	-	-	-	-
4961.387		0.630	-0.710	-	19.9	113.3	-	-	42.3	-	72.5	-	-
4989.953		0.680	-1.400	-	-	144.9	-	-	-	-	-	-	-
5212.361		0.204	-0.870	-	52.1	138.7	-	-	-	-	-	22.7	36.2
5293.169		0.823	-0.060	39.0	-		-	-	-	-	-	46.8	60.2
5276.878		0.859	-0.440	-	-	93.0	-	-	-	-	-	-	-
5287.133		0.745	-1.300	-	14.9	71.6	-	-	-	-	-	-	-

Table A.4 – continued from previous page

Wavelength Å	Element	E_{low} eV	log gf	4395 mÅ	5395 mÅ	16458 mÅ	48565 mÅ	81192 mÅ	125079 mÅ	188650 mÅ	201626 mÅ	214714 mÅ	216219 mÅ
5311.480		0.990	-0.560	-	-	117.8	18.2	-	-	-	47.8	-	-
5319.820		0.550	-0.210	35.8	-		46.1	-	-	-	76.9	51.5	59.3
5356.967		1.264	-0.250	-	-	81.5	-	-	-	-	-	-	-
5361.510		0.68	-0.400	-	-		-	-	-	35.2	61.4	49.9	-
5371.927		1.412	0.003	-	-		-	-	-	-	-	-	30.1
5603.648		0.380	-1.830	-	-	111.5	-	-	44.7	13.8	-	-	-
5718.118		1.410	-0.340	-	-	68.1	-	-	-	-	-	-	-
5825.857		1.081	-0.760	-	-	74.9	-	-	-	-	-	-	-
4318.927	Sm II	0.280	-0.270	-	-	151.6	-	37.7	-	-	53.0	-	-
4424.337		0.485	-0.260		-		-	-	-	-	70.0	-	-
4434.318		0.378	-0.576	53.5	-	116.9	-	60.4	-	26.1	-	-	52.8
4499.475		0.248	-1.413	-	-	71.9	10.8	-	-	-	28.9	-	-
4519.630		0.540	-0.430	20.2	-	-	28.3	-	-	-	-	-	37.5
4577.690		0.250	-0.770	-		-	-	22.7	36.4	-	-	-	-
4566.210		0.330	-1.245	13.8	-	-	-	-	-	-	44.4	-	16.7
4674.600		0.180	-0.560	-	-	-	27.4	-	-	27.9	-	-	37.7
4704.400		0.000	-1.562	30.2	-	-	-	33.1	-	-	-	23.8	32.8
4615.444		0.544	-1.262	-	-	-	-	-	-	-	18.7		-

Table A.4 – continued from previous page

Wavelength Å	Element	E_{low} eV	log gf	4395 mÅ	5395 mÅ	16458 mÅ	48565 mÅ	81192 mÅ	125079 mÅ	188650 mÅ	201626 mÅ	214714 mÅ	216219 mÅ
4726.026		0.333	-1.849	-	-	-	-	-	-	-	29.8	-	-
4791.580		0.104	-1.846	-	-	77.5	-	-	-	-	24.0	-	-
4815.805		0.185	-1.501	-	-		-	-	- -	-	-	16.2	-
4129.700	Eu II	0.000	+0.204		-	-	74.9	-	-	-	-	-	80.3
4205.050		0.000	+0.117	-	-	-	-	-	-	-	-	-	97.2
6437.640		1.319	-0.276	-	14.8	27.3	-	-	-	-	-	-	-
6645.130		1.380	+0.204	-	-	61.9	-	-	-	-	-	-	-
4103.310	Dy II	0.103	-0.346		-		-	68.9	- -	-	46.7	-	-
4923.167		0.103	-2.384		26.1		-	-	- -	-	-	-	-

Table A.5: Lines used for the calculation of elemental abundances for HD 55496, HD 89668, HD 92545, HD 104979, HD 107574, HD 111721

Wavelength Å	Element	E_{low} eV	log gf	HD 55496 mÅ	HD 89668 mÅ	HD 92545 mÅ	HD 104979 mÅ	HD 107574 mÅ	HD 111721 mÅ
5682.650	Na I	2.100	-0.700	58.07	208.7	63.7	115.9	50.1	-
5688.220		2.100	-0.400	-	205.3	89.9	131.6	-	29.9
5889.950		0.000	0.100	275.5	-	-	450.2	253.8	263.3
5895.920		0.000	-0.200	-	-	225.4	379.5	226.1	245.6
4702.990	Mg I	4.350	-0.666	103.2	-	172.8	188.9	-	143.1
6318.720		5.108	-1.730	15.88	86.1	82.6	137.4	-	79.4
5528.000		4.350	-0.490	142.3	-	162.6	202.4	-	139.0
4098.500	Ca I	2.525	-0.540	-	-	-	-	-	-
4283.010		1.885	-0.224	-	-	-	-	-	-
4425.430		1.879	-0.385	-	-	-	154.6	-	-
4435.679		1.890	-0.520	-	-	-	-	-	-
4455.890		1.900	-0.510	-	-	-	180.4	-	114.8
4578.550		2.521	-0.560	-	-	59.5	94.79	-	-
5261.710		2.521	-0.730	51.41	188.5	63.4	111.8	55.9	74.9
5265.560		2.520	-0.110	-	-	-	-	-	-
5512.990		2.932	-0.290	-	181.2	55.1	93.58	-	-
5581.980		2.523	-0.710	69.85	175.4	72.9	111.0	49.5	80.4

Table A.5 – continued from previous page

Wavelength Å	Element	E_{low} eV	log gf	HD 55496 mÅ	HD 89668 mÅ	HD 92545 mÅ	HD 104979 mÅ	HD 107574 mÅ	HD 111721 mÅ
5588.760		2.530	0.360	104.7	-	113.4	153.1	109.0	112.7
5590.130		2.521	-0.710	74.9	167	69.0	108.1	-	61.9
5594.470		2.520	0.100	94.9	-	-	-	-	62.1
5857.450		2.930	0.240	87.9	-	128.5	137.1	84.9	90.9
6162.170		1.900	-0.090	144.9	-	137.0	194.4	115.4	142.2
6439.070		2.530	0.390	-	-	118.6	-	110.1	120.7
6449.820		2.520	-0.550	-	-	83.5	-	50.9	-
6455.590		2.523	-1.350	58.94	119.7	-	-	-	31.8
6471.670		2.525	-0.590	-	168.4	62.2	111.1	55.8	-
6493.790		2.521	0.140	118.3	-	104.6	158.2	-	95.7
6499.650		2.523	-0.590	70.35	155.2	58.9	107.8	-	60.4
6717.690		2.709	-0.610	-	-	89.1	142.6	53.8	72.9
4431.110		6.035	-2.520	-	-	-	-	-	-
4400.389	Sc II	0.606	-0.510	-	-	-	-	-	-
5031.021		1.360	-0.260	-	26.1	-	115.6	-	55.7
6604.600		1.357	-1.480	47.35	37.3	-	73.27	-	74.7
6245.630		1.507	−1.03	-			69.39	25.7	31.9
4512.700	Ti I	0.836	-0.480	49.03	144.8	37.7	89.85	-	-

Table A.5 – continued from previous page

Wavelength Å	Element	E_{low} eV	log gf	HD 55496 mÅ	HD 89668 mÅ	HD 92545 mÅ	HD 104979 mÅ	HD 107574 mÅ	HD 111721 mÅ
4453.710		1.873	-0.010	-	-	-	77.33	-	-
4533.239		0.848	0.476	86.5	-	-	139.9	-	92.4
4617.250		1.748	0.389	33.5	117.6	41.8	87.01	-	53.2
4656.468		0.000	-1.345	51.0	157.2	-	109.8	-	-
4759.272		2.255	0.514	-	91.7	-	67.37	-	-
4820.410		1.502	-0.441	-	92.5	-	102.0	-	45.2
4840.880		0.899	-0.509	43.45	134.4	35.2	95.31	-	52.8
4778.250		2.236	-0.220	-	-	-	30.33	-	-
4999.500		0.830	0.310	123.2	-	63.8	191.8	79.9	96.6
4937.730		0.813	-2.230	-	59.5	-	31.09	-	-
5007.210		0.820	0.170	158.5	249.5	-	180.8	-	121.8
5039.960		0.020	-1.130	73.92	171.1	-	120.2	-	81.3
5064.650		0.050	-0.940	60.15	145.9	-	132.7	-	85.9
5087.060		1.429	-0.780	-	207.1	-	61.23	-	18.5
5210.390		0.048	-0.884	73.41	-	68.4	146.1	33.6	89.7
6556.060		1.460	-1.074	-	98.2	-	51.69	-	12.9
4161.530	Ti II	1.080	-2.160	-	-	-	-	-	-
4417.710		1.160	-1.430	-	78.5	116.7	153.2	-	74.5

Table A.5 – continued from previous page

Wavelength Å	Element	E_{low} eV	log gf	HD 55496 mÅ	HD 89668 mÅ	HD 92545 mÅ	HD 104979 mÅ	HD 107574 mÅ	HD 111721 mÅ
4418.330		1.240	-1.990	100.9	-	93.1	123.0	84.6	-
4443.790		1.080	-0.700	-	152.0	-	-	-	-
4468.520		1.130	-0.600	46.3	136.2	-	-	-	111.5
4470.900		1.164	-2.280	51.34	48.9	-	108.4	-	-
4493.510		1.080	-2.730	-	-	-	-	-	-
4563.760		1.221	-0.960	110.4	167.1	169.8	168.3	-	125.4
4571.960		1.571	-0.530	75.23	-	125.9	181.0	163.7	-
4568.310		1.224	-2.650	-	-	-	60.37	-	-
4657.210		1.240	-2.320	49.48	-	-	89.28	-	41.6
4708.665		1.240	-2.370	29.16	35.9	-	74.04	36.2	50.81
4798.510		1.080	-2.670	-	-	-	-	-	63.0
4805.090		2.060	-1.100	-	76.6	93.0	127.3	102.7	78.4
5185.900		1.890	-1.350	62.53	-	87.2	90.35	49.5	70.0
5226.530		1.570	-1.300	82.5	-	-	135.1	-	107.4
4090.570	V I	1.853	-2.099	-	-	-	112.5	-	-
4379.230		0.300	0.580	-	221.0	-	135.9	-	-
4406.630		0.300	-0.190	48.63	151.2	-	143.3	-	-
4876.430	V I	2.115	-2.714	-	-	80.1	80.9	-	-

Table A.5 – continued from previous page

Wavelength Å	Element	E_{low} eV	log gf	HD 55496 mÅ	HD 89668 mÅ	HD 92545 mÅ	HD 104979 mÅ	HD 107574 mÅ	HD 111721 mÅ
6531.420		1.218	-0.840	-				-	-
5727.048		1.08	−0.012	-	63.4	-	23.3	-	48.1
4274.800	Cr I	0.000	-0.230	-	-	-	-	-	-
4289.720		0.000	-0.360	-	-	-	-	-	81.1
4351.050		0.970	-1.450	-	116.8	-	-	-	-
4600.750		1.000	-1.260	-	-	-	-	-	50.9
4616.140		0.980	-1.190	43.64	179.5	-	123.6	-	63.8
4626.190		0.970	-1.320	60.19	160.1	41.3	110.0	-	46.7
4652.160		1.000	-1.030	-	211.5	71.9	128.1	-	81.2
4737.380		3.087	-0.099	-	73.8	-	100.5	32.0	-
4942.490		0.941	-2.294	-	201.5	-	119.9	-	52.1
5206.040		0.940	0.020	100.6	-	-	246.4	-	122.1
5247.570		0.961	-1.640	50.28	101.2	-	113.7	-	54.7
5345.810		1.003	-0.980	85.61	-	85.3	157.5	-	80.5
5348.312		1.003	-1.290	72.24	-	-	130.8	34.9	69.1
4588.190	Cr II	4.072	-0.630	-	36.1	-	81.3	-	43.2
4592.040		4.073	-1.220	-	-	-	-	-	-
4812.350		3.864	-1.800	-	-	-	57.4	-	-

Table A.5 – continued from previous page

Wavelength Å	Element	E_{low} eV	log gf	HD 55496 mÅ	HD 89668 mÅ	HD 92545 mÅ	HD 104979 mÅ	HD 107574 mÅ	HD 111721 mÅ
4634.070		4.073	-1.240	20.6	-	83.2	113.5	-	-
4848.250		3.864	-1.140	-	88.9	-	-	58.1	39.4
4030.750	Mn I	0.000	-0.470	-	-	-	-	-	-
4034.480		0.000	-0.810	-	-	-	-	-	-
4041.360		2.110	0.280	-	-	-	144.1	-	-
4451.580		2.890	0.280	46.9	136.6	-	110.6	-	-
4470.140		2.941	-0.444	-	77.7	-	55.3	-	-
4739.080		2.941	-0.490	-	86.7	-	85.5	-	-
4761.530		2.953	-0.138	-	105.2	-	95.1	-	-
4765.860		2.941	-0.080	-	97.4	-	86.4	-	31.9
4766.420		2.919	0.100	-	166.7	-	108.5	-	39.4
4783.430		2.300	0.040	-	54.6	-	152.6	-	-
5516.770		2.178	-1.847	-	118.3	-	82.4	-	-
4813.480	Co I	3.216	0.050	-	63.9	-	66.5	-	-
4121.320		0.920	-0.320	-	-	-	119.4	-	-
4118.770		1.050	-0.490	-	-	-	-	-	-
4749.660		3.053	-0.321	-	64.2	-	-	-	-
4771.080		3.133	-0.504	-	27.6	-	50.9	-	-

Table A.5 – continued from previous page

Wavelength Å	Element	E_{low} eV	log gf	HD 55496 mÅ	HD 89668 mÅ	HD 92545 mÅ	HD 104979 mÅ	HD 107574 mÅ	HD 111721 mÅ
4781.430		1.882	-2.150	-	-	16.1	24.0	-	-
4792.850		3.252	-0.067	-	46.4	-	47.9	-	-
5530.770		1.710	-2.060	-	53.0	-	53.3	-	-
5590.720		2.042	-1.870	-	-	68.9	46.6	-	-
5991.870		2.080	-1.850	-	-	17.2	-	-	-
6454.990		3.632	-0.233	-	-	-	188.3	34.7	-
6632.430		2.280	-2.000	-	37.6	-	26.9	-	-
4470.470	Ni I	3.699	-0.400	-	103.8	-	83.8	-	-
4714.420		3.380	0.230	-	169.8	-	175.7	-	74.2
4732.460		4.106	-0.550	-	-	-	62.1	-	-
4814.590		3.597	-1.680	-	-	-	31.32	-	-
4821.130		4.153	-0.850	-	-	-	39.0	-	-
4852.560		3.542	-1.070	-	49.3	-	61.3	-	-
4855.410		3.540	0.000	-	-	-	-	-	64.0
4857.390		3.740	-1.199	-	82.6	-	65.9	-	48.5
4953.200		3.740	-0.670	-	82.7	25.8	77.8	-	26.1
4937.340		3.606	-0.390	-	65.9	-	91.2	-	51.7
4980.160		3.610	-0.110	-	121.3	69.8	123.0	65.4	58.8

Table A.5 – continued from previous page

Wavelength Å	Element	E_{low} eV	log gf	HD 55496 mÅ	HD 89668 mÅ	HD 92545 mÅ	HD 104979 mÅ	HD 107574 mÅ	HD 111721 mÅ
5035.370		3.630	0.290	-	107.7	-	103.4	-	62.4
5081.120		3.847	0.300	-	-	-	104.6	54.7	-
5082.350		3.657	-0.540	-	-	-	82.11	-	26.2
5084.080		3.678	0.030	36.5	55.8	73.2	90.7	-	52.6
5099.930		3.678	-0.100	-	-	-	93.11	-	33.9
5102.960		1.676	-2.620	45.8	-	-	94.1	-	-
5259.470		3.740	-1.502	-	47.1	-	38.3	-	-
6086.280		4.266	-0.530	-	39.0	-	51.8	-	11.7
6111.070		4.088	-0.785	-	31.8	-	44.22	-	-
6176.810		4.088	-0.148	-	64.9	44.4	75.9	18.2	20.3
6186.710		4.106	-0.777	-	36.5	14.3	-	-	-
6204.600		4.088	-1.060	-	29.5	-	29.2	-	-
6643.640		1.676	-2.300	-	125.0	57.2	141.2	-	73.3
4722.150	Zn I	4.029	-0.370	-	-	-	92.3	-	-
4810.530		4.080	-0.170	56.4	-	-	80.1	-	-
4607.327	Sr I	0.000	-0.570	36.42	140.9	-	91.55	-	-
4854.863	Y II	0.992	-0.380	-	90.5	57.6	120.6	-	-
4883.685		1.084	0.070	-	74.4	89.9	121.2	106.8	51.7

Table A.5 – continued from previous page

Wavelength Å	Element	E_{low} eV	log gf	HD 55496 mÅ	HD 89668 mÅ	HD 92545 mÅ	HD 104979 mÅ	HD 107574 mÅ	HD 111721 mÅ
5087.416		1.080	-0.170	103.5	-	72.1	91.82	-	56.2
5119.112		0.992	-1.360	41.16	-	27.4	55.28	-	-
5205.724		1.033	-0.340	42.89	-	-	-	-	-
5289.815		1.033	-1.850	27.11	-	-	33.81	-	-
5544.611		1.738	-1.090	-	-	-	36.53	-	-
5546.009		1.748	-1.100	-	-	22.3	59.74	16.14	o-
5662.925		1.944	0.160	-	92.0	66.8	92.26	83.82	33.8
6613.733		1.748	-1.110	-	39.0	-	61.85	30.5	-
4048.670	Zr II	0.800	-0.480	-	-	-	156.1	-	-
4208.990		0.710	-0.460	-	-	-	-	-	-
4317.321		0.713	-1.380	42.23	-	-	76.87	-	-
4554.036	Ba II	0.000	0.120	193.3	195.0	205.3	383.2	-	181
4130.650		2.720	+0.560	-	-	-	-	-	-
4934.076		0.000	-0.150	186.2	-	230.3	-	241.6	176.0
5853.668		0.604	-1.020	114.9	60.34	119.3	155.6	124.2	61.3
6141.727		0.704	-0.076	137.3	133.8	167.1	247.3	205.3	111.1
6496.897		0.604	-0.377	137.4	105.5	161.0	240.9	193.9	120.1
4123.230	La II	0.320	+0.120	-	-	-	-	-	-

Table A.5 – continued from previous page

Wavelength Å	Element	E_{low} eV	log gf	HD 55496 mÅ	HD 89668 mÅ	HD 92545 mÅ	HD 104979 mÅ	HD 107574 mÅ	HD 111721 mÅ
4238.380		0.400	-0.058	-	-	-	108.2	-	-
4322.510		0.170	-1.050	-	-	-	70.35	-	-
4333.760		0.170	-0.160	-	-	-	-	-	-
4619.874		1.754	-0.140	-	-	-	75.11	-	-
4748.726		0.927	-0.860	-	-	-	40.6	-	-
5808.313		0.000	-2.200	-	-	-	24.0	-	-
6320.376		0.170	-1.610	21.49	-	-	66.2	-	-
4073.470	Ce II	0.480	+0.320	-	-	-	47.32	-	-
4117.290		0.740	-0.450	-	-	-	-	-	-
4190.630		0.900	-0.390	-	-	-	-	-	-
4193.870		0.550	-0.400	-	-	-	-	-	-
4257.120		0.460	-1.110	-	-	-	-	-	-
4336.244		0.704	-0.564	-	-	-	52.1	-	-
4418.790		0.860	+0.310	-	-	-	-	-	-
4427.920		0.540	-0.380	-	-	-	78.8	-	-
4460.207		0.477	0.171	-	-	-	193	-	58.6
4560.280		0.910	0.000	-	-	-	-	-	58.6
4562.359		0.478	0.081	28.68	-	-	80.5	-	-

Table A.5 – continued from previous page

Wavelength Å	Element	E_{low} eV	log gf	HD 55496 mÅ	HD 89668 mÅ	HD 92545 mÅ	HD 104979 mÅ	HD 107574 mÅ	HD 111721 mÅ
4628.160		0.520	+0.260	82.66	-	-	91.84	-	-
4747.167		0.320	-1.246	-	37.7	18.7	41.46	-	-
4773.941		0.924	-0.498	-	-	-	44.8	-	-
4873.999		1.107	-0.892	-	-	-	47.3	-	21.9
5274.230		1.044	0.323	-	-	-	57.9	20.1	-
5330.556		0.869	-0.760	-	-	-	43.0	-	-
5188.217	Pr II	0.922	-1.145	-	-	-	-	-	-
5259.740		0.630	-0.070	-	-	-	40.7	-	-
5219.045		0.795	-0.240	7.624	-	7.8	25.2	-	-
5292.619		0.648	-0.300	-	36.1	-	50.5	-	-
5322.772		0.482	-0.315	-	-	-	43.7	-	-
5892.251		1.439	-0.352	-	-	-	-	-	19.8
6278.676		1.196	-0.630	-	-	-	-	-	-
4021.327	Nd II	0.320	0.230	-	-	-	53.0	-	-
4059.951		0.205	-0.360	-	-	-	-	-	-
4061.080		0.471	0.550	-	-	-	68.9	-	-
4069.270		0.060	-0.400	-	-	-	-	-	-
4109.448		0.320	+0.180	-	-	-	108.4	-	-

Table A.5 – continued from previous page

Wavelength Å	Element	E_{low} eV	log gf	HD 55496 mÅ	HD 89668 mÅ	HD 92545 mÅ	HD 104979 mÅ	HD 107574 mÅ	HD 111721 mÅ
4446.390		0.200	-0.630	-	18.1	-	76.6	-	-
4451.563		0.381	-0.040	47.08	136.2	-	110.6	-	-
4451.980		0.000	-1.340	-	97.9	-	81.5	-	-
4556.133		0.064	-1.610	-	154.2	-	120.1	-	70.7
4797.153		0.559	-0.950	-	-	-	44.7	-	-
4811.342		0.063	-1.140	19.97	21.4	-	72.5	-	-
5089.832		0.204	-1.160	-	-	-	37.6	-	-
5130.590		1.300	+0.100	-	-	-	-	-	-
4859.039		0.320	-0.830	-	44.0	-	102.6	-	-
4947.020		0.559	-1.250	-	-	-	22.7	-	-
4961.387		0.630	-0.710	-	25.9	-	58.3	-	-
4989.953		0.680	-1.400	-	59.7	-	76.5	-	-
5212.361		0.204	-0.870	-	74.3	-	80.7	-	-
5293.169		0.823	-0.060	-	-	-	90.3	-	-
5276.878		0.859	-0.440	-	-	-	37.8	-	-
5287.133		0.745	-1.300	-	41.5	-	22.2	-	-
5311.480		0.990	-0.560	-	-	-	45.5	-	40.1
5319.820		0.550	-0.210	-	-	-	90.1	-	-

Table A.5 – continued from previous page

Wavelength Å	Element	E_{low} eV	log gf	HD 55496 mÅ	HD 89668 mÅ	HD 92545 mÅ	HD 104979 mÅ	HD 107574 mÅ	HD 111721 mÅ
5356.967		1.264	-0.250	-	-	-	37.7	-	-
5361.510		0.68	-0.400	-	88.8	-	-	-	23.1
5371.927		1.412	0.003	-	-	-	-	-	-
5603.648		0.380	-1.830	-	-	-	45.1	-	47.5
5718.118		1.410	-0.340	-	-	-	-	-	-
5825.857		1.081	-0.760	-	8.662	-	27.8	-	-
4318.927	Sm II	0.280	-0.270	-	-	-	-	-	-
4424.337		0.485	-0.260	-	-	-	-	-	-
4434.318		0.378	-0.576	-	-	-	93.0	-	-
4499.475		0.248	-1.413	-	-	-	35.9	-	-
4519.630		0.540	-0.430	-	-	-	60.7	-	-
4577.690		0.250	-0.770	-	-	-	45.7	-	-
4566.210		0.330	-1.245	-	20.8	-	37.9	-	-
4674.600		0.180	-0.560	-	-	-	121.5	-	-
4704.400		0.000	-1.562	-	-	-	55.2	-	-
4615.444		0.544	-1.262	-	48.2	-	-	-	-
4726.026		0.333	-1.849	14.25	-	-	-	-	-
4791.580		0.104	-1.846	-	14.1	-	-	-	-

Table A.5 – continued from previous page

Wavelength Å	Element	E_{low} eV	log gf	HD 55496 mÅ	HD 89668 mÅ	HD 92545 mÅ	HD 104979 mÅ	HD 107574 mÅ	HD 111721 mÅ
4815.805		0.185	-1.501	-	-	-	-	-	-
4129.700	Eu II	0.000	+0.204	-	-	-	-	-	-
4205.050		0.000	+0.117	-	-	-	-	-	-
6437.640		1.319	-0.276	-	-	-	-	-	-
6645.130		1.380	+0.204	-	-	-	31.1	-	-
4103.310	Dy II	0.103	-0.346	-	-	-	83.1	-	-
4923.167		0.103	-2.384	-	36.6	-	23.1	-	-

Table A.6: Lines used for the calculation of elemental abundances for HD 122202, HD 126681, HD 148897, HD 164922, HD 167768, HD 204613

Wavelength Å	Element	E_{low} eV	log gf	HD 122202 mÅ	HD 126681 mÅ	HD 148897 mÅ	HD 164922 mÅ	HD 167768 mÅ	HD 204613 mÅ
5682.650	Na I	2.100	-0.700	-	22.8	73.7	137.6	93.2	87.5
5688.220		2.100	-0.400	-	-	93.0	143.4	118.7	106.2
5889.950		0.000	0.100	-	263.2	396.5	-	379.1	377.3
5895.920		0.000	-0.200	-	234.5	340.2	601.4	329.7	-
4702.990	Mg I	4.350	-0.666	147.3	-	186.2	334.3	182.4	232.6
6318.720		5.108	-1.730	-	60.7	35.3	133.2	35.5	88.3
5528.000		4.350	-0.490	-	156.7	212.2	320	205.3	201.8
4098.500	Ca I	2.525	-0.540	-	-	-	130.6	-	79.2
4283.010		1.885	-0.224	-	-	116.9	-	142.3	145.7
4425.430		1.879	-0.385	-	-	158.9	193.2	163.8	142.1
4435.679		1.890	-0.520	-	-	-	140.6	-	139.1
4455.890		1.900	-0.510	-	-	166.8	182.4	141.1	-
4578.550		2.521	-0.560	-	-	117.3	100.2	102.1	77.3
5261.710		2.521	-0.730	-	48.9	120.7	124.8	102.6	86.9
5265.560		2.520	-0.110	-	107.3	-	-	-	-
5512.990		2.932	-0.290	-	42.5	94.6	110.4	87.4	70.4
5581.980		2.523	-0.710	-	50.7	118.2	120.4	99.5	84.1

Table A.6 – continued from previous page

Wavelength Å	Element	E_{low} eV	log gf	HD 122202 mÅ	HD 126681 mÅ	HD 148897 mÅ	HD 164922 mÅ	HD 167768 mÅ	HD 204613 mÅ
5588.760		2.530	0.360	-	109.2	162.4	181.7	147.7	129.4
5590.130		2.521	-0.710	-	50.6	115.2	114.3	98.9	80.6
5594.470		2.520	0.100	107.1	89.9	-	-	-	-
5857.450		2.930	0.240	108.7	81.1	149.3	178.7	143.0	111.2
6162.170		1.900	-0.090	-	143.4	223.6	286.2	191.8	174.3
6439.070		2.530	0.390	-	113.7	187.5	200.4	163.9	144.3
6449.820		2.520	-0.550	-	53.9	-	-	113.4	91.5
6455.590		2.523	-1.350	-	25.8	82.3	78.12	-	43.2
6471.670		2.525	-0.590	-	-	122.4	143.0	100.8	81.5
6493.790		2.521	0.140	-	144.1	156.0	160.7	135.7	118.1
6499.650		2.523	-0.590	-	29.9	117.7	112.4	94.4	80.9
6717.690		2.709	-0.610	-	62.3	145.5	155.7	127.6	97.7
4431.110		6.035	-2.520	-	-	-	37.3	67.2	46.5
4400.389	Sc II	0.606	-0.510	-	-	-	-	-	-
5031.021		1.360	-0.260	-	37.0	123.4	81.5	113.6	46.1
6604.600		1.357	-1.480	-	-	75.2	49.3	71.6	41.7
6245.630		1.507	– 1.03			75.6	43.6	64.1	38.9
4512.700	Ti I	0.836	-0.480	-	-	134.8	82.8	89.9	61.7

Table A.6 – continued from previous page

Wavelength Å	Element	E_{low} eV	log gf	HD 122202 mÅ	HD 126681 mÅ	HD 148897 mÅ	HD 164922 mÅ	HD 167768 mÅ	HD 204613 mÅ
4453.710		1.873	-0.010	-	-	93.1	72.2	75.3	46.1
4533.239		0.848	0.476	-	-	194.8	152.7	-	100.4
4617.250		1.748	0.389	-	-	110.7	85.7	79.9	52.1
4656.468		0.000	-1.345	-	95.5	156.4	86.3	96.0	59.6
4759.272		2.255	0.514	-	-	78.3	61.5	50.8	39.4
4820.410		1.502	-0.441	-	-	116.0	70.2	-	42.3
4840.880		0.899	-0.509	-	57.9	134.0	84.6	90.2	60.9
4778.250		2.236	-0.220	-	-	37.9	34.3	111.3	13.2
4999.500		0.830	0.310	-	71.7	201.3	140.0	138.6	111.3
4937.730		0.813	-2.230	-	-	62.7	21.9	69.3	-
5007.210		0.820	0.170	-	108.3	201.7	177.6	162.1	139.5
5039.960		0.020	-1.130	-	-	140.3	103.6	111.2	76.7
5064.650		0.050	-0.940	-	-	192.8	119.3	122.5	78.6
5087.060		1.429	-0.780	-	-	89.2	69.4	45.4	-
5210.390		0.048	-0.884	-	58.4	222.4	140.8	115.1	84.1
6556.060		1.460	-1.074	-	-	84.2	47.3	42.8	-
4161.530	Ti II	1.080	-2.160	-	-	-	-	-	75.2
4417.710		1.160	-1.430	101.1	-	156.2	97.7	131.8	123.8

Table A.6 – continued from previous page

Wavelength Å	Element	E_{low} eV	log gf	HD 122202 mÅ	HD 126681 mÅ	HD 148897 mÅ	HD 164922 mÅ	HD 167768 mÅ	HD 204613 mÅ
4418.330		1.240	-1.990	-	-	132.4	87.8	113.7	89.5
4443.790		1.080	-0.700	-	-	195.6	142.4	-	146.4
4468.520		1.130	-0.600	-	-	-	130.3	-	151.3
4470.900		1.164	-2.280	-	-	70.3	57.7	-	76.4
4493.510		1.080	-2.730	-	-	107.3	-	-	44.1
4563.760		1.221	-0.960	-	76.7	189.9	148.8	174.5	136.2
4571.960		1.571	-0.530	-	-	223.8	-	150.6	144.2
4568.310		1.224	-2.650	-	-	88.82	36.9	63.2	33.8
4657.210		1.240	-2.320	-	-	116.8	48.1	92.6	65.3
4708.665		1.240	-2.370	-	-	95.2	43.7	83.8	60.9
4798.510		1.080	-2.670	-	-	-	49.5	-	53.9
4805.090		2.060	-1.100	-	-	122.2	119.5	121.3	100.8
5185.900		1.890	-1.350	88.3	32.1	111.1	51.7	93.0	77.5
5226.530		1.570	-1.300	-	49.9	-	-	-	101.8
4090.570	V I	1.853	-2.099	-	-	70.4	92.4	-	69.1
4379.230		0.300	0.580	-	-	176.4	146.8	-	101.7
4406.630		0.300	-0.190	-	-	147.5	133.6	127.3	90.9
4876.430	V I	2.115	-2.714	-	-	61.1	60.5	79.2	67.2

Table A.6 – continued from previous page

Wavelength Å	Element	E_{low} eV	log gf	HD 122202 mÅ	HD 126681 mÅ	HD 148897 mÅ	HD 164922 mÅ	HD 167768 mÅ	HD 204613 mÅ
6531.420		1.218	-0.840			56.5	85.7	17.0	
5727.048		1.08	– 0.012	-	-	37.7	-	-	-
4274.800	Cr I	0.000	-0.230	-	-	-	-	-	-
4289.720		0.000	-0.360	-	-	-	-	-	-
4351.050		0.970	-1.450	-	-	-	77.3	-	42.9
4600.750		1.000	-1.260	-	-	-	113.8	-	-
4616.140		0.980	-1.190	-	-	141.7	111.9	104.2	78.0
4626.190		0.970	-1.320	-	71.3	133.3	99.5	98.6	68.6
4652.160		1.000	-1.030	-	91.4	146.0	133.2	109.6	87.9
4737.380		3.087	-0.099	-	-	66.3	76.2	56.0	51.3
4942.490		0.941	-2.294	-	-	126.2	130.7	95.1	62.9
5206.040		0.940	0.020	-	122.4	297.2	-	193.5	162.6
5247.570		0.961	-1.640	-	29.9	135.2	105.4	74.7	61.6
5345.810		1.003	-0.980	74.2	62.5	179.3	157.2	140.5	95.8
5348.312		1.003	-1.290	-	67.8	155.5	127.7	111.8	82.1
4588.190	Cr II	4.072	-0.630	-	-	65.0	61.6	59.8	16.1
4592.040		4.073	-1.220	-	-	-	40.4	-	-
4812.350		3.864	-1.800	-	-	51.3	-	-	31.3

Table A.6 – continued from previous page

Wavelength Å	Element	E_{low} eV	log gf	HD 122202 mÅ	HD 126681 mÅ	HD 148897 mÅ	HD 164922 mÅ	HD 167768 mÅ	HD 204613 mÅ
4634.070		4.073	-1.240	-	-	105.8	69.0	69.2	67.3
4848.250		3.864	-1.140	-	-	-	-	-	-
4030.750	Mn I	0.000	-0.470	-	-	-	-	-	-
4034.480		0.000	-0.810	-	-	-	-	-	-
4041.360		2.110	0.280	-	-	-	-	-	-
4451.580		2.890	0.280	-	-	111.3	108.0	-	84.7
4470.140		2.941	-0.444	-	-	36.7	58.5	-	38.1
4739.080		2.941	-0.490	-	-	57.8	81.5	48.3	34.5
4761.530		2.953	-0.138	-	-	74.9	99.5	64.9	53.1
4765.860		2.941	-0.080	-	-	82.0	90.2	71.4	57.5
4766.420		2.919	0.100	-	-	112.8	120.2	-	74.9
4783.430		2.300	0.040	-	-	162.6	181.5	132.0	110.8
5516.770		2.178	-1.847	-	-	72.2	86.6	35.3	16.7
4813.480	Co I	3.216	0.050	-	-	59.3	64.9	44.8	34.7
4121.320		0.920	-0.320	-	-	-	-	-	118.2
4118.770		1.050	-0.490	-	-	-	-	-	-
4749.660		3.053	-0.321	-	-	79.3	72.7	44.9	-
4771.080		3.133	-0.504	-	-	59.8	56.6	-	-

Table A.6 – continued from previous page

Wavelength Å	Element	E_{low} eV	log gf	HD 122202 mÅ	HD 126681 mÅ	HD 148897 mÅ	HD 164922 mÅ	HD 167768 mÅ	HD 204613 mÅ
4781.430		1.882	-2.150	-	-	74.9	-	-	-
4792.850		3.252	-0.067	-	-	43.8	47.3	39.1	-
5530.770		1.710	-2.060	-	-	66.4	40.4	-	12.6
5590.720		2.042	-1.870	-	-	51.7	33.7	99.1	-
5991.870		2.080	-1.850	-	-	-	23.9	46.6	-
6454.990		3.632	-0.233	-	-	20.7	25.6	-	-
6632.430		2.280	-2.000	-	-	32.4	22.4	-	-
4470.470	Ni I	3.699	-0.400	-	-	69.2	81.1	62.8	72.7
4714.420		3.380	0.230	-	-	135.2	177.9	125.3	127.0
4732.460		4.106	-0.550	-	-	-	47.3	32.4	37.3
4814.590		3.597	-1.680	-	-	-	19.5	-	-
4821.130		4.153	-0.850	-	-	25.9	48.9	35.9	-
4852.560		3.542	-1.070	-	-	44.7	50.5	41.6	31.5
4855.410		3.540	0.000	-	-	-	108.5	-	76.7
4857.390		3.740	-1.199	-	-	50.3	63.8	51.4	34.2
4953.200		3.740	-0.670	-	22.8	83.8	63.5	57.9	41.8
4937.340		3.606	-0.390	-	23.4	83.1	84.1	68.7	69.3
4980.160		3.610	-0.110	54.9	-	118.2	134.1	-	90.6

Table A.6 – continued from previous page

Wavelength Å	Element	E_{low} eV	log gf	HD 122202 mÅ	HD 126681 mÅ	HD 148897 mÅ	HD 164922 mÅ	HD 167768 mÅ	HD 204613 mÅ
5035.370		3.630	0.290	-	71.6	103.7	99.7	88.6	88.0
5081.120		3.847	0.300	53.2	50.1	100.7	108.4	76.7	81.3
5082.350		3.657	-0.540	-	21.1	82.0	72.8	66.1	55.4
5084.080		3.678	0.030	83.2	-	85.9	85.2	78.3	79.3
5099.930		3.678	-0.100	-	23.9	74.9	98.3	73.8	83.3
5102.960		1.676	-2.620	-	-	95.8	65.5	70.5	37.6
5259.470		3.740	-1.502	-	-	-	-	-	-
6086.280		4.266	-0.530	-	-	30.8	57.4	38.9	31.9
6111.070		4.088	-0.785	-	-	28.6	46.8	-	18.4
6176.810		4.088	-0.148	-	-	55.9	76.4	62.2	50.1
6186.710		4.106	-0.777	-	-	23.4	44.2	26.9	14.7
6204.600		4.088	-1.060	-	-	-	-	27.7	-
6643.640		1.676	-2.300	-	43.9	160.2	-	121.3	72.9
4722.150	Zn I	4.029	-0.370	78.0	-	65.2	81.9	82.7	79.2
4810.530		4.080	-0.170	-	-	70.9	70.8	-	75.6
4607.327	Sr I	0.000	-0.570	-	-	89.9	58.5	68.6	77.3
4854.863	Y II	0.992	-0.380	-	-	98.6	53.8	72.2	82.6
4883.685		1.084	0.070	129.5	28.6	114.5	-	80.6	101.4

Table A.6 – continued from previous page

Wavelength Å	Element	E_{low} eV	log gf	HD 122202 mÅ	HD 126681 mÅ	HD 148897 mÅ	HD 164922 mÅ	HD 167768 mÅ	HD 204613 mÅ
5087.416		1.080	-0.170	-	23.8	82.3	40.5	66.1	86.5
5119.112		0.992	-1.360	-	-	41.6	19.0	16.2	47.0
5205.724		1.033	-0.340	-	-	-	-	-	92.2
5289.815		1.033	-1.850	-	-	-	-	14.2	15.2
5544.611		1.738	-1.090	-	-	18.6	-	11.7	29.5
5546.009		1.748	-1.100	-	-	32.0	-	15.2	28.1
5662.925		1.944	0.160	-	34.8	83.8	67.8	64.8	72.0
6613.733		1.748	-1.110	-	67.7	26.5	21.2	21.2	27.4
4048.670	Zr II	0.800	-0.480	-	-	181.2	150.6	73.4	170.2
4208.990		0.710	-0.460	-	-	79.1	41.8	-	87.5
4317.321		0.713	-1.380	-	-	87.6	-	44.8	53.4
4554.036	Ba II	0.000	0.120	323.4	139.3	263.4	177.2	206.3	296.6
4130.650		2.720	+0.560	-	-	-	-	-	-
4934.076		0.000	-0.150	334.5	125.8	302.0	-	243.8	-
5853.668		0.604	-1.020	158.0	41.9	128.1	66.0	95.2	106.3
6141.727		0.704	-0.076	263.0	84.8	192.0	125.0	149.4	179.7
6496.897		0.604	-0.377	-	113.5	196.9	123.0	144.3	160.2
4123.230	La II	0.320	+0.120	-	-	-	-	-	-

Table A.6 – continued from previous page

Wavelength Å	Element	E_{low} eV	log gf	HD 122202 mÅ	HD 126681 mÅ	HD 148897 mÅ	HD 164922 mÅ	HD 167768 mÅ	HD 204613 mÅ
4238.380		0.400	-0.058	-	-	79.4	-	-	62.1
4322.510		0.170	-1.050	-	-	40.3	-	-	34.5
4333.760		0.170	-0.160	-	-	-	-	-	88.1
4619.874		1.754	-0.140	-	-	-	-	19.7	-
4748.726		0.927	-0.860	-	-	16.0	-	-	-
5808.313		0.000	-2.200	-	-	12.2	-	-	-
6320.376		0.170	-1.610	-	-	25.1	-	-	-
4073.470	Ce II	0.480	+0.320	-	-	-	-	-	-
4117.290		0.740	-0.450	-	-	-	-	-	-
4190.630		0.900	-0.390	-	-	166.6	110.1	-	40.0
4193.870		0.550	-0.400	-	-	-	-	-	-
4257.120		0.460	-1.110	-	-	-	-	-	-
4336.244		0.704	-0.564	-	-	22.6	-	-	14.3
4418.790		0.860	+0.310	-	-	-	-	19.1	59.9
4427.920		0.540	-0.380	-	64.8	-	31.7	31.7	-
4460.207		0.477	0.171	-	-	193.6	161.0	118.4	-
4560.280		0.910	0.000	-	-	-	-	-	-
4562.359		0.478	0.081	75.7	-	-	20.8	57.7	51.0

Table A.6 – continued from previous page

Wavelength Å	Element	E_{low} eV	log gf	HD 122202 mÅ	HD 126681 mÅ	HD 148897 mÅ	HD 164922 mÅ	HD 167768 mÅ	HD 204613 mÅ
4628.160		0.520	+0.260	-	18.4	66.5	19.1	39.9	41.4
4747.167		0.320	-1.246	-	-	27.3	-	-	-
4773.941		0.924	-0.498	-	-	16.69	-	-	-
4873.999		1.107	-0.892	-	-	40.1	22.4	-	39.4
5274.230		1.044	0.323	-	-	28.5	-	-	24.6
5330.556		0.869	-0.760	-	-	16.6	-	-	-
5188.217	Pr II	0.922	-1.145	-	-	-	-	-	-
5259.740		0.630	-0.070	8.14	-	24.6	-	-	-
5219.045		0.795	-0.240	-	-	14.2	-	61.3	-
5292.619		0.648	-0.300	7.1	-	29.2	51.3	-	22.2
5322.772		0.482	-0.315	-	-	28.9	-	-	-
5892.251		1.439	-0.352	51.3	-	18.6	-	116.3	-
6278.676		1.196	-0.630	-	-	33.2	-	76.6	-
4021.327	Nd II	0.320	0.230	-	-	47.0	-	-	49.5
4059.951		0.205	-0.360	-	-	49.3	-	-	-
4061.080		0.471	0.550	-	-	83.6	-	-	74.2
4069.270		0.060	-0.400	-	-	-	-	-	-
4109.448		0.320	+0.180	-	-	-	-	-	62.2

Table A.6 – continued from previous page

Wavelength Å	Element	E_{low} eV	log gf	HD 122202 mÅ	HD 126681 mÅ	HD 148897 mÅ	HD 164922 mÅ	HD 167768 mÅ	HD 204613 mÅ
4446.390		0.200	-0.630	-	-	79.8	-	-	35.1
4451.563		0.381	-0.040	-	-	111.4	108.0	76.9	84.4
4451.980		0.000	-1.340	-	-	101.0	55.5	47.4	25.9
4556.133		0.064	-1.610	-	49.6	-	139.0	-	99.7
4797.153		0.559	-0.950	-	-	24.9	-	-	-
4811.342		0.063	-1.140	-	-	64.5	14.3	34.1	-
5089.832		0.204	-1.160	-	-	30.7	-	-	-
5130.590		1.300	+0.100	-	9.2	-	-	-	-
4859.039		0.320	-0.830	-	-	85.5	46.2	45.7	42.1
4947.020		0.559	-1.250	98.0	-	12.8	-	11.3	-
4961.387		0.630	-0.710	-	-	30.8	-	-	14.5
4989.953		0.680	-1.400	-	-	52.8	-	-	19.7
5212.361		0.204	-0.870	-	15.4	66.4	42.2	34.9	
5293.169		0.823	-0.060	-	-	67.8	-	-	29.1
5276.878		0.859	-0.440	-	-	19.2	-	-	-
5287.133		0.745	-1.300	-	-	-	19.6	-	-
5311.480		0.990	-0.560	-	-	24.5	-	-	-
5319.820		0.550	-0.210	-	-	73.5	-	-	29.9

Table A.6 – continued from previous page

Wavelength Å	Element	E_{low} eV	log gf	HD 122202 mÅ	HD 126681 mÅ	HD 148897 mÅ	HD 164922 mÅ	HD 167768 mÅ	HD 204613 mÅ
5356.967		1.264	-0.250	-	-	-	-	-	-
5361.510		0.68	-0.400	-	-	-	80.1	-	-
5371.927		1.412	0.003	-	-	-	-	-	-
5603.648		0.380	-1.830	-	-	23.6	39.2	-	-
5718.118		1.410	-0.340	-	-	-	-	-	-
5825.857		1.081	-0.760	-	-	10.2	-	-	-
4318.927	Sm II	0.280	-0.270	-	-	-	-	-	-
4424.337		0.485	-0.260	-	-	-	-	107.9	64.9
4434.318		0.378	-0.576	-	-	84.0	37.7	-	56.2
4499.475		0.248	-1.413	-	-	26.7	-	-	-
4519.630		0.540	-0.430	-	-	47.6	-	-	18.6
4577.690		0.250	-0.770	-	-	42.0	-	-	-
4566.210		0.330	-1.245	-	-	40.1	16.6	19.1	14.2
4674.600		0.180	-0.560	-	14.4	115.7	-	61.7	-
4704.400		0.000	-1.562	-	-	60.7	29.6	42.2	23.8
4615.444		0.544	-1.262	-	-	-	49.0	-	-
4726.026		0.333	-1.849	-	-	59.1	-	-	-
4791.580		0.104	-1.846	-	-	26.0	-	-	-

Table A.6 – continued from previous page

Wavelength Å	Element	E_{low} eV	log gf	HD 122202 mÅ	HD 126681 mÅ	HD 148897 mÅ	HD 164922 mÅ	HD 167768 mÅ	HD 204613 mÅ
4815.805		0.185	-1.501	14.1	-	-	24.8	-	-
4129.700	Eu II	0.000	+0.204	-	-	-	-	84.0	57.4
4205.050		0.000	+0.117	-	-	-	89.6	-	138.4
6437.640		1.319	-0.276	-	-	16.1	-	-	-
6645.130		1.380	+0.204	-	-	29.9	-	22.12	-
4103.310	Dy II	0.103	-0.346	-	-	113.7	-	-	-
4923.167		0.103	-2.384	-	20.5	23.7	8.56	8.56	9.615

Table A.7: Elemental abundances: Light elements C, Na, Mg, Ca and Ti

Star	[C]	[Na I]	[Mg I]	[Ca I]	[Sc II]	[Ti I]	[Ti II]
Group I							
*HD 16458	8.65	6.17± 0.14	6.92± 0.04	5.94	2.50	4.56± 0.23	4.66± 0.28
#HD 122202	8.26	-	7.22	6.01	-	-	4.63 ± 0.17
HD 201626	8.22	5.19	6.83± 0.20	5.57± 0.15	1.70	4.25±0.27	4.32±0.25
#HD 204613	8.64	6.01±0.24	7.40±0.16	6.20±0.18	2.98	4.92±0.24	5.07±0.20
#HD 216219	8.55	6.32±0.12	7.51±0.20	6.28±0.22	2.70	4.84±0.20	5.02±0.27
Group II							
#HD 4395	8.09	6.24±0.19	7.49±0.28	6.16±0.22	2.80	4.78±0.22	4.96±0.24
*HD 55496	7.91	5.08	6.37	5.28	-	3.31	3.25
*HD 48565	8.39	5.76±0.04	7.09±0.23	5.83±0.22	2.35	4.35±0.07	4.61±0.23
HD 92545	8.86	5.87±0.03	7.23±0.12	6.05±0.23	-	4.72±0.20	5.20±0.24
HD 104979	8.16	5.90±0.04	7.34±0.06	6.10±0.24	2.78	4.78±0.16	4.96±0.20
HD 107574	8.21	6.01±0.18	-	5.85±0.09	2.27	4.57±0.20	4.60

Table A.7 – continued from previous page

Star	[C]	[Na I]	[Mg I]	[Ca]	[Sc II]	[Ti I]	[Ti II]
Group III							
*HD 5395	8.09	5.54±0.14	7.41±0.27	6.09±0.18	2.85	4.74±0.21	4.84±0.25
HD 81192	-	5.38±0.15	7.32±0.11	5.99±0.19	2.8	4.65±0.20	4.65±0.20
HD 89668	8.31	6.12±0.23	7.68	6.81±0.17	2.92	4.51±0.20	4.39±0.22
HD 111721	7.36	5.13±0.14	6.88±0.16	5.61±0.21	-	4.25±0.24	3.82±0.25
HD 125079	8.39	6.33±0.09	7.32±0.27	6.16±0.20	2.89	5.08±0.25	5.17
HD 126681	-	5.01±0.14	7.07	5.48±0.20	-	4.50±0.01	4.60±0.15
HD 148897	7.16	4.86±0.14	7.14±0.07	5.48±0.23	1.70	3.99±0.27	4.34±0.20
HD 164922	8.47	6.38±0.27	8.12	6.47±0.20	2.81	5.38±0.19	5.18±0.23
HD 167768	7.91	5.70±0.25	7.19±0.26	6.02±0.22	2.91	4.56±0.22	3.90±0.28
HD 188650	8.09	6.47±0.09	7.34±0.11	5.83±0.20	2.05	2.83±0.10	2.83±0.20
HD 214714	8.09	6.29±0.15	7.18±0.21	6.13±0.20	2.16	4.36±0.20	4.89±0.15

[#] Sub-giant CH stars

[*] Objects are also included in Ba star catalogue of Lu (1991)

Table A.8: Elemental abundances: Light elements V, Cr, Mn, Co, Ni and Zn

Star	[V I]	[Cr I]	[Cr II]	[Mn I]	[Co I]	[Ni I]	[Zn I]
Group I							
*HD 16458	3.60	5.28± 0.26	-	4.80	4.76± 0.18	5.73± 0.25	4.38± 0.20
#HD 122202	-	5.12	-	-	-	5.74 ± 0.16	4.56
HD 201626	-	3.66±0.25	-	-	3.53	4.73±0.25	3.17
#HD 204613	3.75	5.34±0.28	5.48±0.25	4.82	4.49±0.07	6.03	-
#HD 216219	3.70	5.38±0.20	5.59	4.90	4.78±0.25	6.40±0.23	4.59±0.21
Group II							
#HD 4395	3.70	5.49±0.29	5.63±0.03	5.00	4.57±0.25	6.05±0.21	4.62
*HD 55496	2.70	3.80	3.94	-	-	4.56	3.13
*HD 48565	3.20	4.86±0.15	4.73±0.02	-0.42	-0.15±0.25	-0.17±0.20	-0.18±0.13
HD 92545	-	5.28±0.25	-	-	5.51±0.11	6.03±0.12	-
HD 104979	3.79	5.36±0.23	5.44±0.24	4.90	4.94±0.13	6.01±0.24	4.31±0.20
HD 107574	-	5.09±0.25	4.73	-	-	5.59±0.12	-

Table A.8 – continued from previous page

Star	[V I]	[Cr I]	[Cr II]	[Mn I]	[Co I]	[Ni I]	[Zn I]
Group III							
*HD 5395	3.52	5.21±0.06	5.88	4.65	4.88±0.20	5.90±0.21	4.65
HD 81192	3.60	4.81±0.19	4.91±0.19	4.49	4.70±0.08	5.81±0.18	3.98±0.22
HD 89668	-	5.42±0.23	5.24	5.60	4.56±0.25	5.98±0.23	-
HD 111721	-	4.32±0.20	4.22±0.14	-	-	5.05±0.22	-
HD 125079	3.94	5.40±0.25	-	4.99	4.77±0.20	6.12±0.24	4.55±0.11
HD 126681	-	4.84±0.25	-	-	-	5.25±0.23	-
HD 148897	2.80	4.40±0.20	4.62	3.83	3.94±0.15	5.08±0.20	3.86±0.18
HD 164922	4.63	5.91±0.17	5.93±0.03	5.76	5.28±0.25	5.28±0.25	4.98±0.26
HD 167768	5.33	5.04±0.20	4.92	4.32	4.38±0.11	5.63±0.27	4.29±0.03
HD 188650	3.30	5.14±0.23	5.19	4.69	4.52±0.27	5.61±0.17	4.11±0.04
HD 214714	3.21	4.97±0.20	5.06±0.15	4.55	4.51±0.25	5.62±0.17	4.14

[#] Sub-giant CH stars

[*] Objects are also included in Ba star catalogue of Lu (1991)

Table A.9: Elemental abundances : Heavy elements

Star	[Sr I]	[Y II]	[Zr II]	[Ba II]	[La II]	[Ce II]	[Pr II]	[Nd II]	[Sm II]	[Eu II]	[Dy II]
Group I											
*HD 16458	3.64	3.02±0.25	3.11±0.21	2.70	1.90	2.40±0.21	1.88±0.08	2.35±0.17	2.23±0.18	0.53	-
#HD 122202	-	3.02	-	1.87	1.40	2.57	1.34±0.14	-	2.50	-	-
HD 201626	-	-	-	2.90	1.50	2.08±0.21	1.41	2.30±0.22	1.25±0.25	-	0.72
#HD 204613	4.31	2.94±0.11	3.49±0.04	2.97	2.10	2.58±0.04	1.99	2.23±0.20	2.38±0.17	0.34	2.67
#HD 216219	4.54	3.03±0.22	3.39±0.15	3.13	1.99	2.43	1.67±0.15	2.17±0.25	1.74±0.20	0.41	-
Group II											
#HD 4395	3.81	2.67±0.21	2.98±0.22	2.77	1.97	1.81±0.25	1.05	2.06±0.17	1.90±0.24	-	-
*HD 48565	4.06	2.70±0.13	2.90±0.04	3.10	2.00	2.41±0.17	1.10±0.02	2.37±0.05	1.60±0.02	0.22	-
*HD 55496	2.35	1.65±0.19	1.70	1.33	-	0.30	0.27	-	-	-	-
HD 92545	-	0.23±0.21	-	0.91	0.95	1.6	-	-	-	-	-
HD 104979	3.60	2.61±0.23	3.13	2.80	1.93	2.33±0.25	1.44±0.20	2.25±0.25	2.05±0.24	0.61	-
HD 107574	-	2.57±0.19	-	2.48	1.51	1.52	-	-	-	-	-

Table A.9 – continued from previous page

Star	[Sr I]	[Y II]	[Zr II]	[Ba II]	[La II]	[Ce II]	[Pr II]	[Nd II]	[Sm II]	[Eu II]	[Dy II]
Group III											
*HD 5395	2.94	2.02±0.11	-	1.96	1.13	1.40±0.17	1.26±0.20	1.95±0.12	-	0.62	2.28
HD 81192	2.99	1.80±0.11	2.20±0.12	1.79	0.90	0.92±0.11	-	2.00±0.16	1.35±0.25	-	1.84
HD 89668	3.79	2.57±0.30	-	1.74	2.78	2.91	2.18	2.65±0.20	2.05	0.71	-
HD 111721	-	1.15±0.21	-	0.97	0.33	2.07±0.09	-	2.44±0.14	-	-	-
#HD 125079	4.33	3.08±0.17	-	3.05	-	2.41±0.27	1.53	2.46±0.14	1.39	-	-
HD 126681	-	1.31±0.06	-	1.52	-	1.25	-	1.73±0.10	1.16	-	-
HD 148897	2.24	1.25±0.17	1.13	0.53	0.43	0.43±0.21	-	0.59±0.21	0.60±0.20	-	0.17
HD 164922	3.94	2.58±0.30	-	2.68	1.51	1.72±0.15	-	-	-	-	-
HD 167768	3.13	2.21±0.24	2.23±0.02	1.25	0.03	1.08±0.30	-	1.55±0.22	1.35±0.24	0.22	1.62
HD 188650	-	1.71±0.16	-	1.69	-	1.08±0.17	0.81	1.37	0.42±0.14	-	-
HD 214714	-	2.08±0.20	1.96±0.27	1.51	-	1.28±0.17	1.29±0.28	1.46±0.24	1.20±0.16	-	-

Sub-giant CH stars

* Objects are also included in Ba star catalogue of Lu (1991)

REFERENCES

Abate C., Pols O. R., Izzard R. G., Mohamed S. S., de Mink S. E., 2013, A&A, 552, A26

Abia C., Domínguez I., Gallino R., Busso M., Masera S., Straniero O., de Laverny P., Plez B., Isern J., 2002, ApJ, 579, 817

Abia C., Isern J., 2000, ApJ, 536, 438

Abia C., Rebolo R., Beckman J. E., Crivellari L., 1988, A&A, 206, 100

Allen D. M., Barbuy B., 2006a, A&A, 454, 895

Allen D. M., Barbuy B., 2006b, A&A, 454, 917

Allen D. M., Ryan S. G., Rossi S., Beers T. C., Tsangarides S. A., 2012, A&A, 548, A34

Alonso A., Arribas S., Martinez-Roger C., 1994, A&AS, 107, 365

Alonso A., Arribas S., Martinez-Roger C., 1996, A&A, 313, 873

Alonso A., Arribas S., Martinez-Roger C., 1998, A&AS, 131, 209

Alonso A., Arribas S., Martínez-Roger C., 1999, A&AS, 140, 261

Aoki W., Beers T. C., Christlieb N., Norris J. E., Ryan S. G., Tsangarides S., 2007, ApJ, 655, 492

Aoki W., Honda S., Beers T. C., Kajino T., Ando H., Norris J. E., Ryan S. G., Izumiura H., Sadakane K., Takada-Hidai M., 2005, ApJ, 632, 611

Aoki W., Norris J. E., Ryan S. G., Beers T. C., Ando H., 2002, ApJ, 567, 1166

Aoki W., Ryan S. G., Norris J. E., Beers T. C., Ando H., Iwamoto N., Kajino T., Mathews G. J., Fujimoto M. Y., 2001, ApJ, 561, 346

Arlandini C., Käppeler F., Wisshak K., Gallino R., Lugaro M., Busso M., Straniero O., 1999, ApJ, 525, 886

Asplund M., Grevesse N., Sauval A. J., 2005, in Barnes III T. G., Bash F. N., eds, Cosmic Abundances as Records of Stellar Evolution and Nucleosynthesis Vol. 336 of Astronomical Society of the Pacific Conference Series, The Solar Chemical Composition. p. 25

Baird S. R., Roberts W. J., Snow T. P., Wallerstein G., 1975, PASP, 87, 385

Baranne A., Queloz D., Mayor M., Adrianzyk G., Knispel G., Kohler D., Lacroix D., Meunier J.-P., Rimbaud G., Vin A., 1996, A&AS, 119, 373

Barbuy B., Spite M., Spite F., Hill V., Cayrel R., Plez B., Petitjean P., 2005, A&A, 429, 1031

Barnbaum C., Stone R. P. S., Keenan P. C., 1996, ApJS, 105, 419

Bartkevicius A., 1996, Baltic Astronomy, 5, 217

Baumueller D., Butler K., Gehren T., 1998, A&A, 338, 637

Baumueller D., Gehren T., 1997, A&A, 325, 1088

Beers T. C., Christlieb N., 2005, ARA&A, 43, 531

Beers T. C., Preston G. W., Shectman S. A., 1992, AJ, 103, 1987

Bidelman W. P., 1953, ApJ, 117, 25

Bidelman W. P., 1981, AJ, 86, 553

Bisterzo S., Gallino R., Straniero O., Cristallo S., Käppeler F., 2012, MNRAS, 422, 849

Bladh S., Höfner S., 2012, A&A, 546, A76

Bond H. E., 1974, ApJ, 194, 95

Bondi H., Hoyle F., 1944, MNRAS, 104, 273

Bothun G., Elias J. H., MacAlpine G., Matthews K., Mould J. R., Neugebauer G., Reid I. N., 1991, AJ, 101, 2220

Burbidge E. M., Burbidge G. R., Fowler W. A., Hoyle F., 1957, Reviews of Modern Physics, 29, 547

Busso M., Gallino R., Lambert D. L., Travaglio C., Smith V. V., 2001, ApJ, 557, 802

Busso M., Gallino R., Wasserburg G. J., 1999, ARA&A, 37, 239

Carollo D., Beers T. C., Bovy J., Sivarani T., Norris J. E., Freeman K. C., Aoki W., Lee Y. S., Kennedy C. R., 2012, ApJ, 744, 195

Castelli F., Hack M., 1990, Mem. Soc. Astron. Italiana, 61, 595

Cavallo R. M., Pilachowski C. A., Rebolo R., 1997, PASP, 109, 226

Cayrel R., Depagne E., Spite M., Hill V., Spite F., François P., Plez B., Beers T., Primas F., Andersen J., Barbuy B., Bonifacio P., Molaro P., Nordstroem B., 2004, A&A, 416, 1117

Christlieb N., Bessell M. S., Beers T. C., Gustafsson B., Korn A., Barklem P. S., Karlsson T., Mizuno-Wiedner M., Rossi S., 2002, Nature, 419, 904

Christlieb N., Green P. J., Wisotzki L., Reimers D., 2001, A&A, 375, 366

Clayton D. D., Ward R. A., 1974, ApJ, 193, 397

Cohen J. G., Shectman S., Thompson I., McWilliam A., Christlieb N., Melendez J., Zickgraf F.-J., Ramírez S., Swenson A., 2005, ApJ, 633, L109

Cottrell P. L., Sneden C., 1986, A&A, 161, 314

de Medeiros J. R., Mayor M., 1999, A&AS, 139, 433

Dominy J. F., 1984, ApJS, 55, 27

Evans T. L., 2010, Journal of Astrophysics and Astronomy, 31, 177

Fernandez-Villacanas J. L., Rego M., Cornide M., 1990, AJ, 99, 1961

Frasca A., Covino E., Spezzi L., Alcalá J. M., Marilli E., Fżrész G., Gandolfi D., 2009, A&A, 508, 1313

Frebel A., 2008, in Frebel A., Maund J. R., Shen J., Siegel M. H., eds, New Horizons in Astronomy Vol. 393 of Astronomical Society of the Pacific Conference Series, Metal-poor Stars. p. 63

Frebel A., Aoki W., Christlieb N., Ando H., Asplund M., Barklem P. S., Beers T. C., Eriksson K., et al.. 2005, Nature, 434, 871

Frebel A., Christlieb N., Norris J. E., Beers T. C., Bessell M. S., Rhee J., Fechner C., Marsteller B., Rossi S., Thom C., Wisotzki L., Reimers D., 2006, ApJ, 652, 1585

Fulbright J. P., 2000, AJ, 120, 1841

Gallino R., Arlandini C., Busso M., Lugaro M., Travaglio C., Straniero O., Chieffi A., Limongi M., 1998, ApJ, 497, 388

Gilroy K. K., 1989, ApJ, 347, 835

Girardi L., Bressan A., Bertelli G., Chiosi C., 2000, A&AS, 141, 371

Gontcharov G. A., 2006, Astronomy Letters, 32, 759

Goswami A., 2005, MNRAS, 359, 531

Goswami A., Aoki W., 2010, MNRAS, 404, 253

Goswami A., Aoki W., Beers T. C., Christlieb N., Norris J. E., Ryan S. G., Tsangarides S., 2006, MNRAS, 372, 343

Goswami A., Bama P., Shantikumar N. S., Devassy D., 2007, Bulletin of the Astronomical Society of India, 35, 339

Goswami A., Karinkuzhi D., 2013, A&A, 549, A68

Goswami A., Karinkuzhi D., Shantikumar N. S., 2010a, ApJ, 723, L238

Goswami A., Karinkuzhi D., Shantikumar N. S., 2010b, MNRAS, 402, 1111

Goswami A., Prantzos N., 2000, A&A, 359, 191

Gratton R. G., Carretta E., Castelli F., 1996, A&A, 314, 191

Gratton R. G., Sneden C., 1991, A&A, 241, 501

Gratton R. G., Sneden C., 1994, A&A, 287, 927

Gratton R. G., Sneden C., Carretta E., Bragaglia A., 2000, A&A, 354, 169

Gray D. F., 1992, The observation and analysis of stellar photospheres.

Green P. J., Margon B., Anderson S. F., MacConnell D. J., 1992, ApJ, 400, 659

Hansen T., Andersen J., Nordström B., Buchhave L. A., Beers T. C., 2011, ApJ, 743, L1

Hill V., Barbuy B., Spite M., Spite F., Cayrel R., Plez B., Beers T. C., Nordstroem B., Nissen P. E., 2000, A&A, 353, 557

Höfner S., 2009, in Henning T., Grün E., Steinacker J., eds, Cosmic Dust - Near and Far Vol. 414 of Astronomical Society of the Pacific Conference Series, Dust Formation and Winds around Evolved Stars: The Good, the Bad and the Ugly Cases. p. 3

Howard W. M., Mathews G. J., Takahashi K., Ward R. A., 1986, ApJ, 309, 633

Iben Jr. I., 1991, in Michaud G., Tutukov A. V., eds, Evolution of Stars: the Photospheric Abundance Connection Vol. 145 of IAU Symposium, Asymptotic Giant Branch Stars: Thermal Pulses, Carbon Production, and Dredge Up; Neutron Sources and S-Process Nucleosynthesis. p. 257

Ivans I. I., Sneden C., James C. R., Preston G. W., Fulbright J. P., Höflich P. A., Carney B. W., Wheeler J. C., 2003, ApJ, 592, 906

Izumiura H., Noguchi K., Aoki W., Honda S., Ando H., Takada-Hidai M., Kambe E., Kawanomoto S., Sadakane K., Sato B., Tajitsu A., Tanaka W., Okita K., Watanabe E., Yoshida M., 2008, ApJ, 682, 499

Izzard R. G., Jeffery C. S., Lattanzio J., 2007, A&A, 470, 661

Jonsell K., Barklem P. S., Gustafsson B., Christlieb N., Hill V., Beers T. C., Holmberg J., 2006, A&A, 451, 651

Jorissen A., Mayor M., 1992, in Kondo Y., Sistero R., Polidan R. S., eds, Evolutionary Processes in Interacting Binary Stars Vol. 151 of IAU Symposium, Orbital Elements of a Sample of S-Stars - Testing the Barium - S Evolutionary Connection. p. 407

Jorissen A., van Eck S., 2000, in Wing R. F., ed., The Carbon Star Phenomenon Vol. 177 of IAU Symposium, Barium Stars and Tc-Poor S Stars: Binary Masqueraders within the Carbon-Star Family. p. 259

Karakas A. I., 2010, in Goswami A., Reddy B. E., eds, Principles and Perspectives in Cosmochemistry Nucleosynthesis of Low and Intermediate-mass Stars. p. 107

Keenan P. C., 1942, ApJ, 96, 101

Keenan P. C., 1993, PASP, 105, 905

Koleva M., Vazdekis A., 2012, A&A, 538, A143

Krishnaswamy K., Sneden C., 1985, PASP, 97, 407

Kurucz R. L., 1991, in Bulletin of the American Astronomical Society Vol. 23 of Bulletin of the American Astronomical Society, A New Theoretical Model Photosphere. p. 1047

Kurucz R. L., 1993, in Dworetsky M. M., Castelli F., Faraggiana R., eds, IAU Colloq. 138: Peculiar versus Normal Phenomena in A-type and Related Stars Vol. 44 of Astronomical Society of the Pacific Conference Series, A New Opacity-Sampling Model Atmosphere Program for Arbitrary Abundances. p. 87

Kurucz R. L., 1995a, in Sauval A. J., Blomme R., Grevesse N., eds, Laboratory and Astronomical High Resolution Spectra Vol. 81 of Astronomical Society of the Pacific Conference Series, An Atomic and Molecular Data Bank for Stellar Spectroscopy. p. 583

Kurucz R. L., 1995b, in Adelman S. J., Wiese W. L., eds, Astrophysical Applications of Powerful New Databases Vol. 78 of Astronomical Society of the Pacific Conference Series, The Kurucz Smithsonian Atomic and Molecular Database. p. 205

Kyrolainen J., Tuominen I., Vilhu O., Virtanen H., 1986, A&AS, 65, 11

Lambert D. L., Gustafsson B., Eriksson K., Hinkle K. H., 1986, ApJS, 62, 373

Lambert D. L., Ries L. M., 1981, ApJ, 248, 228

Lawler J. E., Bonvallet G., Sneden C., 2001, ApJ, 556, 452

Lowrance P. J., Kirkpatrick J. D., Reid I. N., Cruz K. L., Liebert J., 2003, ApJ, 584, L95

Lu P. K., 1991, AJ, 101, 2229

Lucatello S., Beers T. C., Christlieb N., Barklem P. S., Rossi S., Marsteller B., Sivarani T., Lee Y. S., 2006, ApJ, 652, L37

Lucatello S., Tsangarides S., Beers T. C., Carretta E., Gratton R. G., Ryan S. G., 2005, ApJ, 625, 825

Luck R. E., 1991, ApJS, 75, 579

Luck R. E., Bond H. E., 1982, ApJ, 259, 792

Luck R. E., Bond H. E., 1983, ApJ, 271, L75

Luck R. E., Bond H. E., 1985, ApJ, 292, 559

Luck R. E., Bond H. E., 1991, ApJS, 77, 515

Luck R. E., Heiter U., 2007, AJ, 133, 2464

MacConnell D. J., Frye R. L., Upgren A. R., 1972, AJ, 77, 384

Massarotti A., Latham D. W., Stefanik R. P., Fogel J., 2008, AJ, 135, 209

Masseron T., Johnson J. A., Plez B., van Eck S., Primas F., Goriely S., Jorissen A., 2010, A&A, 509, A93

Mauron N., Gigoyan K. S., Kendall T. R., 2007, A&A, 463, 969

McClure R. D., 1983, ApJ, 268, 264

McClure R. D., 1984, ApJ, 280, L31

McClure R. D., 1997, PASP, 109, 536

McClure R. D., Woodsworth A. W., 1990, ApJ, 352, 709

McWilliam A., 1990, ApJS, 74, 1075

McWilliam A., 1998, AJ, 115, 1640

McWilliam A., Preston G. W., Sneden C., Searle L., 1995, AJ, 109, 2757

Mishenina T. V., Pignatari M., Korotin S. A., Soubiran C., Charbonnel C., Thielemann F.-K., Gorbaneva T. I., Basak N. Y., 2013, A&A, 552, A128

Mohamed S., Podsiadlowski P., 2007, in Napiwotzki R., Burleigh M. R., eds, 15th European Workshop on White Dwarfs Vol. 372 of Astronomical Society of the Pacific Conference Series, Wind Roche-Lobe Overflow: a New Mass-Transfer Mode for Wide Binaries. p. 397

Morgan W. W., Keenan P. C., Kellman E., 1943, An atlas of stellar spectra, with an outline of spectral classification

Moultaka J., Ilovaisky S. A., Prugniel P., Soubiran C., 2004, PASP, 116, 693

Mucciarelli A., Caffau E., Freytag B., Ludwig H.-G., Bonifacio P., 2008, A&A, 484, 841

Nidever D. L., Marcy G. W., Butler R. P., Fischer D. A., Vogt S. S., 2002, ApJS, 141, 503

Nissen P. E., Chen Y. Q., Schuster W. J., Zhao G., 2000, A&A, 353, 722

Nissen P. E., Schuster W. J., 2011, A&A, 530, A15

Nordstroem B., Mayor M., Andersen J., Holmberg J., Pont F., Jorgensen B. R., Olsen E. H., Udry S., Mowlavi N., 2004, A&A, 418, 989

Norris J. E., Ryan S. G., Beers T. C., 1997a, ApJ, 488, 350

Norris J. E., Ryan S. G., Beers T. C., 1997b, ApJ, 489, L169

Norris J. E., Ryan S. G., Beers T. C., Aoki W., Ando H., 2002, ApJ, 569, L107

North P., Berthet S., Lanz T., 1994, A&A, 281, 775

North P., Duquennoy A., 1992, in Duquennoy A., Mayor M., eds, Binaries as Tracers of Star Formation Are barium dwarfs progenitors of barium giants?. pp 202–216

Ohnaka K., Izumiura H., Leinert C., Driebe T., Weigelt G., Wittkowski M., 2008, A&A, 490, 173

Paczyński B., 1965, Acta Astron., 15, 89

Pilachowski C. A., Sneden C., Booth J., 1993, ApJ, 407, 699

Pourbaix D., Tokovinin A. A., Batten A. H., Fekel F. C., Hartkopf W. I., Levato H., Morrell N. I., Torres G., Udry S., 2004, A&A, 424, 727

Prantzos N., Hashimoto M., Rayet M., Arnould M., 1990, A&A, 238, 455

Preston G. W., Sneden C., 2001, AJ, 122, 1545

Prochaska J. X., McWilliam A., 2000, ApJ, 537, L57

Prugniel P., Vauglin I., Koleva M., 2011, A&A, 531, A165

Qian Y.-Z., Wasserburg G. J., 2003, ApJ, 588, 1099

Ramírez I., Meléndez J., 2004, ApJ, 609, 417

Rebolo R., Beckman J. E., Molaro P., 1988, A&A, 192, 192

Rossi S., Beers T. C., Sneden C., 1999, in Gibson B. K., Axelrod R. S., Putman M. E., eds, The Third Stromlo Symposium: The Galactic Halo Vol. 165 of Astronomical Society of the Pacific Conference Series, Carbon Abundances for Metal-Poor Stars Based on Medium-Resolution Spectra. p. 264

Ryan S. G., Aoki W., Norris J. E., Beers T. C., 2005, ApJ, 635, 349

Ryan S. G., Lambert D. L., 1995, AJ, 109, 2068

Ryan S. G., Norris J. E., Beers T. C., 1996, ApJ, 471, 254

Santos N. C., Mayor M., Bonfils X., Dumusque X., Bouchy F., Figueira P., Lovis C., Melo C., Pepe F., Queloz D., Ségransan D., Sousa S. G., Udry S., 2011, A&A, 526, A112

Schwarzschild M., Härm R., 1967, ApJ, 150, 961

Secchi A., 1868, MNRAS, 28, 196

Shane C. D., 1928, Lick Observatory Bulletin, 13, 123

Shetrone M. D., Sneden C., Pilachowski C. A., 1993, PASP, 105, 337

Siebert A., Williams M. E. K., Siviero A., Reid W., Boeche C., Steinmetz M., Fulbright J., Munari U., et al. 2011, AJ, 141, 187

Smith J. A., Demarque P., 1980, A&A, 92, 163

Smith V. V., 1984, A&A, 132, 326

Smith V. V., Coleman H., Lambert D. L., 1993, ApJ, 417, 287

Smith V. V., Lambert D. L., 1986, ApJ, 303, 226

Sneden C., 1983, PASP, 95, 745

Sneden C., Bond H. E., 1976, ApJ, 204, 810

Sneden C., McWilliam A., Preston G. W., Cowan J. J., Burris D. L., Armosky B. J., 1996, ApJ, 467, 819

Sneden C., Pilachowski C. A., Lambert D. L., 1981, ApJ, 247, 1052

Sneden C., Pilachowski C. A., Vandenberg D. A., 1985, in Bulletin of the American Astronomical Society Vol. 17 of Bulletin of the American Astronomical Society, Carbon Isotope Ratios in Field Population II Giant Stars. p. 877

Sneden C. A., 1973, PhD thesis, THE UNIVERSITY OF TEXAS AT AUSTIN.

Soubiran C., Bienaymé O., Mishenina T. V., Kovtyukh V. V., 2008, A&A, 480, 91

Sousa S. G., Santos N. C., Israelian G., Mayor M., Udry S., 2011, A&A, 533, A141

Sozzetti A., Torres G., Latham D. W., Stefanik R. P., Korzennik S. G., Boss A. P., Carney B. W., Laird J. B., 2009, ApJ, 697, 544

Straniero O., Gallino R., Busso M., Chiefei A., Raiteri C. M., Limongi M., Salaris M., 1995, ApJ, 440, L85

Tomkin J., Lambert D. L., 1983, ApJ, 273, 722

Tomkin J., Lambert D. L., 1986, ApJ, 311, 819

Tomkin J., Lemke M., Lambert D. L., Sneden C., 1992, AJ, 104, 1568

Totten E. J., Irwin M. J., 1998, MNRAS, 294, 1

Totten E. J., Irwin M. J., Whitelock P. A., 2000, MNRAS, 314, 630

Tsangarides S. A., 2005, PhD thesis, Open University (United Kingdom), England

Tsuji T., Tomioka K., Sato H., Iye M., Okada T., 1991, A&A, 252, L1

Vanture A. D., 1992a, AJ, 103, 2035

Vanture A. D., 1992b, AJ, 104, 1986

Vanture A. D., 1992c, AJ, 104, 1997

Vassiliadis E., Wood P. R., 1993, ApJ, 413, 641

Wallerstein G., Greenstein J. L., 1964, ApJ, 139, 1163

Wallerstein G., Knapp G. R., 1998, ARA&A, 36, 369

Wanajo S., Nomoto K., Iwamoto N., Ishimaru Y., Beers T. C., 2006, ApJ, 636, 842

Weigert A., 1966, ZAp, 64, 395

Westerlund B. E., Azzopardi M., Breysacher J., Rebeirot E., 1995, A&A, 303, 107

Wilson R. E., 1953, Carnegie Institute Washington D.C. Publication, p. 0

Wisotzki L., Christlieb N., Bade N., Beckmann V., Köhler T., Vanelle C., Reimers D., 2000, A&A, 358, 77

Worley C. C., Hill V., Sobeck J., Carretta E., 2013, A&A, 553, A47

Yamashita Y., 1975, PASJ, 27, 325

Zacs L., 1991, Soviet Astronomy Letters, 17, 261

Zhang B., Ma K., Zhou G., 2006, ApJ, 642, 1075

Zijlstra A. A., 2004, MNRAS, 348, L23